Title

Paraoxonase 2 (PON2) in Cardiovascular Disease (CVD): The Role of PON2 in Acute Myocardial Ischemia-Reperfusion Injury and Diet-Induced Obesity

Author

Abdulmalek, Dawoud Sulaiman

Publication Date

2020

Peer reviewed|Thesis/dissertation

UNIVERSITY OF CALIFORNIA

Los Angeles

Paraoxonase 2 (PON2) in Cardiovascular Disease (CVD): The Role of PON2 in Acute Myocardial Ischemia-Reperfusion Injury and Diet-Induced Obesity

A dissertation submitted in partial satisfaction of the

requirements for the degree Doctor of Philosophy

in Molecular Toxicology

by

Dawoud Sulaiman Abdulmalek

2020

ABSTRACT OF THE DISSERTATION

Paraoxonase 2 (PON2) in Cardiovascular Disease (CVD): The Role of PON2 in Acute Myocardial Ischemia-Reperfusion Injury and Diet-Induced Obesity

by

Dawoud Sulaiman Abdulmalek

Doctor of Philosophy in Molecular Toxicology

University of California, Los Angeles, 2020

Professor Srinivasa T. Reddy, Chair

Paraoxonase 2 (PON2) is a ubiquitously expressed antioxidant, anti-inflammatory protein localized in the inner mitochondrial membrane, where it protects against mitochondrial dysfunction and oxidative stress, among other protective properties. Human PON2 polymorphisms, particularly human PON2 $Ser_{311}Cys$, has been implicated in the development of coronary artery disease, including myocardial infarction and ischemic stroke. Therefore, in this thesis, I explored the cardioprotective capacity of PON2 against myocardial infarction, specifically acute myocardial ischemia-reperfusion injury (IRI). My hypothesis is that PON2 protects against myocardial IRI in cardiomyocytes by modulating mitochondrial dysfunction and oxidative stress, particularly mitigating mitochondrial lipotoxicity (lipid peroxidation). I employed *in vitro*

(rat ventricular cardiomyocyte cell line, H9c2 cells), *ex vivo* (cardiomyocytes derived from PON2-deficient mice hearts), and *in vivo* (PON2-deficient mice) models, subjecting them to cardiac IRI, to test my hypothesis. I determined that PON2 protects against myocardial IRI in cardiomyocytes by reducing mitochondrial dysfunction (stabilizing mitochondrial membrane potential and improving calcium retention capacity) and oxidative stress (reducing mitochondrial reactive oxygen species) via the reperfusion injury salvage kinase pathway (increasing phosphorylated glycogen synthase kinase-3β). Furthermore, there is an increase in mitochondrial lipid peroxidation in PON2-deficient mice subjected to myocardial IRI, with an increase in oxidized phosphatidylcholine species and eicosanoids (12, 15- hydroxyeicosatetraeonic acid), and a decrease in prostanoid production. These injuries are rescued by PON2 overexpression. Also, I observe an increase in cytoplasmic phospholipase A_2 in the hearts of PON2-def mice subjected to myocardial IRI, serving as a potential mechanism by which PON2 modulates the increase in unesterified eicosanoid production. In order to further examine whether PON2 deficiency, exclusively in cardiomyocytes, is sufficient to induce increased myocardial IRI, I generated cardiomyocyte-specific PON2-KO mice. Lastly, I investigated the protective role of a novel drug, HSG4112, against cardiovascular risk factor, diet-induced obesity. I found that HSG4112 protects against diet-induced obesity by enhancing lactonase/arylesterase activity, reducing body weight and fat mass, and increasing lean (muscle) mass. Nevertheless, the protective effects of HSG4112 are significantly reduced in PON2-def mice, suggesting that PON2 is at least partly involved as a mode of action for HSG4112's protective capacity.

The dissertation of Dawoud Sulaiman Abdulmalek is approved.

Oliver Hankinson

Jesus A. Araujo

Mansoureh Eghbali

Srinivasa T. Reddy, Committee Chair

University of California, Los Angeles

2020

TABLE OF CONTENTS

List of Figures

Figure 4: Overexpression of human PON2 in H9c2 cells results in increased pGSK-3β following HRI.

Figure 5: Figure 5: PON2 overexpression is cardioprotective and activates the RISK (PI3K/Akt/GSK-3β) pathway.

Figure 26: Limited capacity of HSG4112 to rescue obesity phenotype in PON2-def mice.

Figure 27: HSG4112 Protection Against Diet-Induced Obesity in Hyperlipidemic Mice.

List of Tables

ACKNOWLEDGEMENTS

Chapter 2 was previously published as: Sulaiman D, Li J, Devarajan A, Cunningham CM, Li M, Fishbein GA, Fogelman AM, Eghbali M, Reddy ST. Paraoxonase 2 protects against acute myocardial ischemia-reperfusion injury by modulating mitochondrial function and oxidative stress via the PI3K/Akt/GSK-3 RISK pathway. Journal of Molecular and Cellular Cardiology. 2019 April; 129: 154-164..

For this work, I would like to acknowledge Li J for LAD ligations, mitochondria assays, protein characterization; Devarajan for early cardiomyocyte studies; Cunningham for ex vivo Langenderoff experiments; Li M for LAD ligations, Fishbein for IHC help; Fogelman for guidance; Eghbali for mentorship and guidance; Reddy ST was the principal investigator for this work.

Overall, I would like to acknowledge my funding sources: NIH/NHLBI grant RO1 HL071776-01.

Lastly, I would not be here today without the endless and unconditional support and love of my family, friends and mentors: my father, Sulaiman Abdulmalek; my mother, Nehal Abdulkareem; my brothers, Abdulmalek and Abdullah Sulaiman; my sister, Noor Sulaiman; my wife, Alba Ortez; my in-laws, the Ortez family, and my close friends: Bakir Silajdzic, Daniyal Ahmed, Michael Robertson, Maureen Sampson. Additionally, I would like to thank and acknowledge everyone during my time at UCLA: my lab members: Victor, Ellen, David, Arnab, Pallavi, Nasrin, and Prisca; the tremendous support and mentorship of my committee members: Dr. Oliver Hankinson, Dr. Jesus Araujo, and Dr. Eghbali, and, most importantly, my thesis advisor/PI, Dr. Srinivasa T. Reddy. Dr. Reddy has been a continuous source of support and guidance, both scientifically and professionally, always pushing me to better myself and pursue excellence in everything I do. Thank you all!

Vita

Education:

University of California, Irvine	BS	2011	Biology

Positions/Employment, Memberships and Honors

2007-2011	Dean's Honor List, University of California, Irvine (UCI)
2011	Excellence in Research in the Biological Sciences, UCI
2012-2014	Staff Research Associate, Department of Medicine-Cardiology, UCLA
2015-2020	Graduate Student Researcher, Molecular Toxicology, UCLA
2017-2018	Molecular Toxicology Student Representative, Molecular Toxicology, UCLA
2017	Poster Presentation Award, Graduate Division, 2017 UCLA Cardiovascular Symposium
2018	Poster Presentation Award, Graduate Division, 2018 UCLA Cardiovascular Symposium

Publications

Meriwether D, **Sulaiman D**, Volpe C, Dorfman A, Grijalva V, Dorreh N, Solorzano-Vargas RS, Wang J, O'Connor E, Papesh J, Larauche, M, Trost H, Palgunachari MN, Anantharamaiah GM, Herschman HR, Martin MG, Fogelman AM, Reddy ST. Apolipoprotein A-1 mimetics mitigate intestinal inflammation in COX2-dependent inflammatory bowel disease model. Journal of Clinical Investigation. 2019 Jun.

Sulaiman D, Li J, Devarajan A, Cunningham CM, Li M, Fishbein GA, Fogelman AM, Eghbali M, Reddy ST. Paraoxonase 2 protects against acute myocardial ischemia-reperfusion injury by modulating mitochondrial function and oxidative stress via the PI3K/Akt/GSK-3 RISK pathway. Journal of Molecular and Cellular Cardiology. 2019 April; 129: 154-164.

Chattopadhyay A, Yang X, Mukherjee P, **Sulaiman D**, Fogelman HR, Grijalva V, Dubinett S, Wasler TC, Paul MK, Salehi-Rad R, Mack JJ, Iruela-Arispe ML, Navab M, Fogelman AM and Reddy ST. Treating the Intestine with Oral ApoA-I Mimetic Tg6F Reduces Tumor Burden in Mouse Models of Metastatic Lung Cancer. Sci Rep. 2018;8:9032.

Zhang M, Nakamura K, Kageyama S, Lawal AO, Gong KW, Bhetraratana M, Fujii T, **Sulaiman D**, Hirao H, Bolisetty S, Kupiec-Weglinski JW, Araujo JA. Myeloid HO-1 modulates macrophage polarization and protects against ischemia-reperfusion injury. JCI Insight; 2018 October; 3(19).

Meriwether D, **Sulaiman D**, Wagner A, Grijalva V, Kaji I, Williams KJ, Yu L, Fogelman S, Volpe C, Bensinger SJ, Anantharamaiah GM, Shechter I, Fogelman AM, Reddy ST. Transintestinal transport of the anti-inflammatory drug 4F and the modulation of transintestinal cholesterol efflux. Journal of Lipid Research. 2016 July; 57(7): 1175-93.

Li R, Navab K, Hough G, Daher N, Zhang M, Mittelstein D, Lee K, Pakbin P, Saffari A, Bhetraratana M, **Sulaiman D**, Beebe T, Wu L, Jen N, Wine E, Tseng CH, Araujo JA, Fogelman A, Sioutas C, Navab M and Hsiai TK. Effect of exposure to atmospheric ultrafine particles on production of free fatty acids and lipid metabolites in the mouse small intestine. *Environ Health Perspect*. 2015;123:34-41

Chapter 1: Introduction

Abbreviations:

CVD	Cardiovascular Disease
PON	Paraoxonase
WT	Wild-type
PON2-def	PON2-deficient
LDLR-KO	Low density lipoprotein receptor knock-out
WD	Western diet
HF/HS	High fat/high sucrose
CL	Cardiolipin
PC	Phosphatidylcholine
PE	Phosphatidylethanolamine
ROS	Reactive oxygen species
HETE	5-Hydroxyeicosatetraenoic acid
POVPC	1-palmitoyl-2-(5'-oxo-valeroyl)-sn-glycero-3-phosphocholine
PGPC	1-palmitoyl-2-glutaryl-sn-glycero-3-phosphocholine
$cPLA_2$	Cytoplasmic phospholipase A_2
IRI	Ischemia-reperfusion injury
ROS	Reactive oxygen species
mPTP	Mitochondrial permeability transition pore
Akt	Protein kinase B
IMM	Inner mitochondrial membrane
SNP	Single nucleotide polymorphism

Cardiovascular disease (CVD) is the leading cause of morbidity and mortality worldwide, including the United States.[1-3] In the United States, CVD deaths surpass that of cancer and chronic lung disease combined, with one person dying from CVD every 37 seconds, with deaths from heart disease accounting for about one in four deaths.[1-3] CVD includes an array of diseases associated the entire vasculature, including stroke,

heart failure, high blood pressure, and coronary heart diseases (CHD), which includes coronary artery diseases (CAD) like atherosclerosis. Subsequently, CAD can lead to CHD manifesting as ischemia and myocardial infarction (MI). Moreover, CHD is the leading cause of CVD deaths (43.2%) in the United States, with an American experiencing a MI every 40 seconds.[1] Additionally, diet-induced obesity in adults is one of the leading risk factors (~40%) for many individuals suffering from CVD/CHD or are at a higher risk for developing CVD.[1] The financial impact of CVD is tremendous, with an estimated $351.2 billion in direct and indirect costs.[1] In 2016, The American Heart Association estimated that by 2035, the direct and indirect costs of CVD will reach $1.1 trillion.[1]

There is a lack of therapeutic agents to treat MI and diet-induced obesity. Therefore, discovery of novel molecules and mechanisms that protect against the debilitating outcomes of MI, specifically ischemia-reperfusion injury (IRI) and diet-induced obesity are of vital importance, particularly for the development of therapeutic targets. An underlying feature of both diseases is oxidative stress and mitochondrial dysfunction.[4] Therefore, studying a therapeutic target that can modulate these pathologies is critical. Paraoxonase 2 (PON2), a ubiquitously expressed anti-oxidant and anti-inflammatory protein located in the mitochondria, has been shown to be protective against atherosclerosis, obesity and heart failure.[5-7] Moreover, the human PON2 $Ser_{311}Cys$ ($S_{311}C$) polymorphism, a fairly common SNP, has been linked to coronary artery disease, including myocardial infarction and ischemic stroke.[8-13] Consequently, the primary aim of my thesis will be to examine the role of PON2 against myocardial IRI, particularly in cardiomyocytes. In addition, I will examine the potential role of PON2 in

modulating the protective effects of a novel therapeutic, HSG4112, in mitigating diet-induced obesity, one of the largest risk factors associated with CHD.

The mitochondria are intimately involved in the pathogenesis of myocardial IRI, which is characterized by the ischemic injury, or occlusion of a coronary artery (myocardial infarction), and the subsequent reperfusion injury upon restoration of blood flow to the myocardium *via* primary percutaneous coronary intervention (PPCI).[14] A primary outcome of ischemia is the switch from aerobic to anaerobic respiration, resulting in the depletion of ATP.[15] A key consequence is the inhibition of crucial ATP-dependent ion channels that result in the accumulation of sodium and, more critically, calcium. Furthermore, oxygen, an electron acceptor in the electron transport chain, is absent, resulting in a large build-up of electrons within the mitochondrial membranes.[16] These ischemic injuries prime the cell for a further injury upon reperfusion. The reintroduction of oxygen during reperfusion interacts with the free electrons in the mitochondrial membrane, resulting in the formation of reactive oxygen species (ROS), specifically superoxides.[17] The influx of ROS, coupled with the unresolved calcium overload, trigger the opening of mitochondrial permeability transition pore (mPTP). [15, 16] mPTP is a nonselective channel of the inner mitochondrial membrane (IMM) and its opening results in mitochondrial membrane depolarization, uncoupling of oxidative phosphorylation, release of ROS and cytochrome c to the cytosol, inducing pro-apoptotic, caspase signaling cascade ultimately leading to the death of cardiomyocytes.[15, 16, 18, 19] Nevertheless, despite the seemingly paradoxical reperfusion injury, quick and timely PPCI upon the onset of the ischemia results in a critically significant salvaging of the myocardium that would otherwise be lost if the ischemic

injury is allowed to persist.[14] Consequently, discovering novel genetic targets and pharmacological interventions that aim to mitigate reperfusion injury, i.e. by reducing ROS generation or mPTP opening, prior/during PPCI are instrumental in the fight against myocardial IRI. Yet, many therapies have been largely unsuccessful.[20, 21]

During IRI, a fraction of glycogen synthase kinase-3β (GSK-3β), a ubiquitously expressed serine/threonine kinase, is localized to the sarcoplasmic reticulum/endoplasmic reticulum (SR/ER) and the mitochondria-associated ER membranes (MAMs) in the heart.[22] In addition, the inhibition, via phosphorylation, of GSK-3β inhibits the opening of mPTP and is regulated by the reperfusion injury salvage kinases (RISK), including phosphatidylinositol 3-kinase (PI3K) and Akt.[23-25] Therefore, discovering a molecule that modulates the phosphorylation of GSK-3β will serve as a potential therapeutic target of IRI.

Mitochondrial membrane lipids, especially within the IMM like CL, play various roles within the mitochondria including protein biogenesis, energy production, membrane function, and apoptosis.[26] The major phospholipids in the mitochondrial membranes are PC, PE, and CL, which make-up ~40%, 30%, and 15% of the total lipids respectively.[26] These mitochondrial membrane lipids are susceptible to oxidative damage during IRI, which leads to lipid peroxidation of the phospholipids and their esterified polyunsaturated fatty acid tails, like linoleic and arachidonic acid, which can be further oxidized to pro-inflammatory eicosanoids and prostanoids.[27-34] Furthermore, this mitochondrial lipid peroxidation causes the loss of IMM organization, decreases in CL content, increases in CL peroxidation and increases the permeability of the plasma membrane that lead to increases the release of cytochrome c into the cytosol and

disruption of membrane potential.[27, 28, 35-38] Consequently, lipid peroxidation and or their secondary, endogenous toxic products also have the potential to be promising therapeutic targets against IRI.

PON2 is part of a gene family consisting of three members, PON1, PON2, and PON3, which are located adjacent to each other on the long arm of chromosome 7 in humans and chromosome 6 in mice.[4, 39] Although PON1 was discovered first, PON2 is the oldest member of the gene family, which gave rise to PON1 and PON3 by gene duplication. All three genes are highly conserved in mammals and exhibit great homology with each other, sharing approximately 60% at the amino acid level and about 70% at the nucleic acid level. [40] PON1 and PON3 are mainly expressed in the liver and associate with High Density Lipoproteins (HDL) in the circulation (PON3 on a much smaller scale), while PON2 is ubiquitously expressed as an intracellular protein in nearly all tissue types.[41] PON1 was initially discovered as an enzyme with the ability to hydrolyze organophosphates like chlorpyrifos oxon, dizoxon, and paraxon, the active metabolite of insecticide parathion.[4, 41] Nevertheless, all three PONs exhibit lactonase activity, in which they can hydrolyze a variety of lactones, namely acyl- homoserine lactones (AHLs) that mediate bacterial quorum-sensing (QS) signals. More specifically, PON2 is responsible for attenuating the biological effects of the Pseudomonas aeruginosa QS molecule N-(3-oxo-dodecanoyl)-L-homoserine lactone (3OC12) by decreasing its availability for receptor-mediated effects as well as promoting calcium release and stress signaling via intracellular acidification.[42] Recently, Li et al. generated soluble human PON2 that has shown promise as a novel therapeutic approach for

reducing antibiotic resistance and fighting chronic infections through the enzymatic inactivation of QS signaling molecules, like AHLs.[43]

PON2 has been shown to have various anti-oxidant and anti-inflammatory properties, is protective against a range of diseases including bacterial infection, cancer, and cardiovascular disease.[4, 5, 44-46] However, the physiological substrates and molecular mechanisms through which the PON enzymes exhibit these anti-oxidant and anti-inflammatory properties remain generally unknown. PON2 is a ~43 kDa protein localized within the mitochondria, specifically associating with complex III of the IMM.[5] A PON2-deficient mouse model was developed by our lab to test the role of PON2 in various disease models.[44] PON2 deficiency alters mitochondrial function by decreasing mitochondrial complex I and III activity and total ATP levels and alters mitochondrial oxidative stress by increasing mitochondrial superoxide production, increasing lipid peroxidation and decreasing reduced glutathione levels.[5, 45] Additionally, PON2 deficiency aggravated the development of atherosclerosis.[5, 47] Moreover, PON2 is associated with endoplasmic reticulum (ER) and its expression is induced in response ER stress pathway unfolded protein response (UPR), which reduces intracellular ROS and UPR-associated oxidative stress and caspase induced cell death by regulation of calcium homeostasis.[46, 48] Within the IMM, PON2 attenuated CL peroxidation, cytochrome c release and caspase activation.[49] **Therefore, given that the pathophysiology of myocardial IRI largely converges onto the mitochondria and the well-established protective capacity of PON2 against mitochondrial dysfunction and oxidative stress, I hypothesize that PON2 is protective against**

myocardial IRI by mitigating mitochondrial dysfunction, oxidative stress, and lipid peroxidation.

Recently, I have reported the critical protective role that PON2 plays in modulating myocardial Ischemia-Reperfusion Injury, which I further discuss in chapter 2.[50] In brief, our study demonstrates that PON2 expression is inversely related to IRI severity as PON2-def mice subjected to IRI exhibited a significant increase in infarct size when compared to WT controls. Since mitochondrial dysfunction and oxidative stress are hallmark consequences of myocardial IRI, we tested the mitochondrial integrity of PON2-def mice following IRI. Our findings reveal that PON2-def mice have an inherent mitochondrial defect that, when in the presence of an exogenous stressor (i.e. extramitochondrial calcium), manifests into basal mitochondrial dysfunction. Furthermore, mitochondria isolated from PON2-def mice subjected to IRI had a significant reduction in calcium retention capacity (CRC) and oxidative stress, when compared to WT controls. We further examined and validated these results specifically within mitochondria from the cardiomyocyte subpopulation. In addition, PON2 modulates mitochondrial membrane potential, an essential consequence of mitochondrial dysfunction, driven in part by mPTP opening. These observations demonstrate a clear role for PON2 in protection against myocardial IRI as lack of PON2 results in increased IRI, in the form of mitochondrial dysfunction and oxidative stress, specifically within the cardiomyocyte subpopulation.

In chapter 3, I investigate the role novel role that PON2 plays in modulating mitochondrial phospholipid composition and lipid peroxidation, specifically evaluating eicosanoid and prostanoid production. In brief, PON2 deficiency significantly modulates

mitochondrial membrane phospholipid composition by reducing PC and increasing PE species under baseline conditions, which largely held true post-IRI. Many of significantly altered mitochondrial phospholipids contain esterified linoleic acid (18:2) and arachidonic acid (20:4), which serve as substrates for oxidation (enzymatic or non-enzymatic) into various eicosanoids and prostanoids.[51] In fact, I observe that there is a significant increase in both eicosanoid and prostanoid production as well as PC oxidation (POVPC and PGPC) in the mitochondria of hearts from PON2-def mice under baseline and post-IRI conditions. Furthermore, PON2 overexpression rescues this phenotype, supporting its protective capacity. Lastly, cytoplasmic phospholipase 2 is upregulated in PON2 deficient hearts subjected to IRI, serving as a potential molecular mechanism for PON2's capacity to modulate mitochondrial lipid composition and peroxidation.

Consequently, I set out to determine if PON2 deficiency specifically within cardiomyocytes is sufficient to inducing the increase in myocardial IRI that I observed in my global PON2 knockout (PON2-def) mouse model.[50] Therefore, I generated two novel cardiomyocyte specific PON2-KO transgenic mouse models to explore this hypothesis, using both CRISPR-Cas9 and FLP/Cre recombinase systems, which I outline in chapter 3.

Lastly, in chapter 5, I explore the capacity of novel drug, HSG4112, to protect against the CVD risk factor, diet-induced obesity, and the potential role of PON2 as a mode of action for its protective properties. In brief, HSG4112 enhances lactonase and arylesterase activity and induces PON1 and PON3 protein expression in WT, PON1-KO and PON2-KO mice under baseline, chow fed conditions. HSG4112's protective effects

are partly reduced with PON2 deficiency. This is observed in preserved capacity of HSG4112 to reduce body weight in both WT and PON2-def mice, while losing its potential to reduce fat mass, increase muscle mass, enhance lactonase activity, and decrease plasma glucose levels. Nevertheless, HSG4112 was able to significantly reduce the body weight and fat mass, increase muscle mass, and decrease plasma glucose levels in hyperlipidemic mice fed a western diet.

Chapter 2: Paraoxonase 2 protects against acute myocardial Ischemia-reperfusion injury by modulating mitochondrial function and oxidative stress via the PI3K/Akt/GSK-3β RISK pathway

Abbreviations:

AMI	Acute myocardial infarction
CM	Cardiomyocytes
IRI	Ischemia-reperfusion injury
LAD	Left anterior descending
ROS	Reactive oxygen species
mPTP	Mitochondrial permeability transition pore
RISK	Reperfusion injury salvage kinase
PI3K	Phosphoinositide 3-kinase
Akt	Protein kinase B
WT	Wild-type
PON2-def	PON2 deficient
CM	Cardiomyocyte
IMM	Inner mitochondrial membrane
OMM	Outer mitochondrial membrane
CRC	Calcium retention capacity
GSK-3β	Glycogen synthase kinase 3β
MAMs	Mitochondria-associate ER membranes

2.1 Introduction

Acute myocardial infarction (AMI) is one of the leading causes of morbidity and mortality worldwide.[14, 52] AMI is characterized by blocked blood flow to the coronary arteries, resulting in various biochemical and metabolic alterations within the myocardium, including mitochondrial dysfunction and, if prolonged, the death of cardiomyocytes (CM). Surgical interventions, like stents, are critical in mitigating the

damage to the myocardium by reperfusing, or restoring blood flow to the heart; however, AMI induced ischemic injury primes the cells for further injury once reperfusion occurs.[14, 15]

Mitochondria are intimately involved in the pathogenesis of myocardial ischemia-reperfusion injury (IRI). A primary outcome of AMI induced ischemic injury is the switch from aerobic to anaerobic respiration, resulting in the depletion of ATP.[15] A key consequence is the inhibition of crucial ATP-dependent ion channels that result in the accumulation of sodium and calcium. In addition, oxygen, an electron acceptor in the electron transport chain, is absent during ischemia, resulting in a large build-up of electrons within the mitochondrial membranes.[16] Upon reperfusion, the restoration of oxygen results in the formation of ROS, specifically superoxides.[17] The calcium overload and ROS generation converge onto the mitochondria and trigger the opening of the mitochondrial permeability transition pore (mPTP) during reperfusion injury resulting in cell death.[16] The reperfusion injury salvage kinases (RISK) pathway, PI3K/Akt/GSK-3β, has been shown to be cardioprotective against IRI by phosphorylating glycogen synthase kinase-3β (GSK-3β), a ubiquitously expressed serine/threonine kinase, which inhibits the opening of the mPTP.[23-25] There are many therapies currently attempting to mitigate myocardial IRI by targeting mPTP opening or the RISK pathway, but have largely been unsuccessful.[14, 21] These therapies only target one aspect of a highly complex disease. Consequently, the need to find a novel therapeutic agent that has a multifaceted connection with myocardial IRI pathogenesis is critical.

PON2 is part of a gene family consisting of three members, PON1, PON2, and PON3, which are located adjacent to each other on the long arm of chromosome 7 in humans and chromosome 6 in mice.[4] PON2 polymorphisms, particularly PON2 Ser311Cys, have been associated with increased risk of coronary heart disease and ischemic stroke in various human populations.[9, 10, 12, 13, 53-56] PON2 has been shown to have various anti-oxidant and anti-inflammatory properties.[4, 5, 44-46] PON2 deficiency alters mitochondrial function by decreasing mitochondrial complex I and III activity and total ATP levels and alters mitochondrial oxidative stress by increasing mitochondrial superoxide production, increasing lipid peroxidation and decreasing reduced glutathione levels.[5, 45] Additionally, PON2 deficiency aggravated the development of atherosclerosis.[5, 47] PON2 is localized within the mitochondria, specifically associating with complex III of the IMM.[5] Furthermore, PON2 attenuates cardiolipin peroxidation, cytochrome c release and caspase activation.[49]

The role of PON2 against acute IRI has not been investigated to date. Many of the injuries resulting from IRI converge on the mitochondria, making it a fundamental organelle to study in this disease model. Since PON2 and its antioxidant activity are localized to the mitochondria, we hypothesized that PON2 plays a protective role against acute myocardial IRI by modulating mitochondrial function and oxidative stress.

2.2 Materials and Methods

2.2.1 Experimental Animals

C57BL/6J, wild-type (WT) mice and PON2 deficient (PON2-def) male mice 8-10 weeks of age were used for the *in vivo* studies. The wild type controls used for all our studies were derived from PON2 heterozygous intercrosses. All animal studies were approved by the IACUC and Animal Research Committee (ARC) at UCLA, and designed to prevent/reduce any stress/pain.

2.2.2 H9c2 Cell Culture Methods

H9c2(2-1) (ATCC CRL-1446), a rat ventricular cardiomyocyte cell-line, was utilized for the *in vitro* studies. ATCC-formulated DMEM (catalog#30-2002, ATCC) was used to culture the cells, with the addition of 10% FBS (Catalog#26140079, ThermoFisher) and 1% Penicillin-Streptomycin (catalog#15140122, ThermoFisher) for complete growth medium. H9c2 cells were transfected with pcDNA3.1+ plasmid expressing human PON2 (H9c2-hPON2) or empty vector (H9c2-EV) (Catalog#V790-20, Addgene) using Lipofectamine 2000 transfection reagent (catalog#11668027, ThermoFisher). Stable cell-lines were generated by selection of positive colonies via neomycin selection (Geneticin, catalog#10131035, ThermoFisher).

2.2.3 Ischemia-Reperfusion Injury

In vivo IRI- Left Anterior Descending (LAD) Coronary Artery Occlusion: Mice were subjected to vivo IRI as previously described.[57] In brief, mice were anesthetized with ketamine (100 mg/kg i.p.) and xylazine (10 mg/kg i.p.). After general anesthesia, the baseline ECG and ECHO were performed. Under mechanical ventilation, the chest was opened and the heart exposed. A suture was placed around the left anterior descending

coronary artery (LAD) three quarters of the distance from the base to the apex, and tightened to occlude the LAD permanently for 30 minutes, which was confirmed by ST elevation in ECG. The ligature was released to start reperfusion. The chest was then closed and the mice were allowed to recover. Twenty-four hours later, Evans Blue dye was injected through the right ventricle to assess area at risk, and mice were euthanized using approved procedures and the hearts removed. 2 mm thick sections of the ventricles were then incubated in 1% triphenyltetrazolium chloride (TTC) at 37^{o}C for 15 minutes to assess infarct size.

Ex vivo IRI- Mouse hearts were subjected to ex vivo IR via the Langendorff Apparatus as previously described.[57] In brief, mice were anesthetized with an intraperitoneal injection of pentobarbital sodium (50 mg/kg). Heparin (200 IU/kg) was also administered to prevent blood coagulation. Once anesthetized, the heart was quickly (within 60 seconds) removed, mounted, and perfused through the ascending aorta in a Langendorff apparatus with Krebs Henseleit bicarbonate buffer (KH Buffer) (mM): glucose 11.1, NaCl 118, KCl 4.7, $MgSO_4$ 1.2, KH_2PO_4 1.2, $NaHCO_3$ 25.0, $CaCl_2$ 2 at pH 7.4 bubbled with 95% O_2/5% CO_2 at 37 °C. Following a 10 minute stabilization period, a global normothermic (37^{o}C) ischemic episode was induced by stopping perfusate for 20 minutes followed by a 5-minute reperfusion of the heart with KH. CM were immediately isolated post-reperfusion (refer to Cardiomyocyte Isolation).

In vitro IRI- Hypoxia-Reoxygenation via Hypoxia Chamber: To induce hypoxia in cells, cell media was changed from normal, growth media (refer to H9c2 Cell Culture Methods) to a low nutrient DMEM (Life Technologies, Catalog# 11966-025) without growth factors and were placed into a hypoxic plastic chamber under hypoxic gas

conditions (≤2% O_2, 5% CO_2, nitrogen balanced) at 37ºC for 3 hours. Hypoxia was confirmed by HIF-1α upregulation (data not shown). The cells were then reoxygenated by replacing the media back to regular growth media and placing the cells back to normoxic gas conditions (~20-21% O_2 and 5% CO_2) at 37ºC for 2 hours. The cells were then used for all downstream assays.

2.2.4 Mitochondrial Isolation and Protein Quantification

Mitochondria were isolated from whole hearts of PON2-def and WT, C57Bl/6J, mice, as previously described.[24, 57, 58] In brief, the heart were finely minced with scissors and homogenized in buffer A (containing in mM: 70 sucrose, 210 mannitol, 1 EDTA, 50 Tris-HCl, pH 7.4 at 4ºC) and centrifuged at 1,300 g for 3 minutes. The supernatant was filtered through cheesecloth and centrifuged at 10,000g for 10 minutes; the pellet was then resuspended in in buffer C (containing in mM: 150 sucrose, 50 KCl, 2 KH_2PO_4, 5 succinic acid, and 20 Tris-HCl, pH7.4 at 4ºC); protein concentration was measured by Bradford Assay.

2.2.5 Cardiomyocyte Isolation

CM were isolated as previously described.[59, 60] In brief, mice were anesthetized with an intraperitoneal injection of pentobarbital sodium (50 mg/kg). Heparin (200 IU/kg) was also administered to prevent blood coagulation. The heart was quickly (within 60 seconds) removed and mounted on a modified Langendorff apparatus and secured by the ascending aorta. The heart was then perfused with Tyrode's solution [130 mM NaCl, 5.4 mM KCL, 0.6 mM NaH_2PO_4*H20, 1 mM $MgCl_2$*$6H_20$, 10 mM HEPES, 10 mM Glucose, 5 mM Taurine; oxygenated with 95% O_2, 5% CO_2; at pH 7.4] at 37ºC for 5 minutes. The heart is then perfused for 5-6 minutes at 37ºC with Tyrode's solution

containing 0.5 U/mL Protease Type-XIV (Sigma, catalog# P5147) and 140.5 U/mL Collagenase Type-2 (Worthington Biochemicals, catalog# LS004176). Lastly, the heart was perfused for 5 minutes at 37^{o}C with KB solution [25 mM KCL, 10 mM KH2PO4, 2 mMMgSO4*7H20, 5 mM HEPES, 20 mM Glucose, 20 mM Taurine, 5 mM Creatine, 100 mM K-Glutamate, 10 mM Aspartic Acid, 5 mM EGTA, and 0.10% BSA (fatty acid free); oxygenated with 95% O_2, 5% CO_2; at pH 7.4]. The atria were removed and the ventricles were minced in KB solution to dissociate the cells. The CM were then filtered through a 100 µm strainer and centrifuged for 5 minutes at 1000xg. The CM were then ready for downstream use.

2.2.6 Calcium Retention Capacity

The calcium retention capacity (CRC) assay was performed to determine the threshold for mPTP opening in response to calcium overload.[25, 57, 58] In brief, 0.5 µM calcium green-5N was used to determine free calcium concentration outside the mitochondria using excitation and emission wavelengths set at 500 and 530 nm, respectively.

In vivo IRI: 500µg protein of isolated mitochondria from the whole heart of the mice was resuspended in 2mL buffer C (containing in mM: 150 sucrose, 50 KCl, 2 KH_2PO_4, 5 succinic acid, and 20 Tris-HCl, pH7.4 at 4^{o}C); $CaCl_2$ pulses (20 nmoles) were added every minute until a sustained calcium increase is established, indicating mPTP opening. The results were measured as nmoles of calcium per milligram of mitochondrial protein.

Ex vivo IRI and *in vitro* HRI: CM and H9c2 cells are resuspended in 2mL buffer C and permeabilized with an optimized concentration of 25 µM and 3 µM digitonin,

respectively. $CaCl_2$ pulses (16 nmoles) were added every minute until a sustained calcium increase is established, indicating mPTP opening. The results were measured as nmoles of calcium per $5.0x10^4$ cells (CM) and $1.5x10^6$ cells (H9c2 cells).

2.2.7 Reactive Oxygen Species (ROS) Production

Mitochondrial ROS production was assessed.

In vivo IRI: In brief, mitochondria (100µg) were resuspended in 50µL reaction buffer (containing in mM: 125 KCl, 10 HEPES, 5 $MgCl_2$, 2 K_2HPO_4, pH 7.4 at 4°C) to determine complex I or complex II driven H_2O_2 production; mitochondrial H_2O_2 production was assessed by using horseradish peroxidase (2 units/mL) H_2O_2-dependent oxidation of nonfluorescent Amplex Ultra Red (50µM) to fluorescent resorufin red, at an excitation wavelength of 545 nm and an emission wavelength of 590 nm for 20 minutes.[61] The results were measured as nmoles of H_2O_2 divided by minutes per microgram of mitochondrial protein, but expressed as fold change.

Ex vivo IRI and *in vitro* HRI: MitoSox Red mitochondrial superoxide indicator (Molecular Probes, catalog# M36008) was utilized and the assay was run based on manufacturer recommendations. In brief, an optimized 5 µM concentration of MitoSox Red was determined to be the most effective concentration. In brief, CM and H9c2 cells were plated and subjected to IRI or HRI, respectively. The cells were washed with PBS. Then, the cells were incubated with unsupplemented media containing a concentration of 5 µM MitoSox Red for 45 minutes. Afterward, the cells were washed 3 times with PBS. The cells were then pelleted (5 minute spin at 1000xg) and resuspended with 300 µL of PBS in placed plastic culture tubes (Fisher, catalog# 14-961-10A). Mitochondrial

superoxide levels were then determined in the live cells via flow cytometry using an absorption/emission maxima of ~510/580 nm. The data is expressed as fold change.

2.2.8 Quantitative RT-PCR Analysis

Total RNA was isolated from whole hearts of PON2-def and WT mice post *in vivo* IRI by RNeasy mini kit (Qiagen, USA). 1 microgram of RNA was used to generate cDNA via reverse transcription with a High-Capacity cDNA Reverse Transcription kit (Applied Biosystems, Life Technologies, ThermoFisher, USA). The qPCR reaction mixture consisted of 2 microliters of cDNA, gene specific primers and iQ SYBR Green Supermix (Bio-Rad, Hercules, CA, USA) and was run in a MyiQ Single-Color Real-Time PCR Detection System (Bio-Rad, Hercules, CA, USA). mRNA gene expression levels were quantified and normalized to mouse GAPDH levels. The primer pairs are as follows: mouse PON2 (forward) 5'-GAGTCAGCTGGGGCTTTGACTTGGC-3' and (reverse) 5'-ATTGGTGGCGTAGAAGTGGGTGGGC-3', mouse GAPDH (forward) 5'TTGTCATGGATGGACCTTGGCCAGG-3' and (reverse) 5'-TGCCATTTGCAGTGGCAAAGTGG-3'.

2.2.9 Immunoblotting

50 micrograms of protein from whole heart lysates (PON2-def and WT) or H9c2 cells were loaded on 4-20% Mini-PROTEAN TGX Stain-Free protein gels (Bio-Rad, Hercules, CA, USA) and transferred to nitrocellulose membranes. The membranes were blocked for 1 hour at room temperature in Tris-buffered Saline with 0.1% Tween 20 (TBST) containing 5% (w/v) BSA. The following primary antibodies were used at the specified dilutions: human PON2 (R&D Systems, Biotechne brand, USA) at 1:1000, GSK-3β (27C10) (Cell Signaling Technology, USA) at 1:1000, pGSK-3β (ser9) (Cell

Signaling Technology, USA) at 1:1000, CHOP (Cell Signaling Technology, USA) at 1:750, GAPDH (ab9485) (Abcam, USA) at 1:10,000. Primary antibodies were diluted in TBST containing 5% BSA at 4oC overnight, followed by incubation with appropriate secondary antibody (1:5000 dilution) coupled to HRP for 1 hour. Protein was detected using Immobilon Western Chemiluminescent HRP Substrate (Millipore Sigma, USA).

2.2.10 Cell Apoptosis Assessment

Cell apoptosis was determined in CM ($6x10^4$ cells) isolated from WT and PON2-def mice hearts by evaluating caspase-3/7 activity using the CellEvent Caspase-3/7 Green Detection Reagent (catalog#C10423, ThermoFisher) via live cell fluorescence-imaging as described by manufacturer's protocol.

2.2.11 ATP Quantification

ATP levels were quantified as previously described.[5] In brief, ATP levels from CM ($6x10^4$ cells) isolated from WT and PON2-def mice hearts were evaluated as described by the manufacturer's protocol (Bioassay System).

2.2.12 Statistical Analysis

Student's t-tests were carried out between all studies with two groups. Data from experiments with more than 2 or more groups were compared using a one-way ANOVA model. After a significant overall group effect was established, Tukey's pairwise comparisons were carried out to determine specific group to group differences. Experiments were repeated 2-3 times to ensure that the results were consistent and reproducible. All data is represented as mean±SEM. A p-value less than 0.05 was considered statistically significant.

2.3 Results

2.3.1 PON2 expression is associated with reduced infarct size following myocardial IRI

We confirmed PON2 protein expression in both neonatal and adult WT mice (Figure 1A). When WT mice were subjected to *in vivo* IRI (Figure 1B), PON2 gene expression levels were approximately 2-fold higher in hearts from the IRI mice when compared to the sham group (n=5/group) (Figure 1C). IRI-induced PON2 gene expression further supported our hypothesis that PON2 may play a role in modulating IRI. To further explore the role of PON2 in myocardial IRI, we used a PON2 deficient (PON2-def) mouse line previously generated in our lab.[5, 44, 47] Echocardiograms were performed on both WT and PON2-def mice under baseline (untreated) conditions to assess heart function and structure, and no significant differences were found (Supplemental Figure 1 and 2). Following *in vivo* IR, we observed that PON2-def mice had roughly 2-fold larger infarct size compared to controls (n=8/group, Figure 1D), quantified as the percentage of the infarct size over the area at risk (IS/AAR) and infarct size over left ventricle area (IS/LV) (Figure 1E).

2.3.2 PON2 deficiency leads to cardiac mitochondrial dysfunction and decreased pGSK-3β levels following myocardial IRI

To determine the role of PON2 in modulating mitochondrial dysfunction and oxidative stress against myocardial IRI, we isolated cardiac mitochondria from PON2-def mice and WT controls subjected to *in vivo* IRI and measured the threshold for mPTP opening in response to exogenous calcium overload using the calcium retention capacity (CRC) assay. Mitochondria from the PON2-def mice had significantly lower CRC than WT mice in both baseline (untreated) [274.3±15.39 in WT, 214.9±13.46 in

PON2-def, nmoles Ca^{2+}/mg mitochondrial protein; n=7/group; $p<0.05$] and IR conditions [250±41 in WT, 173±19 in PON2-def, nmoles Ca^{2+}/mg mitochondrial protein; n=6/group; $p<0.05$] (Figure 2A and 2B). Additionally, mitochondrial ROS production was approximately 2-fold greater ($p<0.05$) in the PON2-def mice (n=4) versus WT controls (n=5) following IRI (Figure 2C and 2D), and PON2-def hearts had significantly higher protein expression ($p<0.05$) of endoplasmic reticulum (ER) stress marker, CHOP, versus WT mice (Figure 2E and 2F), suggesting a potential role that PON2 can be playing in modulating ER stress and calcium release in response to IRI. PON2-def hearts also had significantly lower levels of phosphorylated, cardioprotective GSK-3β, the downstream effector in the RISK pathway, compared to WT controls ($p<0.05$), Figure 2H). Taken together, the mitochondria from PON2-def mice exposed to IRI are more dysfunctional, having a reduced calcium retention capacity, increased ROS production, increased ER stress, and decreased pGSK-3β levels when compared to WT controls.

2.3.3 Cardiomyocytes deficient in PON2 exhibit increased mitochondrial dysfunction, oxidative stress, and apoptosis following IRI

While the above studies identified the protective effect of PON2 against IRI in whole heart tissue, we sought to investigate the role of PON2 specifically within CM. Hearts from PON2-def and WT mice were subjected to *ex vivo* IRI via the Langendorff apparatus, with a 20-minute ischemic episode, followed by a 5-minute reperfusion (Figure 3A). CM were isolated from the ventricles of IRI hearts and evaluated for ATP levels, CRC, ROS production and cell apoptosis. CM from PON2-def IRI hearts exhibited a significant decrease in ATP levels versus WT CM controls ($p<0.05$), with no

change in baseline conditions (Figure 3B). CM from PON2-def, non-IR injured hearts showed a baseline decrease in CRC versus WT control CM [267 in WT CM, 123 in PON2-def CM nmoles of Ca^{2+} per $5.0x10^4$ cells; n=3/group; $p<0.05$] (Figure 3C). This data supports an inherent mitochondrial defect in PON2-def mice when handling extramitochondrial calcium (Figure 2B). Furthermore, CM isolated from PON2-def IR injured hearts have further reduction in CRC when compared to CMs from WT IRI hearts [176 in WT CM (IRI), 80 in PON-2-def CM (IRI), nmoles of Ca^{2+} per $5.0x10^4$ cells; n=3/group; $p<0.01$] (Figure 3D). In addition, ROS production, particularly mitochondrial superoxide levels, was significantly increased ($p<0.01$) in CM from PON2-def hearts subjected to IRI versus CM controls, with no change in the baseline conditions (Figure 3E). Lastly, we observed a significant increase in cell apoptosis in the CM from PON2-def hearts subjected to IRI compared to WT controls as assessed by caspase-3/7 activity ($p<0.01$), with no significant baseline differences between the groups (Figure 3F).

2.3.4 Overexpression of human PON2 in H9c2 cells results in increased pGSK-3β following hypoxia-reoxygenation injury

To investigate the molecular mechanism and a potential therapeutic role for PON2 protection against IRI, we stably overexpressed human PON2 in the rat ventricular cardiomyocyte cell-line, H9c2, and subjected them to hypoxia-reoxygenation injury (HRI) (Figure 4A/B). We found a significant decrease in CHOP protein levels in the PON2 overexpression cells (H9c2-hPON2) versus the empty vector controls (H9c2-EV) as determined by western blot (Figure 4C/D). In addition, we found a significant increase in the pGSK-3β/GSK-3β ratio in the H9c2-hPON2 cells versus H9c2-EV

controls (Figure 4F). No differences in pGSK-3β/GSK-3β levels were observed under baseline (untreated) conditions (Supplemental Figure 3).

2.3.5 Overexpression of PON2 rescues IRI via activation of the PI3K/Akt/GSK-3β Pathway

To further elucidate the cardioprotective role that PON2 overexpression could play during IRI and the potential contribution of the RISK pathway, we subjected H9c2-hPON2 cells and H9c2-EV controls to HRI with and without LY294002, a potent PI3K inhibitor, and assessed mitochondrial CRC, ROS production (superoxide levels), and cell apoptosis. H9c2-hPON2 cells subjected to HRI exhibited increased CRC compared to H9c2-EV cells [141.7±16.67 in H9c2-EV, 200±14.43 in H9c2-hPON2, nmoles of Ca^{2+} per $1.5x10^6$ cells, $p<0.05$] (Figure 5B), indicating that PON2 overexpression increases the threshold for the opening of the mPTP in response to calcium overload. In addition, H9c2-hPON2 cells demonstrated a 40% reduction ($p<0.01$) in ROS generation versus the H9c2-EV control cells post HRI (Figure 5D). Following HRI, H9c2-hPON2 cells were markedly resistant to apoptosis when compared to H9c2-EV controls [5% TUNEL Positive cells in H9c2-hPON2 cells versus 34% in H9c2-EV cells, $p<0.0001$] (Figure 5F); however, the protective effects of PON2 overexpression was abolished by inhibition of PI3K. CRC was significantly reduced in the H9c2-hPON2 cells when compared to H9c2-EV control [105±5 in H9c2-EV+PI3Ki, 60±10 in H9c2-hPON2+PI3Ki, nmoles of Ca^{2+} per $1.5x10^6$ cells, $p<0.05$] (Figure 5B). PI3K inhibitor treated H9c2-hPON2 cells also displayed reduced CRC compared to non-PI3k inhibitor treated H9c2-hPON2 cells [200±14.43 in H9c2-hPON2 w/o, 60±10 in H9c2-hPON2+PI3Ki, nmoles of Ca^{2+} per $1.5x10^6$ cells, $p<0.0001$]. Following PI3K inhibition, H9c2-hPON2 cells exposed to HRI

had 50% more mitochondrial ROS production when compared to H9c2-EV controls with inhibitor ($p<0.01$) and approximately 100% increase when compared to the H9c2-PON2 cells without inhibitor (Figure 5D). Lastly, H9c2-PON2 cells treated with PI3K inhibitor had a highly significant increase in apoptosis when compared to the H9c2-hPON2 cells alone [80% TUNEL positive H9c2-hPON2+PI3Ki versus 5% in H9c2-hPON2, $p<0.0001$] (Figure 5F). No differences in cell apoptosis were observed at baseline (untreated) conditions (Supplemental Figure 4).

2.4 Discussion

Myocardial IRI is a highly complex disease characterized by both an ischemic injury, resulting from the occlusion of the coronary arteries, and a paradoxical reperfusion injury following the return of blood flow to the myocardium. During reperfusion, calcium overload and ROS production trigger mitochondrial membrane depolarization, uncoupling of oxidative phosphorylation, and release of cytochrome c to the cytosol initiating caspase induced apoptosis and the death of CM.[15, 16, 18] Therefore, mitochondrial dysfunction and oxidative stress are fundamental components of myocardial IRI pathogenesis.

PON2 plays a protective role in many disease models including atherosclerosis, neurodegenerative disorders, ovarian cancer, and cardiovascular disease. PON2's ability to modulate mitochondrial dysfunction and oxidative stress serves as an underlying mechanism for protection against these diseases.[4, 7, 62, 63] While the role of PON2 in IRI has not been previously investigated, we found that PON2 is upregulated in WT mouse hearts following in vivo IRI. As PON mitigates mitochondrial dysfunction, ER stress and maintains calcium homeostasis, upregulation of PON2 may help the myocardium protect against IRI. As such, we investigated the role of PON2 in conferring protection against acute IRI and its potential as a therapeutic target.

Our study demonstrates that PON2 expression is inversely related to IRI severity as PON2-def mice subjected to IRI exhibited a significant increase in infarct size when compared to WT controls (Figure 1D-E). Since mitochondrial dysfunction and oxidative stress are hallmark consequences of myocardial IRI, we tested the mitochondrial integrity of PON2-def mice following IRI.[4-5] Our findings reveal that PON2-def mice have

an inherent mitochondrial defect that, when in the presence of an exogenous stressor (i.e. extramitochondrial calcium), manifests into basal mitochondrial dysfunction (Figure 2B). Furthermore, mitochondria isolated from PON2-def mice subjected to IRI had a significant reduction in CRC (Figure 2A/B) and oxidative stress (Figure 2C/D), when compared to WT controls. We further examined and validated these results specifically within mitochondria from the CM subpopulation (Figure 3). These observations demonstrate a clear role for PON2 in protection against myocardial IRI as lack of PON2 results in increased IRI, in the form of mitochondrial dysfunction and oxidative stress.

In addition, we determined that the cardioprotective capacity of PON2 is intimately connected to the RISK pathway (PI3K/Akt/GSK-3β), a fundamental cardioprotective pathway involved in mitigating myocardial IRI.[7-9] We previously demonstrated a connection between PON2 deficiency and impaired PI3K/Akt activation when treated with 3OC(12)-HSL, a quorum-sensing molecule.[64] Therefore, we sought to further explore the role of PON2 in modulating myocardial IRI via the RISK pathway. We observed that PON2 deficiency resulted in a significant decrease in cardioprotective pGSK-3β levels in the heart of PON2-def mice subjected to myocardial IRI (Figure 2G-H). Conversely, overexpression of PON2 sufficiently increases pGSK-3β levels and rescues mitochondrial dysfunction and oxidative stress in H9c2 cells, a model cardiomyocyte cell-line, when subjected to HRI (Figure 4-5). This protection conferred by PON2 overexpression is abolished in the presence of LY294992, a potent PI3K inhibitor (Figure 5).

Many studies demonstrate that mitochondrial phospholipids, particularly outer and inner mitochondrial membrane phospholipids like cardiolipin, play a vital role in

maintaining mitochondrial homeostasis by aiding in protein biogenesis and maintaining normal bioenergetics, membrane function and apoptosis.[26, 35] These mitochondrial membrane phospholipids are susceptible to oxidative damage during IRI, which leads to lipid peroxidation, loss of IMM organization and a decrease in cardiolipin content and peroxidation, which in turn leads to poor electron flow, further generation of ROS, and impairment of respiratory complexes and membrane potential.[27, 28, 35-38] As noted earlier, PON2 is localized within the IMM and has a capacity to attenuate cardiolipin peroxidation, cytochrome c release, and caspase activation.[5, 49] PI3K, which exerts its effects through the membrane lipid phosphatidylinositol, is associated with a plethora of cell signaling, membrane trafficking and metabolic processes.[65] In particular, PI3K/Akt signaling has been implicated in cell survival, particularly through intervention in mitochondrial apoptosis via inhibition of cytochrome c release and caspase activation.[66-68] The intimate connection and shared function between PON2 and PI3K/Akt may explain the molecular mechanism of PON2 cardioprotection by modulating mitochondrial membrane homeostasis and apoptosis, although further studies are needed to confirm our hypothesis.

Additionally, X-ray crystallography studies performed on PON1, a paralogue of PON2 that shares 65% amino acid homology, revealed a fatty acid tail binding substrate pocket.[69] We previously demonstrated that PON2 binds Coenzyme Q_{10}, which has a fatty acid tail and is synthesized in the IMM.[5] Moreover, mitochondrial membrane phospholipids, like cardiolipin, contain fatty acid tails that may bind this substrate pocket, and preliminary experiments from our lab demonstrate direct binding of cardiolipin and PON2.[70] A future direction of study includes investigating the effect of

PON2 in modulating mitochondrial membrane phospholipid composition during myocardial IRI.

The role of calcium in modulating IRI is fundamental to the pathogenesis of the disease. As such, there are many pathways involved in maintaining calcium homeostasis in the myocardium including the GSK-3β pathway.[71] A recent study by Gomez et al demonstrated a connection between GSK-3β and ER-mitochondria calcium regulation during IRI, specifically that GSK-3β localizes at the ER and mitochondria-associated ER membranes (MAMs) and, at the MAMs interface, it regulates IP_3R calcium transfer between the ER and mitochondria.[22] mPTP is a nonselective channel of the IMM, and its opening results in mitochondrial membrane depolarization, uncoupling of oxidative phosphorylation, release of cytochrome c to the cytosol and activation of the caspase cascade leading to cardiomyocyte death.[15, 16, 18] In addition, a key organelle responsible for calcium homeostasis is the ER.[72] Not only does our data show the connection between PON2 and GSK-3β in myocardial IRI, but we also demonstrate that PON2-deficiency leads to an increase in CHOP (Figure 2E-F), an ER stress marker responsible for IP_3R-calcium release from the ER and initiating cell apoptosis, among other deleterious consequences. Conversely, overexpression of PON2 in H9c2 cells subjected to HRI results in a significant reduction in CHOP expression (Figure 4C-D). Our lab previously demonstrated the that PON2 deficiency in macrophages results in increased expression of CHOP and dysregulation of calcium homeostasis under ER stress conditions.[46, 47] Consequently, the role that PON2 could play in regulating calcium homeostasis at the MAMs interface via GSK-3β modulation warrants further investigation.

Our study is the first to identify the robust protective role of PON2 in acute IRI. PON2 deficiency in CM leads to increased mitochondrial dysfunction and oxidative stress, which is rescued by PON2 overexpression, reflecting its potential therapeutic potential. Furthermore, attenuation of this rescue by PI3K inhibition highly suggests a casual role that the RISK pathway (PI3K/Akt/GSK-3β) plays as a potential molecular mechanism of PON2 cardioprotection against IRI.

2.5 Conclusion

- PON2 deficient mice have a 2 fold larger infarct size following myocardial IRI.
- PON2 deficiency in cardiomyocytes leads to an increase in mitochondrial dysfunction (reduced calcium retention capacity) and oxidative stress (increased ROS).
- Cardiac IRI leads to a decrease in cardioprotective phosphorylated GSK-3β (pGSK-3β) levels in PON2 deficient mice and an increase in CHOP, an ER stress marker.
- PON2 overexpression rescues mitochondrial dysfunction and oxidative stress during IRI, but inhibition of PI3K ablates PON2's cardioprotective properties.
- The RISK (PI3K/Akt/GSK-3β) pathway acts a potential molecular mechanism for PON2 cardioprotection.

Figure 1A

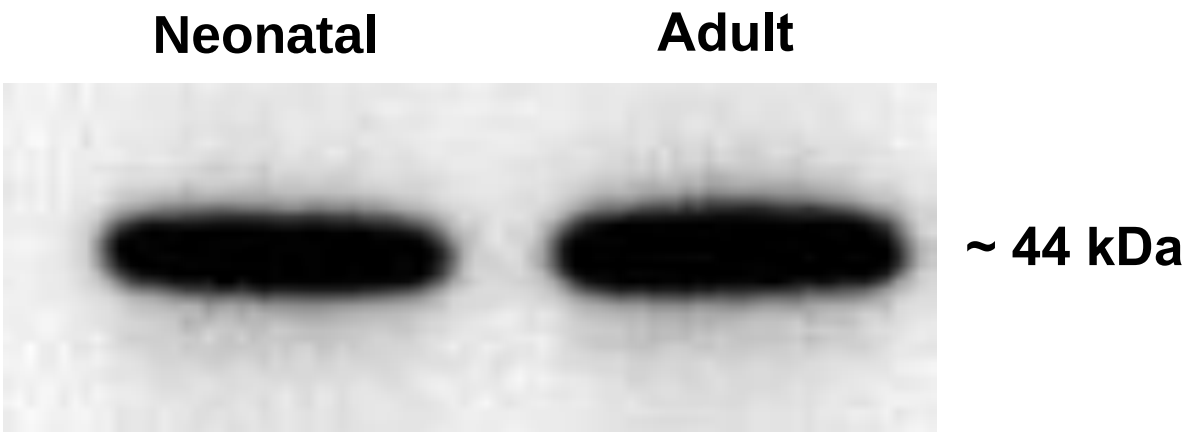

Figure 1B

Figure 1C

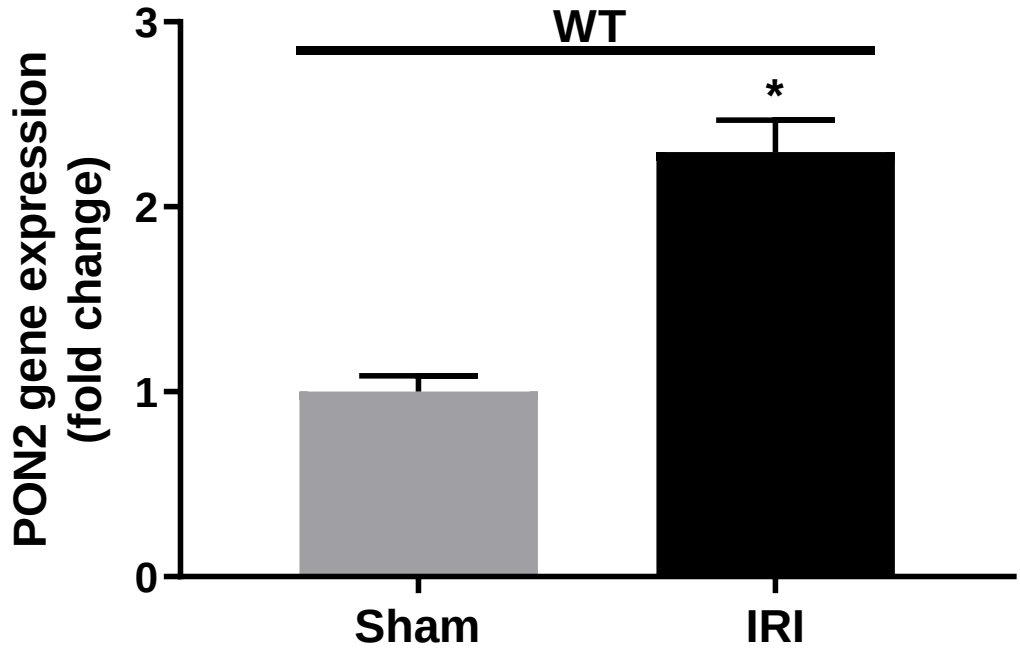

Figure 1D

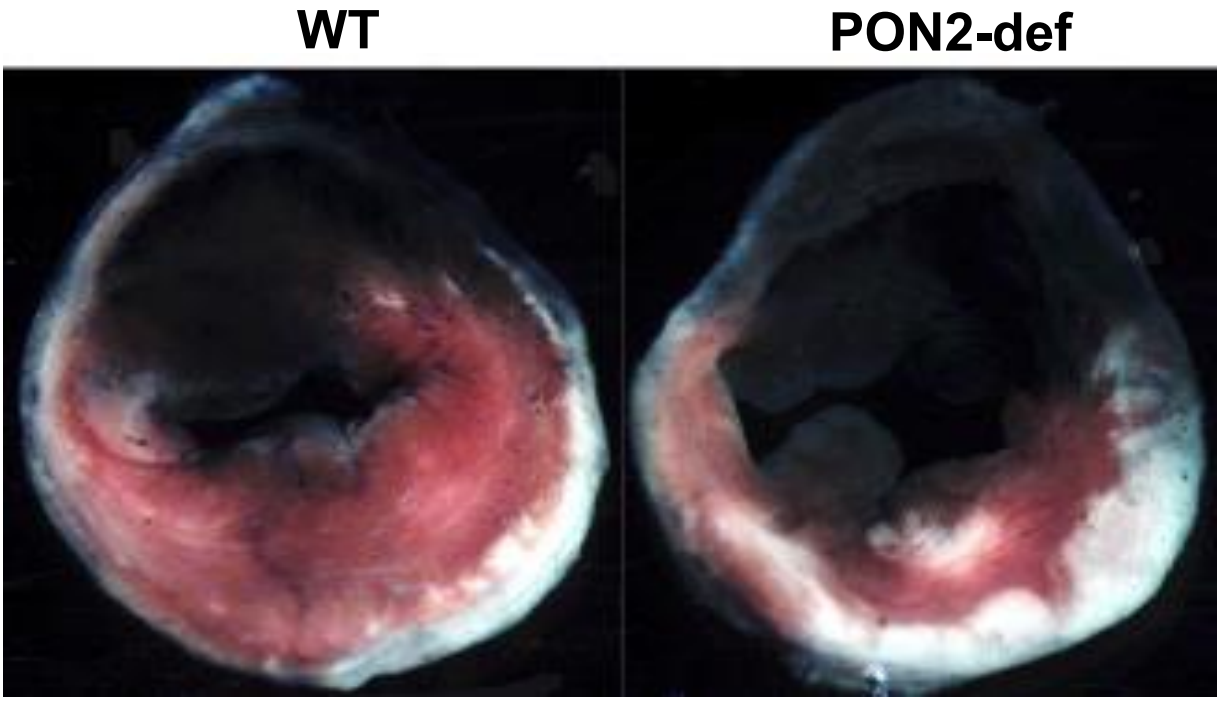

Figure 1E

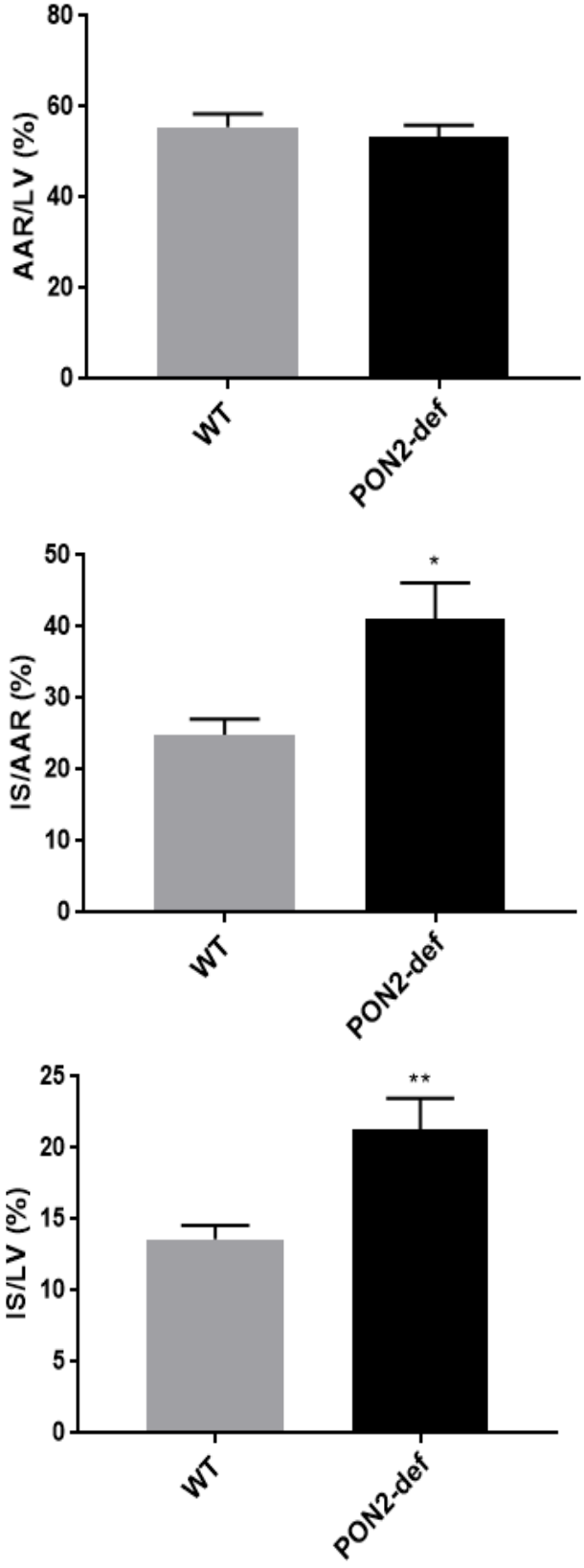
AAR/LV (%)
80
60
40
20
0
WT
PON2-def
IS/AAR (%)
50
40
30
20
10
0
*
WT
PON2-def
IS/LV (%)
25
20
15
10
5
0
**
WT
PON2-def

Figure 1: PON2 expression is associated with reduced infarct size following myocardial IRI. (A) PON2 protein is expressed in both neonatal and adult mouse hearts. (B) In vivo myocardial ischemia-reperfusion injury (IRI) was induced in PON2-deficent mice (PON2-def) and C57Bl/6, wildtype (WT) controls via left anterior descending (LAD) coronary artery occlusion for 30 minutes followed by 24 hours of reperfusion. After 24 hours, Evans Blue Dye was injected to assess AAR. (C) WT mice were subjected to in vivo IRI (n=5) or sham surgery (n=5) and PON2 gene expression levels (as fold change) were then determined in the hearts via real-time PCR. *p<0.05. (D) Representative Evans Blue Dye-stained heart sections from WT and PON2-def mice subjected to in vivo IRI. The white area reflects infarcted area, blue area reflects non-infarcted area, and red and white areas reflect risk area. (E) Quantification of hearts from WT and PON2-def mice (n=8/group) subjected to in vivo IRI assessed by percentage of IS/AAR and IS/LV. Data is represented as mean±SEM; *p<0.05. *p<0.05, **p<0.01. AAR=area at risk; LV=left ventricle; IS=infarct size.

Figure 2A

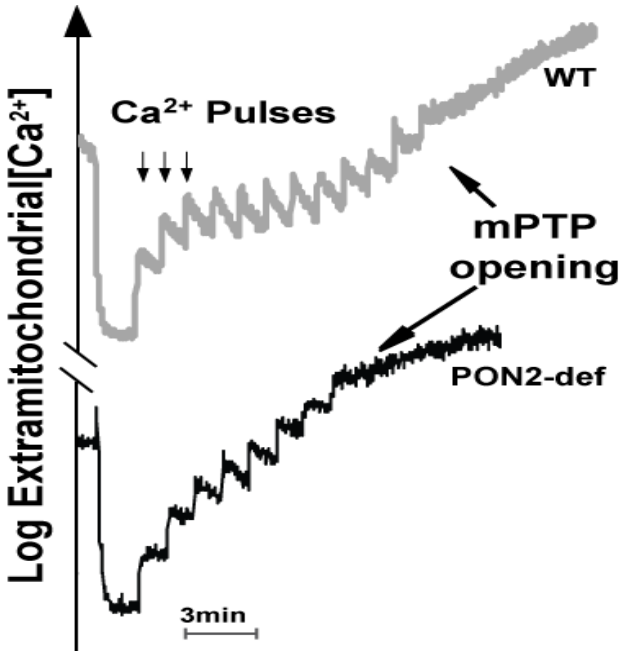

Figure 2B

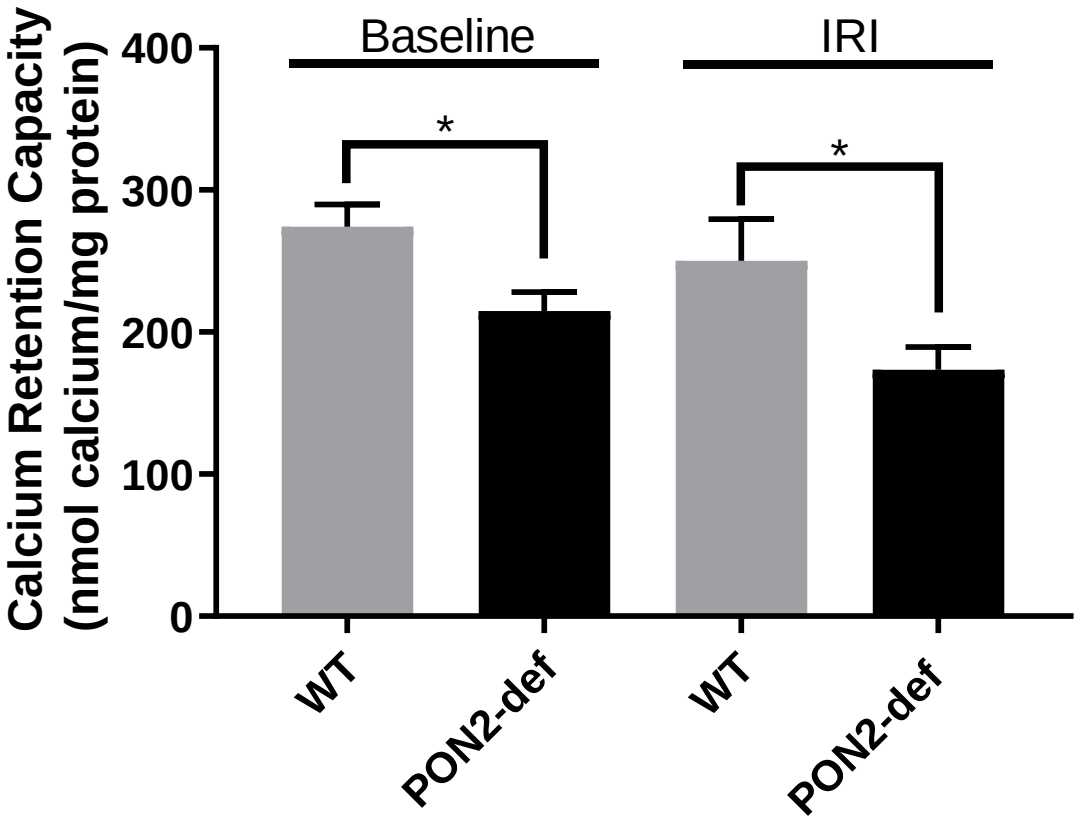

Figure 2C

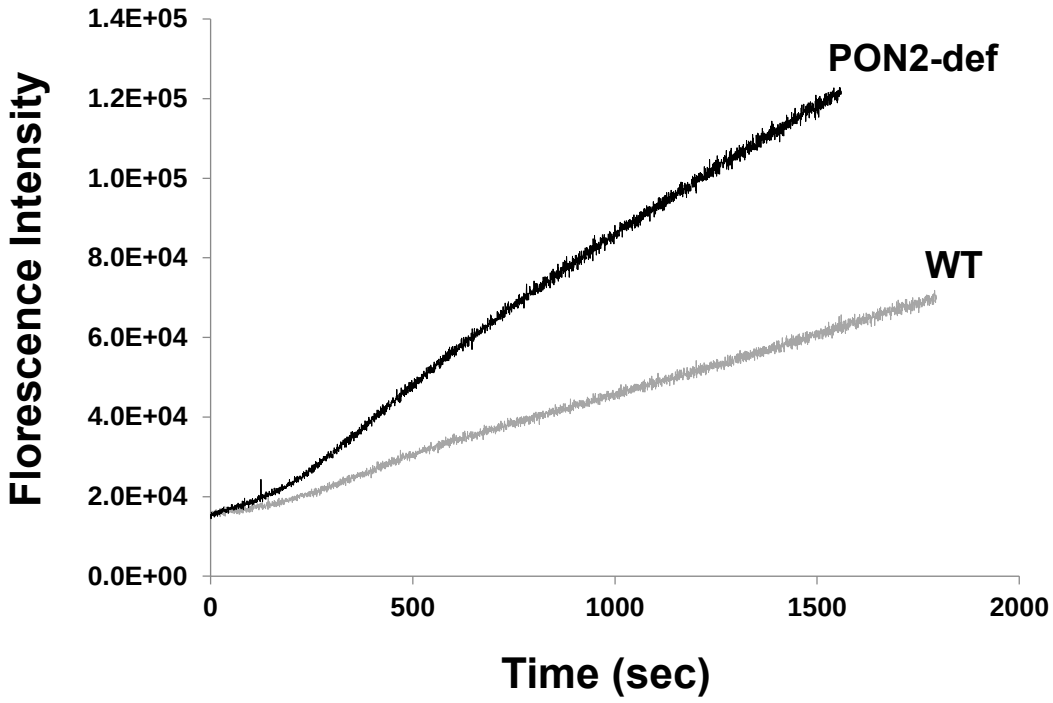

Figure 2D

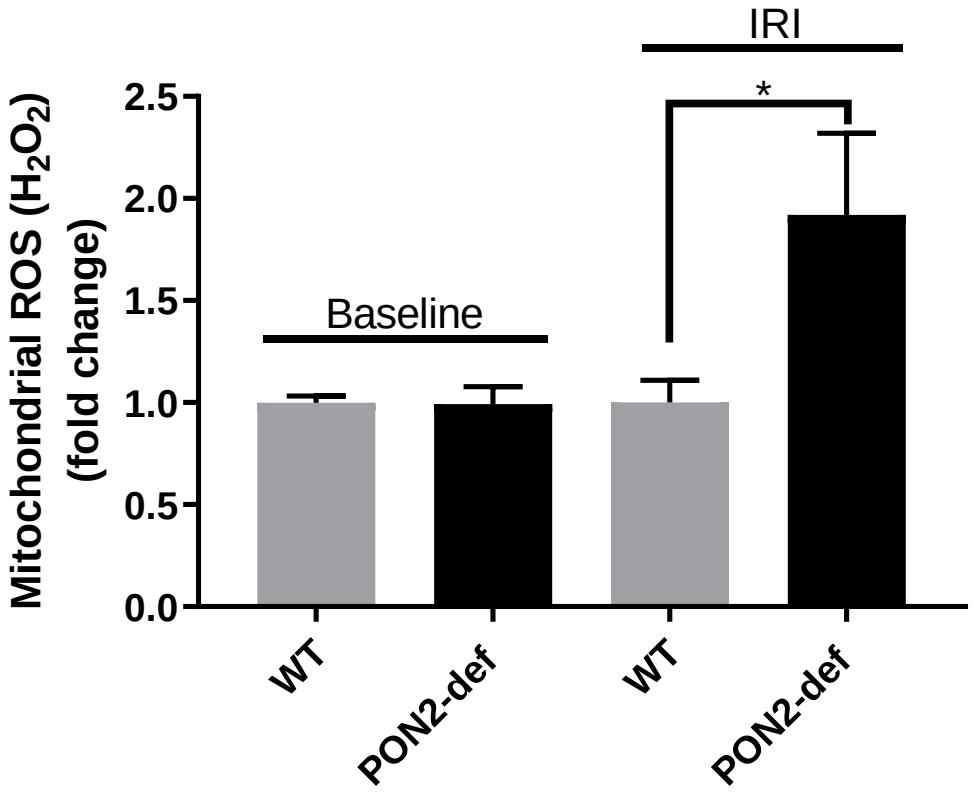

Figure 2E

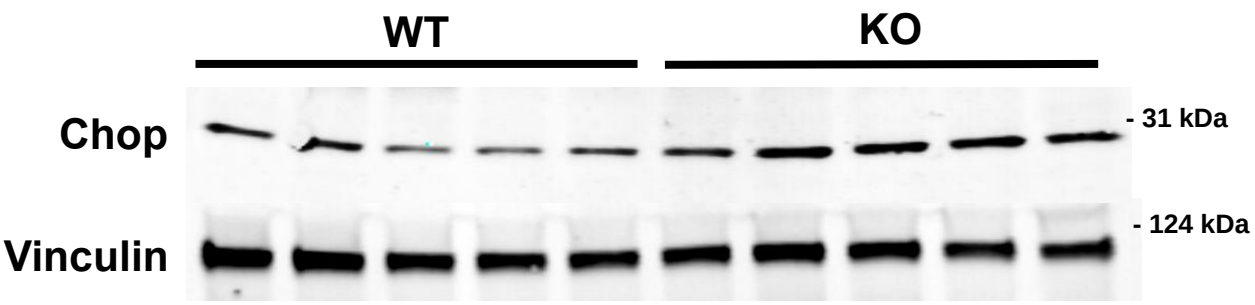

Figure 2F

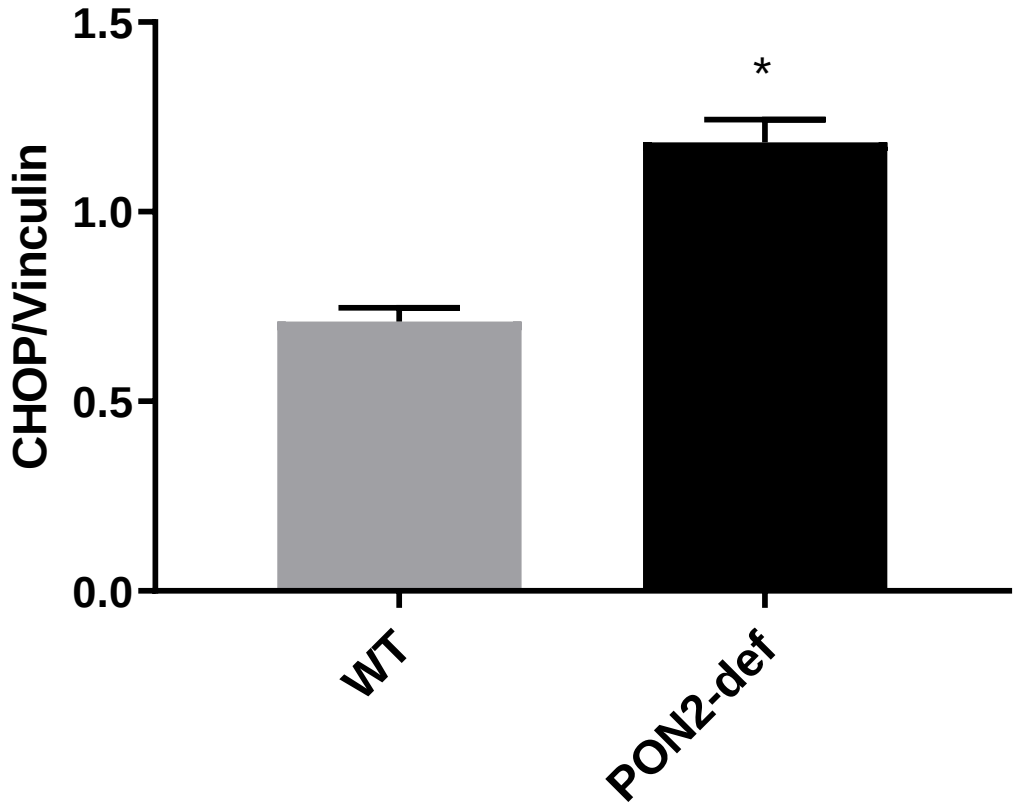

Figure 2G

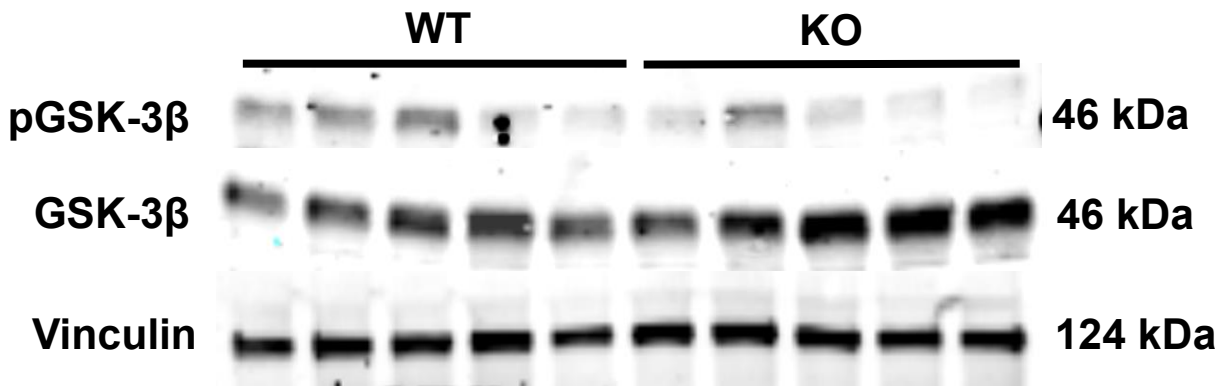

Figure 2H

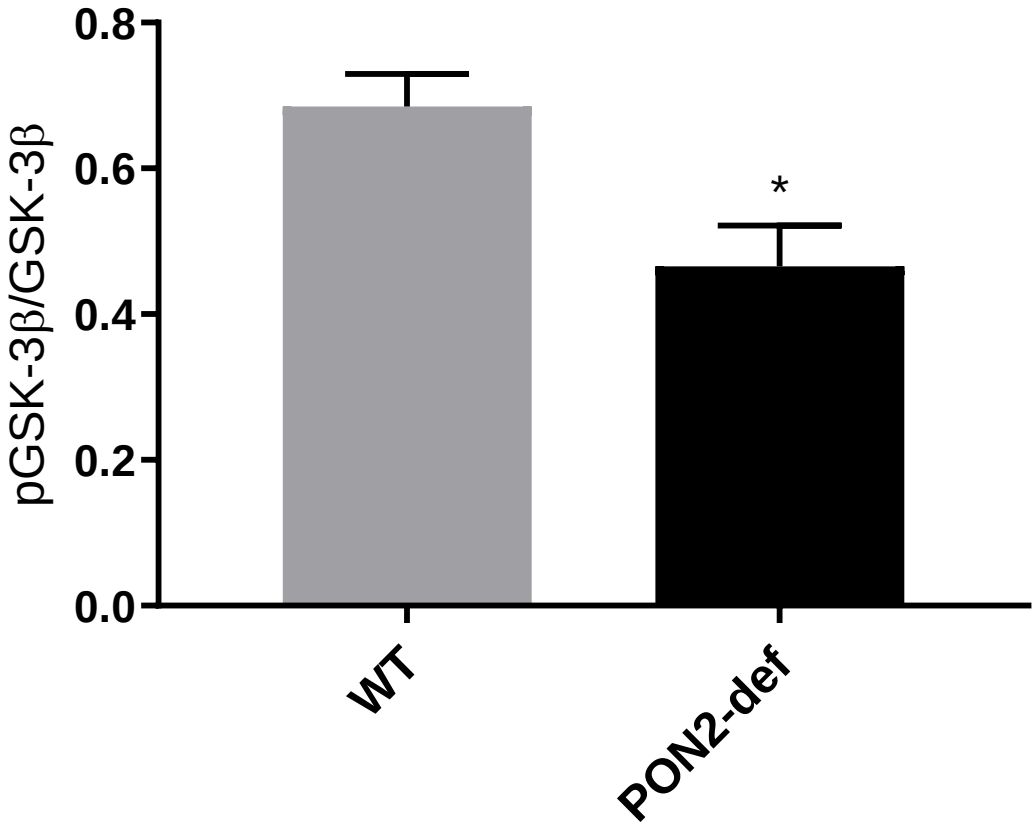

Figure 2: PON2 deficiency leads to global cardiac mitochondrial dysfunction and decreased pGSK-3β levels following myocardial IRI. (A-F) WT and PON2-def mice were subjected to *in vivo* IRI (as shown in Figure 1B). (A) Representative recordings of the calcium retention capacity (CRC) assay from WT and PON2-def mice (n=6/group), which indicates the threshold of isolated myocardial mitochondria to extramitochondrial calcium on mitochondrial permeability transition pore (mPTP) opening post *in vivo* IRI. CRC was evaluated and quantified as nmoles of calcium per mg of mitochondrial protein under baseline (untreated) conditions and under *in vivo* IRI (B). (C) A representative recording of ROS generation, specifically H_20_2, from isolated myocardial mitochondria from WT (n=5) versus PON2-def mice (n=4) post *in vivo* IRI. ROS generation was quantified as nmole of H_20_2 per min per mg of mitochondrial protein and represented as fold change under baseline (untreated) conditions and under *in vivo* IRI (D). GSK-3β and pGSK-3β expression was evaluated, as represented in (G), normalized to Vinculin, and quantified as a ratio of pGSK-3β to GSK-3β (H). CHOP expression was evaluated, as represented in (E), normalized to Vinculin, and quantified as a ratio of CHOP to Vinculin (F). Data is represented as mean±SEM; *$p<0.05$.

Figure 3A

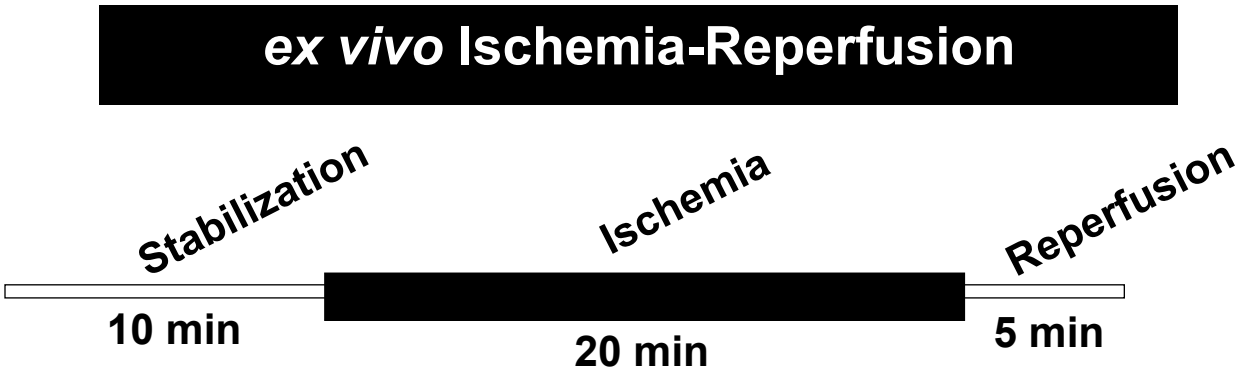

Figure 3B

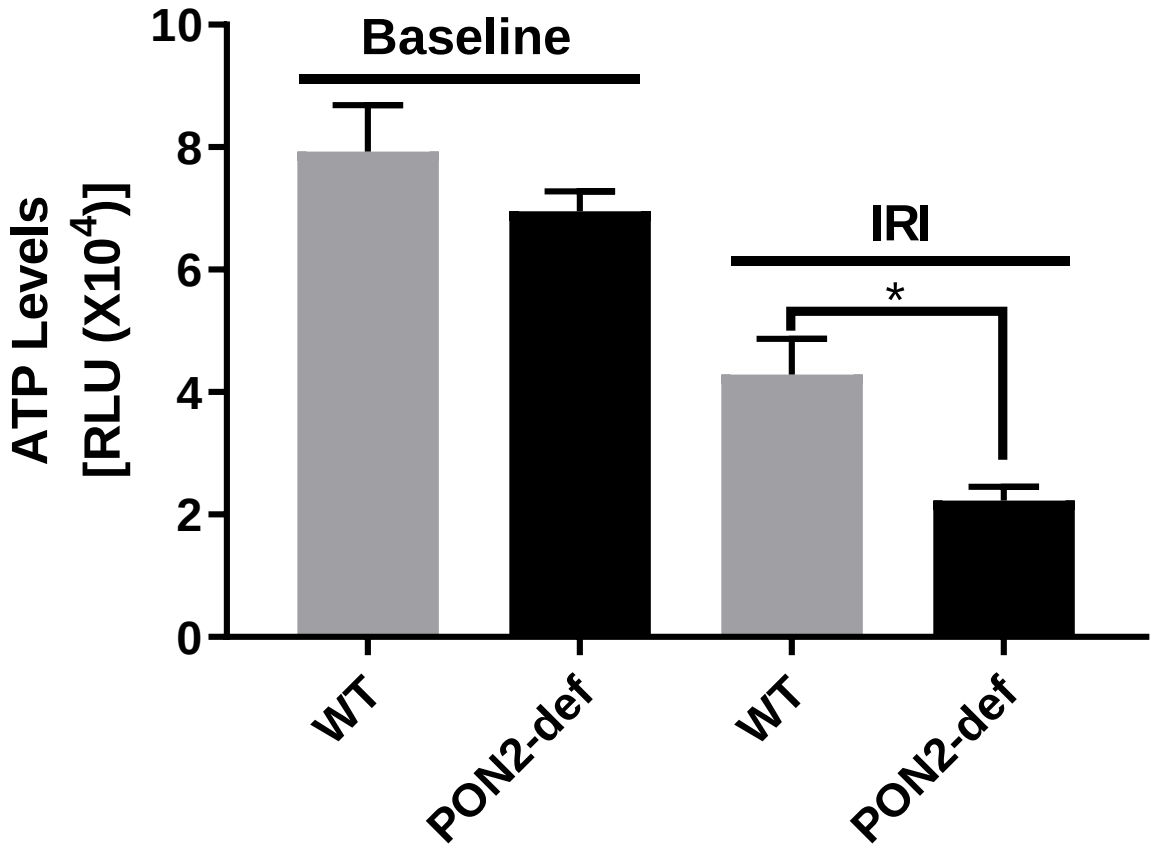

Figure 3C

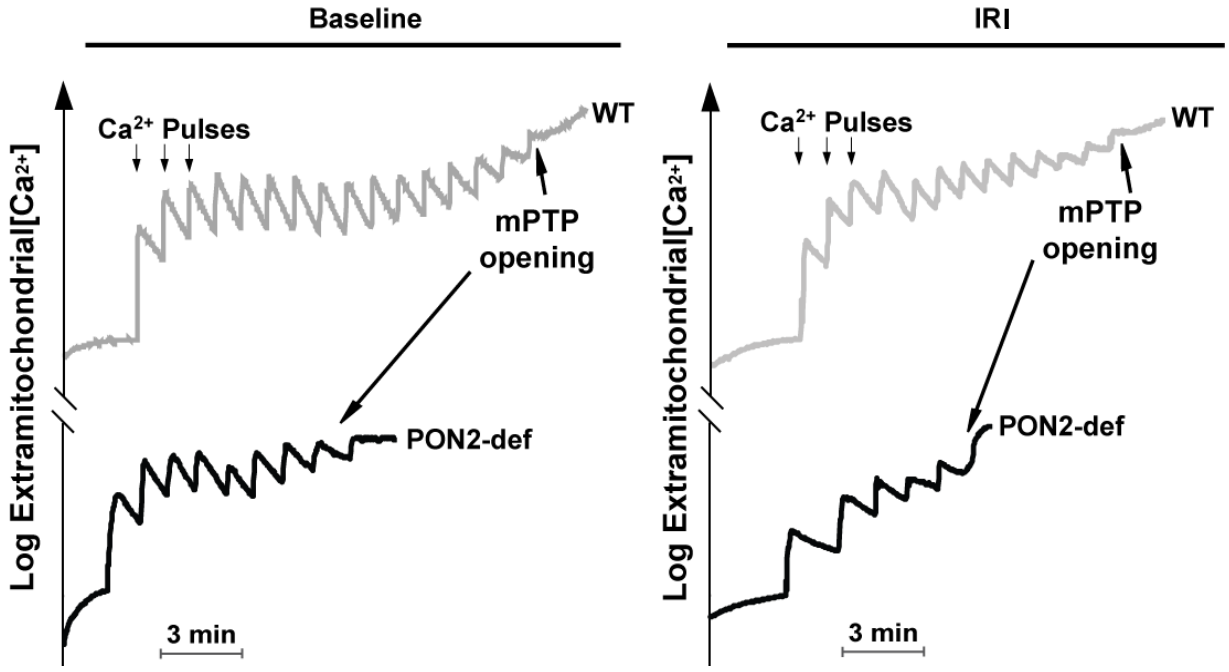

Figure 3D

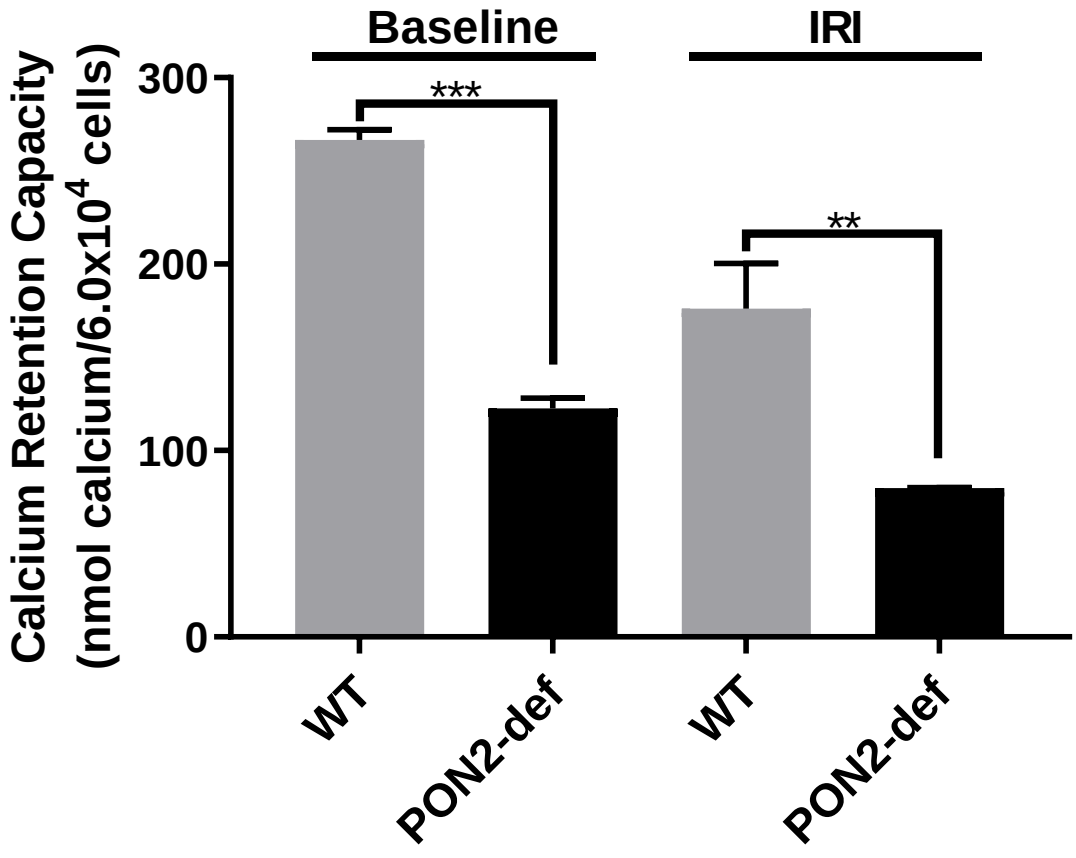

Figure 3E

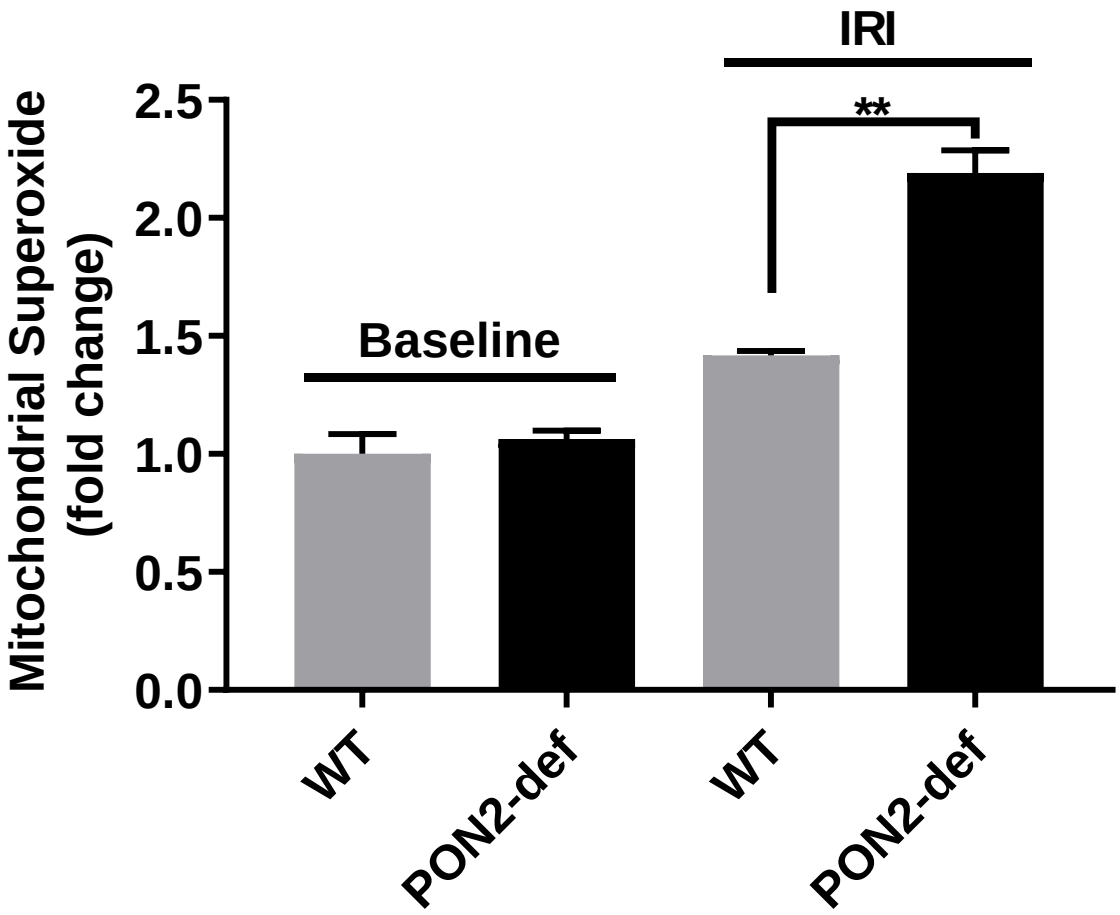
IRI
**
Baseline
Mitochondrial Superoxide
(fold change)
2.5
2.0
1.5
1.0
0.5
0.0
WT
PON2-def
WT
PON2-def

Figure 3F

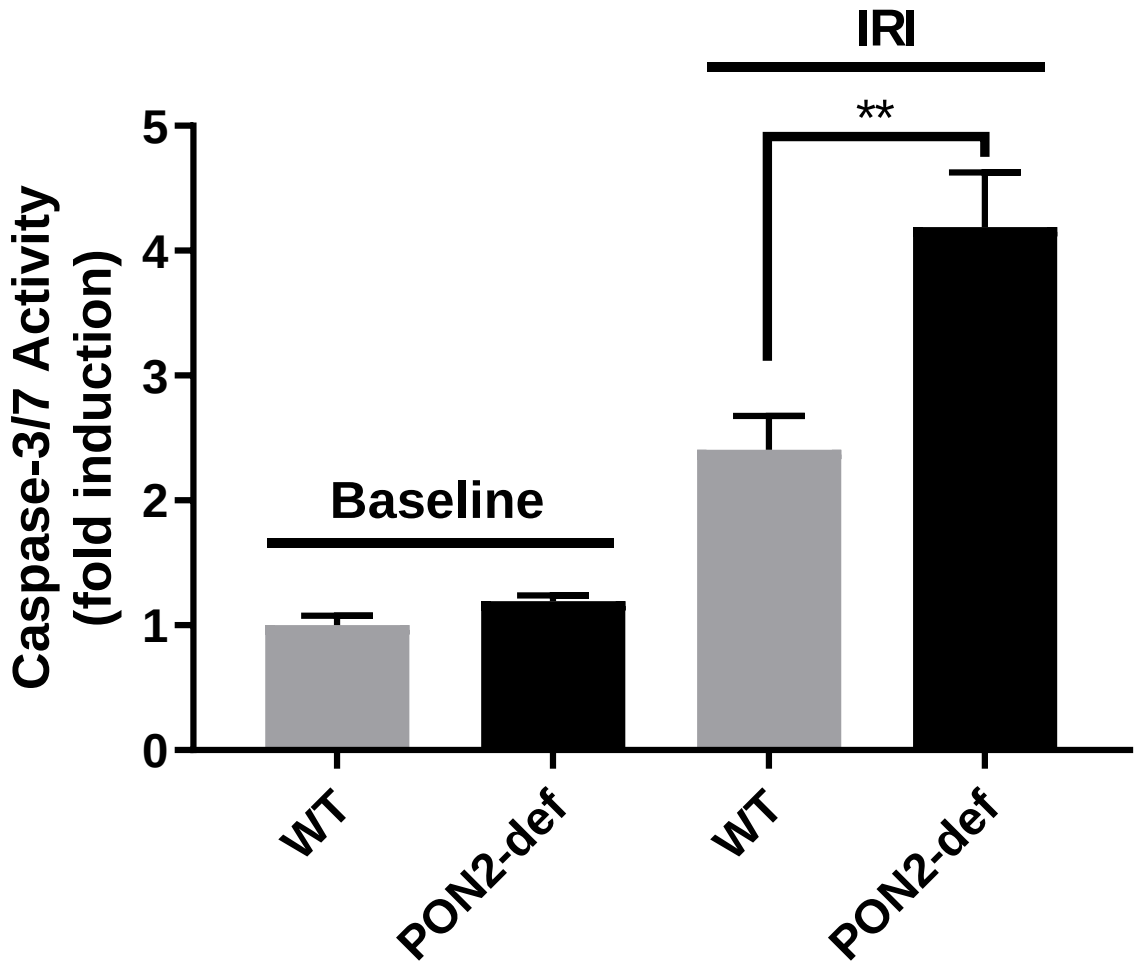
IRI
**
Caspase-3/7 Activity
(fold induction)
5
4
3
2
1
0
Baseline
WT
PON2-def
WT
PON2-def

Figure 3: Cardiomyocytes deficient in PON2 exhibit increased mitochondrial dysfunction, oxidative stress, and apoptosis following IRI. (A) *Ex vivo* ischemia-reperfusion protocol, via the Langendorff Apparatus, was performed. Hearts were cannulated onto a Langendorff apparatus and allowed to stabilize for 10 minutes with oxygenated, KH buffer. The aorta was clamped for 20 minutes, inducing the hypoxic episode, followed by a 5 minute reperfusion with oxygenated, KH buffer. (B) ATP levels were assessed in WT and PON2-def cardiomyocytes under baseline (untreated) and *ex vivo* IR injured conditions (n=3/group) and represented as relative luminescence units ($x10^4$). (C) Representative recordings of the calcium retention capacity (CRC) assay from cardiomyocytes isolated from WT and PON2-def mice (n=3/group), which indicates the threshold of mitochondrial permeability transition pore (mPTP) opening of isolated cardiomyocytes to extramitochondrial calcium. (D) CRC was evaluated under baseline (untreated) and *ex vivo* IR injured conditions (n=3/group) and quantified as nmoles of calcium per 6.0 x 10^4 cells. (E) ROS generation was evaluated in baseline (untreated) and *ex vivo* IR injured cardiomyocytes (n=3/group) and represented as fold change of mitochondrial superoxide production. (F) Apoptosis, evaluated as caspase-3/7 activity, was assessed in baseline (untreated) and *ex vivo* IR injured cardiomyocytes (n=3/group) and quantified as relative luminescence units ($x10^4$). Data is represented as mean±SEM; *p<0.05, **p<0.01, ***p<0.001.

Figure 4A

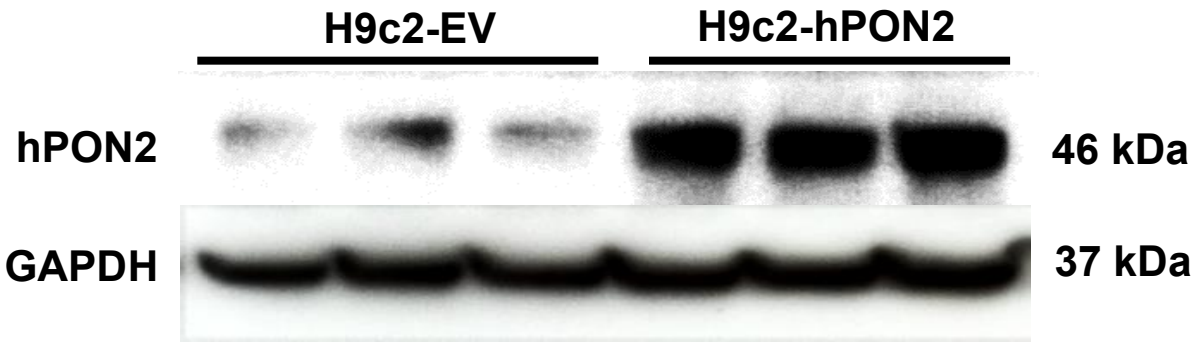

Figure 4B

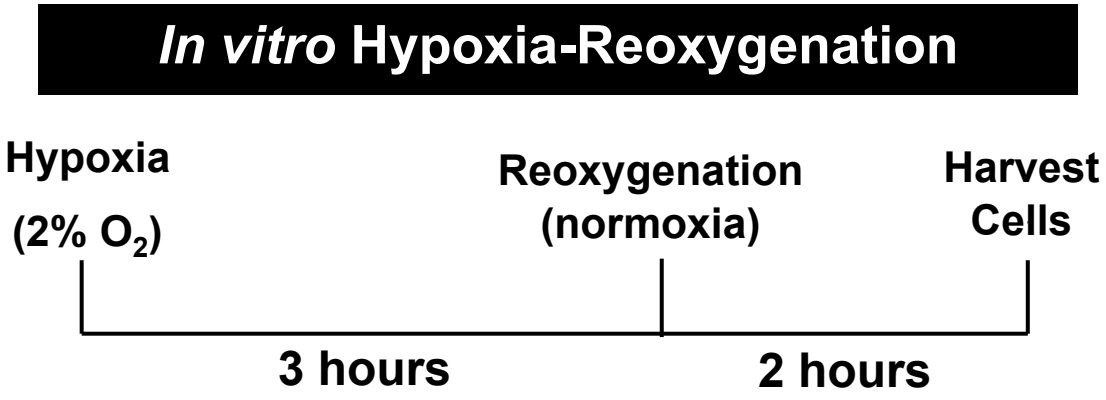

Figure 4C

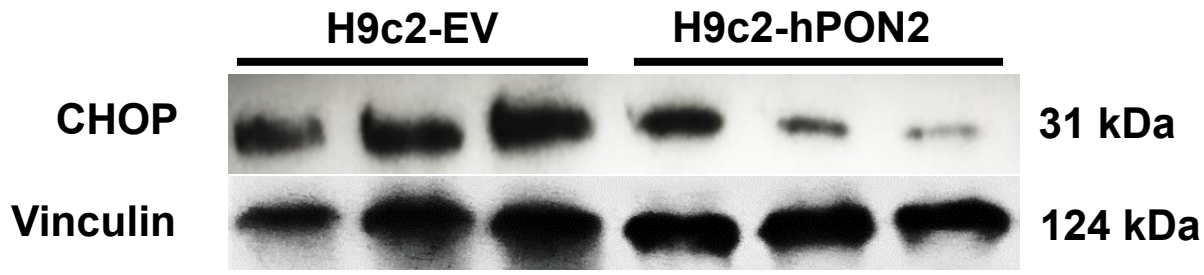

Figure 4D

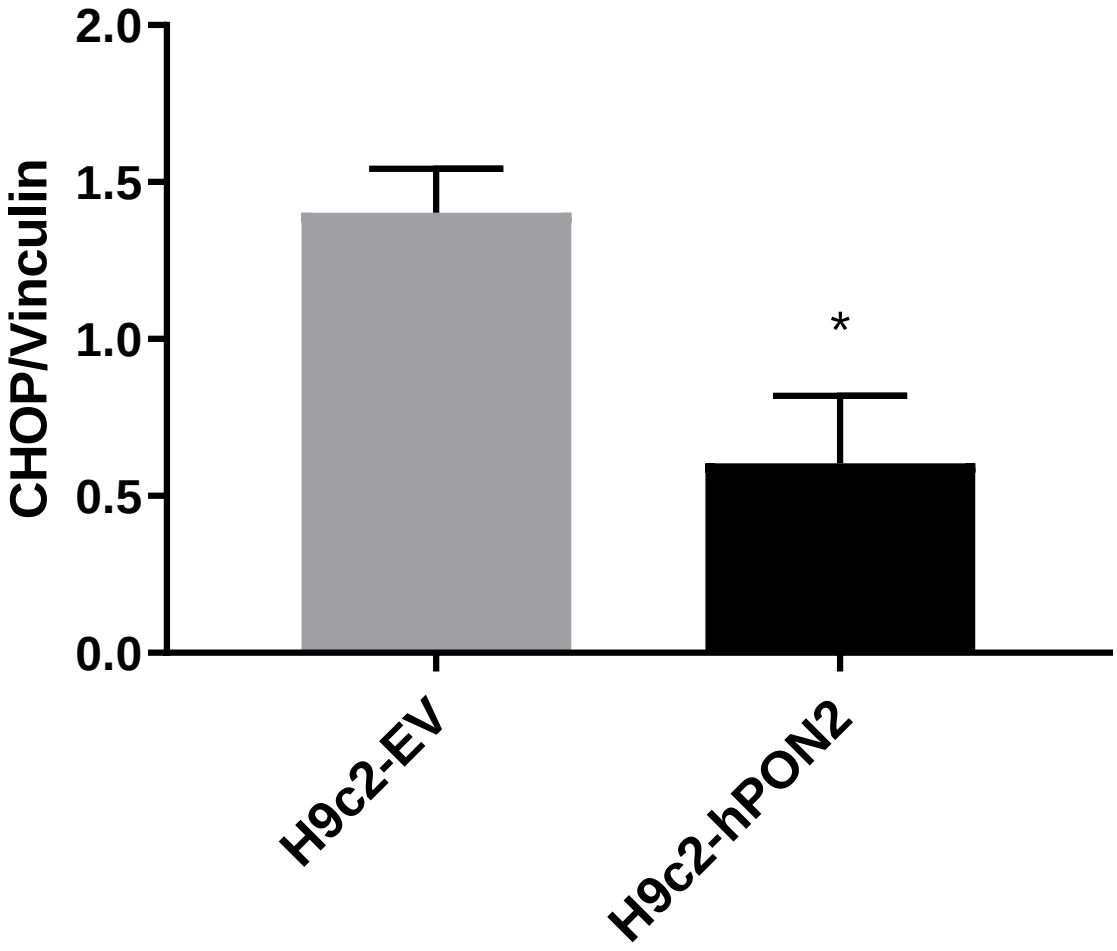

Figure 4E

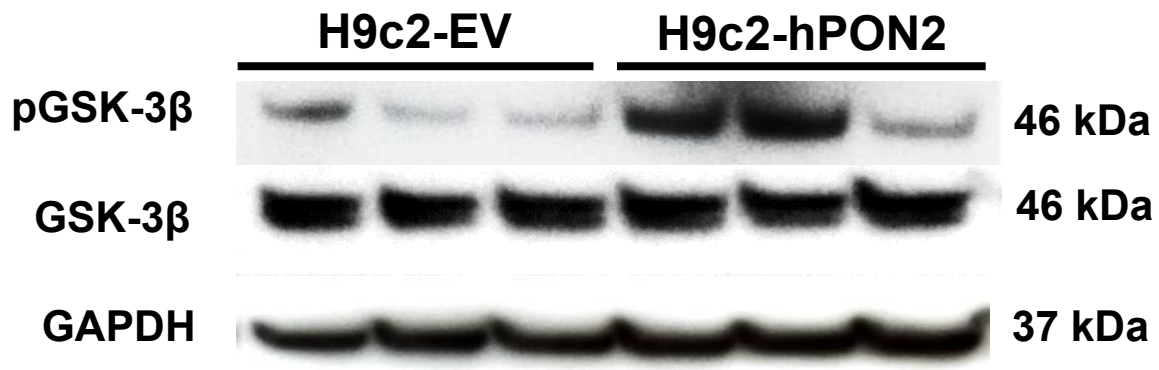

Figure 4F

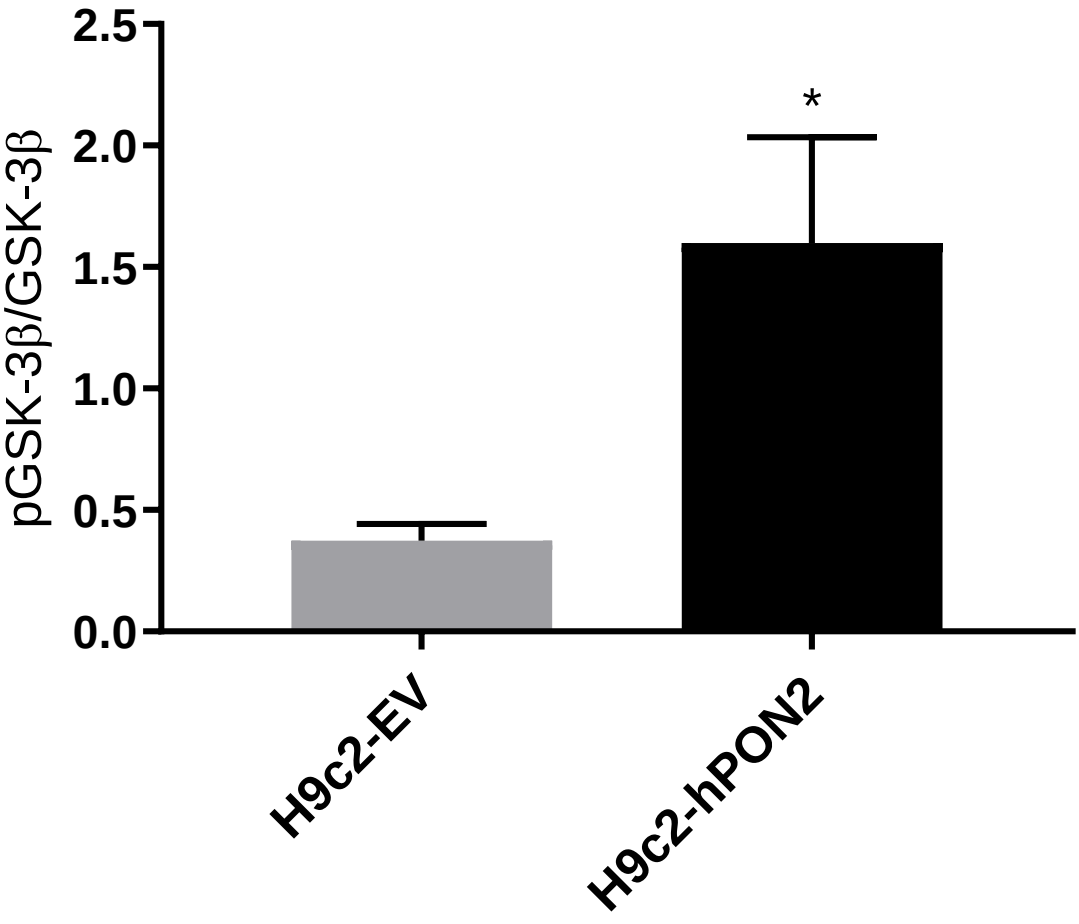

Figure 4: Overexpression of human PON2 in H9c2 cells results in increased pGSK-3β following HRI. (A) H9c2 cells were stably transfected with an empty pcDNA3.1+ plasmid (H9c2-EV) or a pcDNA3.1+ plasmid containing human PON2 gene (H9c2-hPON2). (B) H9c2-EV and H9c2-hPON2 cells were subjected to hypoxia-reoxygenation injury (HRI) [3-hour hypoxia at 2% O_2, followed by a 2-hour reoxygenation at normoxic conditions]. CHOP expression (n=4/group) was evaluated via western blot analysis (C), normalized to vinculin, and quantified as a ratio of CHOP to Vinculin (D). GSK-3β and pGSK-3β expression (n=3/group) was evaluated via western blot (E), both normalized to GAPDH and then quantified as a ratio of pGSK-3β to GSK-3β (F). Data is represented as mean±SEM; *$p<0.05$.

Figure 5A

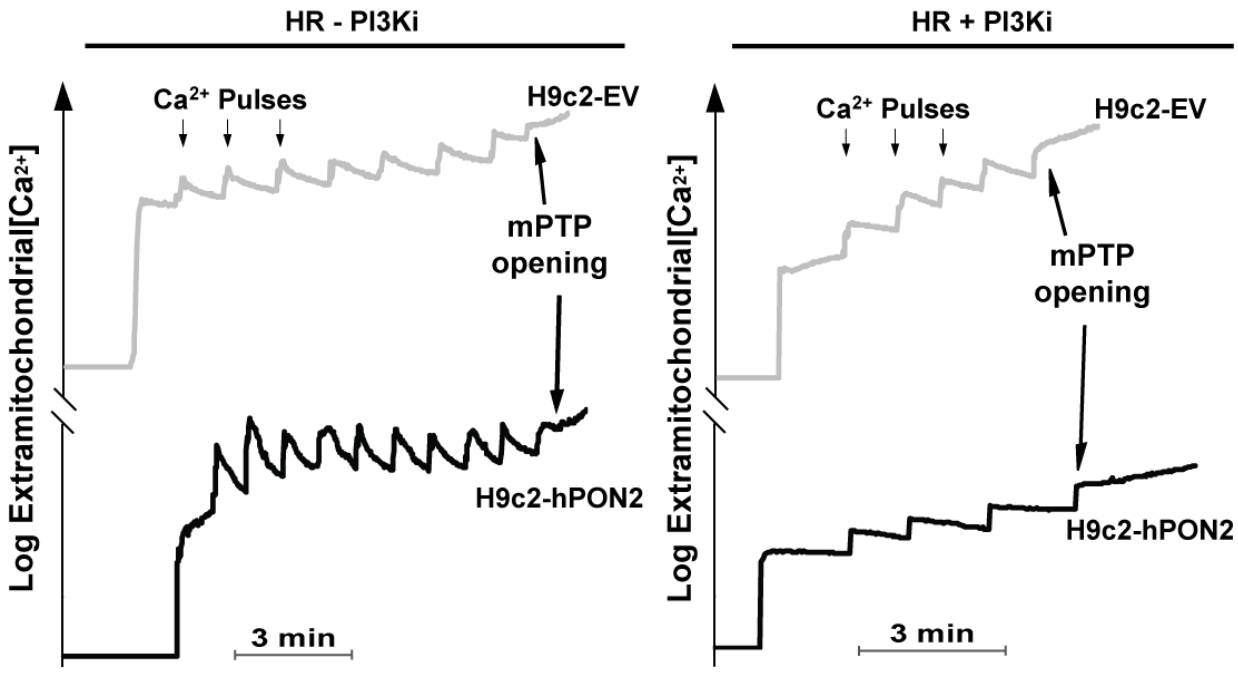

Figure 5B

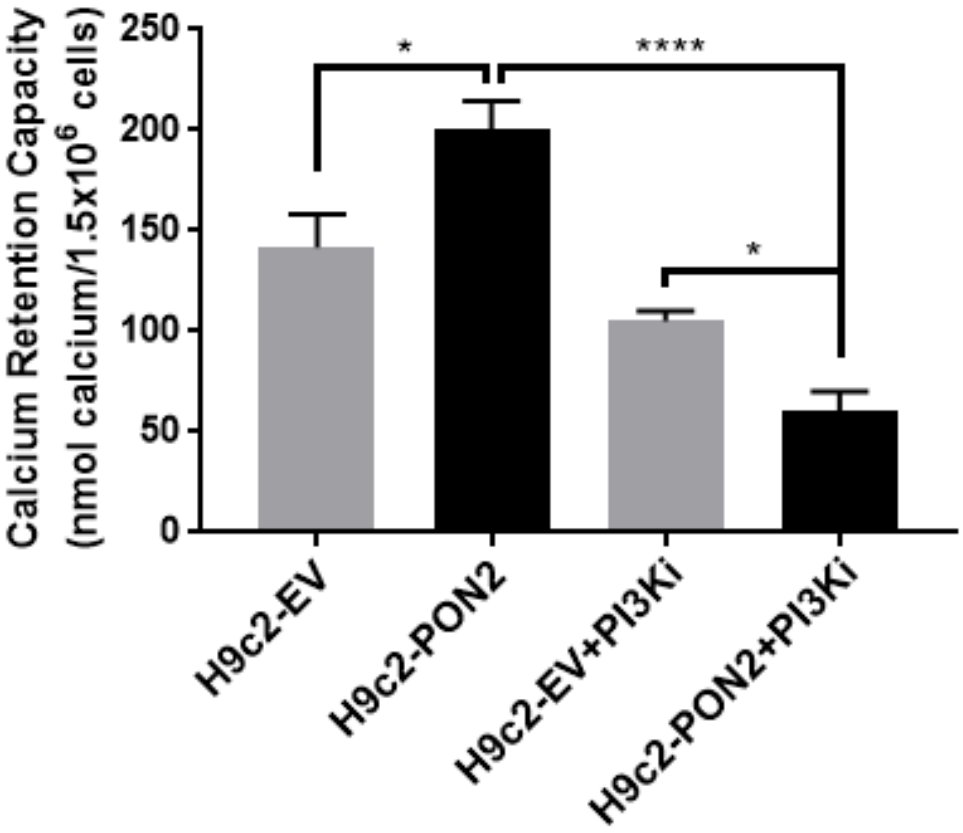

Figure 5C

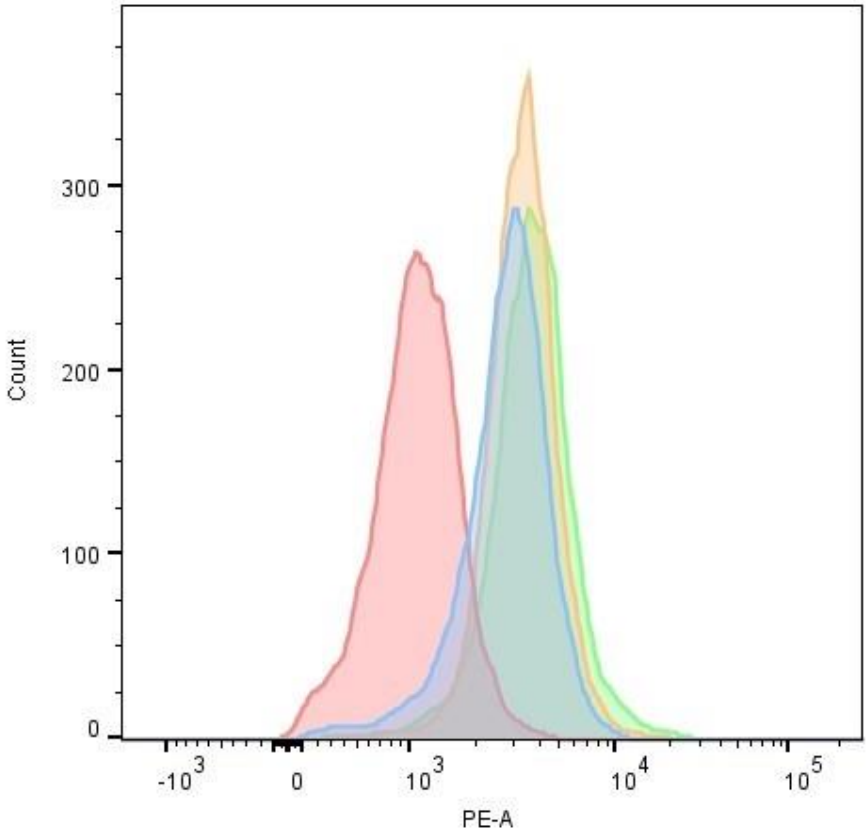

	Sample Name	Mean: PE-A
	H9c2-EV	3106
	H9c2-hPON2	1176
	H9c2-EV + PI3Ki	3670
	H9c2-hPON2 + PI3Ki	4246

Figure 5D

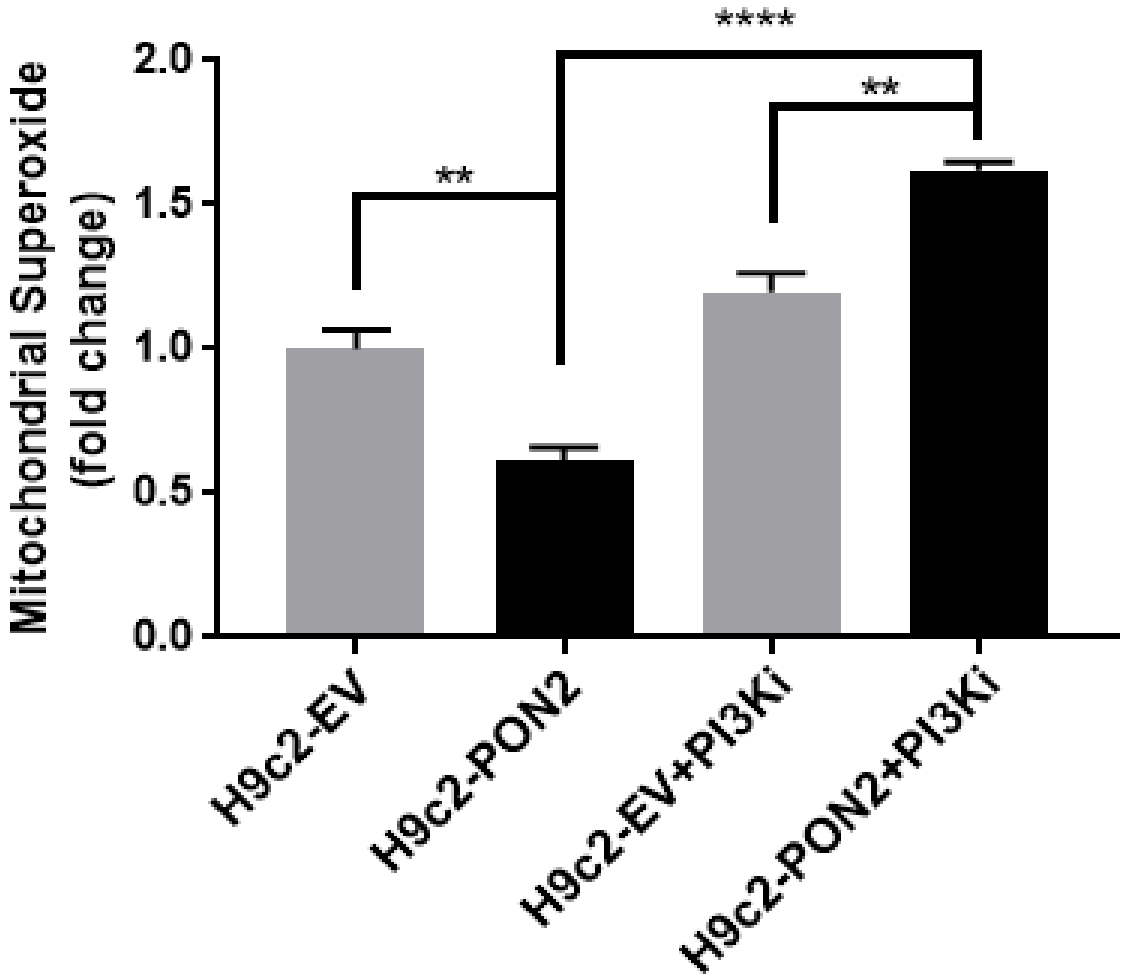
Mitochondrial Superoxide
(fold change)
2.0
1.5
1.0
0.5
0.0
****
**
**
H9c2-EV
H9c2-PON2
H9c2-EV+PI3Ki
H9c2-PON2+PI3Ki

Figure 5E

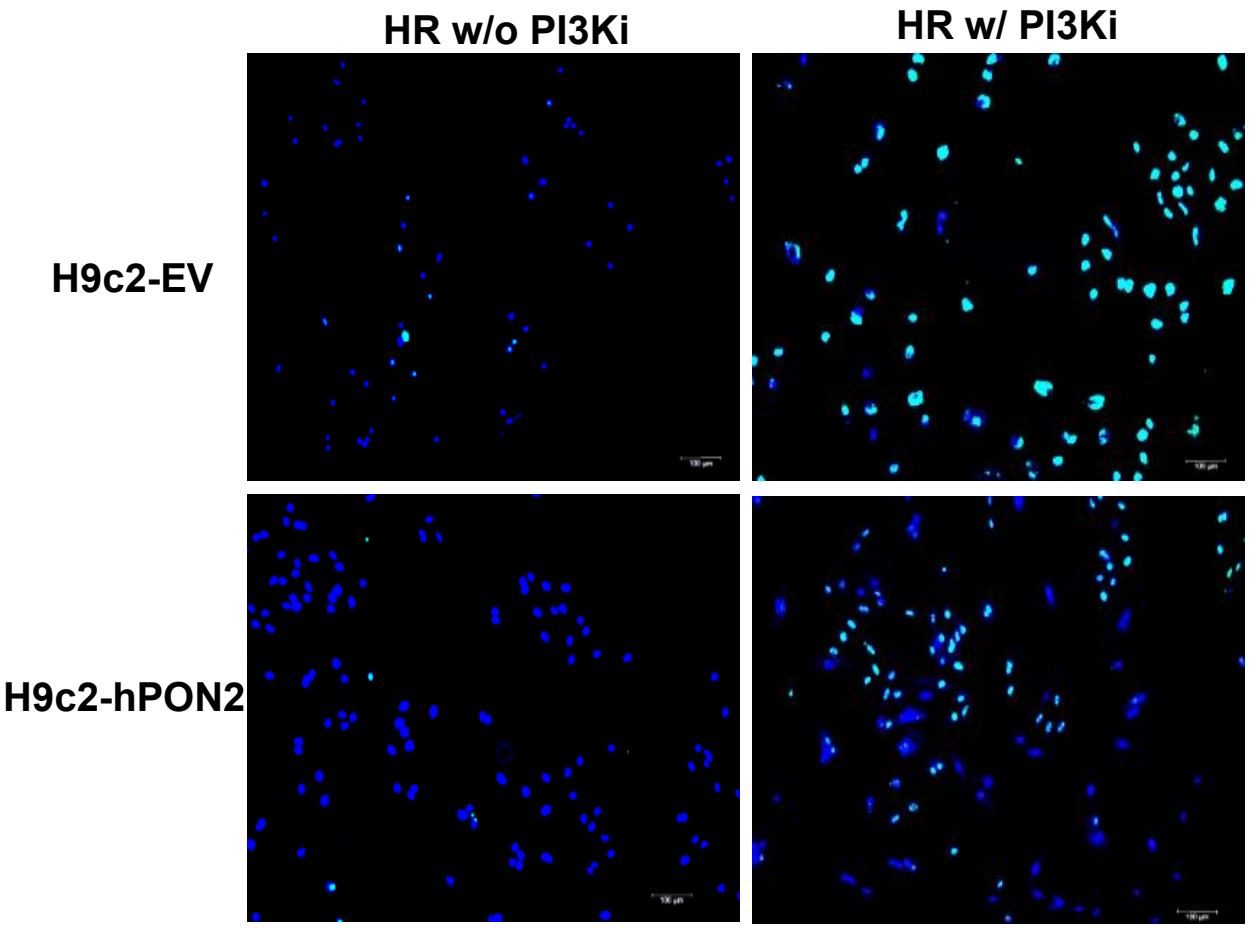

Figure 5F

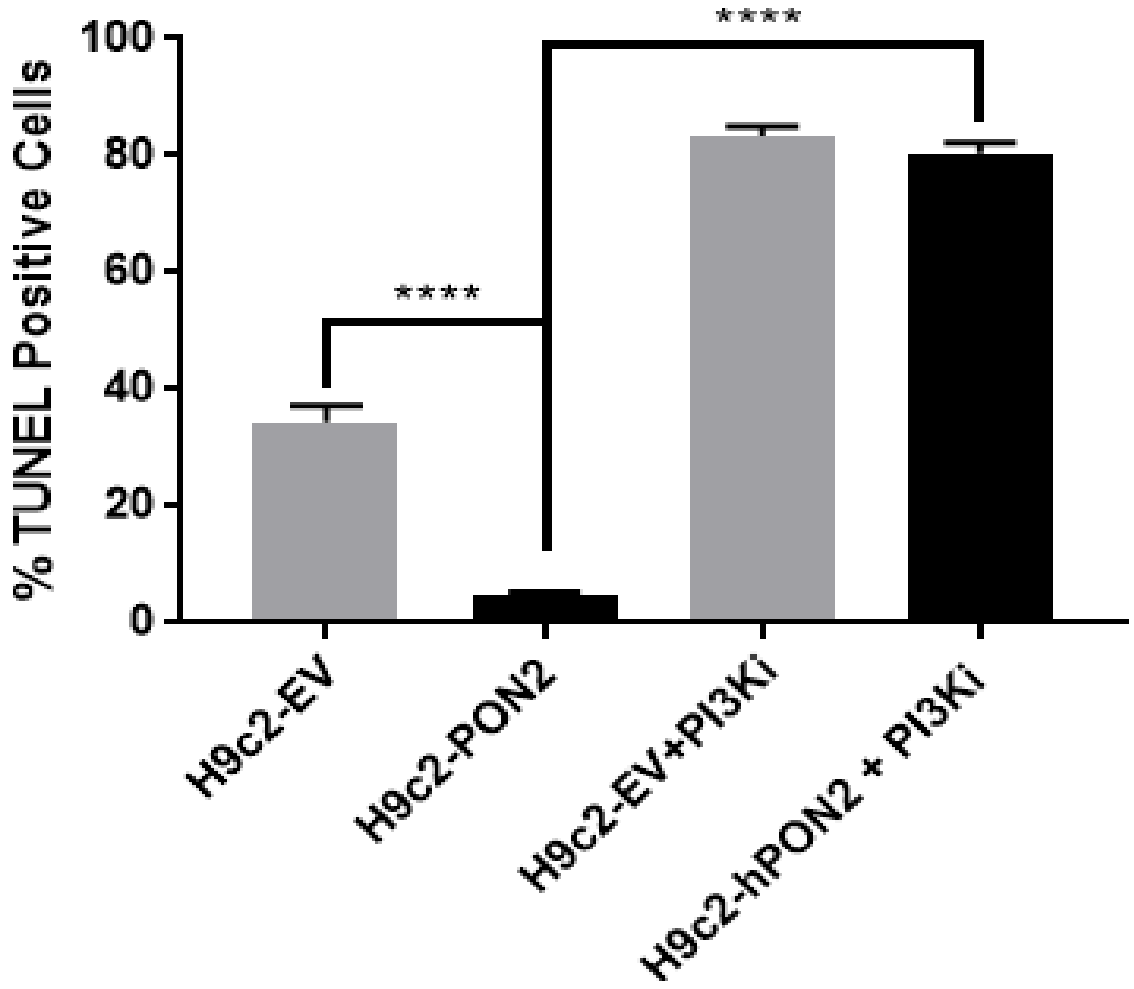
% TUNEL Positive Cells
100
80
60
40
20
0
****
****
H9c2-EV
H9c2-PON2
H9c2-EV+PI3Ki
H9c2-hPON2 + PI3Ki

Figure 5: PON2 overexpression is cardioprotective and activates the RISK (PI3K/Akt/GSK-3β) pathway. (A-F) H9c2-EV and H9c2-hPON2 cells were subjected to hypoxia-reoxygenation injury ± PI3K inhibitor, LY294002 (n=3/group). (A) Representative recordings of the calcium retention capacity (CRC) assay indicating the threshold of mitochondrial permeability transition pore (mPTP) opening of H9c2-EV/hPON2 cells to extramitochondrial calcium. (B) CRC was evaluated and quantified as nmoles of calcium per 1.5 x 10^6 cells. (C) Representative measurement of mitochondrial superoxide production via live cell analysis using flow cytometry. (D) ROS production was quantified and represented as fold change of mitochondrial superoxide production. (E) Representative images of cell apoptosis, via TUNEL assay (Blue=DAPI and Green=TUNEL positive nuclei). (F) Cell apoptosis, via TUNEL assay, was quantified as percent of TUNEL positive cells. Data is represented as mean±SEM; *p<0.05, **p<0.01, ****p<0.0001.

Supplementary Figure 1A

WT

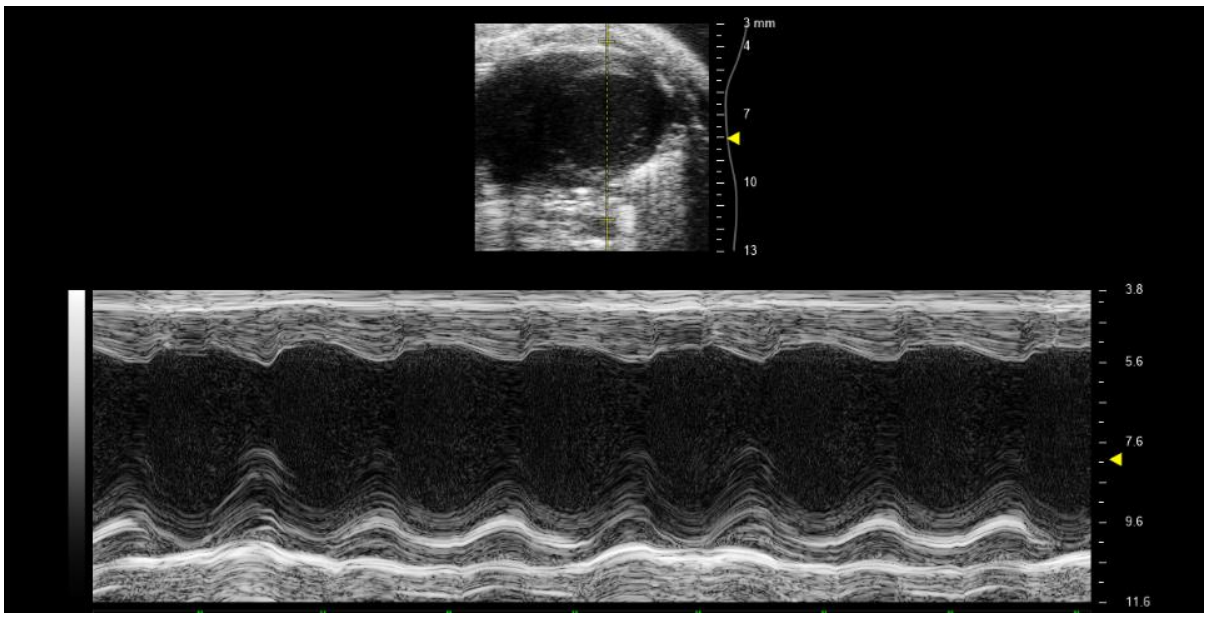

PON2-def

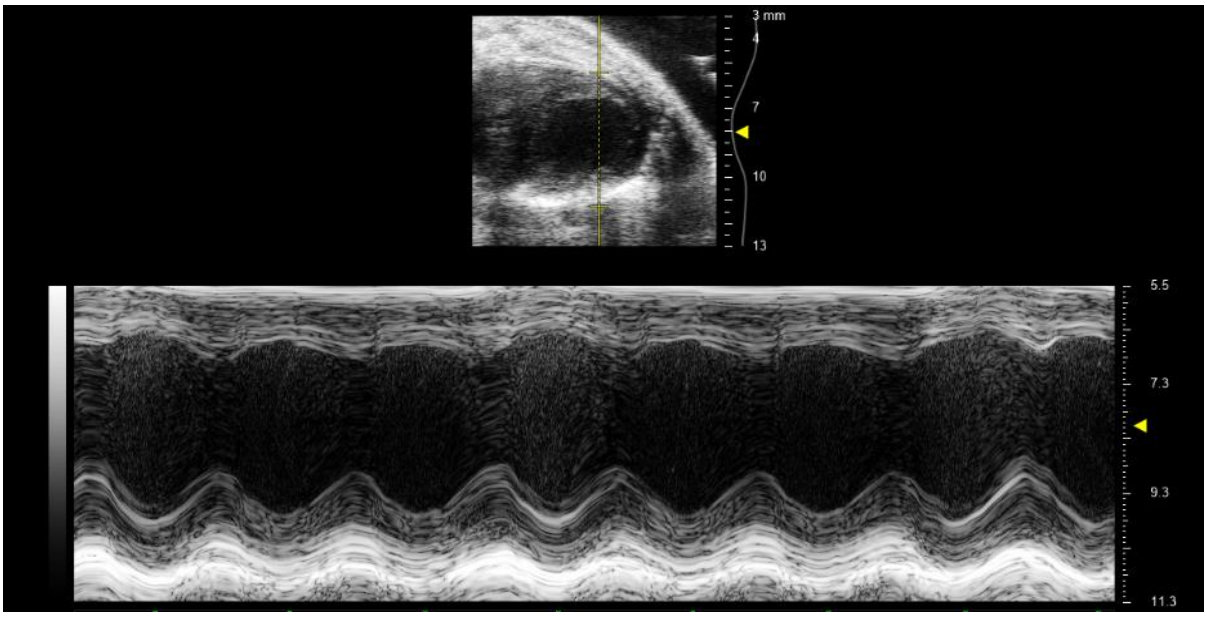

Supplementary Figure 1B

	LV-EF%	LV-FS%	IVS(mm) Diastolic	IVS(mm) Systolic	LV PW(mm) Diastolic	LV PW(mm) Systolic
WT	**63.1±3.45**	**33.5±2.4**	**0.6±0.03**	**0.9±0.03**	**0.70±0.03**	**0.99±0.06**
PON2-def	**65.0±2.86**	**35.2±2.2**	**0.5±0.03**	**1.0±0.09**	**0.67±0.04**	**1.05±0.07**

	LV Diameter(mm) Diastolic	LV Diameter(mm) Systolic	LV Volume(ul) Diastolic	LV Volume(ul) Systolic
WT	**3.1±0.06**	**2.10±0.07**	**44.09±4.16**	**14.30±1.47**
PON2-def	**3.31±0.21**	**2.16±0.16**	**55.37±4.52**	**19.71±2.45**

Supplemental Figure 1: Heart Function and Structure of PON2-def mice are similar to WT at the Baseline. (A) M-mode echocardiograms were performed on WT and PON2-def mice (n=3/group) at baseline (untreated). (B) LV-EF (%), LV-FS (%), IVS systolic (mm), LV PW diastolic and systolic (mm), LV diameter diastolic and systolic (mm), and LV volume diastolic and systolic (uL) were evaluated. Data is represented as mean±SEM.

Supplementary Figure 2A

WT

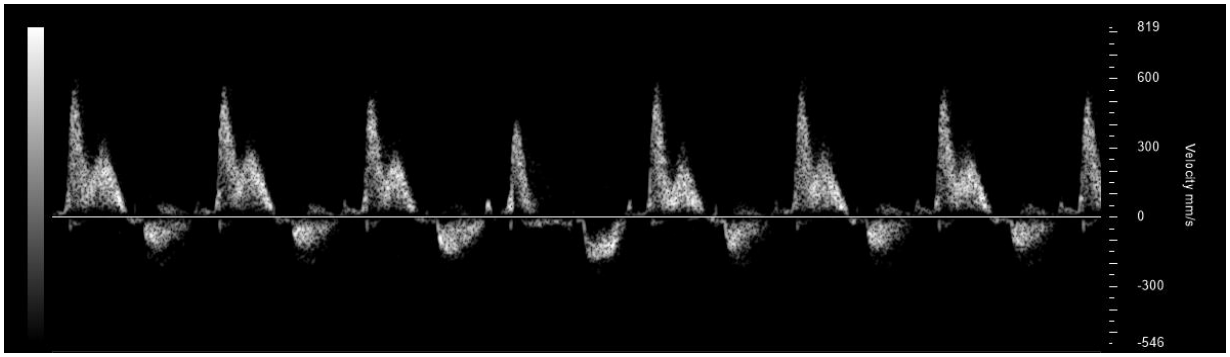

PON2-def

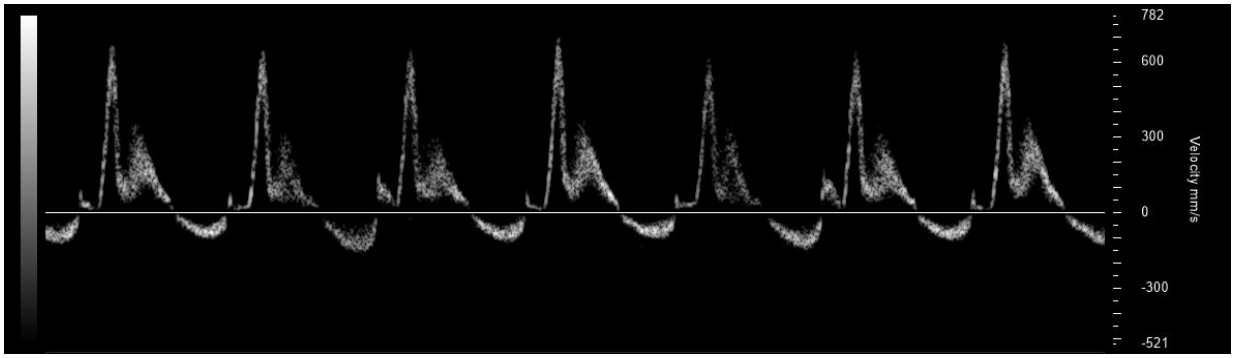

Supplementary Figure 2B

	E/A
WT	1.6±0.07
PON2-def	1.6±0.06

Supplemental Figure 2: Heart function and structure of PON2-def mice are similar to WT at Baseline. (A) Doppler echocardiograms were performed on WT and PON2-def mice (n=3/group) at baseline (untreated). (B) E/A ratio: Early (E) to late (A) ventricular filling velocities were determined. Data is represented as mean±SEM.

Supplementary Figure 3A

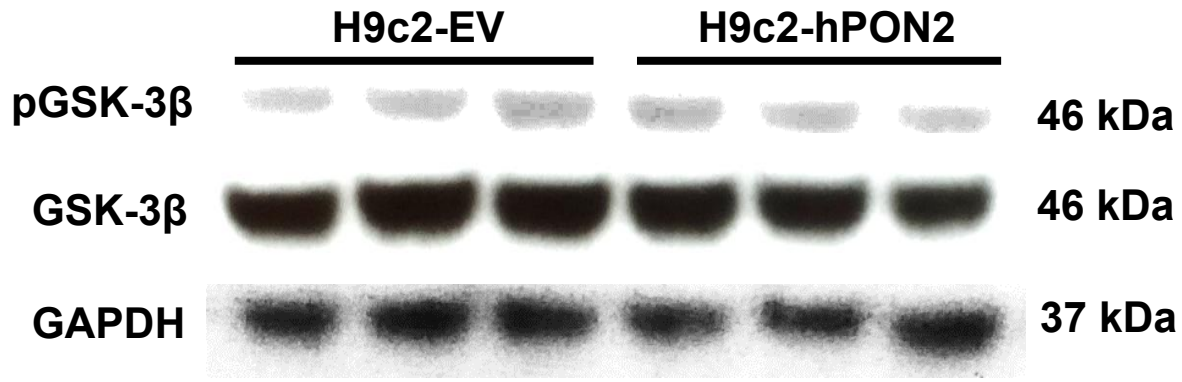

Supplementary Figure 3B

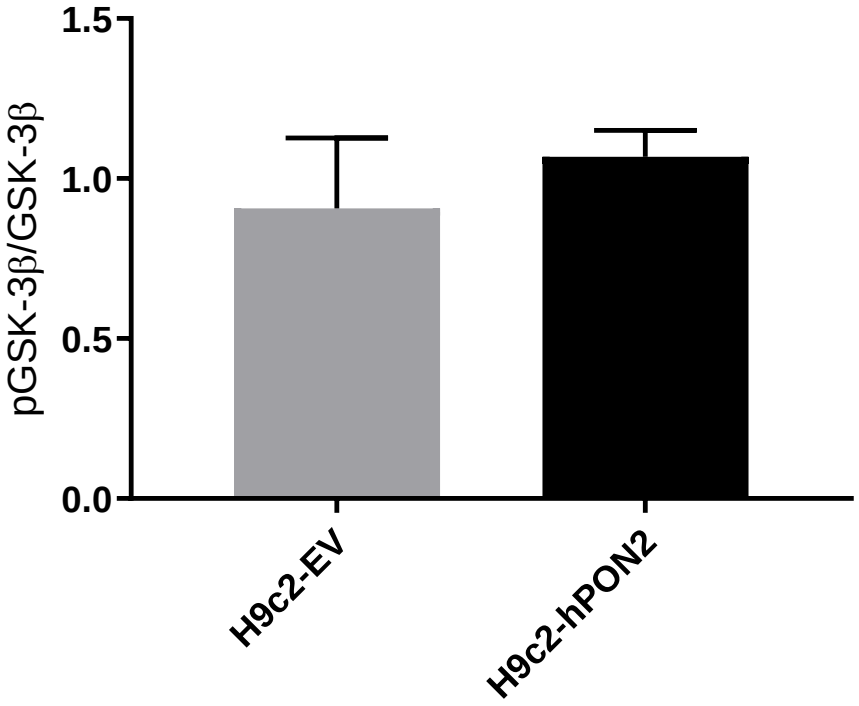

Supplemental Figure 3: No differences in pGSK-3β levels in H9c2 cell-lines under baseline conditions. GSK-3β and pGSK-3β levels were evaluated via western blot (A), both normalized to GAPDH, and then quantified as a ratio of pGSK-3β to GSK-3β in H9c2-EV and H9c2-hPON2 cells (B) under baseline (untreated) conditions (n=3/group). Data is represented as mean+SEM.

Supplementary Figure 4A

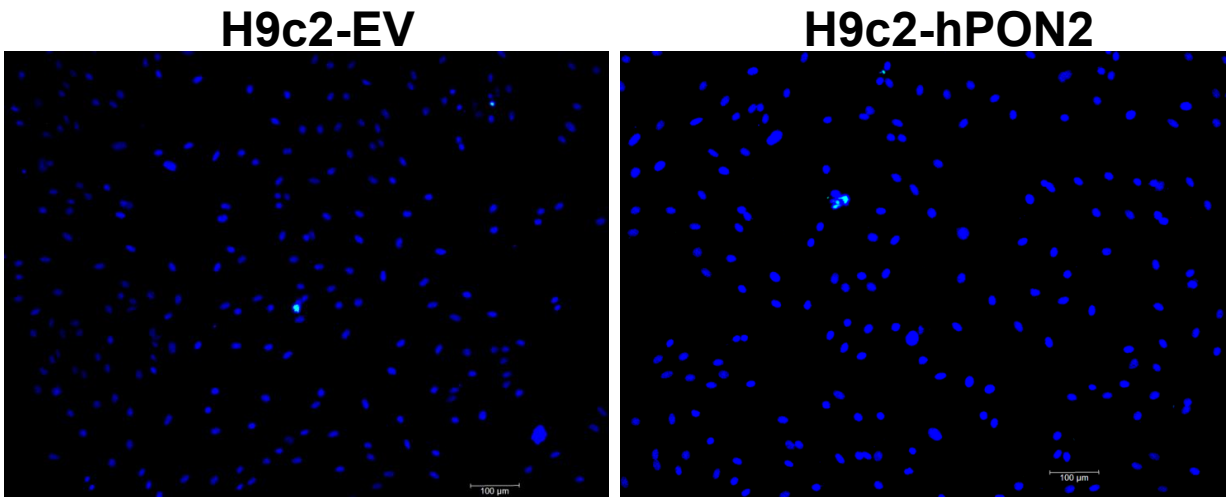

Supplementary Figure 4B

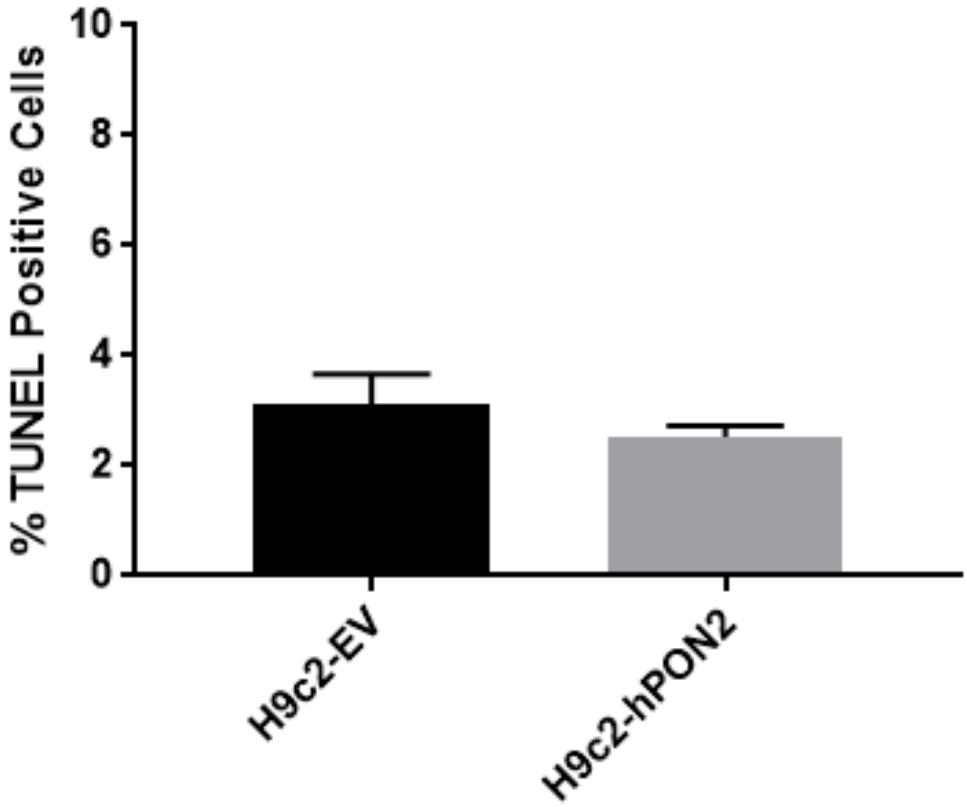

Supplemental Figure 4: No differences in cell apoptosis under baseline conditions. Cell apoptosis, via TUNEL assay, was quantified as percent of TUNEL positive cells in H9c2-EV and H9c2-hPON2 cells under baseline (untreated) conditions (n=3/group). Data is represented as mean+SEM.

Chapter 3: PON2 Modulates Mitochondrial Lipid Composition and Peroxidation via Phosphatidylcholine Oxidation and Production of Eicosanoids and Prostanoids

Abbreviations:

IMM	Inner mitochondrial membrane
OMM	Outer mitochondrial membrane
CL	Cardiolipin
PC	Phosphatidylcholine
PE	Phosphatidylethanolamine
PUFA	Polyunsaturated fatty acids
CAD	Coronary Artery Disease
IRI	Ischemia-reperfusion injury
MI	Myocardial Infarction
ROS	Reactive oxygen species
WT	Wild-type
PON-def	PON2-deficient
LAD	Left anterior descending
oxPAPC	Oxidized 1-palmitoyl-2-arachidonyl-sn- glycero-3-phosphorylcholine
POVPC	1-palmitoyl-2-(5'-oxo-valeroyl)-sn-glycero-3-phosphocholine
PGPC	1-palmitoyl-2-glutaryl-sn-glycero-3-phosphocholine
AA	Arachidonic Acid
LA	Linoleic Acid
HETE	5-Hydroxyeicosatetraenoic acid
HODE	13-Hydroxyoctadecadienoic acid
$cPLA_2$	Cytoplasmic phospholipase A_2
6-keto PGF1α	6-keto prostaglandin F 1α
PGE_2	Prostaglandin E2
PGF2α	Prostaglandin F2α
PGD_2	Prostaglandin D2

3.1 Introduction:

Many pharmacological interventions that aim to mitigate the negative effects of IRI have been largely unsuccessful.[20, 21] Therefore, finding a novel molecular modulator that is connected to multiple IR pathophysiologies may prove instrumental in the fight against myocardial IRI.

PON2 has been shown to have various anti-oxidant and anti-inflammatory properties.[4, 5, 44-46] A PON2-deficient mouse model was developed by our lab to test the role of PON2 in various disease models.[44] PON2 deficiency alters mitochondrial function by decreasing mitochondrial complex I and III activity and total ATP levels and alters mitochondrial oxidative stress by increasing mitochondrial superoxide production, increasing lipid peroxidation and decreasing reduced glutathione levels.[5, 45] PON2 is localized within the mitochondria, specifically associating with complex III of the IMM.[5] Within the IMM, PON2 attenuated CL peroxidation, cytochrome c release and caspase activation.[49]

Mitochondrial lipid composition is a vital aspect of maintaining normal mitochondrial bioenergetics and function. [35] The major phospholipids in the mitochondrial membranes are PC, PE, and CL, which make-up ~40%, 30%, and 15% of the total lipids respectively.[26] IRI promotes the loss of IMM organization and decrease in CL content and peroxidation, which in turn leads to poor electron flow, further generation of ROS, and impairment of respiratory complexes and membrane potential.[35-38] Considering the localization of PON2 within the IMM, earlier, unpublished work in our lab sought to investigate whether PON2 associates with CL, a key lipid in the IMM.[73] Using surface plasmon resonance, it was demonstrated that PON2 binds to

CL in a concentration-dependent manner (Figure 6A).[73] In addition, the ability of PON2 to further interact with cardiolipin and potentially aid in its transport across the inner and outer mitochondrial membranes was tested. The fluorescent probe octadecyl-rhodamine (R18) was used as a marker for cardiolipin. Transfer of R18 was examined from R18 labeled vesicles that mimic the IMM (DOPC:DOPE:TOCL [1:1:1]) to either another set of unlabeled IMM vesicles or to a set of vesicles mimicking the composition of the OMM (DOPC:DOPE:DOPS:bbPI:TOCL[38:28:9:9:4]). The results demonstrated that PON2 indeed transports CL from the IMM to the outer mitochondrial membrane (OMM) (Figure 6B).

Mitochondrial membrane lipids like phospholipids phosphatidylcholine (PC), phosphatidylethanolamine (PE), and cardiolipin (CL), contain esterified polyunsaturated fatty acids (PUFAs), particularly arachidonic acid (AA) and linoleic acid (LA), that are susceptible to oxidative damage during myocardial IRI leading to lipid peroxidation.[33, 74] Furthermore, these AA and LA PUFAs can be unesterified by phospholipases and oxidized into potent lipid signaling molecules like eicosanoids and prostanoids, which play significant inflammatory and anti-inflammatory roles in a variety of diseases, including myocardial IRI.[29, 33, 34, 75, 76]

We have shown that PON2 is present in cardiomyocytes, localized in the IMM,[5] binds to CL and transports CL from the IMM to the OMM. These data support the hypothesis that PON2 does associate with mitochondrial membrane lipids and can potentially play a role in modulating lipid composition against IRI. Therefore, I hypothesize that PON2 plays a protective role against IRI in cardiomyocytes by

modulating mitochondrial lipotoxicity, in the form of lipid composition and lipid peroxidation.

3.2 Materials and Methods

3.2.1 Experimental Mice

C57BL/6J, wild-type (WT) mice and PON2 deficient (PON2-def) male mice 8-10 weeks of age were used for the *in vivo* studies. The wild type controls used for all our studies were derived from PON2 heterozygous intercrosses. All animal studies were approved by the IACUC and Animal Research Committee (ARC) at UCLA, and designed to prevent/reduce any stress/pain.

3.2.2 H9c2 Cell Culture Methods

H9c2(2-1) (ATCC CRL-1446), a rat ventricular cardiomyocyte cell-line, was utilized for the *in vitro* studies. ATCC-formulated DMEM (catalog#30-2002, ATCC) was used to culture the cells, with the addition of 10% FBS (Catalog#26140079, ThermoFisher) and 1% Penicillin-Streptomycin (catalog#15140122, ThermoFisher) for complete growth medium. H9c2 cells were transfected with pcDNA3.1+ plasmid expressing human PON2 (H9c2-hPON2) or empty vector (H9c2-EV) (Catalog#V790-20, Addgene) using Lipofectamine 2000 transfection reagent (catalog#11668027, ThermoFisher). Stable cell-lines were generated by selection of positive colonies via neomycin selection (Geneticin, catalog#10131035, ThermoFisher).

3.2.3 Ischemia-Reperfusion Injury

In vivo IRI

Left Anterior Descending (LAD) Coronary Artery Occlusion: Mice were subjected to vivo IRI as previously described.[57] In brief, mice were anesthetized with ketamine (100 mg/kg i.p.) and xylazine (10 mg/kg i.p.). After general anesthesia, the baseline ECG and ECHO were performed. Under mechanical ventilation, the chest was opened

and the heart exposed. A suture was placed around the left anterior descending coronary artery (LAD) three quarters of the distance from the base to the apex, and tightened to occlude the LAD permanently for 30 minutes, which was confirmed by ST elevation in ECG. The ligature was released to start reperfusion. The chest was then closed and the mice were allowed to recover. Twenty-four hours later, the mice were euthanized using approved procedures and the hearts removed for downstream lipid extraction.

In vitro IRI

Hypoxia-Reoxygenation via Hypoxia Chamber: To induce hypoxia in cells, cell media was changed from normal, growth media (refer to H9c2 Cell Culture Methods) to a low nutrient DMEM (Life Technologies, Catalog# 11966-025) without growth factors and were placed into a hypoxic plastic chamber under hypoxic gas conditions (0% O_2, 5% CO_2, nitrogen balanced) at 37^{o}C for 3 hours. Hypoxia was confirmed by HIF-1α upregulation (data not shown). The cells were then reoxygenated by replacing the media back to regular growth media and placing the cells back to normoxic gas conditions (~20-21% O_2 and 5% CO_2) at 37^{o}C for 2 hours. The cells were then used for all downstream assays.

3.2.2 Mitochondrial Isolation from Heart Tissue

Fresh relaxation buffer (55.5mg Sodium Pyrophosphate, 5 ml KCL 1M, 500ul EGTA 500mM, 250ul HEPES 1M, Add 40ml milliQ water, pH to 7.4, and adjust final volume to 50ml) was prepared. Mice were anesthetized using isoflurane and sacrificed the animal by cervical dislocation. Hearts were removed then immediately immersed heart in 3ml ice cold relaxation buffer on a 6 well plate (on ice). The hearts were

incubated in the solution for 3-5 minutes, pressing/squeezing the heart with tweezers to remove blood from inside the heart. Hearts were moved to next well with clean relaxation buffer and repeated heart perfusion is continued as detailed above. Lastly, hearts were moved to third well containing 2 mL of ice cold homogenization solution (4.28g Sucrose (0.25M), 30ml milliQ water, 250ul HEPES 1 M (5mM), 100ul EDTA 500 mM (1mM), pH to 7.4, with 1M KOH), and water adjusted to 50ml. The heart was minced to approximately 0.5cm (very small) pieces. The heart pieces were collected with tweezers and transferred to ice-cold Glass Teflon homogenizer (Fisher) with 2ml of ice cold homogenization solution. 20 Strokes were performed (up and down IN ICE) with the loose pestle. Homogenates were transferred to glass on glass homogenizer and another 20 strokes were performed with tight pestle in ice. A homogenous solution should be seen. The homogenate is centrifuged in 2 mL Eppendorf tubes at 900 xg for 10 minutes in centrifuge (4^{o}C). The pellet is discarded and the supernatant is collected, which contains the mitochondria (avoiding pellet), and transferred to a fresh 2ml Eppendorf tube. The supernatant is centrifuged at 9000xg for 15 minutes (4^{o}C). A pellet containing the mitochondria should be seen. Supernatant is carefully removed, avoiding sucking up the pellet. The pellet in resuspended in 100 µl of water (HPLC-grade water) and protein concentration is measured via Bradford Assay.

3.2.3 Phospholipid Extraction

Equal mitochondrial protein is added from each sample and volume is adjusted to 100 µl with more HPLC grade water into a new glass tube (13x100mm) and then another 200 µl of HPLC grade water is added (total 300 µl). 1.8 mL of 2:1 $CHCl_3$:MeOH (HPLC grade) is added to each glass tube in addition to 20 µl of 20 mM BHT and 5 µl of

internal standard mixture (Kansas Lipidomics). Samples are vortexed for 30 seconds and then centrifuged at 1000 rpm for 10 minutes to separate phases. The organic layer (bottom phase) is transferred so that the aqueous layer is excluded to a new tube (13x100mm). 600 µl MeOH and 1.2 ml water are added. Sample are vigorously vortexed for 30 seconds and centrifuged at 1000rpm for 10 minutes. The organic phase (lower phase) is harvested and transferred to a new tube (12x75mm). Samples are dried under Argon and resuspended in 100 µl HPLC-grade MeOH and transferred into 1.5ml Eppendorf tubes and centrifuged at 13,600 rpm for 10-15 minutes to remove any potential debris. 50 µl of supernatant were transferred into a labelled mass spec vial. Sample were either ready to be run on mass spectrometer or stored at -80^{o}C for future run.[51]

3.2.4 Lipid Extraction for Lipid Panel from Mitochondria Isolated from Heart Tissue and Cells

Equal mitochondrial protein is added from each sample and volume is adjusted to 100 µl with more HPLC grade water into a new 1.5 ml Eppendorf tube and then another 200 µl of HPLC grade water is added (total 300 µl). 5 µl of BHT (10mM) and 20ul of 5x Lipid Panel IS mix (final concentration 10ng/ml extract) is added. 180ul MeOH is added, and the sample are vortexed well (30 seconds minimum). Samples are centrifuged at 13,000rpm for 10 minutes, and supernatant is transferred to 13x100mm glass tube. 2.5ml of acidified HPLC grade water (pH 3-4) is added to the tubes and vortexed. Supernatant were extracted using 3 cc Oasis HLB SPE cartridge on manifold: Cartridges are activated with 2 ml HPLC-grade MeOH; Washed with 2 ml H2O; Samples were then added to cartridge, Washed with 2 ml 5% MeOH (HPLC-grade);

Final collection tubes (13x100mm glass) were placed into manifold; and finally the samples were eluted with 2 ml 100% HPLC-grade MeOH. Samples were dried to completion under argon in 37^{o}c water bath. Samples were then reconstituted with 100 µl HPLC-grade MeOH and transferred to a labelled 1.5ml Eppendorf tube. Tubes are centrifuged at 13,600rpm for 10 minutes at 4^{o}C. 50 µl of the sample were transferred to labelled mass spec vials and delivered for analysis. Remainder of samples are stored in Eppendorf tube at -80^{o}C under argon atmosphere.[51]

3.2.5 Mitochondrial Lipid Saponification

Mitochondrial samples were thawed in their original Eppendorf tubes and any remaining solvent were evaporated under argon/N_2. 1ml of MeOH is added, and then vortexed/sonicated and then the supernatant was transferred to 16ml screw-top glass tubes. 50ul of 50% KOH (made with HPLC-grade water) was added, vortexed, and capped. The samples were then heated in 60^{o}C water bath or oven for 1 hour. The reaction was arrested by cooling in ice water bath briefly, then adding 450 µl of 1M HCl (made with HPLC-grade water), and vortexed. 1 ml HPLC-grade Hexane was added, tubes capped, and vortexed for 30 seconds. Tubes were centrifuged for 10 minutes at 2000rpm until 2 distinct layers were seen. The lower organic layer was transferred using a glass Pasteur pipet to a new 13x100mm tube. The organic layer were completely dried down under argon. Samples were then reconstituted with 180 µl of HPLC-grade MeOH. Lipid signals were extracted using lipid extraction for panel method, as noted above.

3.2.6 OxPAPC Lipid Extraction from Mitochondria Isolated from Heart Tissue and Cells

Equal mitochondrial protein were added from each sample and the volume adjusted to 100 µl with more HPLC grade water into a new 1.5 ml Eppendorf tube and then the following were added: 600 µl of HPLC-grade 1-butanol, 30 µl of internal standard mix (500 ng/ml), and 400 µl brine (10% NaCl made with HPLC-grade water). Samples were vortexed for 1 minute and centrifuged at 2000rpm for 10 minutes. Upper organic phase were transferred to new 12x75mm glass tubes and the butanol was evaporated under argon. Samples were reconstituted with 150 µl HPLC-grade MeOH and transferred to a labelled 1.5ml Eppendorf tube. Tubes were then centrifuged at 13,600rpm for 10 minutes. 50 µl of the sample were then transferred to labelled MS Vial and delivered for analysis. The remainder of samples were stored in Eppendorf tube at -80^{o}C under argon atmosphere.[51]

3.2.7 LC-MS/MS Methods

Lipid Panel and oxPAPC Panel

The LC-MS/MS methods utilized for the lipid and oxPAPC panels were adopted from Meriwether, et al., as previously described.[51]

Phospholipid Analysis

We modified a method outlined by Vu, et al., for our initial baseline mitochondrial membrane phospholipid characterization.[77] For our subsequent evaluation of the 13 lipid classes post-IRI, we utilized the services of the UCLA Lipidomics Core, which uses the following method: “This is a mass spectrometry-based approach that involves direct infusion of lipid samples into the AB SCIEX Lipidyzer Platform: a SCIEX 5500 triple-quadrupole (QQQ) with a Shimadzu auto-sampler configured for direct infusion experiments, SelexION ion mobility device, and Shimadzu LC. Backend analysis is

performed using Sciex proprietary Lipidyzer software. When combined with SCIEX's proprietary lipids standard sets, this instrument can provide accurate, quantitative measurements of over 1000 lipid species across 13 lipid classes within a biological sample." (this method is taken directly from the website of the UCLA Lipidomics Core [https://www.uclalipidomics.net/services-755110.html]).

3.2.8 Statistical Analysis

Student's t-tests were carried out between all studies with two groups. Data from experiments with more than 2 or more groups were compared using a one-way ANOVA model. After a significant overall group effect was established, Tukey's pairwise comparisons were carried out to determine specific group to group differences. All data is represented as mean±SEM. A p-value less than 0.05 was considered statistically significant.

3.3 Results

3.3.1 PON2 deficiency alters mitochondrial membrane phospholipid composition.

To determine if PON2 deficiency inherently affects the mitochondria membrane, specifically the phospholipid composition, I sought to characterize the mitochondrial membrane phospholipid composition in WT and PON2-def mice (n=4/group) under baseline conditions (Figure 7). Mitochondria were isolated from both WT and PON2-def mice and phospholipids were extracted. The phospholipid composition, including various acyl chain combinations, of LPC, PC, PE, PG, PI, and PS was determined via LC-MS/MS. Many PC species were significantly reduced compared WT controls (Figure 7A), while PE had one species (42:9) that was significantly elevated (Figure 7B). There were no significant changes observed between the groups for PG, PI, and PS (Figure 7C-E).

Subsequently, I wanted to evaluate the phospholipid changes in both WT and PON2-def mice (n=4/group) post-IRI. 13 lipid classes were then evaluated in the mitochondria from the heart of these mice, along with the whole heart lysate generated during the mitochondria isolation process, via LC-MS/MS, as summarized in Supplemental Figure 5. Triglyceride levels were significantly down in the mitochondria and whole hearts of PON2-def mice versus WT controls (Supplementary Figure 5). Furthermore, when exploring specific lipid species, many PE and PC species containing linoleic acid (LA, 18:2) or arachidonic acid (AA, 20:4) esterified as one or both of their associated fatty acids were significantly increased in the PON2-def mice versus WT controls (Figure 8). Due to variation of the phospholipid classes and the increased

oxidative stress that occurs during myocardial IRI, I sought to further characterize and explore the potential lipid peroxidation that could be occurring in PON2-def mice.

3.3.2 Mitochondrial lipids experience increased oxidation under baseline conditions in PON2-def mice

Prior to exploring the role that PON2 deficiency has on mitochondrial lipid peroxidation, I characterized the mitochondrial lipid peroxidation in WT and PON2-def mice (n=6/group) under baseline conditions (Figure 9). Initially, free, unbound lipids (pre-saponification) were evaluated. Subsequently, the mitochondrial preps were saponified (post-saponification), releasing all the bound fatty acids from their respective phospholipids. Various oxidized lipids were measured, including oxidized metabolites of linoleic (HODEs) and arachidonic (HETEs) acid were measured. I observe that there was a significant increase in eicosanoid products (5-HETE, 12-HETE and 5-oxoETE) and oxidized LA metabolites (9-HODE and 13-HODE) in the mitochondria of PON2-def mice pre-saponification (Figure 9A) as well as 11-HETE and 12-HETE ($p=0.052$) post-saponification (Figure 9B), compared to WT controls. Lastly, oxidation of mitochondrial phospholipids was assessed, specifically measuring the levels of two prominent oxidized products of PC, POVPC and PGPC. I observe that there was a significant increase in both POVPC and PGPC in the mitochondria of PON2-def mice versus WT controls (Figure 9C).

Having determined that there is an inherent susceptibility for oxidation in mitochondrial lipids of PON2-def mice, I investigated the effects of this phenotype during IRI as well as measuring any further mitochondrial lipid peroxidation.

3.3.3 PON2 deficiency leads to increased mitochondrial lipid peroxidation during myocardial IRI

To study the effects that myocardial IRI has on mitochondrial lipids, WT and PON2-def mice (n=4/group) were subjected to IRI. The mitochondria were isolated from the hearts of the mice and lipids were extracted, both pre-saponification and post-saponification. Various eicosanoid products, including oxidized metabolites of LA (HODEs) and AA (HETEs) were measured. I observe that in the pre-saponified mitochondria, there is a significant increase in 12-HETE and 15-HETE, while 9-HODE significantly decreases in the PON2-def mice versus controls (Figure 10A). Moreover, 15-HETE is significantly increased post-saponification in the myocardial mitochondria of PON2-def mice when compared to WT mice (Figure 10B). When evaluating phospholipid oxidation, POVPC is significantly increased in the mitochondrial hearts of PON2-def mice versus WT controls.

Given the consistent oxidation of lipids, specifically arachidonic acid, and PC in the myocardial mitochondria of PON2-def mice (versus WT), I sought to determine whether overexpression of PON2 can rescue any of these oxidative phenotypes.

3.3.4 PON2 overexpression has the capacity to partly rescue mitochondrial lipid oxidation post-IRI

H9c2 cells stably expressing EV or hPON2, as described in chapter 2, were utilized to test the protective role that PON2 overexpression could have against mitochondrial lipid peroxidation. These cells were subjected to HRI and lipid

peroxidation was assessed (Figure 11). H9c2-hPON2 cells have significantly reduced 12-HETE (Figure 11A) and POVPC (Figure 11B) levels versus EV controls.

These data suggest the protective role that PON2 plays in mitigating oxidation of mitochondrial lipids. Next, I sought to investigate what potential mechanisms could be underlying this protection against myocardial IRI.

3.3.5 Cytoplasmic PLA2 and prostanoids levels potentially mediate PON2 protective role against mitochondrial peroxidation post myocardial IRI.

I sought to probe the mechanisms behind the changes observed in phospholipid composition and the production of eicosanoids in the mitochondria of my *in vivo* and *in vitro* IRI experiments by examining cytoplasmic PLA2 and downstream production of pro-inflammatory/pro-resolving prostanoids. I examined the expression of cytoplasmic PLA2 (cPLA2) protein levels by western blot, on whole heart lysates from PON2-def mice and WT mice (n=4/group) subjected to myocardial IRI (Figure 12). There is a significant increase of cPLA2 levels in the PON2-def hearts versus WT controls as seen in Figure 12A, and as quantified in Figure 12B. Furthermore, when examining the prostanoid production, specifically of prostaglandins (PGE_2, PGF2α, and PGD_2) and prostacyclin (6-keto PGF1α), I observe that 6-keto PGF1α, PGE_2, PGF2α, and PGD_2, are all significantly decreased in the myocardial mitochondria of PON2-def mice when compared to WT controls (Figure 12A). However, the opposite is observed in the H9c2-hPON2 cells, with a significant increase in 6-keto PGF1α and PGE_2, when compared to EV controls. This data suggests that PON2 plays a role in modulating phospholipid

composition by modulating cPLA$_2$ levels as well as influencing the production of various pro-inflammatory/pro-resolving prostanoids during myocardial IRI.

3.4 Discussion

This study aimed to explore the role that PON2 plays in modulating mitochondrial lipid composition and peroxidation. Initially, I characterized the baseline changes of the mitochondrial phospholipid composition between WT and PON2-def mice. I observed that there is significant decrease in PC species and an increase in one PE species in the myocardial mitochondria of PON2-def mice versus WT controls, with no significant differences in PG, PI, or PS levels (Figure 7A-E). Moreover, when evaluating any mitochondrial lipid changes post-IRI, I observed that the trend towards increased PE species held true, with a significant increase in various PE species, while one PC species increased (Figure 8). Of note, the polyunsaturated fatty acids (PUFA) esterified into these membrane phospholipids are linoleic acid (18:2) and AA (20:4). Moreover, the oxidation of these particular PUFAs, under conditions of oxidative stress or enzymatically via cyclooxygenase and lipoxygenase, results in the formation of eicosanoids and prostanoids, both of which are critical signaling molecules affecting a host of inflammatory responses in various disease models, including CVD and myocardial IRI.[33, 51, 78]

Consequently, I investigated the role that PON2 plays in modulating the levels of free, unesterified (pre-saponification) and esterified (post-saponification) mitochondrial lipid peroxidation of PUFAs. Interestingly, I found that even under baseline conditions, PON2-def mice were more susceptible to oxidation of AA with significantly increased unesterified 15-HETE (Figure 9A) and esterified 12-HETE (Figure 9B) versus controls. Furthermore, there is a significant increase in unesterified 12-HETE and 15-HETE (Figure 10A) and esterified 15-HETE (Figure 10B) post-IRI in the myocardial

mitochondria of PON2-def mice compared to WT controls. Additionally, PON2 overexpression decreased the levels of unesterified 12-HETE in H9c2 cells subjected to HRI (Figure 11A). Although PON2 deficiency increases oxidation of AA into these various eicosanoids, it remains unclear what specific lipoxygenases are being modulated by PON2 as well as the contribution of non-enzymatic oxidation by way of ROS, both of which remain to be elucidated. Next, I examined the role that PON2 plays in modulating prostanoids during myocardial IRI.

Many studies have demonstrated the cardioprotective effects that various prostanoids have against cardiovascular disease, including myocardial IRI.[34, 76] For example, both endogenous PGE_2 and exogenous EP_4 agonists protect the heart from IRI via EP_4, in which EP4-/- mice had a larger infarct size in the heart compared to WT controls.[29] These protective effects were in part by PGE_2 inhibitory effects on neutrophil function and regulation of the production of various inflammatory cytokines, like TNFα and IL-10, in macrophages via EP_4.[29] In addition, PGI_2, and its downstream metabolites including 6keto-PGF1α, have been shown to reduce the infarct size in dog hearts, and pig hearts, both of which demonstrated that the cardioprotective effects were in part mediated to inhibition of neutrophil migration.[31, 32] In this study, I observe that PON2 deficiency in myocardial IRI leads to a significant decrease in mitochondrial prostanoid levels (6-keto PGF1α, PGE_2, PGF2α, and PGD_2) (Figure 12A), while overexpression of PON2 in H9c2 cells subjected to HRI leads to a significant increase in 6-keto PGF1α and PGE_2. PON2 deficiency eliminates the cardioprotective effects afforded by prostanoid production, while PON2 overexpression can partly rescue the loss. Therefore, PON2's ability to differentially affect prostanoid production supports another

potential mechanism of action by which PON2 acts to modulate myocardial IRI, and further supports the therapeutic potential of PON2 against myocardial IRI.

The observed alterations of phospholipid composition and increased levels of oxidized PUFAs with differential PON2 expression, specifically unesterified AA products, led me to consider the potential role that phospholipase expression could play in mediating this response. Cytoplasmic phospholipase 2 ($cPLA_2$), much like the other members of the PLA_2 superfamily, release free FAs and lysophospholipids from bound membrane phospholipids by hydrolyzing the *sn*-2 ester bond in phospholipids.[79] $cPLA_2$ is located in the cytosol and it's activation is calcium-dependent (μM) in order to translocate to membrane phospholipids where it selectively hydrolyzes arachidonylated phospholipids.[79, 80] Moreover, cPLA2 activation has also been shown to be activated by oxidative stress and has been implicated in an array of oxidative and inflammatory pathologies including neurogenerative, cancer, and cardiovascular diseases.[79-81] More specifically, $cPLA_2$ plays a significant role in modulating myocardial IRI through the hydrolysis of cardiac phospholipids resulting in the increased release of unesterified AA and subsequent production of various eicosanoids and prostanoids, with some studies showing improved cardiac recovery with anti-PLA_2 treatment.[33, 75, 82, 83] Therefore, I evaluated the levels of $cPLA_2$ in PON2-def hearts post-IRI and discovered that cPLA2 is significantly increased compared to WT controls (Figure 12). This result sheds some light on a potential mechanism of action for the role that PON2 plays in modulating lipid oxidation during myocardial IRI, particularly in explaining the increase in mitochondrial unesterified PUFA (AA and LA) metabolites in PON2-def mice. Nevertheless, it is worth noting that while cPLA2 may explain the increase in release of AA and subsequent

eicosanoid levels, the decrease in prostanoid levels seems paradoxical. One possible explanation is that PON2 is specifically acting to modulate prostanoid production through cyclooxygenase (COX) 1 and 2, the key enzymes responsible for producing prostaglandins from AA.[51] Given that prostanoid production from AA is largely governed by COX, I hypothesize that PON2's modulation of prostanoids is governed by COX activity. In the context of our studies, PON2 deficiency during myocardial IRI inhibits COX2 thus reducing prostanoid production; and when PON2 is overexpression, COX2 is upregulated, increasing prostanoid production. Many papers have shown that COX2 is protective against myocardial IRI. In fact, recent studies demonstrated the detrimental effects of COX inhibition (via NSAIDs) and protective effects of COX2 overexpression on myocardial IRI, further supporting this hypothesis.[84, 85] However, additional dissection of this mechanism of action needs to be undertaken, specifically in determining the levels of COX 1 and 2 in my studies.

Although membrane phospholipids supply the PUFA associated moieties as substrates for phospholipases to act on, oxidized phospholipids, like POVPC and PGPC, can act as potent mediators of cardiovascular disease.[78, 86, 87] A recent study demonstrated that there was a significant increase in oxidized phospholipids (including POVPC and PGPC) in cardiomyocytes (both cellular and mitochondrial) post IRI.[88] Additionally, treatment with murine IgM natural antibody EO6, which only recognizes and bind oxidized phospholipids, attenuated oxidized phospholipid mediated cell death and resulted in a reduction of myocardial infarct size when transgenically expressed in mice subjected to IRI.[88] In this study, I observed that PON2 deficiency results in a significant increase of POVPC and PGPC under baseline conditions (Figure 9C), which

is then exacerbated following myocardial IRI, with a significant increase of POVPC (Figure 10C). Moreover, PON2 overexpression in H9c2 cells results in a significant reduction of POVPC during HRI (Figure 11B). This observation, coupled with PON2's ability to reduce eicosanoids and increase prostanoid levels during myocardial IRI, not only strengthens the protective role that PON2 can play as a therapeutic agent against myocardial IRI.

Finally, a recent study was just published connecting the association of various AA-derived lipid mediators, particularly HETEs, with the ensuing onset of acute MI in patients with CAD.[74] Our study clearly demonstrates the role of PON2 in modulating lipid peroxidation of AA-derived PUFAs, particularly eicosanoids (HETEs), with PON2 deficiency increasing mitochondrial eicosanoid production post-myocardial IRI. Consequently, this study further supports a mechanism of action for explaining the increased susceptibility of patients with the human PON2 $Ser_{311}Cys$ ($S_{311}C$) polymorphism for CAD, including myocardial MI.[9, 11, 55]

3.5 Conclusion

- Under baseline conditions, myocardial mitochondria from PON2-def mice have a significant reduction in PC species versus WT controls.
- There is a significant increase in unesterified and esterified eicosanoids, specifically 12-HETE and 15-HETE, as well as increased oxidized phospholipid species, POVPC and PGPC, in the cardiac mitochondria of PON2-def mice under baseline conditions and post myocardial IRI compared to WT mice. On the contrary, PON2 overexpression significantly reduces eicosanoid and oxidized phospholipid levels in H9c2 cells post-HRI, compared to EV controls.
- Cardiac mitochondria from PON2-def mice have significantly decreased production of prostanoids post myocardial IRI, while PON2 overexpression in H9c2 cells results in significantly increased prostanoid levels post-HRI, compared to controls.
- PON2 deficiency in the heart results in a significant increase of cPLA2 expression when compared to WT controls.

Figure 6

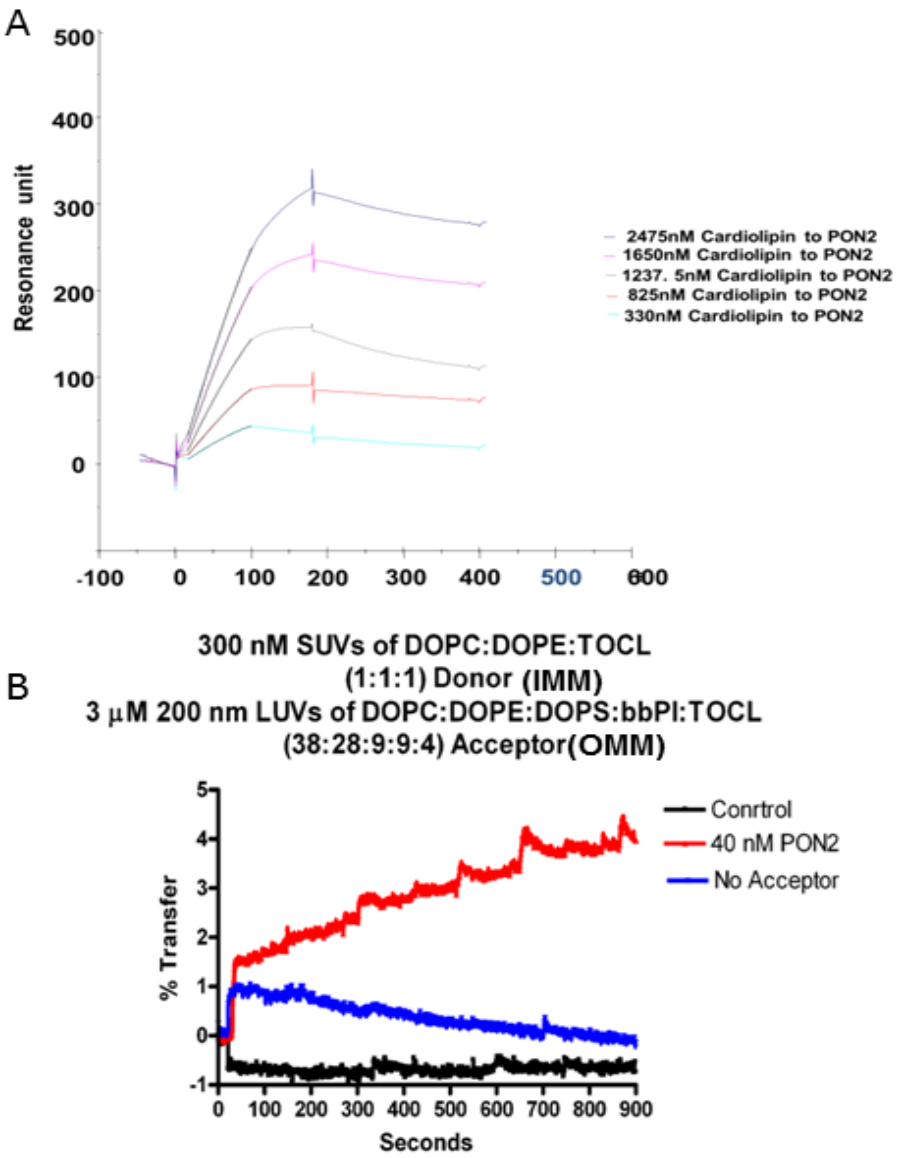

Figure 6: PON2 binds cardiolipin and transfers it from the IMM to OMM. (A) Using surface plasmon resonance, cardiolipin binds PON2 in a dose dependent manner. (B) Cardiolipin is transferred from the donor (IMM) to the acceptor (OMM) with the additon of 40 nM PON2, while no transfer is observed without an acceptor.

Figure 7A

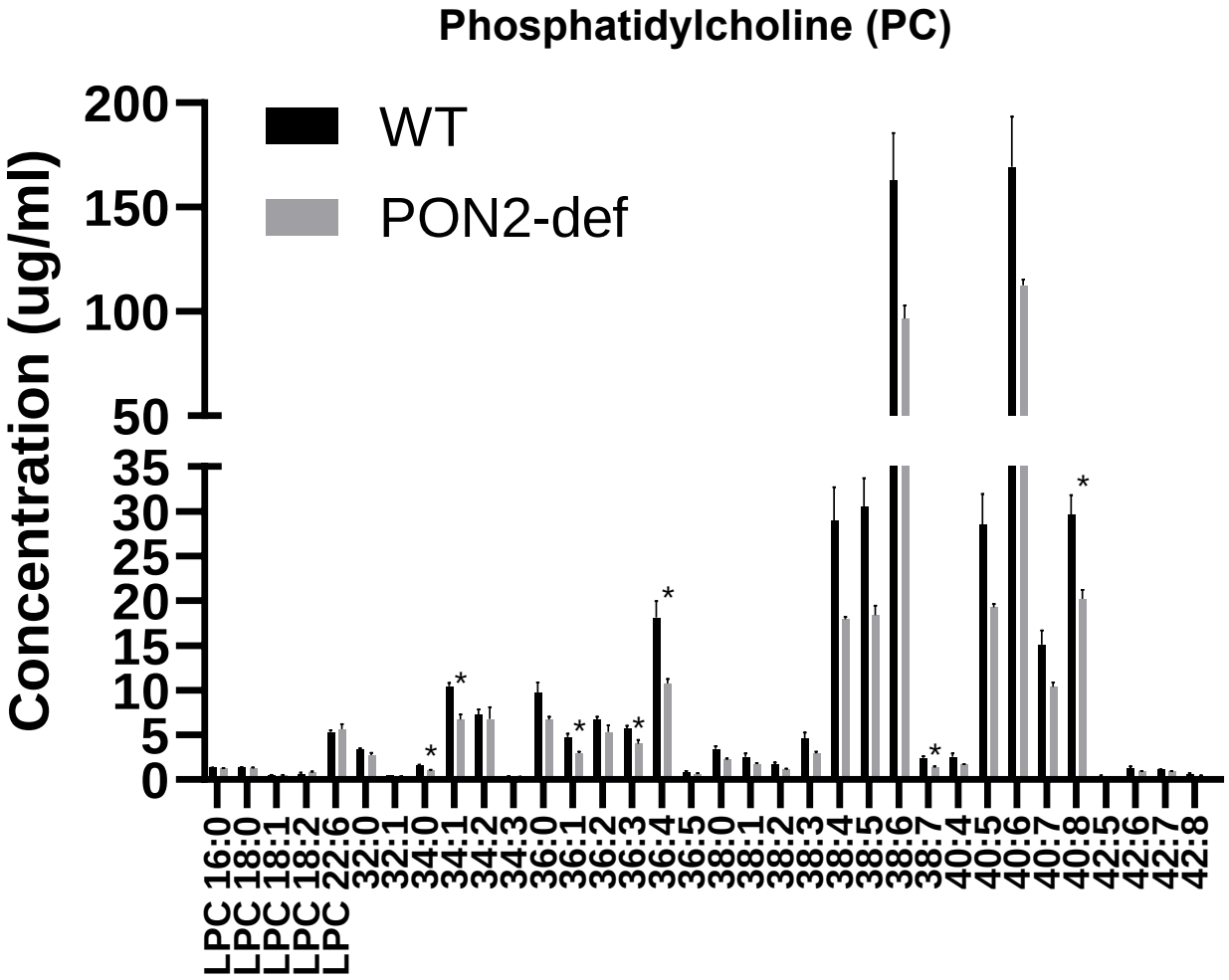
Phosphatidylcholine (PC)
WT
PON2-def
Concentration (ug/ml)
200
150
100
50
35
30
25
20
15
10
5
0
LPC 16:0
LPC 18:0
LPC 18:1
LPC 18:2
LPC 20:6
LPC 32:0
LPC 32:1
LPC 34:0
LPC 34:1
LPC 34:2
LPC 34:3
LPC 36:0
LPC 36:1
LPC 36:2
LPC 36:3
LPC 36:4
LPC 36:5
LPC 38:0
LPC 38:1
LPC 38:2
LPC 38:3
LPC 38:4
LPC 38:5
LPC 38:6
LPC 38:7
LPC 40:4
LPC 40:5
LPC 40:6
LPC 40:7
LPC 40:8
LPC 42:5
LPC 42:6
LPC 42:7
LPC 42:8

Figure 7B

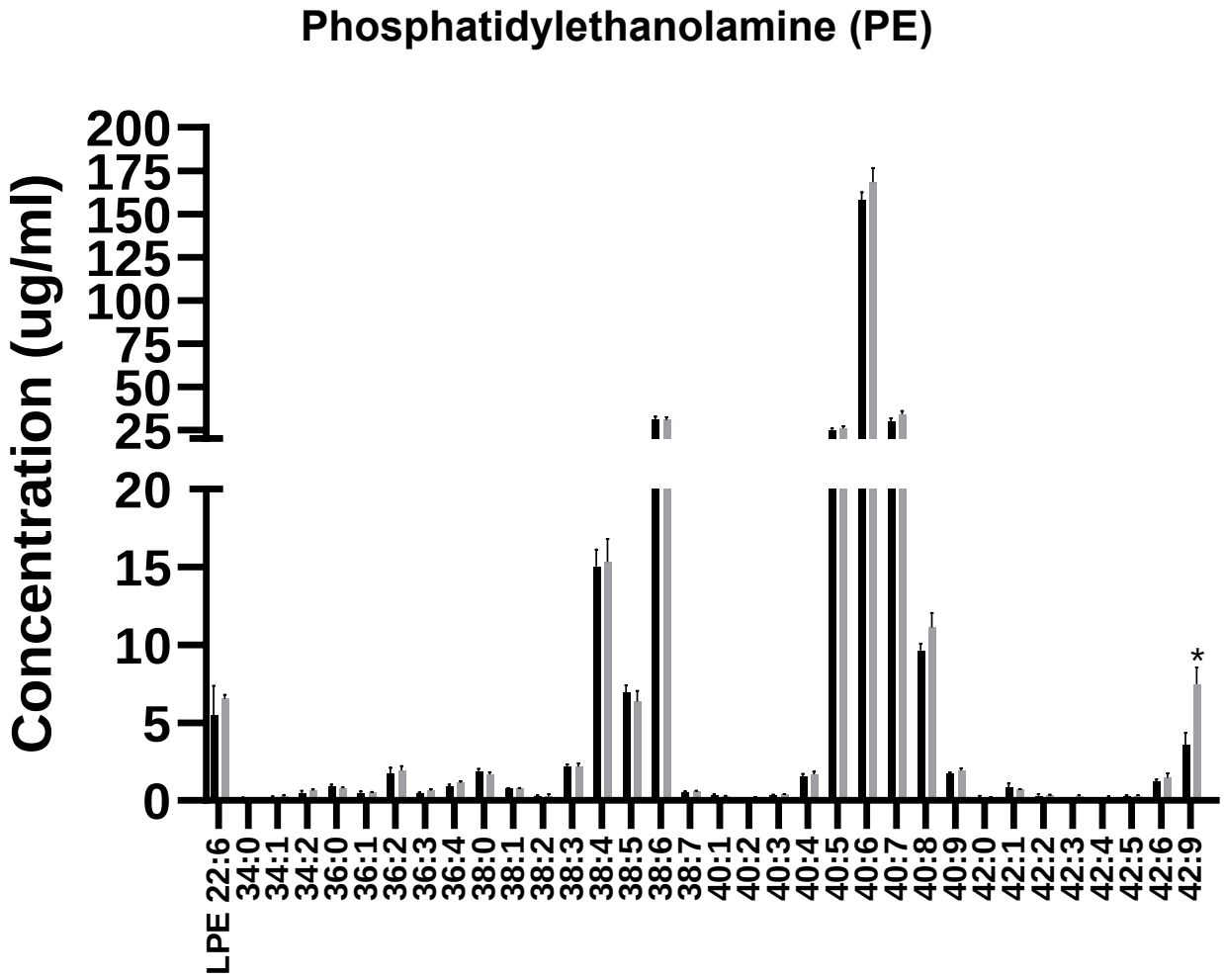
Phosphatidylethanolamine (PE)
Concentration (ug/ml)
200
175
150
125
100
75
50
25
20
15
10
5
0
*
LPE 22:6
34:0
34:1
34:2
36:0
36:1
36:2
36:3
36:4
38:0
38:1
38:2
38:3
38:4
38:5
38:6
38:7
40:1
40:2
40:3
40:4
40:5
40:6
40:7
40:8
40:9
42:0
42:1
42:2
42:3
42:4
42:5
42:6
42:9

Figure 7C

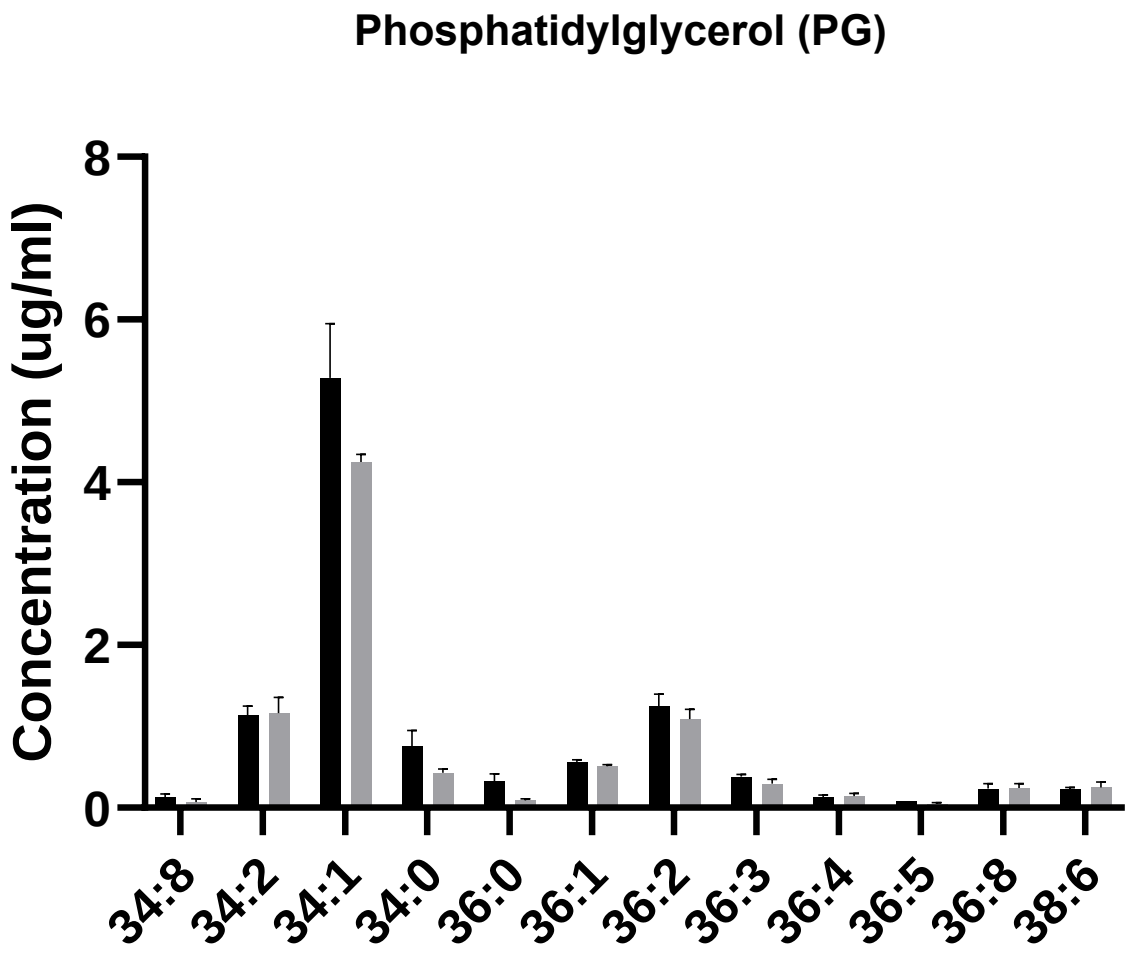
Phosphatidylglycerol (PG)
Concentration (ug/ml)
8
6
4
2
0
34:8
34:2
34:1
34:0
36:0
36:1
36:2
36:3
36:4
36:5
36:8
38:6

Figure 7D

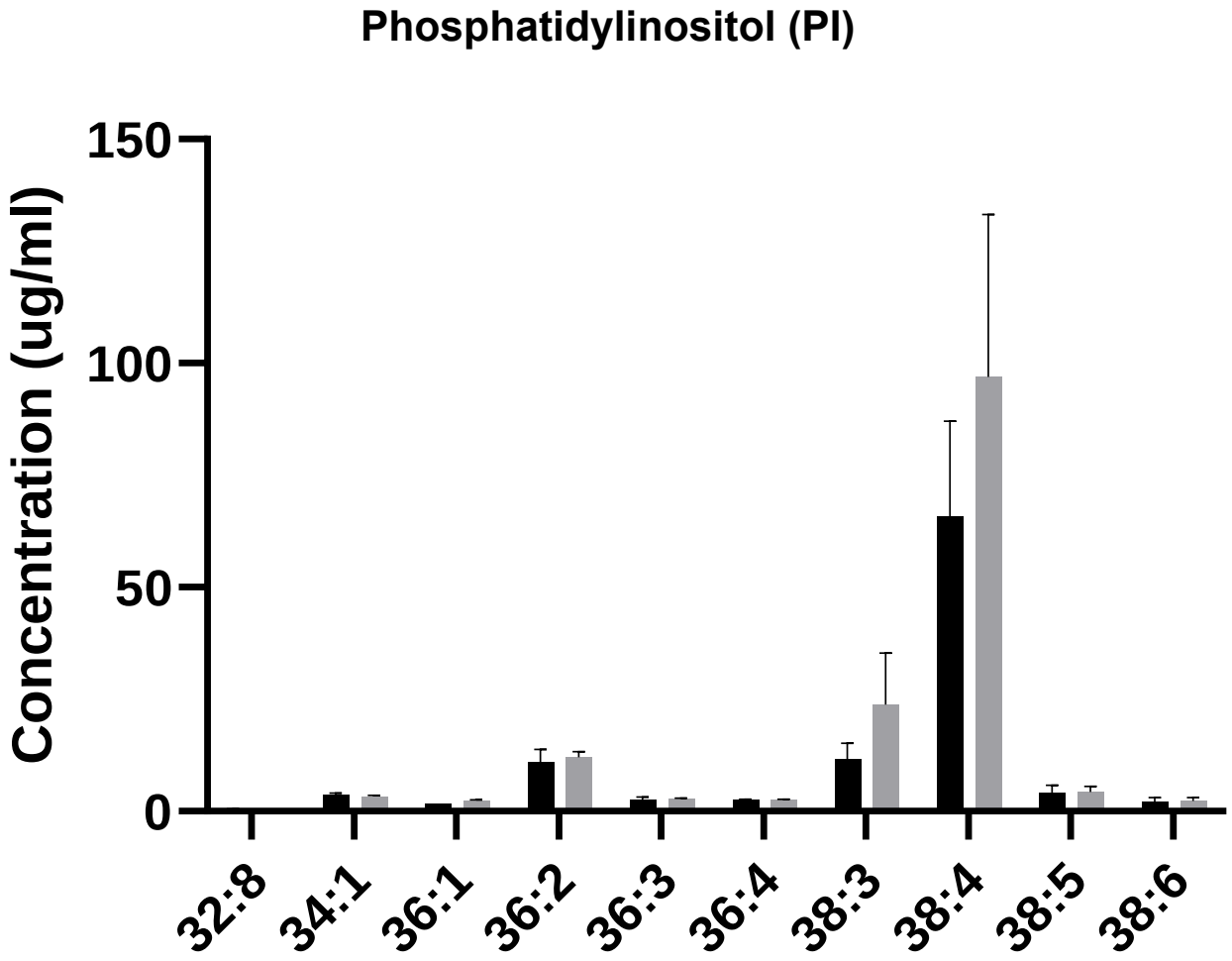
Phosphatidylinositol (PI)
Concentration (ug/ml)
150
100
50
0
32:8
34:1
36:1
36:2
36:3
36:4
38:3
38:4
38:5
38:6

Figure 7E

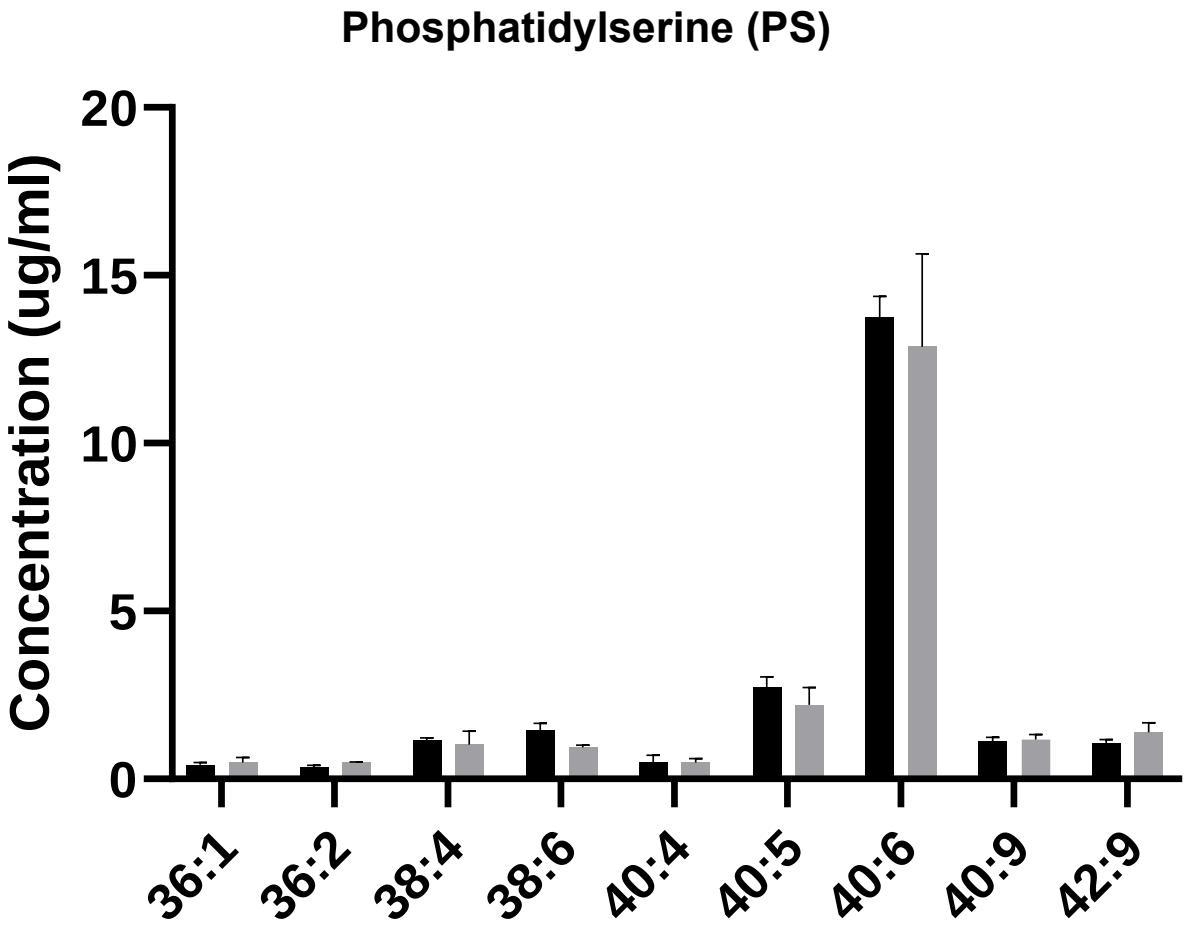
Phosphatidylserine (PS)
Concentration (ug/ml)
20
15
10
5
0
36:1
36:2
38:4
38:6
40:4
40:5
40:6
40:9
42:9

Figure 7: Mitochondrial Phospholipid Composition of WT and PON2-def mice under Baseline Conditions.

Various phospholipid classes and their varying acyl chain compositions, were measured from mitochondria isolated from whole hearts of WT and PON2-def mice (n=4/group) under baseline conditions using LC-MS/MS, including: (A) Lysophosphatidylcholine/Phosphatidylcholine (LPC/PC), (B) Lysophosphatidylethanolamine/Phosphatidylethanolamine (LPE/PE), (C) Phosphatidylglycerol (PG), (D) Phosphatidylinositol (PI), and (E) Phosphatidylserine (PS) were measured from. Concentrations of the phospholipids are in μg/ml. Data is represented as mean±SEM and statistically significant data is noted as *$p<0.05$.

Figure 8

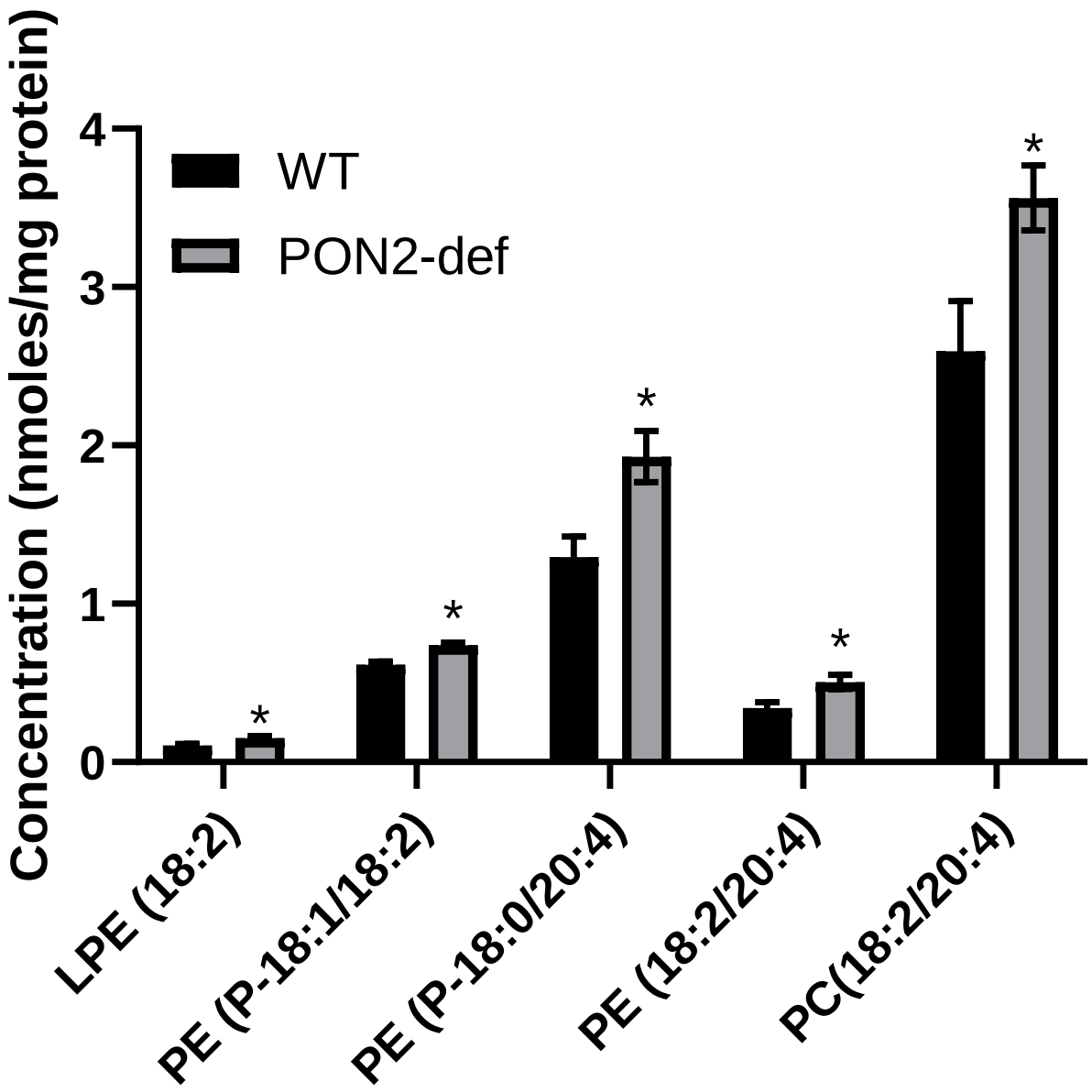
Concentration (nmoles/mg protein)
0
1
2
3
4
WT
PON2-def
*
*
*
*
*
LPE (18:2)
PE (P-18:1/18:2)
PE (P-18:0/20:4)
PE (18:2/20:4)
PC(18:2/20:4)

Figure 8: Mitochondrial Phospholipid Composition of WT and PON2-def mice post-IRI. Various phospholipid classes and their varying acyl chain compositions, were measured from mitochondria isolated from whole hearts of WT and PON2-def mice (n=4/group) post-IRI using LC-MS/MS, including: (A) Lysophosphatidylcholine/Phosphatidylcholine (LPC/PC), (B) Lysophosphatidylethanolamine/Phosphatidylethanolamine (LPE/PE), (C) Phosphatidylglycerol (PG), (D) Phosphatidylinositol (PI), and (E) Phosphatidylserine (PS) were measured from. Concentrations of the phospholipids are in μg/ml. Data is represented as mean±SEM and statistically significant data is noted as *$p<0.05$.

Figure 9A

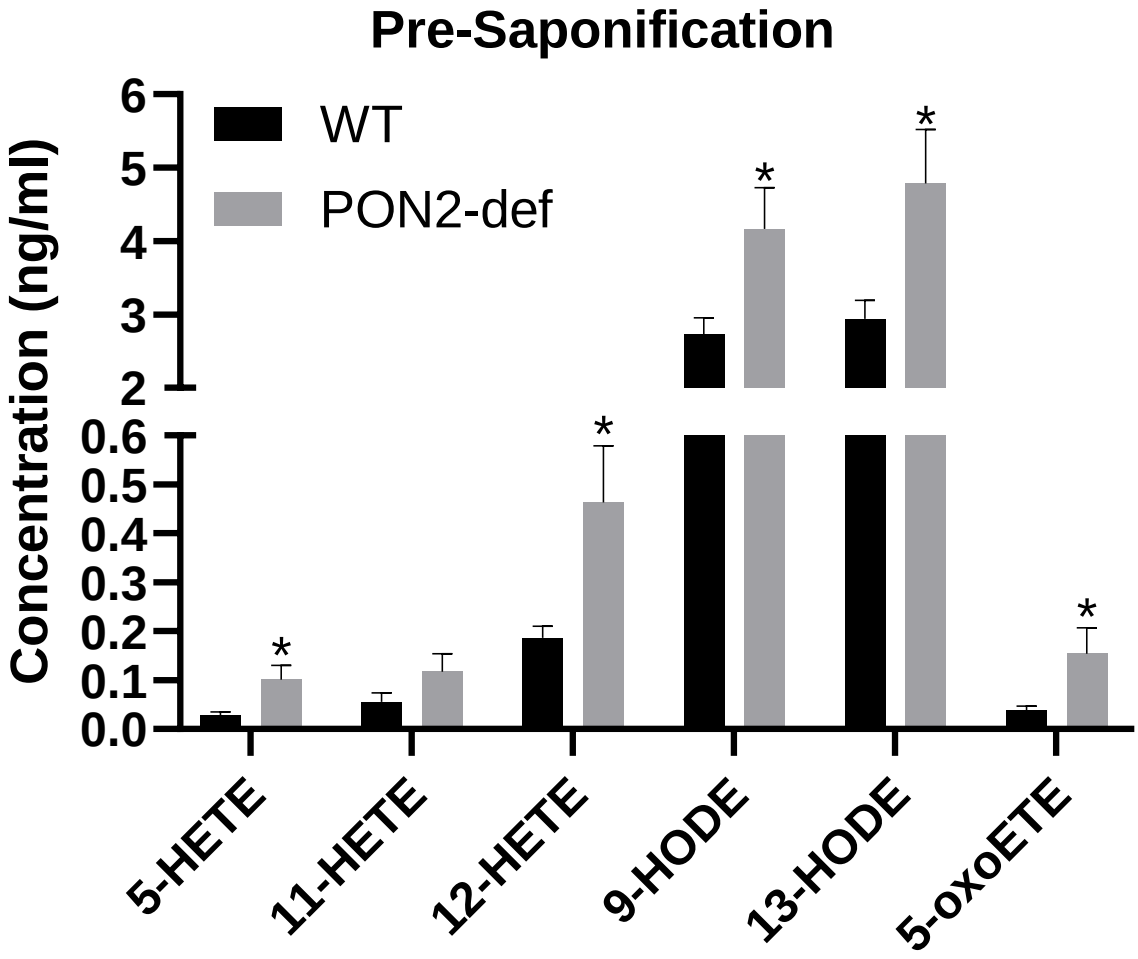
Pre-Saponification
WT
PON2-def
Concentration (ng/ml)
6
5
4
3
2
0.6
0.5
0.4
0.3
0.2
0.1
0.0
*
5-HETE
11-HETE
12-HETE
9-HODE
13-HODE
5-oxoETE

Figure 9B

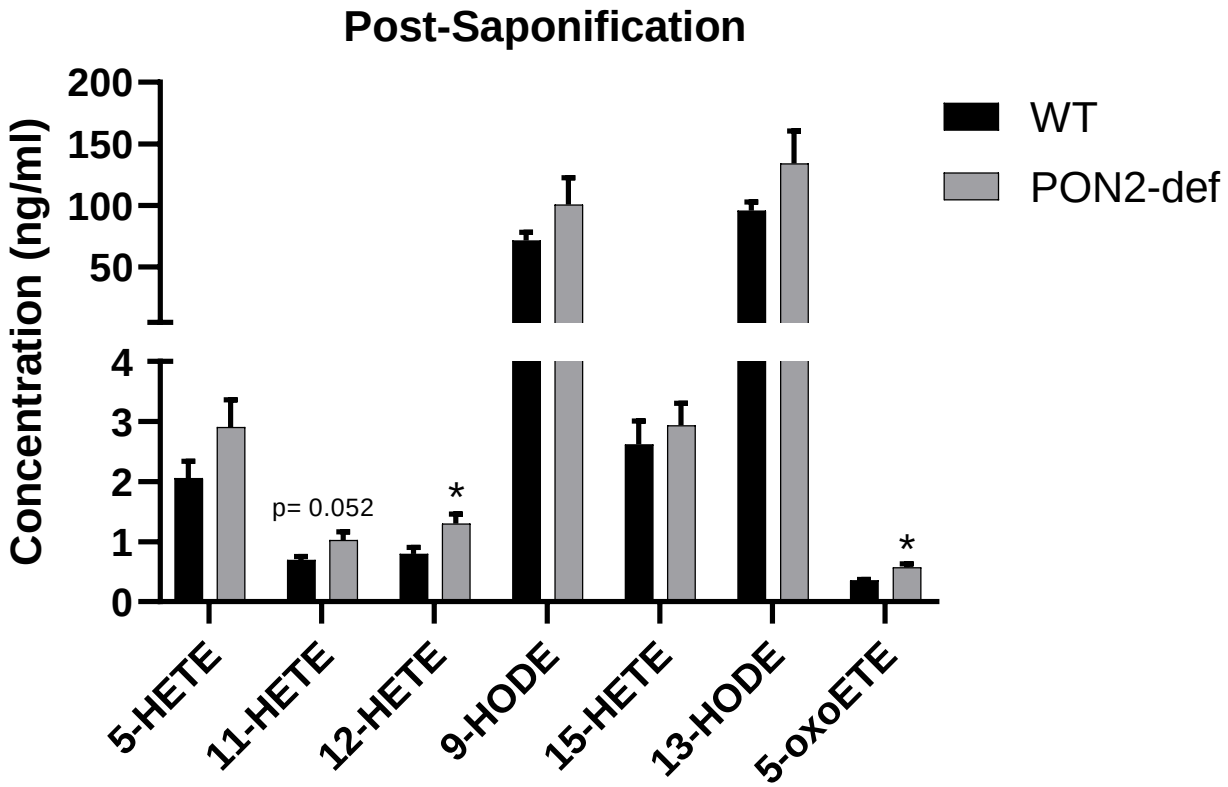
Post-Saponification
Concentration (ng/ml)
200
150
100
50
4
3
2
1
0
p= 0.052
*
*
WT
PON2-def
5-HETE
11-HETE
12-HETE
9-HODE
15-HETE
13-HODE
5-oxoETE

Figure 9C

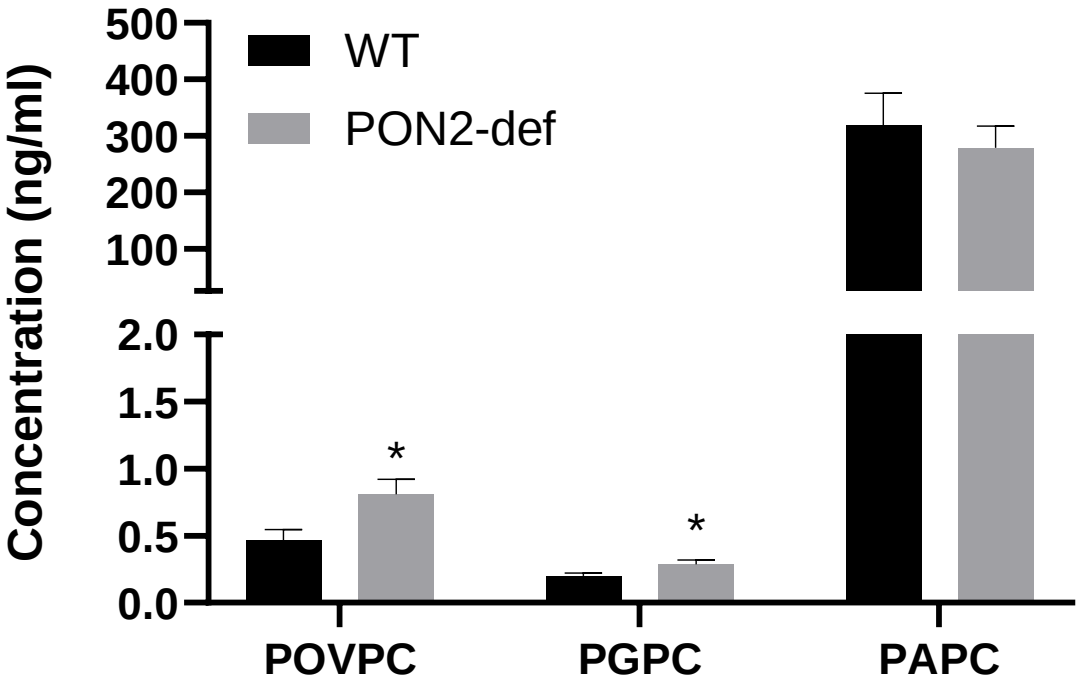
Concentration (ng/ml)
500
400
300
200
100
2.0
1.5
1.0
0.5
0.0
WT
PON2-def
*
*
POVPC
PGPC
PAPC

Figure 9: Mitochondrial phospholipid and lipid oxidation products in WT and PON2-def mice under baseline conditions. Mitochondrial lipids, specifically oxidized fatty acids derived from linoleic and arachidonic acid (11-HETE, 12-HETE, 9-HODE, 15-HETE, 13-HODE, and 5-oxoETE), from the hearts of WT and PON2-def mice (n=6/group) under baseline conditions were measured via LC-MS/MS both pre-sponification (A) and post-sponification (B). Oxidized PC products, POVPC and PGPC, were also measured (C). Concentrations of the lipids/phospholipids are in ng/ml. Data is represented as mean±SEM and statistically significant data is noted as *$p<0.05$.

Figure 10A

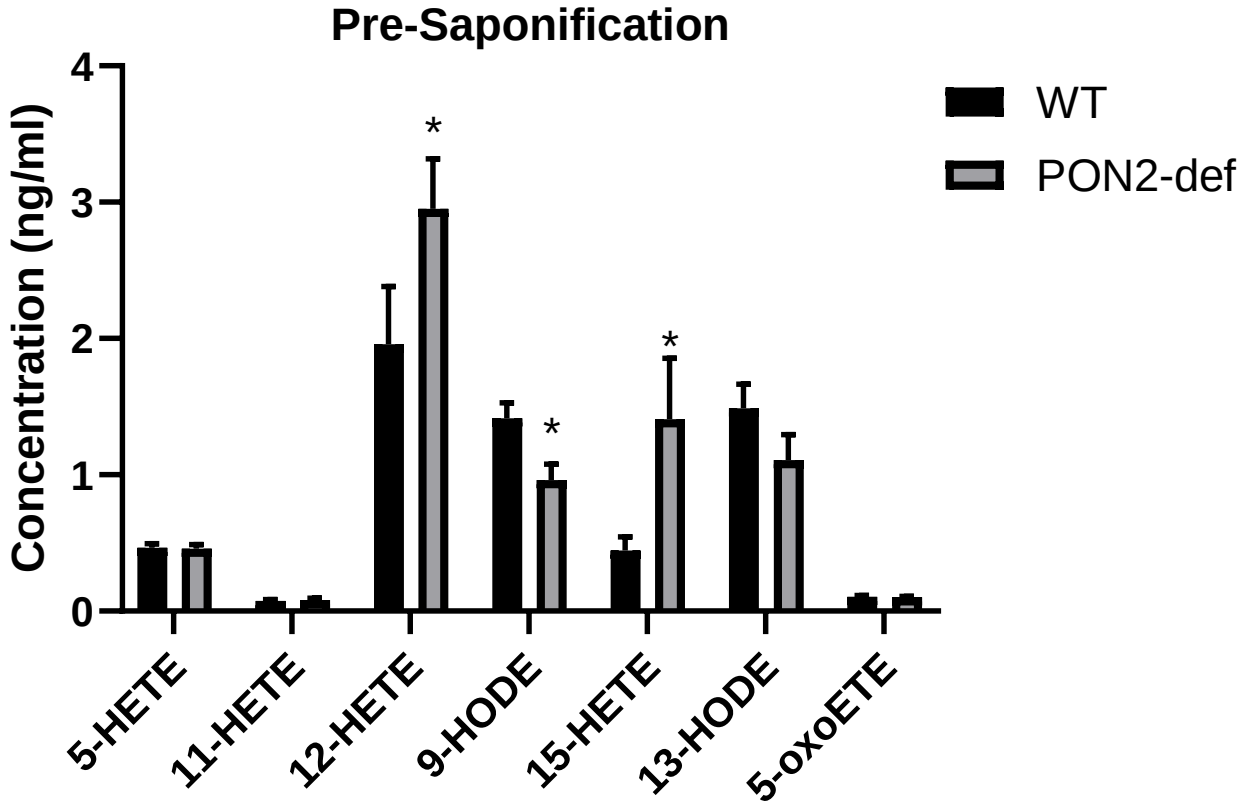
Pre-Saponification
Concentration (ng/ml)
4
3
2
1
0
*
*
*
WT
PON2-def
5-HETE
11-HETE
12-HETE
9-HODE
15-HETE
13-HODE
5-oxoETE

Figure 10B

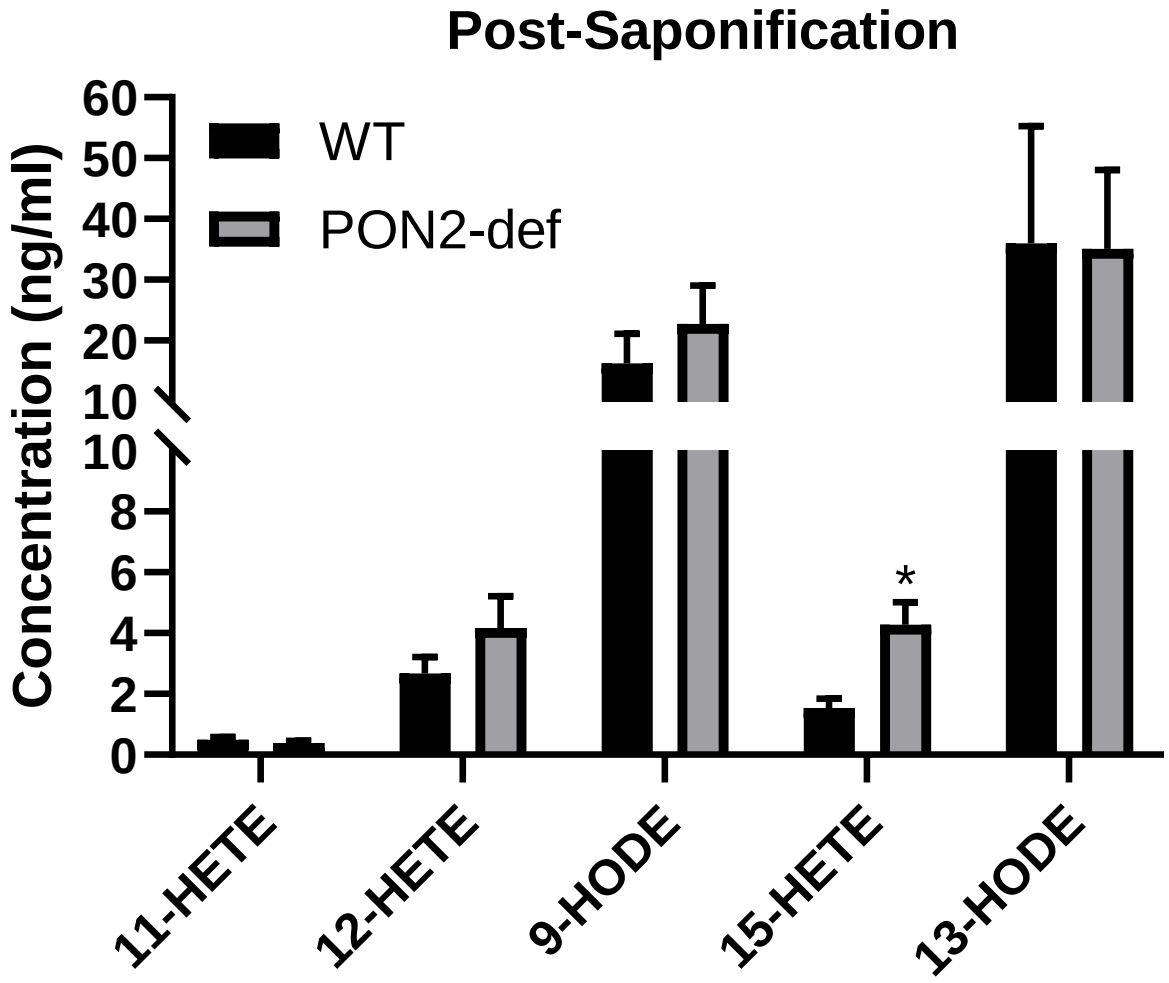
Post-Saponification
Concentration (ng/ml)
60
50
40
30
20
10
10
8
6
4
2
0
WT
PON2-def
*
11-HETE
12-HETE
9-HODE
15-HETE
13-HODE

Figure 10C

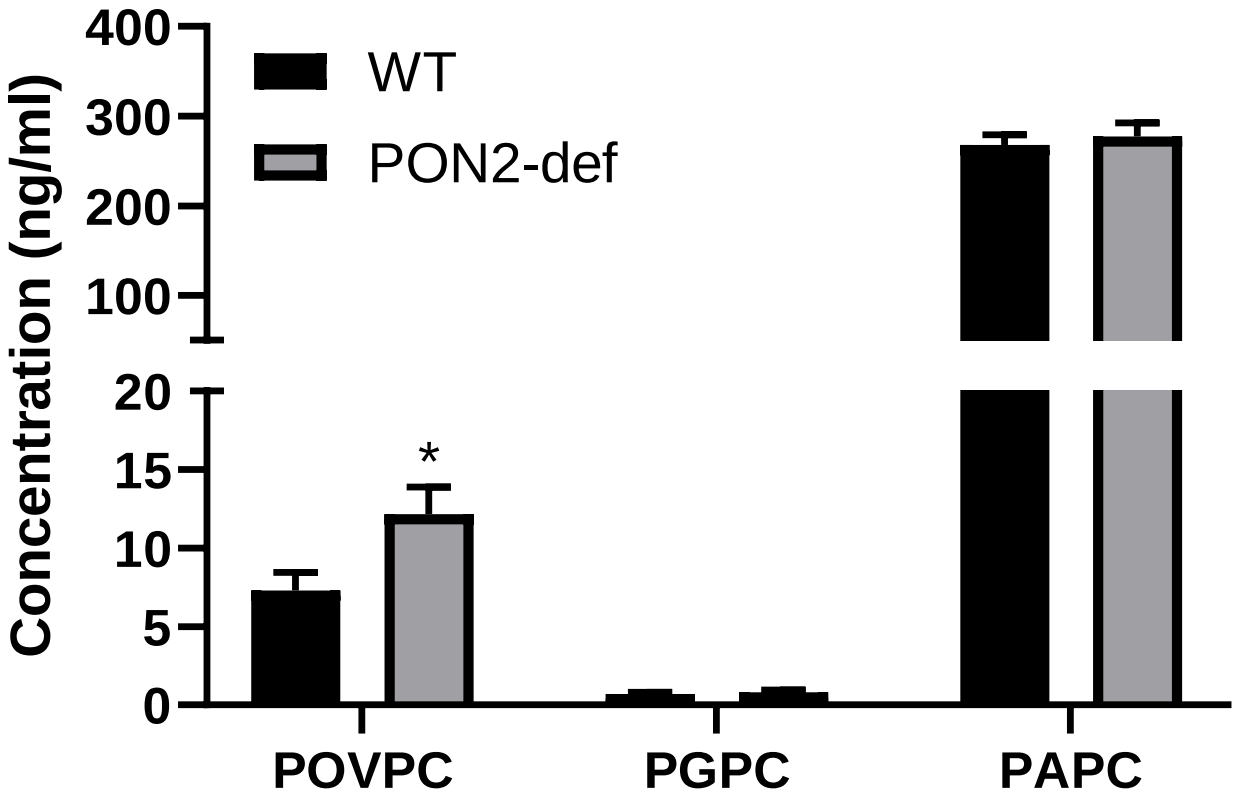
400
300
200
100
20
15
10
5
0
Concentration (ng/ml)
WT
PON2-def
*
POVPC
PGPC
PAPC

Figure 10: Mitochondrial phospholipid and lipid oxidation products in WT and PON2-def mice post-IRI. Mitochondrial lipids, specifically oxidized fatty acids derived from linoleic and arachidonic acid (5-HETE, 11-HETE, 12-HETE, 9-HODE, 15-HETE, 13-HODE, and 5-oxoETE), from hearts of WT and PON2-def mice (n=4/group) under baseline conditions were measured via LC-MS/MS both pre-sponification (A) and post-sponification (B). Oxidized PC products, POVPC and PGPC, were also measured (C). Concentrations of the lipids/phospholipids are in ng/ml. Data is represented as mean±SEM and statistically significant data is noted as *$p<0.05$.

Figure 11A

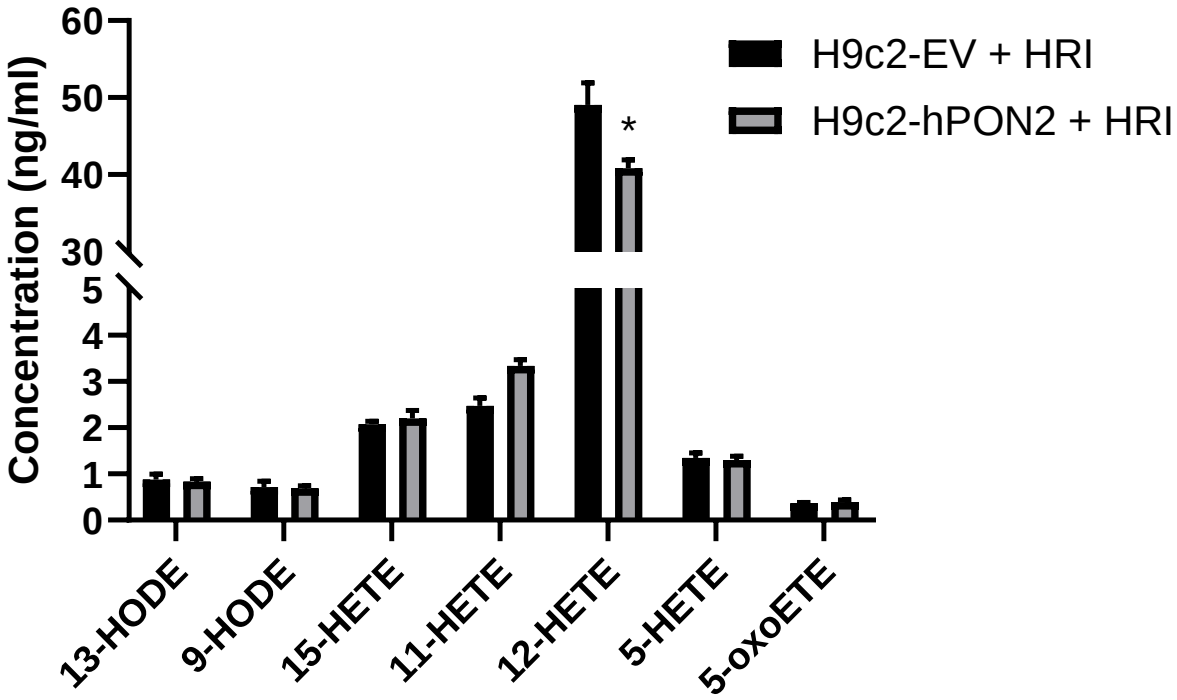
Concentration (ng/ml)
60
50
40
30
5
4
3
2
1
0
*
H9c2-EV + HRI
H9c2-hPON2 + HRI
13-HODE
9-HODE
15-HETE
11-HETE
12-HETE
5-HETE
5-oxoETE

Figure 11B

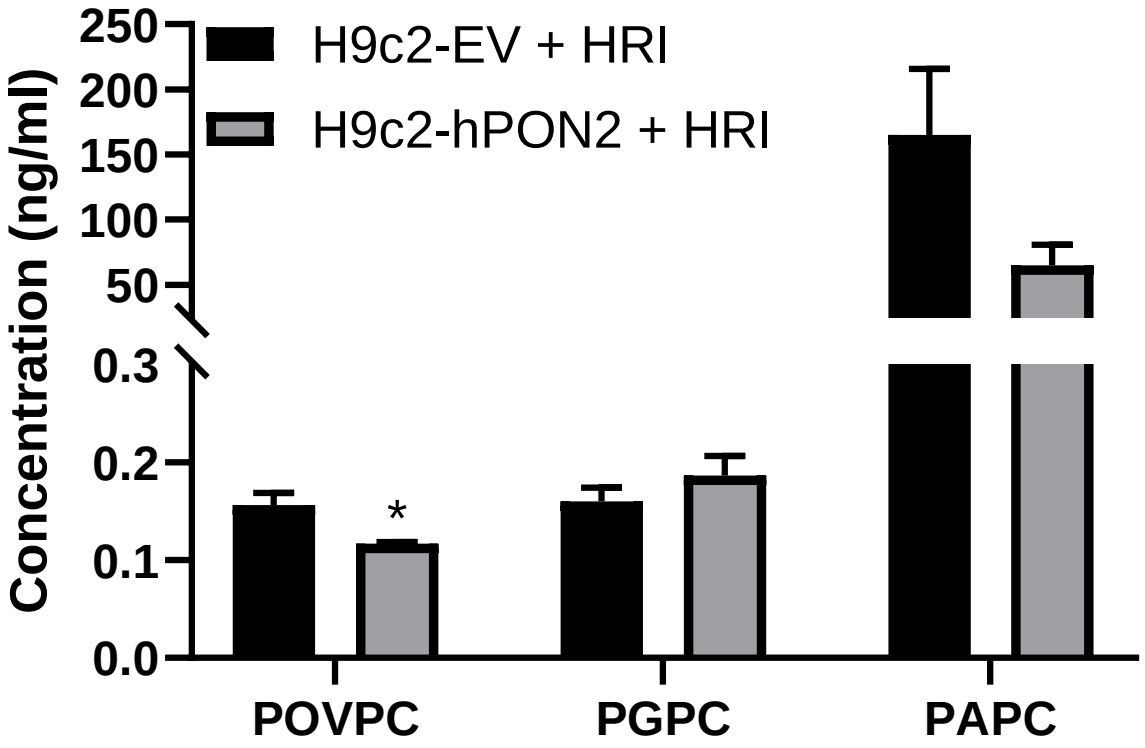
H9c2-EV + HRI
H9c2-hPON2 + HRI
Concentration (ng/ml)
250
200
150
100
50
0.3
0.2
0.1
0.0
*
POVPC
PGPC
PAPC

Figure 11: PON2 overexpression protects against phospholipid and lipid oxidation in H9c2 cells post-HRI. H9c2 cells stably expressing either EV or hPON2 (n=4/group) were treated with HRI (0% O_2) and lipid and phospholipid oxidation was evaluated. 12-HETE levels were significantly decreased in the H9c2-hPON2 group versus EV controls (A). Furthermore, POVPC was significantly reduced in the H9c2-hPON2 group versus EV controls (B). Concentrations of the lipids/phospholipids are in ng/ml. Data is represented as mean±SEM and statistically significant data is noted as *$p<0.05$.

Figure 12A

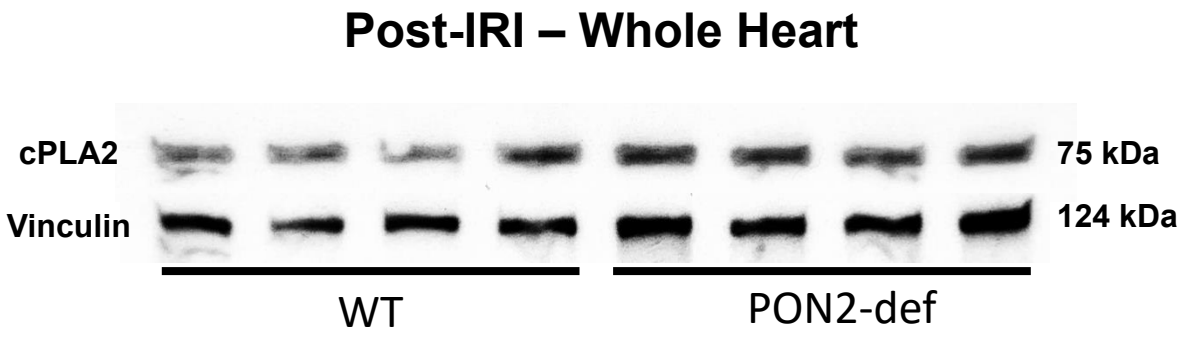

Figure 12B

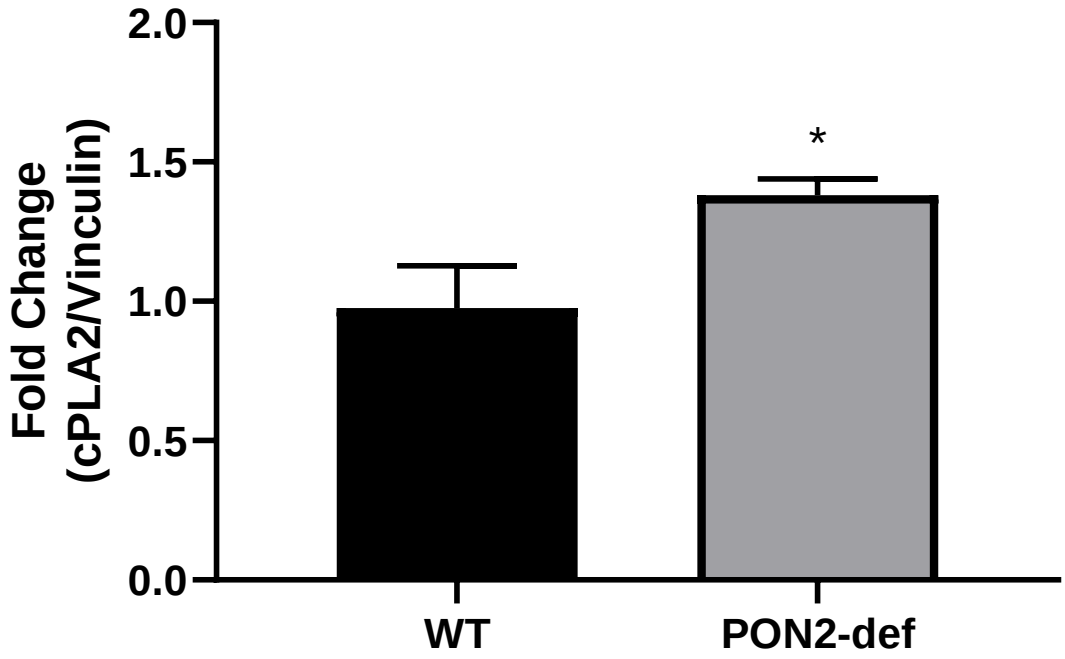

Figure 12: Cytoplasmic PLA2 expression in WT and PON2-def Hearts post-IRI. Cytoplasmic PLA2 (cPLA2) protein expression was determined in whole heart lysates from WT and PON2-def mice (n=4/group) post-IRI via western blot analysis (A), normalized to vinculin (A), and quantified as a ratio of cPLA2 to vinculin (B). The data is represented as Mean ± SEM and statistically significant data is noted as *$p<0.05$.

Figure 13A

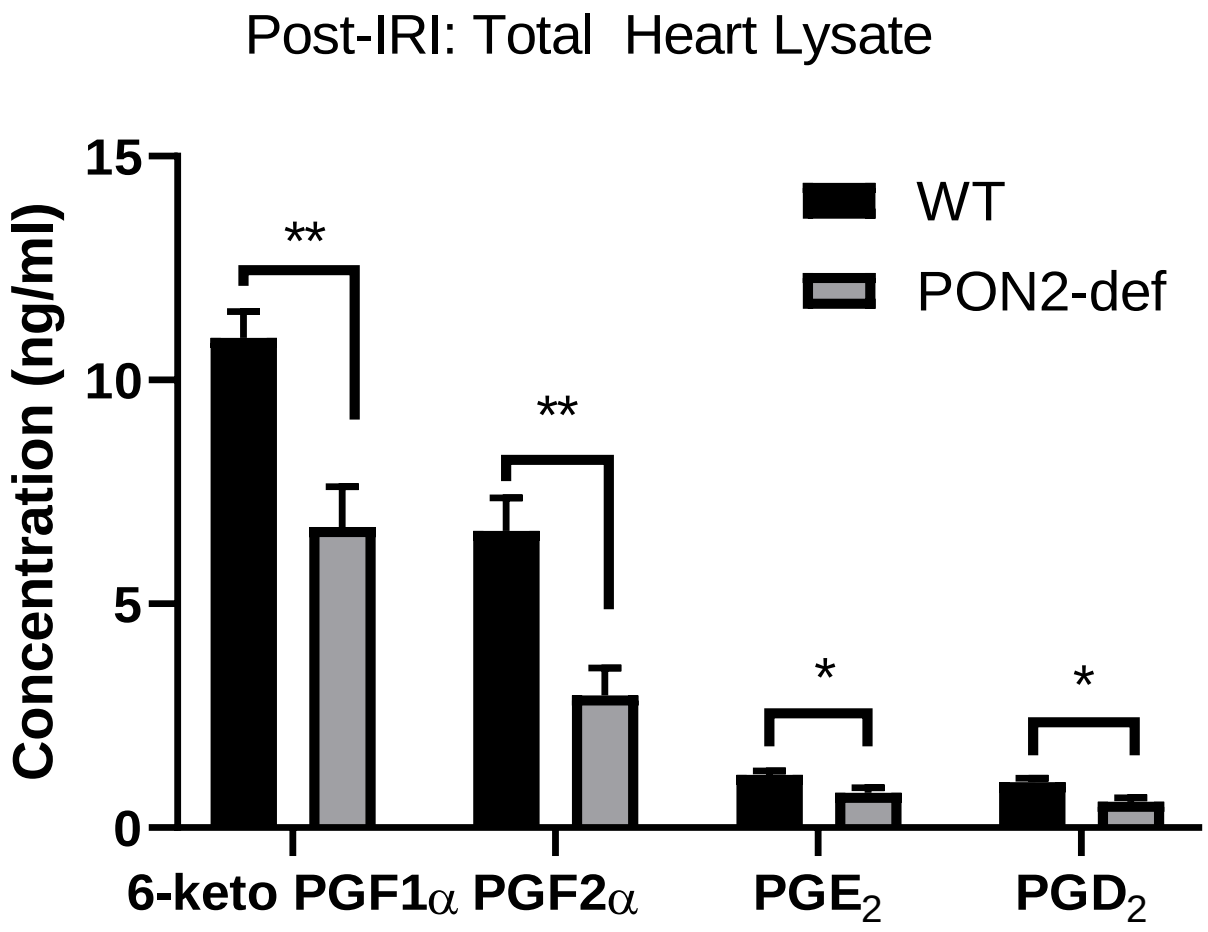
Post-IRI: Total Heart Lysate
Concentration (ng/ml)
15
10
5
0
**
**
*
*
WT
PON2-def
6-keto PGF1α
PGF2α
PGE2
PGD2

Figure 13B

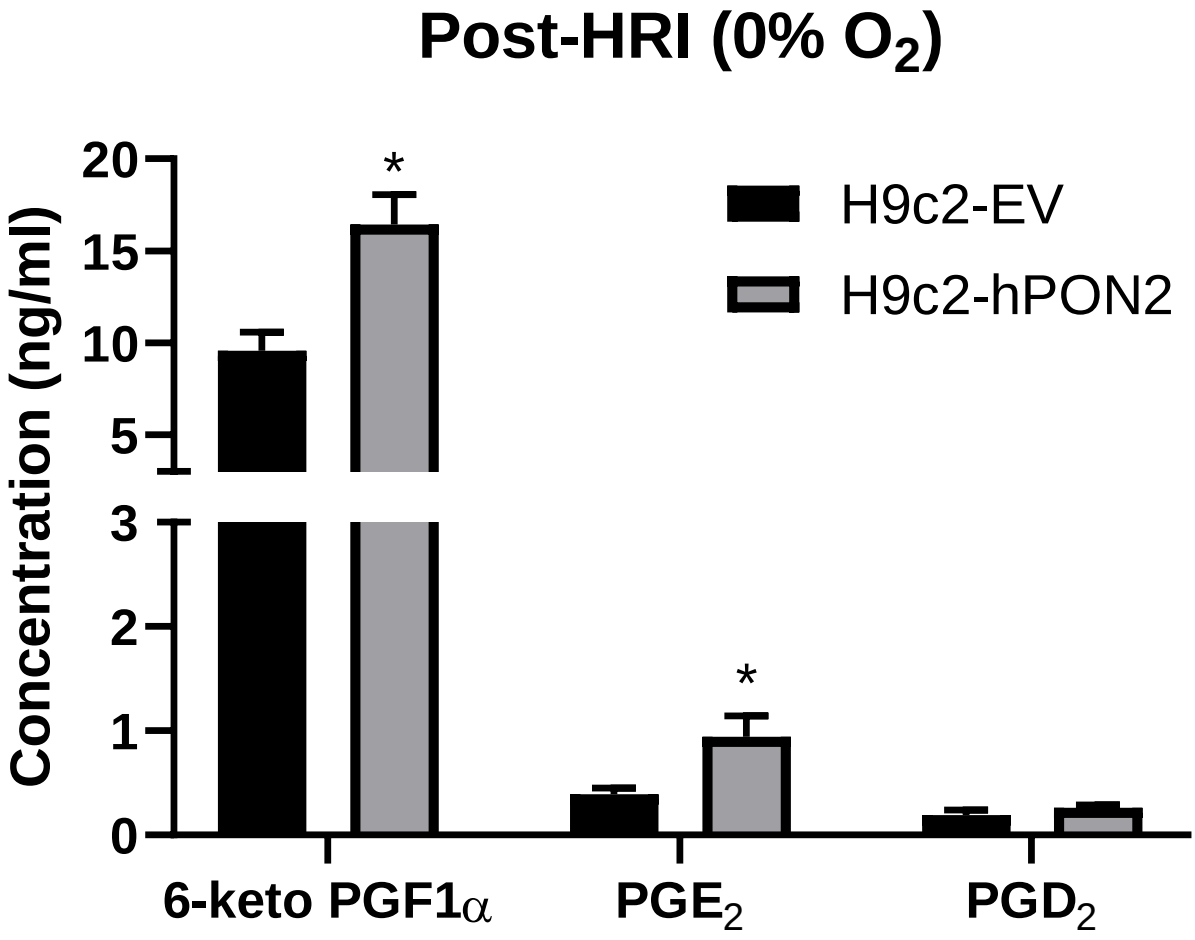
Post-HRI (0% O_2)
Concentration (ng/ml)
20
15
10
5
3
2
1
0
*
*
H9c2-EV
H9c2-hPON2
6-keto PGF1α
PGE_2
PGD_2

Figure 13: Prostaglandin levels in the hearts of WT and PON2-def mice as well as in H9c2 cells (EV vs hPON2) post-IRI. Various prostaglandins, including 6-keto $PGF1_{\alpha}$, PGE_2, $PGF2_{\alpha}$, and PGD_2, were measured in total heart lysates of WT and PON2-def mice post-IRI (n=4/group) (A) and in H9c2 cells (EV and hPON2) subjected to HRI (n=4/group) (B) via LC-MS/MS. Concentrations of the prostaglandins are in ng/ml. Data is represented as mean±SEM and statistically significant data is noted as *$p<0.05$.

Supplementary Figure 5

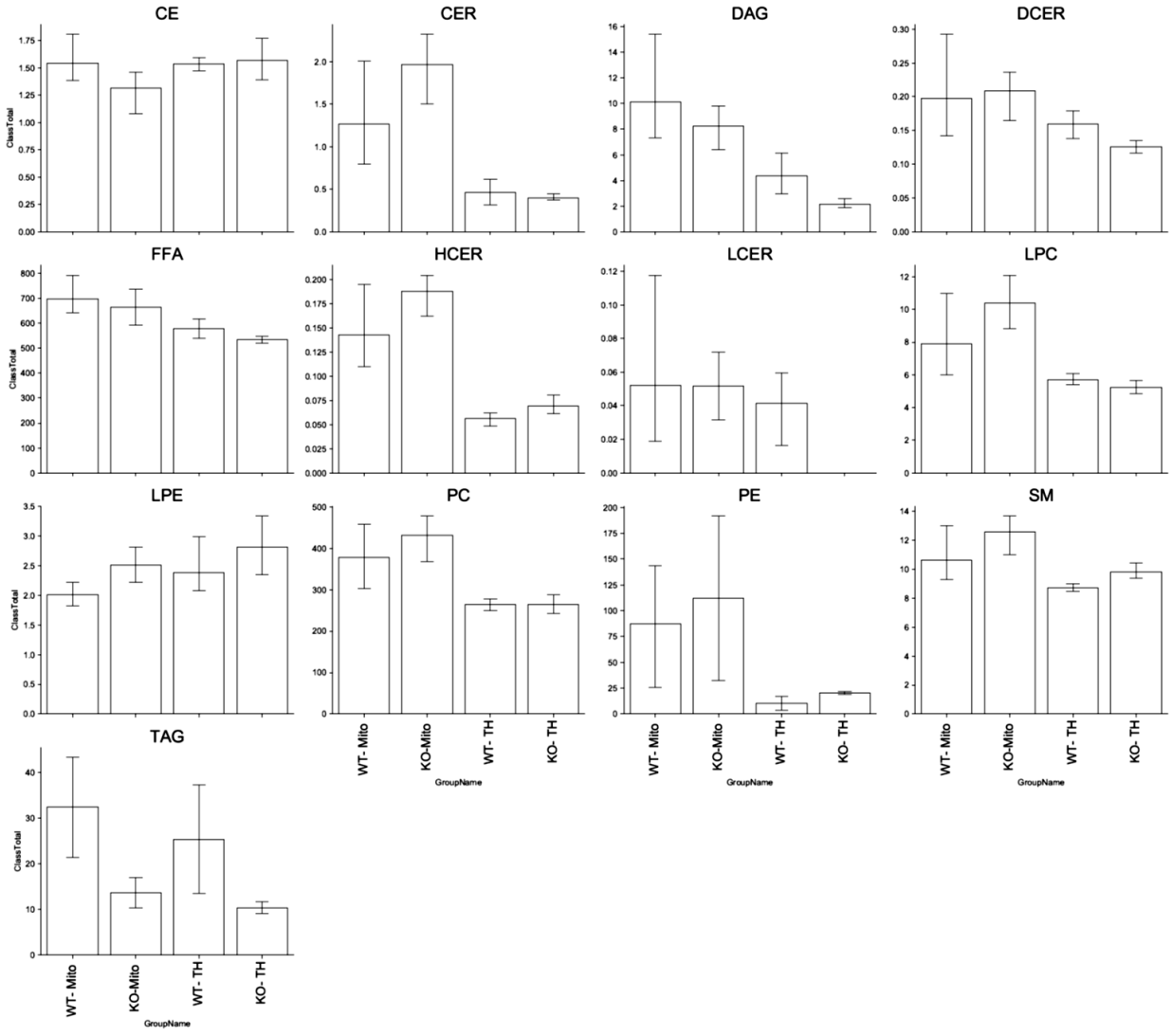

Supplementary Figure 5: Summary of the 13 lipid classes evaluated in both the mitochondria (heart) and whole heart lysates from WT and PON2-def mice (n=4/group) post-IRI. Abbreviations: CE- cholesterol esters, CER- ceramides, DAD- diacylglycerols, DCER- dihydroceramides, FFA- free fatty acids, HCER- hexosylceramides, LCER- lactosylceramide, LPC- lysophosphatidylcholines, LPE- lysophosphatidylethanolamines, PC- phosphatidylcholines, PE- phosphatidylethanolamines, SM- sphingomyelins, TAG- Triacylglycerols. Data is represented as mean±SEM.

Chapter 4: Generation of Cardiomyocyte-Specific PON2-KO Mice

4.1 Introduction

The PON2-deficient mouse model utilized in our various experiments is a global "knock-out" of PON2.[5, 44, 47] Nevertheless, generating cardiac-specific PON2 knockout mouse models allows for the investigation of the role that PON2 plays specifically in the heart, while minimizing any off-target or compensatory responses that can arise from the global PON2 "knockout" model. Therefore, I intended to generate a colony of cardiac-specific PON2 knockout mice to enable a robust and effective model for the investigation of PON2 in myocardial IRI, as well as other cardiovascular disease paradigms. We generated two PON2-cardiac specific knockout mouse models. The first is by implementing a PON2 "knockout-first" mouse breeding strategy and the second is by utilizing the CRISPR/Cas9 gene editing system. Unfortunately, however, I have not been able to test these mice in disease models due to time constraints. Therefore, I will be describing in detail the development and partial characterization of these two mouse models. Our laboratory will utilize these mice to understand the specific mechanisms behind the protective roles of PON2 in mitigating CVD and other related diseases described in my thesis.

4.2 Mice Generation Strategy and Characterization

4.2.1 PON2 "Knockout-First" Mice Generation

In order to have the flexibility of generating not only a PON2-cardiac specific knockout mouse model, but the potential of any other PON2 tissue specific mouse line, we utilized a "knockout-first" reporter tagged insertion allele system, with conditional

potential, generated by the EUCOMM/KOMP-CSD ES cell resource.[89, 90] We specifically used the C57BL/6N-PON2$^{tm1a(EUCOMM)Hmgu}$ mouse, which we obtained from MRC Harwell (MGI ID # 4847743) as cryopreserved sperm.

The cryopreserved sperm came from mice that contain the “knockout-first” allele (tm1a). The basic construct for the PON2-Tm1a allele is as follows: A L1L2_Bact_P cassette is inserted at position 5289544 of Chromosome 6 upstream of exon2, disrupting gene function. The cassette contains an FRT site followed by a lacZ sequence and a loxP site. Following the first loxP site is neomycin (under the control of the human β-actin promoter), SV40 polyA, a second FRT site and a second LoxP site. A third loxP site is inserted downstream of exon 2 at position 5288760. Exon 2 is thus flanked by loxP sites. Therefore, crossing the tm1a mice with Flp recombinase removes the gene-trap cassette reverting the mutation to a “wild-type,” conditional allele (tm1c allele), restoring gene function and leaving loxP sites on either side of exon 2. Subsequent crossing of the tm1c allele mice with tissue-specific cre recombinase allows for conditional, tissue-specific knockout of PON2 by deleting the floxed exon2 of the PON2-tm1c allele to generate a frameshift mutation (tm1d), causing a nonsense mediated decay of the PON2 transcript (Figure 14).[89]

The PON2-tm1a mouse line was reconstituted via IVF in a C57BL/6 female. The resulting mice are heterozygous for the tm1a allele. We then crossed these mice with each other to generate homozygous PON2-Tm1a mice. We are currently breeding these mice to generate and expand our PON2-Tm1a homozygous mouse colony.

Furthermore, we used a Flp recombinase mouse (ROSA26::FLPe knock in, stock#: 016226) from Jackson Lab to cross with our PON2-Tm1a mice in order to

generate the “wild-type,” conditional knockout ready, Tm1c allele. These mice will serve as our experimental wildtype, control group. Furthermore, we generated tm1c homozygous mice, with the Flp-recombinase allele crossed out of the genome. We have set up breeding between homozygous PON2-tm1c male and female mice in order to maintain and expand our tm1c homozygous mouse colony.

We have acquired a cardiac-specific cre recombinase mouse from Jackson Lab (αMyHC-Cre, stock# 011038). This mouse contains a cardiac-specific alpha myosin-heavy chain (Myh6) promoter, that induces greater than 90% recombination in cardiomyocytes, and has no observable recombination in liver, lung, skeletal muscle, spleen, or in extraneous cell types in the heart.[91] We are currently breeding female homozygous PON2-Tm1c mice with our αMyHC-Cre male mouse in order to generate the PON2-Tm1d mice, or PON2 cardiac-specific knockout mice. Our breeding strategy is as follows: Tm1c (fl/fl) x Cardiac Cre = Tm1c (fl/+) and Tm1c (fl/+/cre); then Tm1c (fl/fl) x Tm1c (fl/+/cre) = Tm1d(fl/fl/cre) and Tm1c(fl/+); lastly Tm1c (fl/fl) x Tm1d (fl/fl/cre) = Tm1c (fl/fl) and Tm1d (fl/fl/Cre) (50% each). We have generated PON2-Tm1d, homozygous offspring, which will serve as our final Cardiomyocyte-specific PON2 Knockout experimental mice.

4.2.2 *PON2 “Knockout-First” Mice Genotyping*

Mouse tail biopsies were acquired from pups of potential tm1a, tm1c, and tm1d mice. DNA was isolated from tail biopsies and gel based genotyping strategies were utilized to confirm the genotypes of the mice.

Tm1a Gel Based Genotyping:

Tm1a gel based assays are designed using a universal mutant reverse primer that sits in the sequence just after the 5' homology arm, or 5mut-R1. A forward primer is designed to the 5' homology arm (PON2-5arm-WTF) and designed to give a mutant specific band at 118 bp that will only be present if the cassette is present. Lastly, a wildtype (WT) primer (PON2-Crit-WTR) is designed to the critical region and gives a product of 288 bp, in the case of a heterozygous, Tm1a mouse. Nevertheless, a Tm1a mouse will not produce a WT band, because if the mutant cassette is present the product between the two primers is too large to PCR under standard conditions. This strategy is summarized in Figure 15.

Tm1c Gel Based Genotyping:

Tm1c alleles are produced by exposing tm1a alleles to Flp-recombinase which causes the deletion of Neo and LacZ sequences that are between the FRT sites. The protocol for Tm1a genotyping needs to be run. Both Tm1a and Tm1c alleles will produce a mutant specific product (118 bp) from PON2-5arm-WTF and 5mut-R1. WT and Tm1c alleles will produce PCR products from PON2-5arm-WTF and PON2-Crit-WTR although the Tm1c product (~420 bp) will be bigger due to the presence of the FRT-loxP part of the cassette. In addition to this generic Tm1c assay can be used. This uses the 5'CAS-F1 and 3'CAS-R1 primers, which will produce a product of 218 bp. This strategy is summarized in Figure 16.

Tm1d Gel Based Strategy:

Tm1d mice are produced by crossing tm1c animals with mice expressing cre recombinase (as outlined above), which causes the deletion of the critical region. The tm1d allele produces a 174 bp product from the 5'CAS-F1 and 3'LOXP-R1 primers. A

tm1c allele will produce a larger product which includes the critical region sequence. Alternatively, in all other tissue types other than cardiomyocytes, Tm1d can be confirmed by homozygous Tm1c genotyping and the presence of the αMyHC-Cre allele [Tm1c(fl/fl/cre)]. These mice will be considered the experimental mice for downstream experiments. This genotyping strategy is summarized in Figure 17.

A summary of the gel based genotyping assays and list of the correspond primers can be found in Figure 18 and Table 1, respectively.

4.2.3 PON2 "Knockout-First" Mice Characterization

Two methods were undertaken to characterize the generated mice. The first, as mentioned above, was via gel based genotyping screens, as shown in the representative images in Figure 19.

The second method used to assess the genotype of these mice was via immunofluorescence. For this approach, Tm1a (homozygous), Tm1c (homozygous), and Tm1d mice were euthanized and hearts were collected, paraffin embedded, and finally sectioned in a transverse orientation. The sections were then incubated with two antibodies, anti-PON2 (Green), anti-sarcomeric alpha actinin (red), and stained with DAPI (blue). Representative images are shown below in Figure 20. Tm1a (Figure 20A) and Tm1c (Figure 20B) hearts show the expression of PON2 in cardiomyocytes, while Tm1d (Figure 20C) hearts show a lack of PON2 expression, demonstrating the successful cardiomyocyte-specific deletion of PON2.

4.2.4 CRISPR/Cardiac-Cas9 Mediated Deletion of PON2

The CRISPR/Cas9 system of gene editing offers a fast and effective method to generate targeted gene editing in many model organisms.[92] Consequently, we aim to

generate a cardiomyocyte-specific PON2 knock-out mouse model using CRISPR/Cas9 to investigate and validate the role of PON2 on cardiomyocytes against myocardial IRI.

4.2.5 Cardiac-Cas9 Mouse/Guide RNA Design and Validation

A transgenic mouse line has been generated by Dr. Eric Olson's group at UT Southwestern that expresses Cas9 exclusively in cardiomyocytes.[93] As a proof of concept, Adeno-Associated Virus 9 (AAV9) was used to deliver sgRNA against myosin heavy chain 6 (Myh6), via intraperitoneal injection of postnatal cardiac-Cas9 transgenic mice, inducing Myh6 editing and resulting in cardiomyopathy and heart failure in the mice.[93] We have acquired these cardiac-cas9 transgenic mice from Dr. Olson's group and are now breeding and expanding the colony. A representative gel based genotyping image is shown in Figure 21, in which a Cardiac-Cas9 positive mice produce a band at ~700 bp, whereas wildtype mice do not.

With the acquisition of these mice, we can a generate cardiomyocyte-specific PON2 knock-out mouse model by using AAV to deliver sgRNA against PON2, using the methods detailed by Olson's group.[93] We have tested four predesigned gRNAs (Table 2) against mouse PON2 from Integrated DNA Technologies (IDT), using IDT's patented Alt-R CRISPR-Cas9 system to initially validate the potential success of the guides in deleting PON2 *in vitro* via transfection of the guides into NIH/3T3 cells, a mouse fibroblast cell-line. 48 hours post transfection, the cells were collected and DNA was isolated. The efficiency and efficacy of PON2 deletion was evaluated via the T7 endonuclease I assay, using the respective PON2 guide RNA primers (Table 3). All experimental groups were done in duplicates. Homoduplex and heteroduplex controls were also performed successfully. An HPRT positive control worked successfully,

producing the expected cleaved products: Full length (647 bp), Fragment 1 (512 bp), and Fragment 2 (135 bp). PON2 guides B and C successfully produced the expected cleaved products: Full length (925 bp), Fragment 1 (654 bp), and Fragment 2 (254 bp). The T7E1 assay results are reflected in Figure 22.

The efficacy of *in vitro* mouse PON2 guide RNA deletion was determined by evaluating PON2 protein expression post transfection. Guides B and C were chosen to be tested as they had the most robust cleavage in the T7E1 assay. Both guides B and C were very efficient in knocking out PON2 expression as reflected by the absence of the PON2 protein via western blot as seen in Figure 23.

Lastly, the guides will be cloned into a U6-PON2 gRNA-GFP cassette, which will then be cloned into a double-stranded Adeno-associated (AAV) vector plasmid backbone that will then be packaged into an AAV9 serotype. Large scale AAV9 viral vectors will be produced (~1 x 10^{13} titer). The Cardiac-Cas9 transgenic mice will then be injected with 1 x 10^{12} viral vectors. Cardiomyocytes will then be isolated and PON2 deletion will be determined via qPCR and western blot analysis.

Figure 14

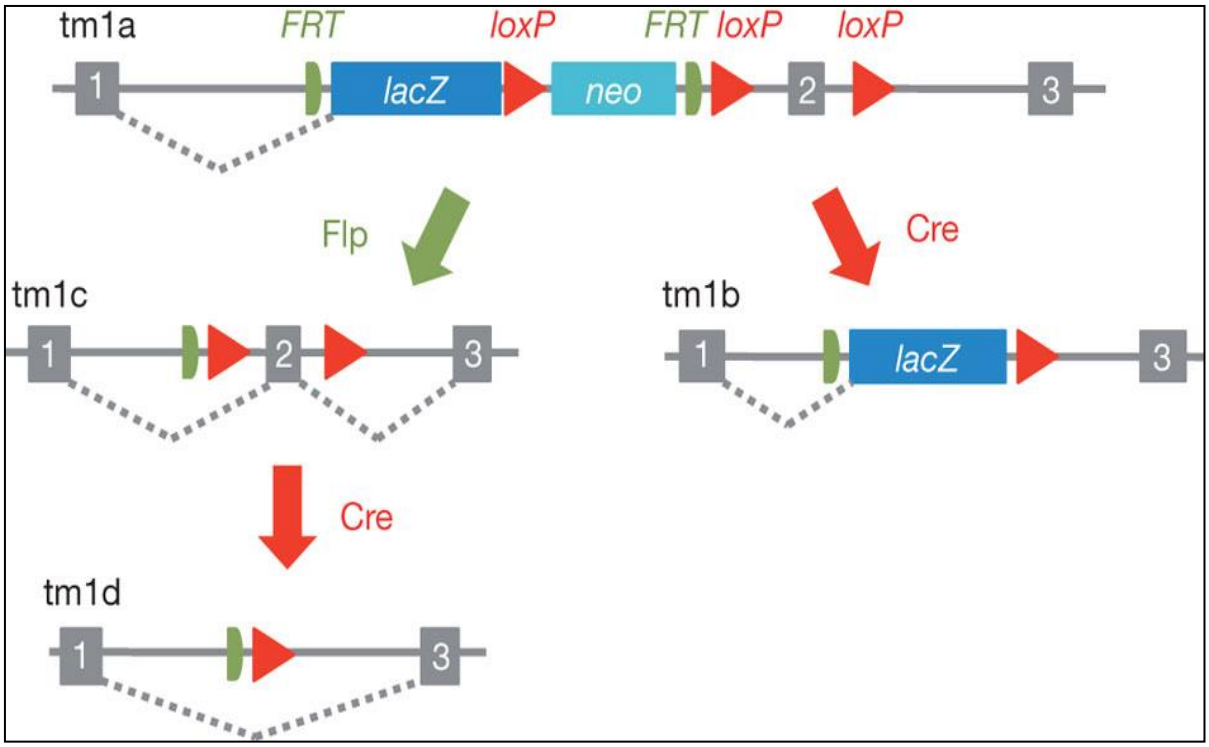

Figure 14: A schematic of the breeding strategy for the PON2-tm1a allele mice (adopted from Skarnes et al.).[89] Tm1a mice bred with Flp-recombinase mice result in tm1c allele, reverting the mice to "wild-type" genotype with loxP site flanking PON2. Further crossing of tm1c mice will result in PON2 deletion. Alternatively, if tm1a mice are crossed with cre-recombinase mice, the resulting mice will have PON2 deleted, with lacZ also expressed and can be used to visualize the deletion.

Figure 15

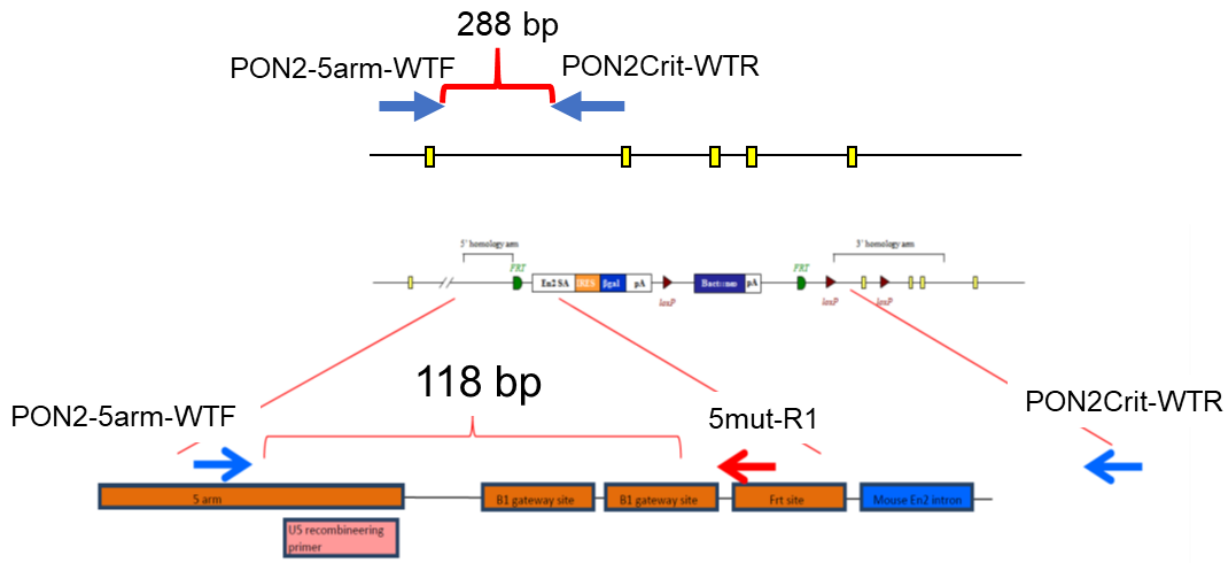

Figure 15: Tm1a gel based genotyping strategy (adopted from MHC Pon2 HEPD0689_5_E02 Protocol). This generic schematic demonstrates the location of the tm1a construct within the gene, in this case PON2, which includes the FRT sites and LOXP sites flanking the exons along with the location of the primers (denoted as the red and blue arrows) that would be used for the gel based genotyping strategy. PON2-5arm-WTF and 5mut-R1(universal mutant reverse primer) primers will amplify a 118bp product, indicating the presence to the Tm1a cassette. Homozygous tm1a will only produce the 118 bp. If mouse contains a WT allele (heterozygous), then the product between the PON2-5arm-WTF and PON2-Crit-WTR would produce a 288 bp product.

Figure 16

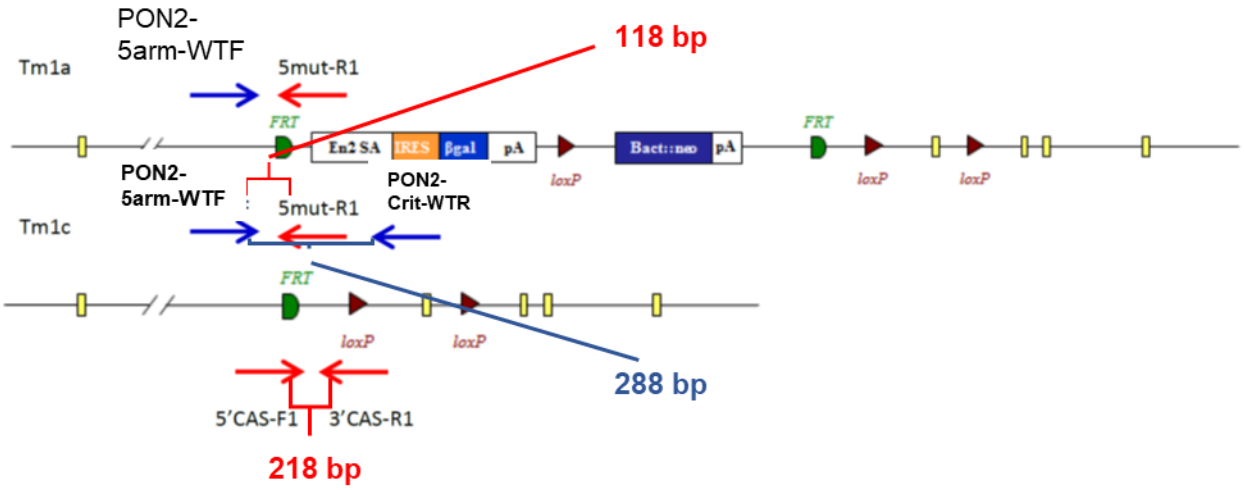

Figure 16: Tm1c gel based genotyping strategy (adopted from MHC Pon2 HEPD0689_5_E02 Protocol). This schematic demonstrates the tm1a construct post-Flp recombination, producing the tm1c allele within the gene (PON2) and resulting in the deletion of the neomyocin (neo) and LacZ sequences between the FRT sites. However, the LOXP sites flank the exons and are ready for cre-recombination. The red and blue arrows denote the location of the primers that would be used for the tm1c gel based genotyping strategy. Tm1a genotyping needs to be run. Tm1c (and Tm1a) alleles will produce the mutant specific product of 118bp (PON2-5arm-WTF and 5mut-R1). WT and tm1c alleles would produce a 288 bp product (PON2-5arm-WTF and PON2-Crit-WTR). Lastly, a generic tm1c assay (5'CAS-F1 and 3'CAS-R1) will produce a product of 218bp.

Figure 17

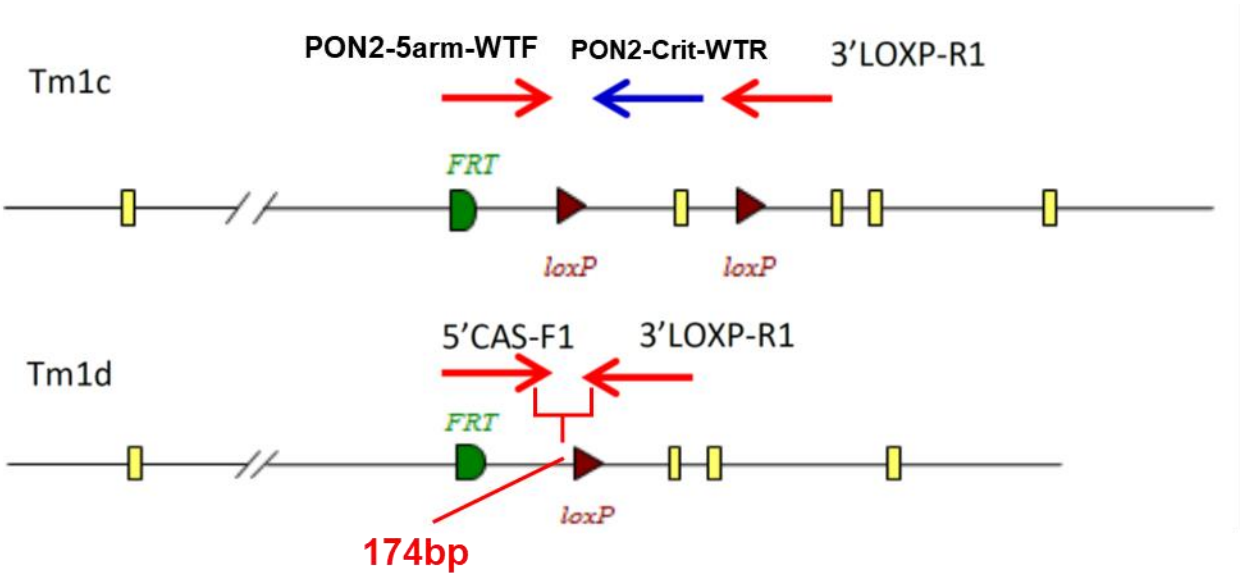

Figure 17: Tm1d gel based genotyping strategy (adopted from MHC Pon2 HEPD0689_5_E02 Protocol). This generic schematic demonstrates the tm1d construct post-Cre recombination, which in our studies is the excision of PON2. The red and blue arrows denote the location of the primers that would be used for the tm1c and tm1d gel based genotyping assays. Tm1d alleles will produce a 174bp product (5'CAS-F1 and 3'LOXP-R1).

Figure 18

	Primers to use										
	5'CAS-F1	5mut-R1	LacZ-F	SV40-FRT-F	3'CAS-R1	3'LOXP-R1	5arm-WTF	Crit-WTF	Crit-WTR	3arm-WTR	Comments
Tm1a + PL		√					√		√		
Tm1b			√					√		√	Run tm1a protocol to identify WT alleles
PL-Tm1b				√				√		√	Run tm1a protocol to identify WT alleles
Tm1c	√	√			√		√		√		Blue =separate reaction
Tm1d	√					√			√		Run tm1a protocol to identify WT alleles

- WT Product between 5arm-WTF and Crit-WTR (product too big in tm1a).
- Tm1a Product between 5arm-WTF and 5mut-R1.
- Tm1b Product between LacZ-F and 3arm-WTR (product too big in tm1a but PCR product from Crit-WTF and 3arm-WTR is made).
- Tm1b-PL Product between SV40-FRT-F and 3arm-WTR (product too big in tm1a but PCR product from Crit-WTF and 3arm-WTR is made).
- Tm1c 218bp product between 5'CAS-F1 and 3'CAS-R1 made. Can also run tm1a protocol for a gene specific assay.
- Tm1d 174bp product produced from 5'CAS-F1 and 3'LOXP-R1. Larger product may be produced by tm1c.

Figure 18: Summary of the primers utilized for the detection of tm1c, tm1b, tm1c, and tm1d alleles via gel based genotyping strategy (adopted from MHC Pon2 HEPD0689_5_E02 Protocol)**.**

Figure 19

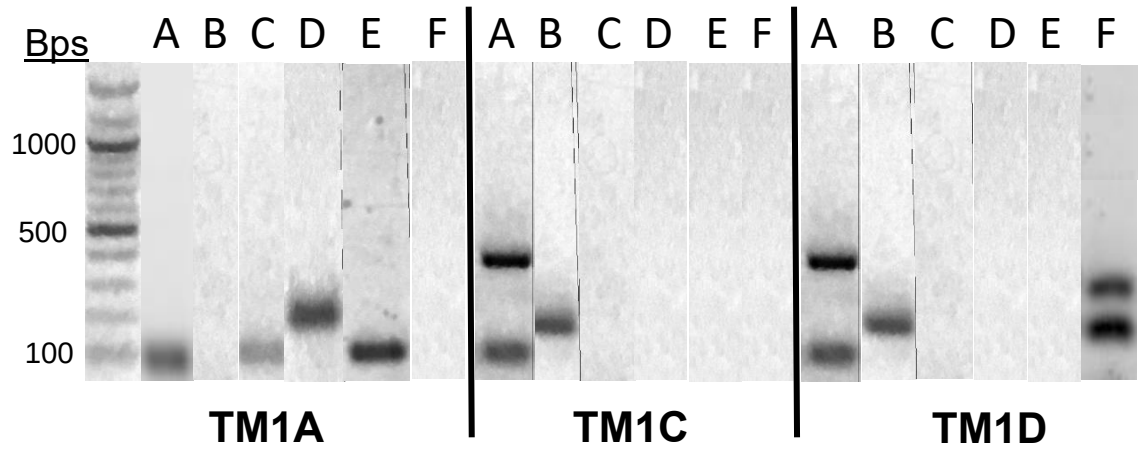

Figure 19: Representative gel based genotyping results for Tm1a, Tm1c, and Tm1d Mice. Representative gel based genotyping results for homozygous Tm1a, Tm1c, and Tm1d mice. Six different PCR reactions were tested in each mouse for the following alleles, with the expected product sizes in parenthesis: (A) Tm1a, (B) tm1c (218 bp), (C) LacZ (108 bp), (D) FRT (204 bp), (E) NEO (186 bp), and (F) Cardiac Cre (300 bp). Furthermore, the tm1a assay will produce the expected product sizes in each of the following strains: Tm1a (1 mutant band- 118 bp), Tm1C and D (2 bands- 1 mutant band and upper band- ~420 bp).

Figure 20

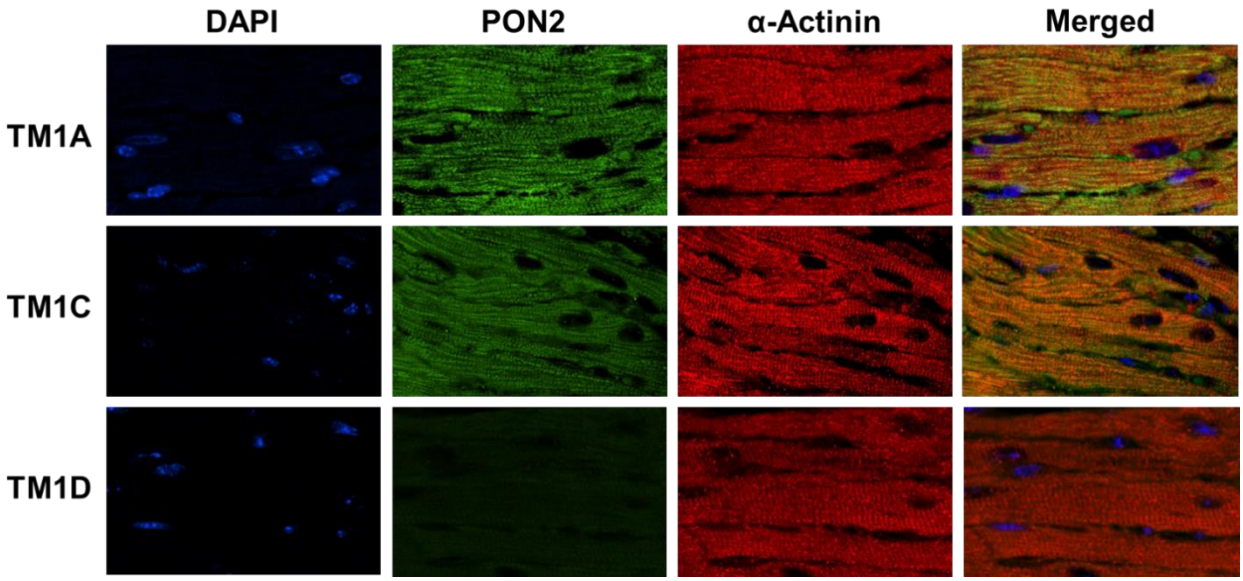

Figure 20: Representative immunofluorescence (IF) images of Tm1a, Tm1c, and Tm1d. Representative IF images of PON2 and sarcomeric α-actinin levels in Tm1a, Tm1c, and Tm1d mouse hearts. Anti-PON2 is green, anti-sarcomeric α-actinin is red, and nuclei is stained with DAPI as blue. Lastly, a merged image is provided combining DAPI, PON2, and α-actinin.

Figure 21

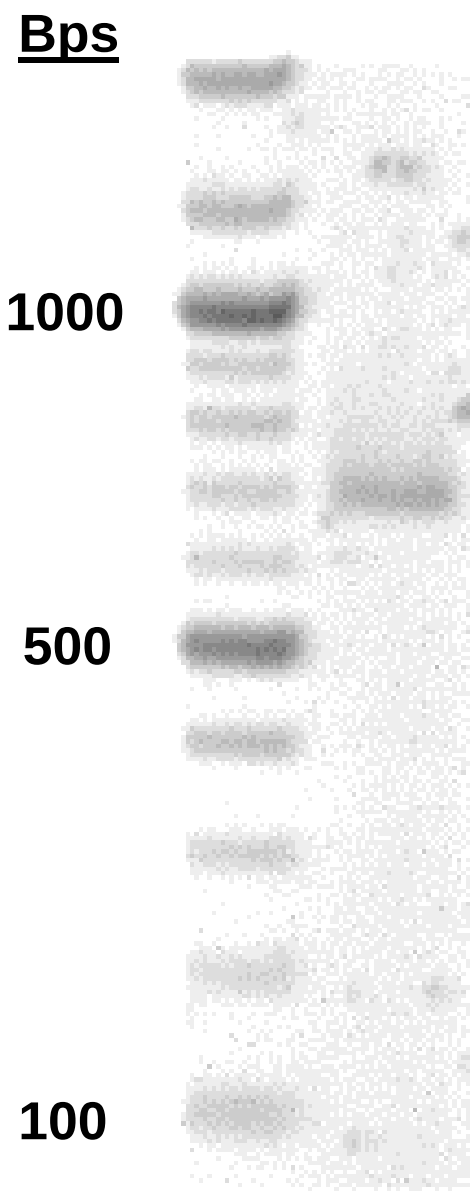

Figure 21: Representative image of Cardiac-Cas9 Gel Based Genotyping. The presence of the Cardiac-Cas9 allele can be seen via gel-based genotyping at around 700 bp.

Figure 22

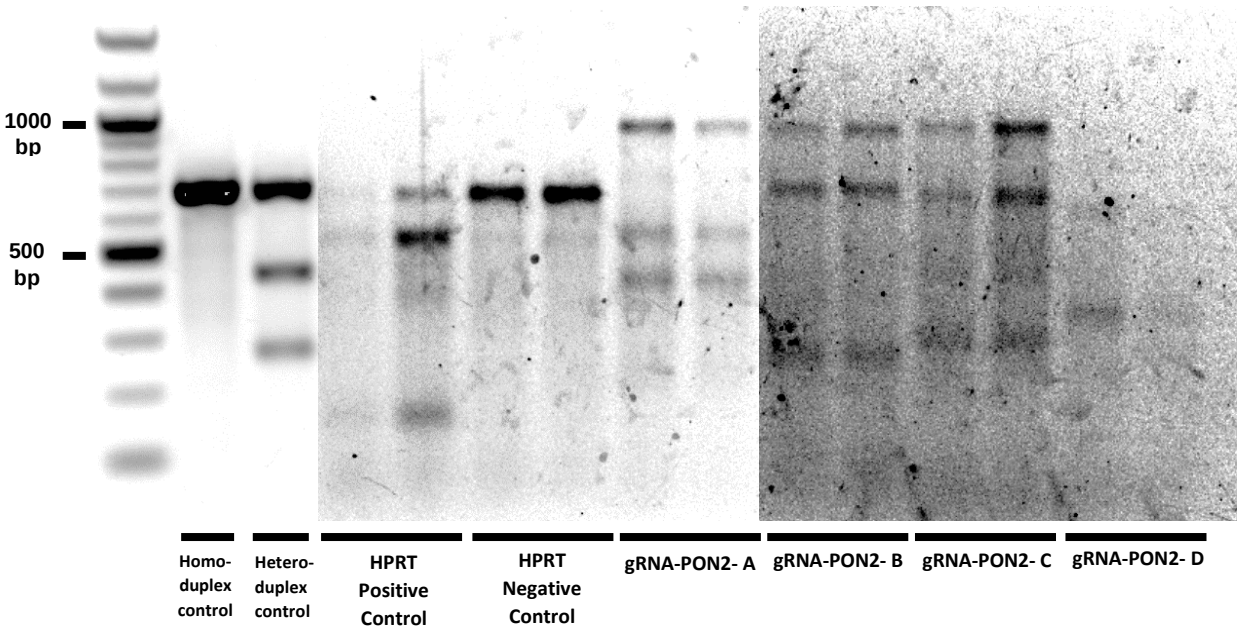
1000 bp
500 bp
Homo-duplex control
Hetero-duplex control
HPRT Positive Control
HPRT Negative Control
gRNA-PON2- A
gRNA-PON2- B
gRNA-PON2- C
gRNA-PON2- D

Figure 22: Results of *in vitro* mouse PON2 guide RNA T7E1 validation experiment. The T7E1 assay was utilized to determine the capacity of the PON2 gRNAs to successfully target PON2 via the CRISPR/Cas9 system. This is accomplished by T7E1 detecting and cleaving mismatched DNA, revealing insertions and deletions that are produced by non-homologous end joining activity. Homoduplex (undigested band at ~700bp) and heteroduplex (full length band at ~700bp, and digested bands seen at ~500 bp and ~300 bp) controls worked successfully. HPRT was used as a positive control and T7E1 cleavage worked successfully, with the following expected results: Full length (647 bp), Fragment 1 (512 bp), and Fragment 2 (135bp). HPRT negative control worked successfully with full length and no digested products. 4 PON2 gRNAs (Guide A, B, C, D) were tested (in duplicates) with the expected products as follows: full length (~925 bp), Fragment 1 (~654 bp), Fragment 2 (~254 bp). Guide A potentially worked, but the digested products are not what was expected; Guide B worked successfully; Guide C worked successfully; and Guide D did not appear to work, although there is a very faint band at around ~300 bp.

Figure 23

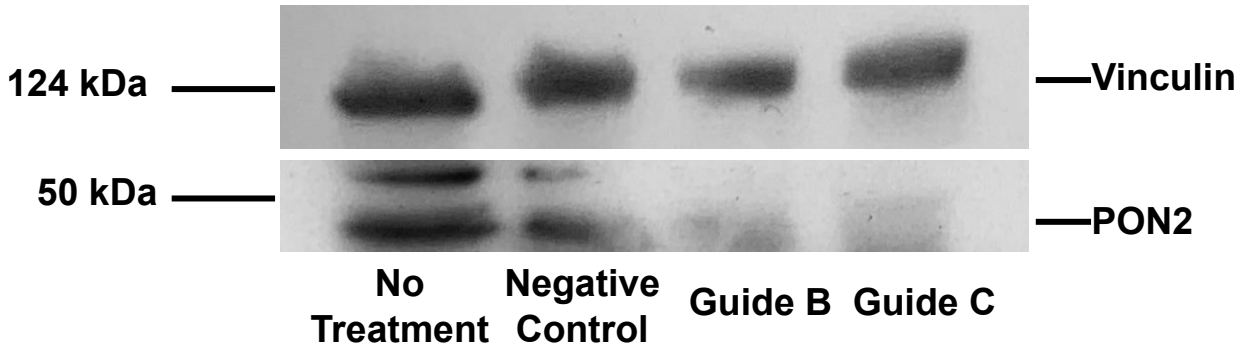

Figure 23: PON2 Knock down by PON2-gRNA B and C via CRISPR/Cas9 system. Protein expression of PON2 in NIH/3T3 cells post CRISPR/Cas9 mediated genetic editing. There four groups tested: no treatment, negative control, PON2-gRNA B, or PON2-gRNA C. Guide B and C successfully deleted PON2 expression (Duplet at ~45 kDa and 55 kDa). Vinculin (124 kDa) was also probed on the same blot as a loading control.

Table 1

Allele	Primer	Sequence	Results (size)
Tm1a	Pon2-5arm-WTF	AGAAAGATGGCTCAGAGGCTA	Tm1a Assay: WT Band—289bp Mutant Band—118bp
	Pon2-Crit-WTR	TGGCTGGGCCTAGATAACTC	Tm1c Assay: Mutant Band—118bp Upper Band—~420bp
	5mut-R1	GAACTTCGGAATAGGAACTTCG	Post-Flp--
Tm1c	5'CAS-F1	AAGGCGCATAACGATACCAC	Tm1c band—218 bp
	3'CAS-R1	CCGCCTACTGCGACTATAGAGA	
Tm1d	5'CAS-F1	AAGGCGCATAACGATACCAC	Tm1d band—174 bp
	3'LOXP-R1	ACTGATGGCGAGCTCAGACC	
	Pon2-Crit-WTR	TGGCTGGGCCTAGATAACTC	
FRT	5FRT_F	AGGCGCATAACGATACCACGAT	5'FRT band—204 bp
	5FRT_R	CCACAACGGGTTCTTCTGTT	
LacZ	LacZ_F	ATCACGACGCGCTGTATC	LacZ band—108 bp
	LacZ_R	ACATCGGGCAAATAATATCG	
Neo	Neo-F	TTGAACAAGATGGATTGCACGC	Neo Band—186 bp
	Neo-F	CCTCGTCCTGCAGTTCATT	
FlpE	FlpE_F	CCTAAGGTCCTGGTTCGTCA	FlpE band—229 bp
	FplE_R	TTGTTGCTTTTTGCGTCTTG	
Cardiac Cre	CRE F	ATG ACA GAC AGA TCC CTC CTA TCT CC	Cre Positive band—300 bp
	CRE R	CTC ATC ACT CGT TGC ATC ATC GAC	Internal Positive Control—100bp

Table 1: Primer sequences for all the primers utilized in the gel based genotyping strategy, including expected band size (in base pairs).

Table 2

Guide RNA	Sequence
Mm.Cas9.PON2.1.AA	GAAGGATTCGATTCCGCCAA CGG
Mm.Cas9.PON2.1.AB	TTTGCACCGGATAAGCCTGG AGG
Mm.Cas9.PON2.1.AC	GTCGGAGAAGTAGTGGTCAT TGG
Mm.Cas9.PON2.1.AD	GACATACTTGAACCTACACT GGG

Table 2: Guide RNA sequences against mouse PON2 used to generate CRISPR mediated Cardiac Specific PON2 KO mice.

Table 3

Primer	Sequence	Amplicon Generated
T7E1 PON2 Guide A,C,D-F	GTTCCGTGGTACTGTGTGTAA	925 bp
T7E1 PON2 Guide A,C,D-R	CTGTGCATAGGCGTCATTCTA	
T7E1 PON2 Guide B-F	CAGCTCCCAGTCACCATTT	910 bp
T7E1 PON2 Guide B-R	GAATGAGAAGGACAGAGCTACG	

Table 3: T7E1 assay primer sequences for PON2 guide RNAs.

Chapter 5: PON2 Mediated Protection of HSG4112 Against Diet-Induced Obesity

Abbreviations:

CVD	Cardiovascular Disease
CHD	Coronary Heart Disease
CAD	Coronary Artery Disease
PON	Paraoxonase
3OC12-HSL	N-(3-oxododecanoyl)-1-homoserine lactone
WT	Wild-type
PON2-def	PON2-deficient
LDLR-KO	Low density lipoprotein receptor knock-out
WD	Western diet
HF/HS	High fat/high sucrose
TG	Triglyceride
TC	Total Cholesterol
HDL	High density lipoprotein
UC	Unesterified cholesterol

5.1 Introduction

Coronary Heart Disease (CHD), particularly myocardial infarction, is the leading cause of global morbidity and mortality.[1, 52, 94] Cardiovascular risk factors for coronary heart disease include dyslipidemia, hypertension, diabetes, and obesity.[1] Obesity accounts for approximately 40% of the risk factors leading to CHD, and over 80% of CHD patients are overweight/obese.[1] Obesity and its subsequently related array of metabolic diseases, including CHD, share various pathophysiological alterations in mitochondrial function, oxidative stress, and inflammation.[6, 95-97] Consequently, discovering a therapeutic agent that can not only reduce obesity, but can also modulate these pathophysiological consequences is of paramount importance.

The Paraoxonase gene family, consisting of PON1, PON2, and PON3, are highly conserved in mammals and have a vast role in modulating various metabolic and inflammatory diseases, including infection, cardiovascular disease, obesity, and cancer.[4, 5, 49, 50, 64, 98] Although each PON member has evolved unique substrates and mechanisms of action, a conserved mechanism shared amongst all three PON enzymes is their ability to hydrolyze lactones, particularly *N*-acyl-homoserine lactones, as well as aromatic esters.[40, 99, 100] Our group and others have demonstrated the ability that all PONs, particularly PON2, have to hydrolyze and inactivate N-(3-oxododecanoyl)-1-homoserine lactone (3OC12-HSL), a quoreum-sensing molecule produced by gram-negative bacteria thereby reducing bacterial infections in various animal models, tissues and cell types.[64, 101, 102] Moreover, other underlying mechanisms driving PON protection is rooted in their antioxidant capacity and modulation of lipid peroxidation.[7, 40, 44, 103, 104] In particular, PON2's protective effects against

proatherogenic effects of chronic infection are not only mediated by its ability to hydrolyze 3OC12-HSL, but also through protection against mitochondrial ROS generation, oxidized phospholipid induced oxidative stress and ER-stress induced unfolded protein response.[47, 64, 105, 106] Therefore, evaluating lactonase and arylesterase activity serves as a valuable method for determining PON activity in experimental settings.

PON2 has been shown in our lab and by others to protect against cardiovascular diseases, including atherosclerosis and myocardial ischemia-reperfusion injury, as well as cancer and, more recently, diet-induced obesity.[5, 6, 48, 50] I and others have demonstrated that a key factor mediating this protection is PON2's capacity to mitigate mitochondrial dysfunction and oxidative stress.[5, 50] Recently, Dr. Shih, et al., demonstrated that PON2 deficient mice (PON2-def) fed a high fat/high (HF/HS) sucrose diet developed a significant increase in body weight due to increased fat mass weight, as compared to wildtype (WT) controls.[6] This phenotype was accompanied by mitochondrial dysfunction, with significant decreases in oxygen consumption and energy expenditure in PON2-def mice as well as lower oxygen consumption rate in the mitochondria derived from white adipose tissue as compared to WT controls.[6] Consequently, the protection afforded by PON2 against diet-induced obesity, makes it a valuable candidate to pursue as a mechanism of preventing further cardiovascular disease, including myocardial IRI.

Glaceum, Inc., a Korean biotech company, is interested in treating metabolic syndrome and used Glabridin, an isoflavan in licorice roots, as pharmacological target to translate into druggable compounds. Isoflavones, including their derivates isoflavoids,

are polyphenolic compounds that possess antioxidant properties and are often referred to as phytoestrogens, or plant-based compounds that have biological activity through the estrogen receptors.[107, 108] Glabridin has been shown to have antioxidant, anti-inflammatory, anti-atherogenic, and anti-bacterial properties, along with protective capacities against cancer, atherosclerosis, and neurological diseases.[109] Furthermore, glabridin was shown to upregulate PON2 expression under hyperglycemia.[110] Subsequently, Glaceum developed and tested over 300 chemical derivates of glabridin, and HSG4112 emerged as one of the lead druggable new chemical entities that the company discovered. They discovered that the mode of action of their lead compound HSG4112, developed for treating metabolic diseases, is via the induction of PON2 protein. HSG4112 oral administration (for 6 weeks) resulted in 38% reduction of food intake, a 62% increase in energy expenditure, and a 26% drop in weight in mice a diet-induced obesity model in mice (data not published). Additionally, HSG4112 treatment resulted in a significant increase in PON2 expression (Supplemental Figure 6) and the proposed mode of action by Glaceum for HSG4112 was determined to be a PON2 dependent modulation of mitochondrial dysfunction (data not published). Glaceum reached out to our lab and requested to collaborate to further explore the role of HSG4112 against diet-induced obesity using our PON2-def mouse model to evaluate the potentially causal role that PON2 plays as a mode of action of HSG4112. Our laboratory signed an MTA with Glaceum, Inc. and obtained HSG4112. My hypothesis is that HSG4112 will be protective against diet-induced obesity by reducing body weight and fat mass, while increasing lean mass, in a PON2 dependent manner.

With this compound in hand, I performed a series of experiments to test my hypothesis: 1) Baseline assessment of Chow diet ± HSG4112 on three mouse models: WT, PON1-KO, and PON2-def. 2) Assessment of HF/HS ± HSG4112 on WT and PON2-def mice. 3) Rescue capacity of HSG4112 against diet-induced obesity on WT and PON2-def mice. 4) Assessment of Chow diet ± HSG4112 and Western Diet ± HSG4112 on a mouse LDLR-KO, or hyperlipidemic, background.

5.2 Materials and Methods

5.2.1 Mice and Diets

All mouse breeding and experimental protocols were approved by the UCLA Animal Research Committee (ARC), in accordance with PHS guidelines. WT and PON2-def mice were generated as a result of a PON2 heterozygous intercross. PON1-KO mice were also generated from a heterozygous intercross. Lastly, the LDLR-KO mice were originally purchased from Jackson Laboratories and obtained from the Department of Laboratory and Animal Medicine at David Geffen School of Medicine at UCLA. All the mice used are on a C57BL/6J background. Both male and female mice were utilized for these experiments and ranged from 8 to 12 weeks of age, which are further specified in each experimental design as noted in the respective figure legends. Based on the experimental design, mice were fed a standard mouse chow diet (Ralston Purina), a western diet (WD; Teklad, Harlan, catalog# TD88137), and/or a high fat/high sucrose diet (HF/HS; Research Labs, catalog# D12266B), with and without HSG4112 (Glaceum Inc.), which was mixed with the diet at a dose of 100mg/kg. All mice were weighed both prior to start of the experiment and every subsequent week until termination. Lastly, mice were fasted overnight prior to blood and tissue collection.

5.2.2 Plasma Lipids and Glucose Measurement

Plasma lipids, including triglycerides, total cholesterol, high density lipoprotein (HDL), and unesterified cholesterol, as well as glucose levels were determined using enzymatic colorimetric assays,[6] with final concentrations expressed as mg/dL.

5.2.3 Body Composition Measurement

Body composition, specifically total body fat and lean mass was determined using quantitative nuclear magnetic resonance (NMR) via the Bruker MiniSpec utilizing software from Echo Medical Systems. The percent of total body fat and lean (muscle) mass was determined by dividing the total body fat/lean mass by total body weight, taken just prior to NMR, and then multiplying by 100.

5.2.4 Immunoblotting

50 micrograms of protein from plasma and liver lysates were loaded on 4–20% Mini-PROTEAN TGX Stain-Free protein gels (Bio-Rad, Hercules, CA, USA) and transferred to nitrocellulose membranes. The membranes were blocked for 1 h at room temperature in Tris-buffered Saline with 0.1% Tween 20 (TBST) containing 5% (w/v) milk. The following primary antibodies were used at the specified dilutions: PON1 (catalog# MAB4926, R&D Systems) at 1:1000, PON2 (Catalog# A00816, GenScript), PON3 (catalog# AF4345, R&D Systems) at 1:1000, Vinculin (catalog# V9131, Sigma-Aldrich) at 1:5,000. Primary antibodies were diluted in TBST containing 5% milk at 4oC overnight, followed by incubation with appropriate secondary antibody (1:5,000 dilution) coupled to HRP for 1 hour. Protein was detected using Immobilon Western Chemiluminescent HRP Substrate (Millipore Sigma, USA). Western blot images were quantified using the ImageJ software.

5.2.5 Lactonase and Arylesterase Assays

Plasma and liver homogenates (20mg) were utilized for the lactonase and arylesterase assays. The protocol for the assays were as follows:

Lactonase Assay[111]

Stock solutions of 100 mM dihydrocumarin (Catalog# 104809-5G, Sigma) in DMSO (can keep for up to 2 weeks at 4°C) were prepared fresh. The stock was diluted to 2 mM with reaction buffer (freshly prepared; 50mM Tris HCl, pH 7.5, 1 mM $CaCl_2$), and a final concentration of 1 mM is used. Dilute plasma 1:10 with reaction buffer (dilution factor depends the activity of PON1). Nondiluted HDL was used. 3 µl of the diluted plasma or 10-15 µl of mouse HDL was added to the wells of a UV microplate. Reaction buffer was added to complete the volume to 100 µl. Also, self hydrolysis of dihydrocoumarin was measured. 100 µl of 2 mM dihydrocumarin was added. Absorbance at 270 nm was read for 10 minutes every 15 seconds. The Mean V mOD/minute values were acquired. Following conditions were utilized for the determination of the final concentration : 1 unit = 1 µmol of dihydrocumarin hydrolyzed per minute per 1 ml; extinction coefficient: E270 = 1295/M/cm; Calculation: - [(Mean V of sample - Mean V of self hydrolysis) × 5 × dilution factor]/700 = units/ml. Serum lactonase activity toward dihydrocoumarin in healthy subjects is in the range of 13–20 units/ml.

Arylesterase Assay[112]

Assay Buffer (9.0 mM Tris.HCl, pH 8.0, 0.9 mM $CaCl_2$) and Substrate Solution (25 µl of phenyl acetate (catalog# P-2396, Sigma) dissolved in 50 ml of assay buffer) were prepared fresh before assay. Plasma was diluted 1:50 (10 µl plasma + 490 µl assay buffer), 20 µl were aliquoted into each well of the 96-well flat bottom UV plate (catalog#: 3635, Costar), with duplicated determinations made for each sample. The plate reader (Molecular Devices, model:Spectra Max 190) was configured with the following settings: Function: Kinetics, Wavelength: 270 nm, Interval time: 15 seconds,

Total Time: 2 minutes. Using a multichannel pipet, 180 µl of substrate solution was added into each well. The plate was then quickly added to the plate reader and readings began right away. The machine computed the rate as follows: v(in mO.D./min). V was multiplied by 2.5 to obtain O.D./min/ml of plasma. The following calculation was utilized for final concentration: L = path length of the spectrometer (cm), Molar E 270 for phenol (product) = 1310, 1 mole/liter = 1310 A270 in a spectrometer of 1 cm path length. Therefore, Arylesterase activity = 2.5 *v *0.7633/L= v * 1.9083/L (Units/ml of plasma).

5.2.6 Statistical Analysis

Student's t-tests were carried out between all studies with two groups. Data from experiments with two or more groups were compared using a one-way ANOVA model. After a significant overall group effect was established, Tukey's pairwise comparisons were carried out to determine specific group to group differences. Experiments were repeated two to three time to ensure that the results were consistent and reproducible. All data are represented as mean ± SEM. A p-value<.05 was considered statistically significant.

5.3 Results

5.3.1 Role of HSG4112 in modulating expression and activity of Paraoxonases.

In order to elucidate the potential role that HSG4112 might play in modulating Paraoxonase expression and activity, I performed a pilot experiment in which Control (WT, C57BL/6J), PON1-KO, and PON2-def mice (n=8/group) were fed Chow ± HSG4112 for 2 weeks (Figure 24A). Subsequently, using both plasma and liver acquired before and after HSG4112 treatment, I evaluated the protein expression of PON1, PON2, and PON3 as well as the lactonase, arylesterase, and paraoxonase activities. Paraoxonase activity in the plasma post-HSG4112 treatment is significantly reduced in the control and PON2-def groups, while it is significantly increased in the PON1-KO group, when compared to pre-HSG4112 treatment (Figure 24B). In addition, arylesterase and lactonase activity was significantly increased in the plasma post-HSG4112 across all three groups (Control, PON1-KO, and PON2-def), when compared to pre-HSG4112 treatment (Figure 24B). Furthermore, when evaluating arylesterase and lactonase activity the liver post-HSG4112, I observed no significant differences in the control group, while there is a significant increase in activity in both assays in the PON1-KO and PON2-def groups, when compared to pre-HSG4112 treatment (Figure 24C).

Next, when looking at the protein expression of PON1, PON2, and PON3 in the plasma post-HSG4112 treatment, I observed that PON1 is significantly increased in the Control, WT group and PON2-def group, with the PON2-def group demonstrating a significant increase in PON3 expression as well, when compared to chow fed controls (Figure 24D). Lastly, PON1 is significantly increased in livers of PON2-def mice, along

with PON3 in PON1-KO and PON2-def mice, treated with HSG4112 versus chow controls (Figure 24E).

HSG4112's ability to increase PON enzymatic activity (lactonase and arylesterase) and induce PON protein expression in the plasma and liver of WT, PON1-KO and PON2-def mice under baseline, untreated conditions supports the role that HSG4112 functions, at least in part, through the PON gene family. Additionally, as noted earlier, Glaceum observed a significant induction of PON2 expression in a diet-induced obesity model (Supplementary Figure 6), and proposed PON2 as a mode of action for HSG4112. Therefore, I sought to determine whether the protective properties of HSG4112 are, at least in part, mediated by PON2.

5.3.2 Role of PON2 in modulating the protective effects of HSG4112

To assess the role that PON2 plays in potentially modulating the protective effects of HSG4112, I utilized PON2-def mice and WT mice as controls (n=10/group). Both male and female mice were used and fed a WD (HF/HS) diet ± HSG4112 for 3 weeks (Figure 25A). Changes in weight (in grams) was determined in WT and PON2-def mice two weeks after being on HF/HS ± HSG4112, with both male and female groups demonstrating a significant decrease in weight with the HSG4112 treatment, when compared to HF/HS controls (Figure 25B). Nevertheless, the PON2-def group fed the HF/HS diet with HSG4112 had a borderline significant ($p=0.054$) reduction in the magnitude of weight change compared to the female, WT group fed the same diet. Fat and muscle mass were also determined via NMR for all mice groups and, as noted above, percent fat and muscle (lean) mass is calculated as fat/muscle mass over total body weight x 100. Percent fat was significantly reduced in both male and female, WT

mice fed HF/HS + HSG4112, when compared to just HF/HS diet alone (Figure 25C). Furthermore, there were no significant differences in percent fat between either male or female, PON2-def diet groups (Figure 25C). Although percent muscle slightly increases in the HSG4112 treated groups, it is only significantly increased in the female, WT mice compared to just WT, HF/HS controls (Figure 25D).

Next, I evaluated lactonase and arylesterase activity in the plasma and liver of these mice. Lactonase activity was only significantly increased in the plasma for the female, WT group fed HF/HS + HSG4112, compared to control (Figure 25E). Moreover, arylesterase activity is significantly increased in the female, PON2-def group on a HF/HS + HSG4112 diet, compared to controls (Figure 25E). Of note, as expected, both lactonase and arylesterase is significantly reduced in the HF/HS fed PON2-def group versus WT controls. There were no significant differences in lactonase activity in the liver between the WT and PON2-def groups fed HF/HS ± HSG4112, except for a significant decrease in the PON2-def fed HF/HS diet versus its WT control (Figure 25F). However, there was a significant decrease in arlyesterase activity in the liver of the WT mice fed a HF/HS + HSG4112, when compared to control (Figure 25F). In addition, arylesterase activity in the liver is significantly decreased in the PON2-def group fed HF/HS diet versus its WT control (Figure 25F).

Plasma lipid panel (triglycerides, total cholesterol, HDL, and unesterified cholesterol) and glucose levels were evaluated in both male and female, WT and PON2-def mice fed HF/HS ± HSG4112 and WD ± HSG4112 diet (Table 4). Triglyceride levels were significantly elevated in the male, WT group on the HF/HS + HGS4112 diet versus WT, HF/HS controls (Table 4). However, there is a significant decrease in the

triglycerides in the female, PON2-def group fed a HF/HS + HSG4112, when compared to HF/HS fed PON2-def controls (Table 4). Also, there is significant decrease in HDL in the female, WT mice on a HF/HS + HSG4112 diet versus HF/HS, WT controls (Table 4). Lastly, there is a significant decrease in glucose levels in the male, WT and male, PON2-def mice on a HF/HS + HSG4112 versus their respective controls (Table 4). Nevertheless, this significant decrease in glucose levels is absent in the female WT, PON2-def groups. (Table 4).

PON2 deficiency significantly limited the protective effects of HSG4112. Although there was a significant reduction in body weight in both WT and PON2-def mice fed the HF/HS diet with HSG4112, the significant reduction of fat mass and lean observed in the WT, HSG4112 treated groups (both male and female) is lost in the PON2-def groups fed HSG4112. Furthermore, the significantly increased lactonase and arylesterase activity observed in the WT groups treated with HSG4112 is absent in the PON2-def groups fed HSG4112. Lastly, the significant reduction of glucose levels in both male, WT and PON2-def groups treated with HSG4112, is lost in the female, PON2-def group treated with HSG4112.

My observation that the protective effects of HSG4112 is reduced in PON2-def mice (specifically females) led me to conduct another experiment in which I would test the potential for HSG4112 to rescue the diet-induced obesity phenotype, in both WT and PON2-def mice fed an obesifying diet.

5.3.3 Limited capacity of HSG4112 to rescue obesity phenotype in PON2-def mice

To investigate the potential role of HSG4112 in rescuing the effect of diet-induced obesity, I performed a study which consisted of WT and PON2-def mice

(n=10/group) that were fed a HF/HS (WD) diet for three weeks, after which they were placed on a HF/HS diet + HSG4112 for another three weeks (Figure 26A). Changes in weight (in grams) were then assessed post-week 3 to assess the changes due to western diet alone, as well as at the end of week 6 to assess a potential rescue effect of HSG4112 on the changes due to the obesifying diet (Figure 26B). There was a significant weight increase in the male, WT mice versus the male, PON2-def mice after three weeks of HF/HS diet (Figure 26B). This increase in body weight was significantly reduced by HSG4112 treatment in the male, WT mice, while not changing significantly in the male, PON2-def group (Figure 26B). Furthermore, there was a significant difference in the change in weight between the male, WT and PON2-def groups after 3 weeks of HSG4112 treatment, with the male, WT group having a greater change in weight versus the male, PON2-def mice (Figure 26B). On the other hand, the female, PON2-def mice significantly gained more weight when on the HF/HS diet for three weeks, when compared to the female, WT group. Nevertheless, treatment with HSG4112 for three weeks significantly reduced the change in weight, causing the mice to actually lose some weight (compared to week 3 weights), in both the WT and PON2-def groups (Figure 26B).

Fat and muscle (lean) mass was determined via NMR for all groups and percent fat/muscle mass is quantified as the fat/muscle mass (g) over total body weight (g) at the given time point x 100. Male, WT mice have a significant increase in percent fat at the end of 3 weeks of HF/HS diet, which is not significantly reduced by HSG4112 treatment for another three weeks (Figure 26C). Male, PON2-def mice do not significantly increase in fat mass after 3 weeks of HF/HS diet, and HSG4112 does not

appear to have a significant effect in modulating fat mass after three weeks as well (Figure 26C). The male, WT mice have a significantly elevated percent of fat after both week 3 and week 6, when compared to the male, PON2-def group. Female, PON2-def mice significantly increase their percentage of fat mass after three weeks of HF/HS diet, but three weeks of HSG4112 treatment does not significantly rescue that phenotype (Figure 26C). Although the female, WT mice are initially resistant to any changes in fat mass during the three weeks of HF/HS feeding, HSG4112 significantly reduces their fat mass after three weeks of treatment (Figure 26C). Furthermore, there is a significant increase in fat mass between female, PON2-def mice compared to the female, WT mice at both week 3 and week 6 of the study (Figure 26C). Muscle mass was significantly reduced in the male, WT mice after three weeks of HF/HS diet, but does not significantly change after three weeks of HSG4112 treatment, although it does not drop further (Figure 26D). Similarly, muscle mass significantly drops in both the female, WT and PON2-def female groups after three weeks of HF/HS diet. In addition, HSG4112 treatment for three weeks fails to improve muscle mass for either female, WT or PON2-def mice (Figure 26D). Nevertheless, at the end of week 6, female, PON2-def mice have a significantly decreased muscle mass when compared to female, WT controls.

Lastly, food consumption was measured over the course of the study (Figure 26E). Food consumption is reduced over time for both male and female WT groups. 90% of HF/HS diet is consumed by both male and female WT mice at the end of week. However, HSG4112 treatment appears to reduce food consumption down to about 82% for males and 75% for females by the end of week 6 of the study. Similarly, both male and female PON2-def mice consume about 90% of the HF/HS diet by the end of week

3. However, there is a more pronounced reduction in food consumption in the female mice (about 55%) versus males (about 80%), by the end of three weeks of HSG4112 treatment.

HSG4112 treatment after diet-induced obesity largely fails to rescue the negative phenotypes in PON2-def groups (particularly females), which includes an inability of HSG4112 treatment to rescue increases in fat mass and decreases in lean mass. Nevertheless, HSG4112 treatment was still successful in significantly reducing the body weight of both WT and PON2-def mice after three weeks of obesifying diet. Given the limited capacity of HSG4112 to protect against diet-induced obesity in PON2-def mice, I sought to investigate the protective properties of HSG4112 against diet-induced obesity in hyperlipidemic mice.

5.3.4 HSG4112 Protection Against Diet-Induced Obesity in Hyperlipidemic Mice

LDLR-KO mice were utilized to test the efficacy of HSG4112 against hyperlipidemia. In this study, male and female LDLR-KO mice (n=10 per group) were fed a Chow diet or WD, both with and without HSG4112 for three weeks (Figure 27A). Changes in weights (in grams) were determined at the end of the study and compared to the initial weights of the mice before the study began. There were no changes observed in both males and females fed the Chow ± HSG4112. Nevertheless, HSG4112 was able to significantly reduce the weight of both male and female mice fed WD with HSG4112, when compared to just WD alone (Figure 27B). Next, using NMR, I determined the changes in fat and muscle (lean) mass, which I represented as a percent change (fat/muscle mass over total body weight x 100). Similar to what I observed in body weight, there were no significant changes in % fat mass in both male

and female mice fed the Chow ± HSG4112 diet (Figure 27C). However, there is a significant drop in % fat mass, about 50% (from ~20% to ~10%) in the male and female fed a WD with HSG4112 versus WD controls (Figure 27C). In addition, the percent muscle mass was significantly increased in the WD + HSG4112 group versus the WD controls, with no change observed in the Chow ± HSG4112 groups (Figure 27D).

Lactonase and arylesterase activities were evaluated in the plasma and livers from this study. Although there were no significant differences in the arylesterase activity between any of the groups, I observed a significant drop in the lactonase activity in the female WD mice versus chow controls (Figure 27E). Yet, there is a strong trend ($p=0.056$) for an increase in lactonase activity in females on a WD with HSG4112 versus WD controls (Figure 27E). On the other hand, the lactonase and arylesterase activity in the liver are significantly decreased between both the Chow + HSG4112 and WD + HSG4112 groups, compared to their respective controls (Figure 27F).

Lastly, plasma lipid panel (triglycerides, total cholesterol, HDL, and unesterified cholesterol) and glucose levels were evaluated in both male and female, Chow ± HSG4112 and WD ± HSG4112 (Table 5). Triglyceride levels were significantly elevated in both the male and female Chow + HGS4112 versus chow controls, while no significant difference is observed in either male or female WD ± HSG4112 groups (Table 5). There is significant decrease in the total cholesterol in the male WD + HSG4112 versus WD controls (Table 5). Lastly, there is a trend ($p=0.09$) in decreased glucose levels in the male, chow + HSG4112 (versus chow), while a significant decrease in glucose is observed in the female, chow + HSG4112 (versus chow) and a strong trend ($p=0.06$) in the female, WD + HSG4112 group (versus WD) (Table 5).

Under a hyperlipidemic, LDLR-KO background, HSG4112 significantly reduced body weight and fat mass, while increased lean mass in male and female mice fed a WD and not in chow. Furthermore, there were no significant enhancements of PON enzymatic activity with HSG4112 treatment. On the contrary, HSG4112 treatment significantly reduced lactonase and arylesterase activity in the plasma of both chow and WD fed mice. Also, HSG4112 treatment affected plasma lipid and glucose level, significantly increasing triglyceride in the chow fed group, decreasing total cholesterol in males fed WD, and decreasing glucose levels in females fed WD.

5.4 Discussion

Diet-induced obesity is major risk factor for cardiovascular disease, specifically coronary heart disease. In this study, I investigated the potential role that a novel therapeutic, HSG4112, could play in mitigating diet-induced obesity via the Paraoxonase gene family, specifically PON2. I utilized four different experimental models to undertake this project.

In order to assess the baseline function of HSG4112 and the role that the Paraoxonase gene family, including PON1, PON2, and PON3, could play in modulating its protective effects, I administered Chow ± HSG4112 (100 mg/kg) to WT (C57BL/6J), PON1-KO, and PON2-def mice for 2 weeks. HSG4112 did not have a pronounced effect on weight (data not shown), however it did have a significant effect on PON meditated activity, namely lactonase and arylesterase. HSG4112 enhances the lactonase and arylesterase activity in the plasma in all three experimental groups (Figure 24B), as well as in the PON1-KO and PON2-KO groups in the liver (Figure 24C). Furthermore, HSG4112 induces the protein expression of PON1 in the plasma of WT mice and plasma and liver of PON2-def mice, while also inducing PON3 in the livers of both PON1-KO and PON2-def mice (Figure 24D,E). These data support the theory that HSG4112's mechanism of action is potentially via the PON gene family, more specifically acting as a mechanism to rescue the loss of function observed in mice genetically deficient of a member of the PON gene family.

A recent study was published by Dr. Shih et al. demonstrating that PON2 deficiency in mice, specifically females not males, led to diet-induced obesity, when the mice were fed a high fat, high sucrose diet. Furthermore, these PON2-def mice

exhibited significantly increased fat mass weight, impaired glucose tolerance, and mitochondrial dysfunction (decreased oxygen consumption and energy expenditure) when fed the obesifying diet, as compared to WT controls.[6] In addition, PON2-def mice have a greater susceptibility to develop atherosclerosis[5] and develop larger infarcts when subjected to acute myocardial ischemia-reperfusion injury.[50] Furthermore, given the potential of HSG4112 to induce PON2 expression in a diet-induced obesity model, I explored the role that PON2 might be playing as a mode of action for HSG4112 by conducting experiments using PON2-def mice on an obesifying diet.

Male and female, WT and PON2-def mice (n=5/group) were fed a high fat, high sucrose diet ± HSG4112 for three weeks (Figure 25A). Male, PON2-def mice did not significantly gain weight after being fed an obesifying diet, while the female, PON2-def group did (Figure 25B). This result mirrors what Dr. Shih observed in her studies and suggests a sex specific effect that PON2 deficiency plays in the development of obesity. HSG4112 significantly reduces the body weight of both male and female, WT and PON2-def groups, compared to controls (Figure 25B). While there is not a significant difference in the change in weight between the male, WT and PON2-def mice on the HF/HS + HSG4112 diet, there is a significantly reduced capacity of the drug to decrease the body weight of the female, PON2-def group when compared to the WT, drug treated group (Figure 25B). This indicates that although HSG4112 appears to have a protective effect in reducing body weight, that capacity is limited when PON2 is deficient, suggesting that PON2 might play a role in HSG4112's mechanism of action. Furthermore, HSG4112 significantly reduces the fat mass (both male and female) and increases muscle mass (male) in the WT group, but that protective effect is absent in

the PON2-def group (Figure 25C-D). Additionally, lactonase activity in the plasma of the PON2-def mice was not significantly changed by HSG4112 treatment (Figure 25E), a shift from its enhancing effect seen under baseline, chow fed conditions, further supporting the theory that HSG4112's protective effect is diminished when encountering an external stressor, in this case an obesifying diet and PON2 deficiency. Moreover, HSG4112 treatment only significantly reduces plasma glucose levels in the WT (male and female) groups, it does not do so in the PON2-def groups (Table 4). These data strongly suggest that PON2 could play a significant role in modulating HSG4112 function.

In order to test whether HSG4112 has potential to rescue the diet-induced obesity phenotype, I conducted a final experiment whereby WT and PON2-def mice were fed HF/HS diet for three weeks, followed by a HF/HS diet with HSG4112 for another three weeks. Body weights were significantly reduced with HSG4112 treatment, for both WT and PON2-def groups (Figure 26B). Fat mass is significantly increased by HF/HS diet after 3 weeks of feeding in both WT and PON2-def groups. Nevertheless, fat mass is only reduced by HSG4112 in the female, WT group, with the female, PON2-def group maintaining significantly higher fat mass content than their WT controls (Figure 26C). Also, HSG4112 is unable to rescue the loss of muscle mass in both WT and PON2-def groups (Figure 26D). Lastly, HSG4112 treatment strongly reduces food consumption in the PON2-def group, particularly in the females (Figure 26E), which can serve as one explanation for the pronounced loss of body weight in the PON2-def groups. Yet it is worth noting that although the PON2-def mice, specifically the females, on the diet with HSG4112 ate dramatically less than their WT controls, they still

maintain a high fat mass indicating that: a) their lack of food consumption has no bearing on their capacity to develop obesity, in terms of fat mass content and b) HSG4112 is confirmed to have no capacity to reduce their fat mass content, which it consistently does in its WT control group (Figure 24C, 25C). Nevertheless, it is important to determine whether the mice are merely not eating the food due to their own desire or whether HSG4112 is suppressing their appetite, which measuring plasma leptin and insulin levels can help delineate. To further elucidate the protective role that HSG4112 plays in modulating diet-induced obesity, I used a hyperlipidemic, LDLR-KO, mouse model.

LDLR-KO mice were fed either a Chow ± HSG4112 or an obesifying western diet (WD) ± HSG4112 for three weeks (Figure 25A). HSG4112 only significantly reduces the body weights and fat mass, while increasing muscle mass in both male and female, LDLR-KO mice on the western diet; while unaltering the body weights, fat mass, or muscle mass of LDLR-KO mice fed a chow diet (Figure 25B-D). This suggests that although someone might be predisposed to obesity, HSG4112's protective effects are only observed when the body is faced with an external stressor, namely an obesifying diet. In this study, lactonase and arylesterase activity was not enhanced in the plasma of any group (Figure 25E). Moreover, HSG4112 treatment in both male and female, LDLR-KO mice fed chow or WD led to a significant decrease in both lactonase and arylesterase activity. Therefore, it might be noted that genetic predisposition for hyperlipidemia might negatively interfere with the pathway by which HSG4112 acts to modulate various innate paraoxonase activities. Furthermore, this paradoxical observation extends to HSG4112's role in modulating plasma lipids. More specifically,

HSG4112 treatment increases triglycerides in all groups, but only significantly in the male and female groups fed chow + HSG4112 (Table 1). On the other hand, HSG4112 treatment decreases plasma glucose levels in all groups, while only significantly in the female chow + HSG4112 group and trending significantly (p=0.06) in the female WD + HSG4112. These data also seem to point to a possible gender specific role for HSG4112.

It is worth noting the gender specificity that PON2 deficiency has in both inducing obesity through a HF/HS diet (previously reported) and the amelioration of HSG4112 protection.[6] One possible explanation could be in the differential expression of PON2 between male and female mice, with WT, female mice expressing higher PON2 levels in all tissues.[113] In fact, estrogen has been shown to induce PON2 expression, with estradiol transcriptionally activating PON2 via activation of estrogen receptor-α.[114] This modulation was further observed in female mice that received an ovariectomy, in which PON2 levels were significantly reduced the striatum, cerebral cortex and liver to levels observed in males.[114] Also, glabridin and derivates has been shown to bind to estrogen receptor and have estrogen-like activities, such as having inhibitory effects on the growth of breast cancer.[115] Therefore, HSG4112's protective effect could also be acting by way of estrogen agonism; thus potentially having more robust effects on females, although that still needs to be determined. Taken together, the increased expression of PON2 in female, WT mice (and thus more pronounced loss in PON2-def mice) coupled with the potential for the involvement of estrogen agonism by HSG4112, could serve as potential explanation for increased susceptibility of female, PON2-def mice to diet-induced obesity and the corresponding loss of HSG4112's protective effects.

The protective capacity of HSG4112 on diet-induced obesity, which is significantly reduced in PON2 deficiency, strongly suggests the role that PON2 plays as a mode of action for the drug. Recent studies by Glaceum have demonstrated that HSG4112 significantly reduces mitochondrial ROS and increases ATP production (unpublished data). This overlaps with PON2's protective capacity of reducing mitochondrial ROS and increasing ATP, among other protective phenotypes, and supports the connection of PON2 in modulating HSG4112's therapeutic effects.[5, 50] Consequently, HSG4112's antioxidant properties in the mitochondria could further extend to modulating lipid peroxidation, leading me to hypothesize that HSG4112 will reduce lipid peroxidation, particularly in the mitochondria. Therefore, evaluating the ability of HSG4112 to modulate systemic and mitochondrial lipid peroxidation, specifically eicosanoid and prostanoid production, will serve as an important mechanism of action to explore; especially given PON2's ability to modulate mitochondrial lipid peroxidation.

5.5 Conclusions

- HSG4112 modulates PON activity under baseline (chow diet) conditions, significantly enhancing lactonase and arylesterase activity in the plasma and livers of WT, PON1-KO, and PON2-def mice, while also enhancing PON1 and PON3 protein expression in these mice as well (compared to chow fed controls).
- PON2 deficiency significantly reduces the protective capacity of HSG4112. Although there is a reduction in body weight in both WT and PON2-def mice fed a HF/HS diet with HSG4112, the difference in body weight loss in the PON2-def (female) mice is significantly reduced compared to the WT controls. Moreover, HSG4112 treatment fails to reduce fat mass, increase muscle mass, enhance lactonase activity or reduce plasma glucose levels.
- HSG4112 treatment has a limited capacity to rescue the obesifying effect of three weeks of HF/HS diet in both WT and PON2-def mice. Although HSG4112 treatment significantly reduced the body weight of both female WT and PON2-def groups treated with HSG4112 after three weeks of obesifying diet, only the female, WT group had a significant reduction of fat mass. This further supports the role that PON2 plays as a mode of action for HSG4112 protection.
- HSG4112 has protective effects against hyperlipidemic (LDLR-KO), western diet fed mice, significantly reducing the body weight and fat mass, while increasing lean mass in both male and female groups. Furthermore, HSG4112's capacity to reduce plasma glucose levels in these mice was only observed in the female mice.

- Of note, HSG4112's protective effect on body weight and fat/muscle mass was only observed in the LDLR-KO mice fed a high fat, western diet and not a chow diet. This suggests that an external stressor (i.e. diet) is needed to trigger the effects of HSG4112, regardless of genetic predisposition to hyperlipidemia.

Figure 24A

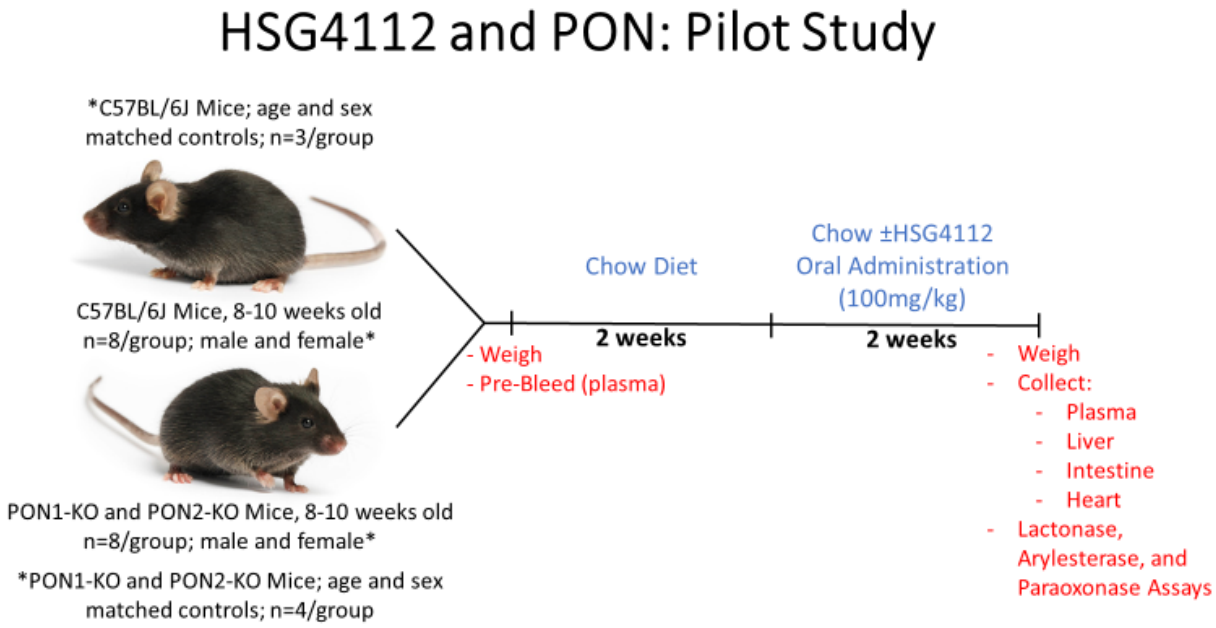
HSG4112 and PON: Pilot Study
*C57BL/6J Mice; age and sex matched controls; n=3/group
C57BL/6J Mice, 8-10 weeks old n=8/group; male and female*
PON1-KO and PON2-KO Mice, 8-10 weeks old n=8/group; male and female*
*PON1-KO and PON2-KO Mice; age and sex matched controls; n=4/group
Chow Diet
2 weeks
Chow ±HSG4112 Oral Administration (100mg/kg)
2 weeks
- Weigh
- Pre-Bleed (plasma)
- Weigh
- Collect:
- Plasma
- Liver
- Intestine
- Heart
- Lactonase, Arylesterase, and Paraoxonase Assays

Figure 24B

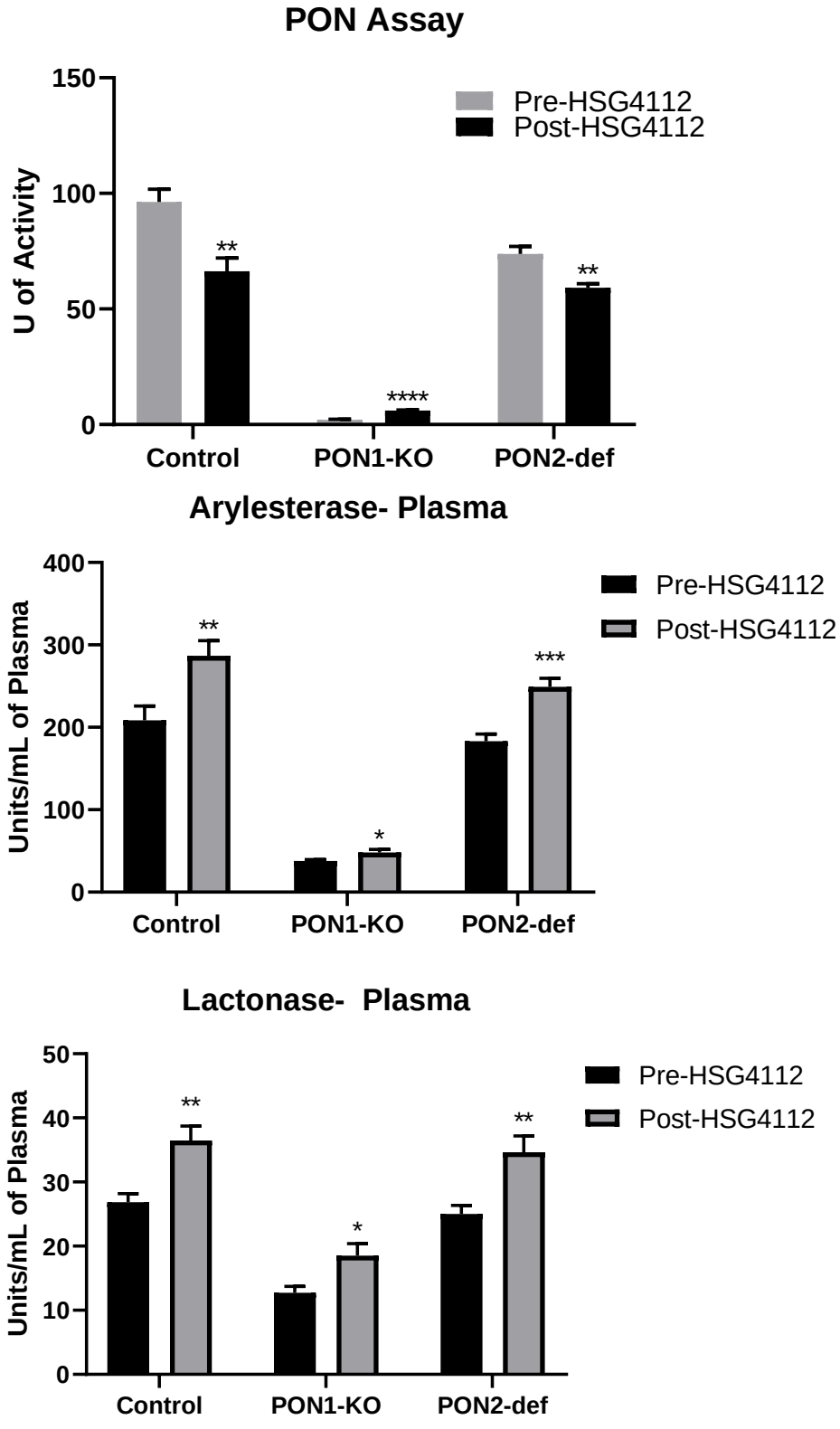
PON Assay
U of Activity
150
100
50
0
Pre-HSG4112
Post-HSG4112
**
****
**
Control
PON1-KO
PON2-def
Arylesterase- Plasma
Units/mL of Plasma
400
300
200
100
0
**
*
***
Pre-HSG4112
Post-HSG4112
Control
PON1-KO
PON2-def
Lactonase- Plasma
Units/mL of Plasma
50
40
30
20
10
0
**
*
**
Pre-HSG4112
Post-HSG4112
Control
PON1-KO
PON2-def

Figure 24C

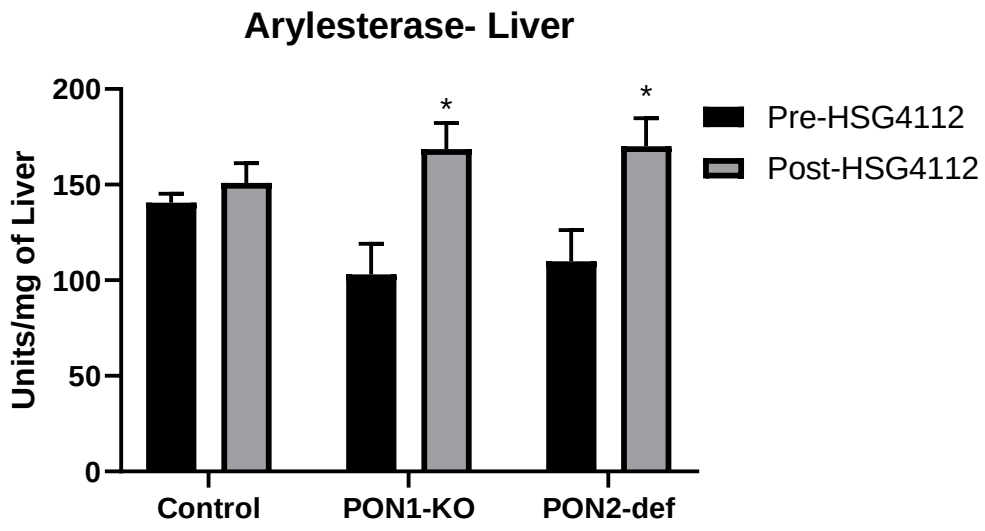
Arylesterase- Liver
Units/mg of Liver
200
150
100
50
0
*
*
Control
PON1-KO
PON2-def
Pre-HSG4112
Post-HSG4112

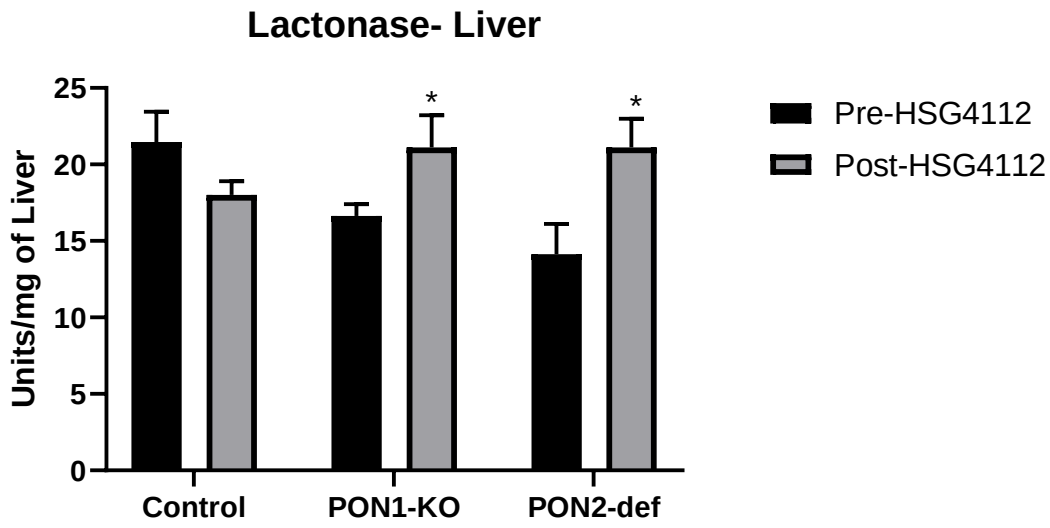
Lactonase- Liver
Units/mg of Liver
25
20
15
10
5
0
*
*
Control
PON1-KO
PON2-def
Pre-HSG4112
Post-HSG4112

Figure 24D

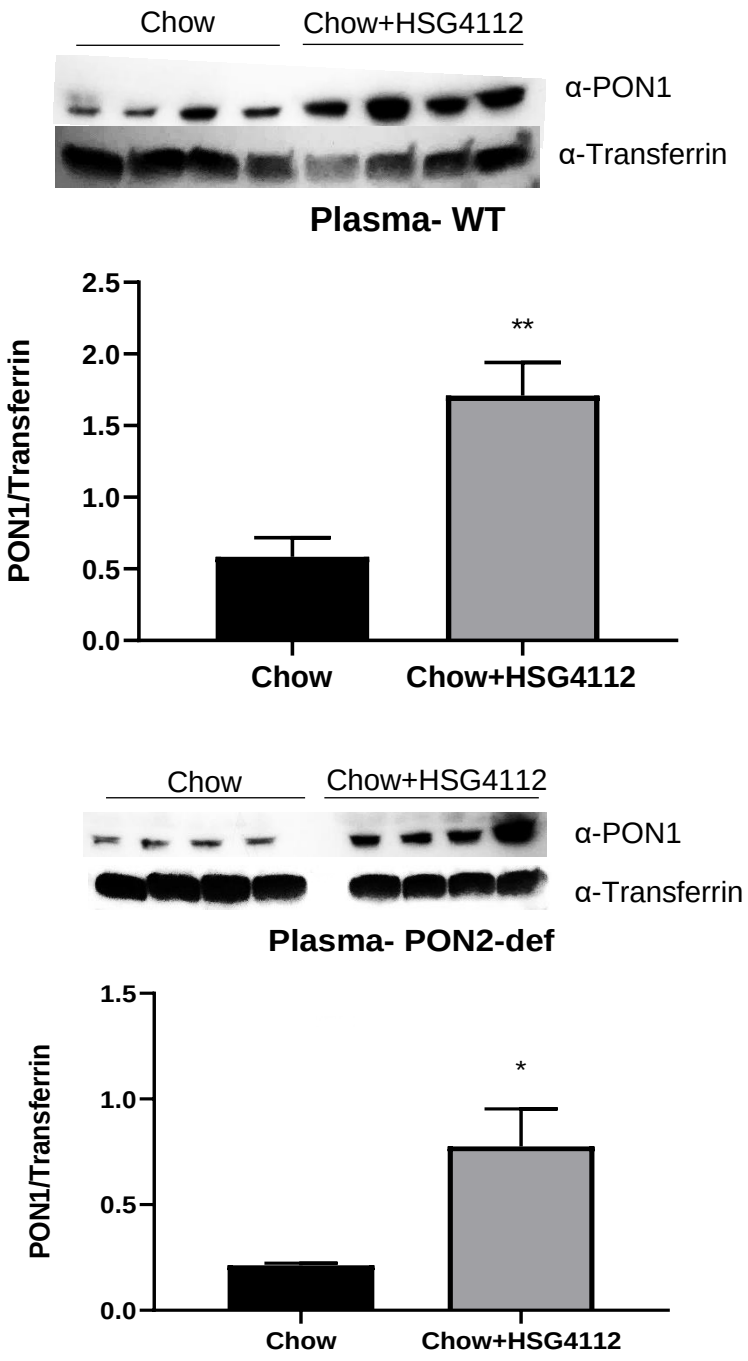
Chow
Chow+HSG4112
α-PON1
α-Transferrin
Plasma- WT
PON1/Transferrin
2.5
2.0
1.5
1.0
0.5
0.0
**
Chow
Chow+HSG4112
Chow
Chow+HSG4112
α-PON1
α-Transferrin
Plasma- PON2-def
PON1/Transferrin
1.5
1.0
0.5
0.0
*
Chow
Chow+HSG4112

Figure 24E

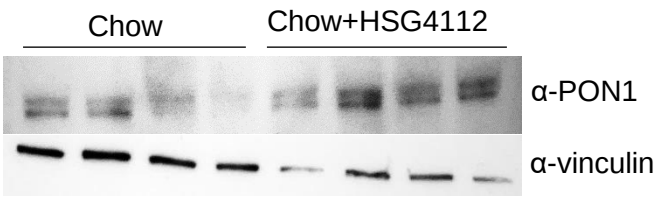
Chow
Chow+HSG4112
α-PON1
α-vinculin

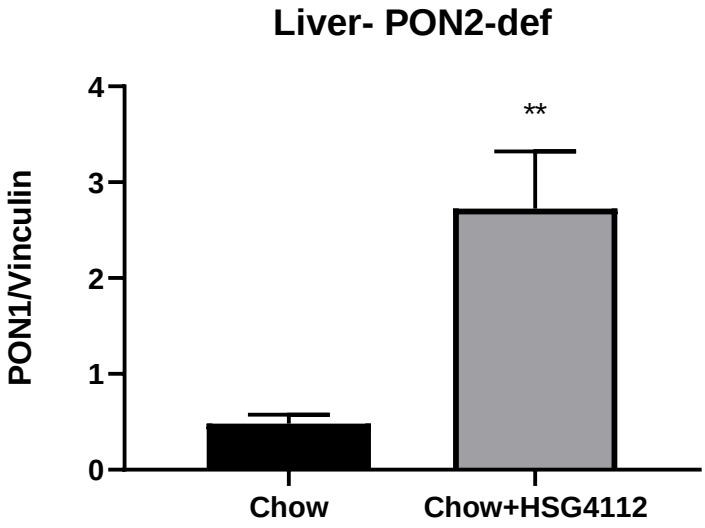
Liver- PON2-def
PON1/Vinculin
4
3
2
1
0
**
Chow
Chow+HSG4112

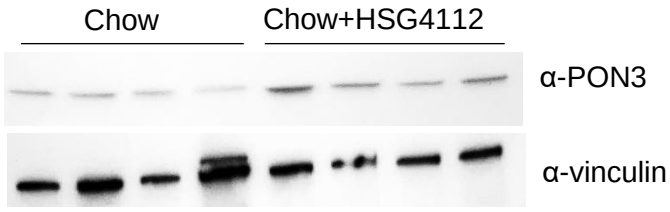
Chow
Chow+HSG4112
α-PON3
α-vinculin

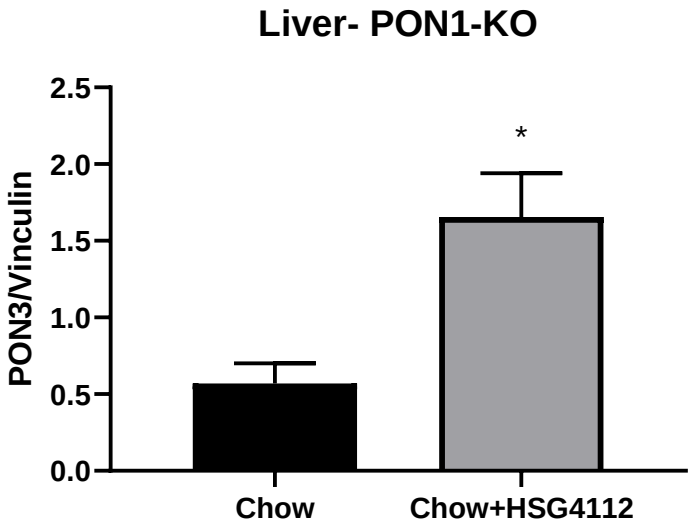
Liver- PON1-KO
PON3/Vinculin
2.5
2.0
1.5
1.0
0.5
0.0
*
Chow
Chow+HSG4112

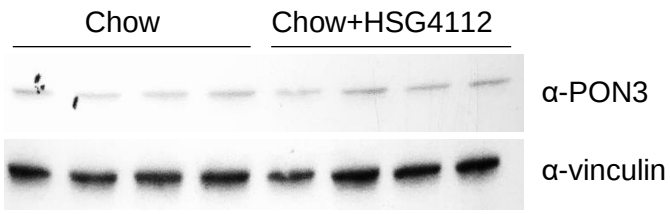
Chow
Chow+HSG4112
α-PON3
α-vinculin

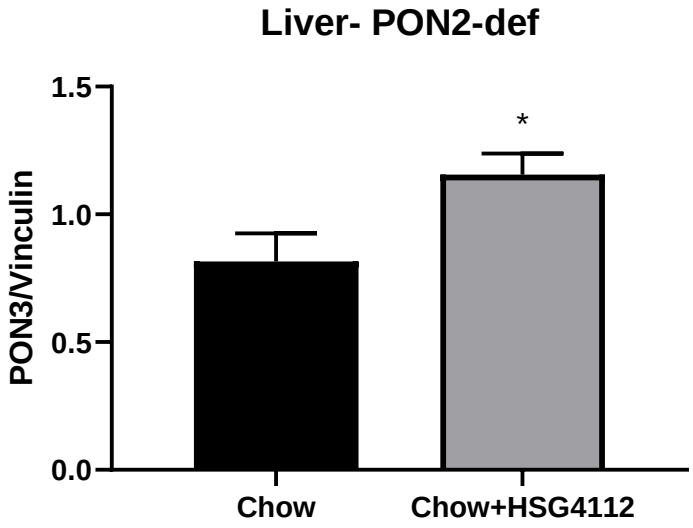
Liver- PON2-def
PON3/Vinculin
1.5
1.0
0.5
0.0
*
Chow
Chow+HSG4112

Figure 24: Role of HSG4112 in modulating expression and activity of Paraoxonases. (A) Three mice stains were utilized for this study, WT (C57BL/6J), PON1-KO, and PON2-def. Both male and females, between 8-10 weeks of age, were used with 8 mice per group for the HSG4112 treated mice, whereas the respective age/sex matched controls were 3-4 mice per group. The mice were weighed and bled prior to the start of the experiment. The mice were left on a standard chow diet for 2 weeks, followed by another two weeks of chow ± HSG4112. At the end of 4^{th} week, the experiment was terminated. Paraoxonase, Arylesterase, and Lactonase assays were performed on the plasma (B) and livers (C) from control, PON1-KO, and PON2-def mice. Of note, the results from the pre-HSG4112 group are from pre-bleeds collected prior to the start of the experiment, while the post-HSG4112 group are from the plasma collected during the termination of the experiment. (D) PON1 expression (n=4/group) was evaluated in the plasma of WT and PON2-def mice via western blot analysis, normalized to transferrin, and quantified as a ratio of PON1 to transferrin. (E) PON1 and PON3 expression (n=4/group) were evaluated in livers of PON1-KO and PON2-def mice fed Chow ± HSG4112, via western blot analysis, normalized to vinculin, and quantified as a ratio of PON1/PON3 to vinculin. 1 unit=μmole of dihydrocumarin (for lactonase) or

phenyl acetate (for arylesterase) hydrolyzed per minute. The data is represented as Mean ± SEM and statistically significant data is noted as *p<0.05,**p<0.01, ***p<0.001, ****p<0.0001.

Figure 25A

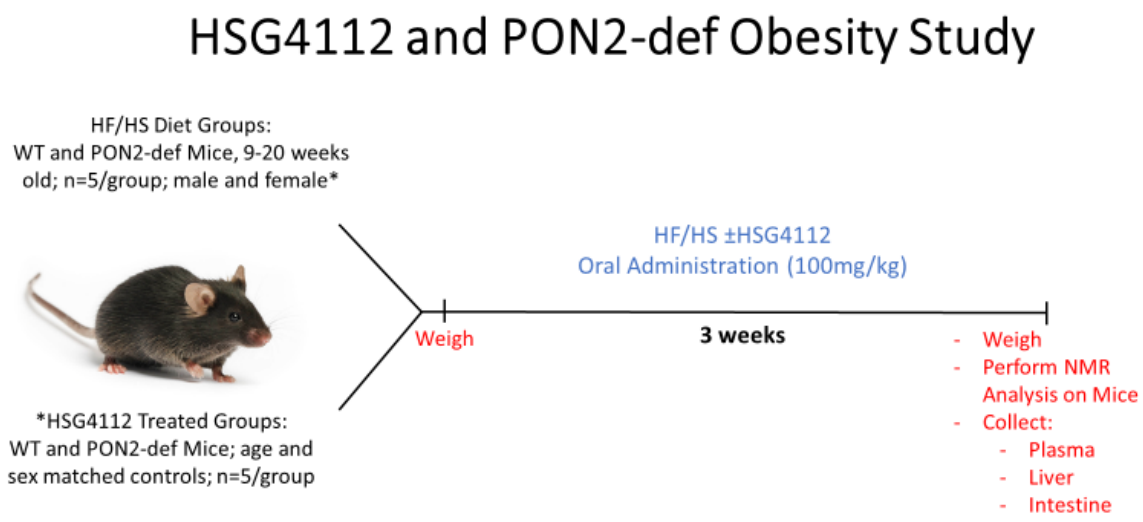

Figure 25B

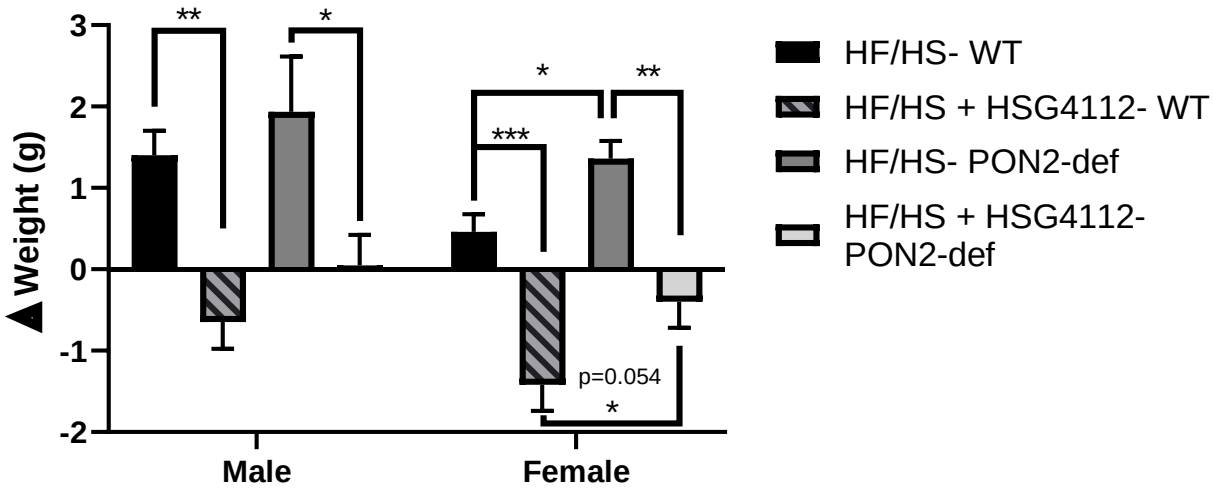

Figure 25C

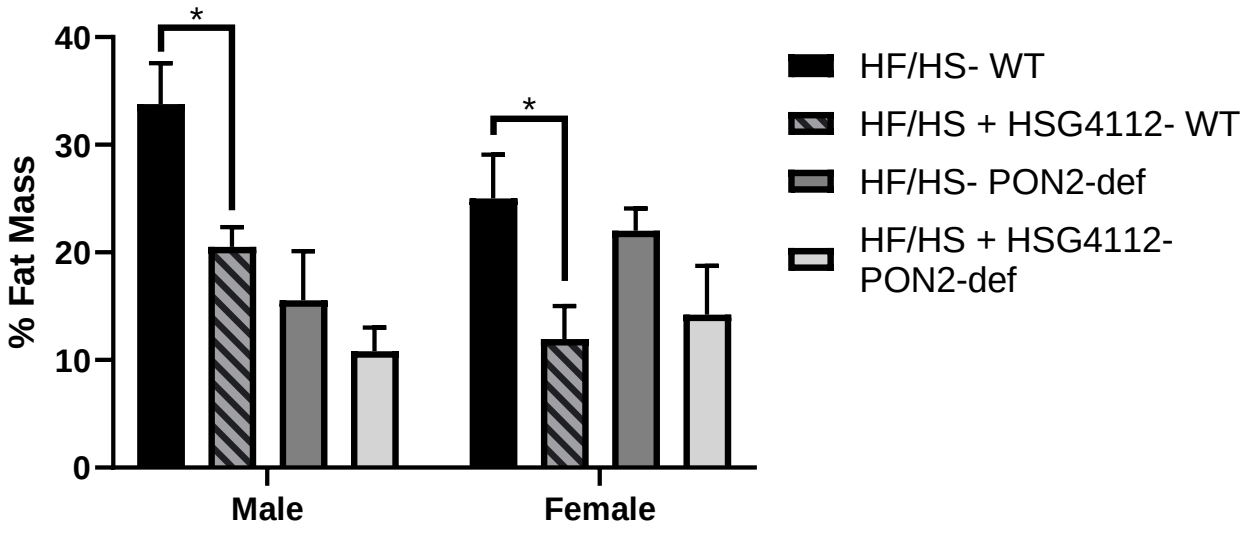

Figure 25D

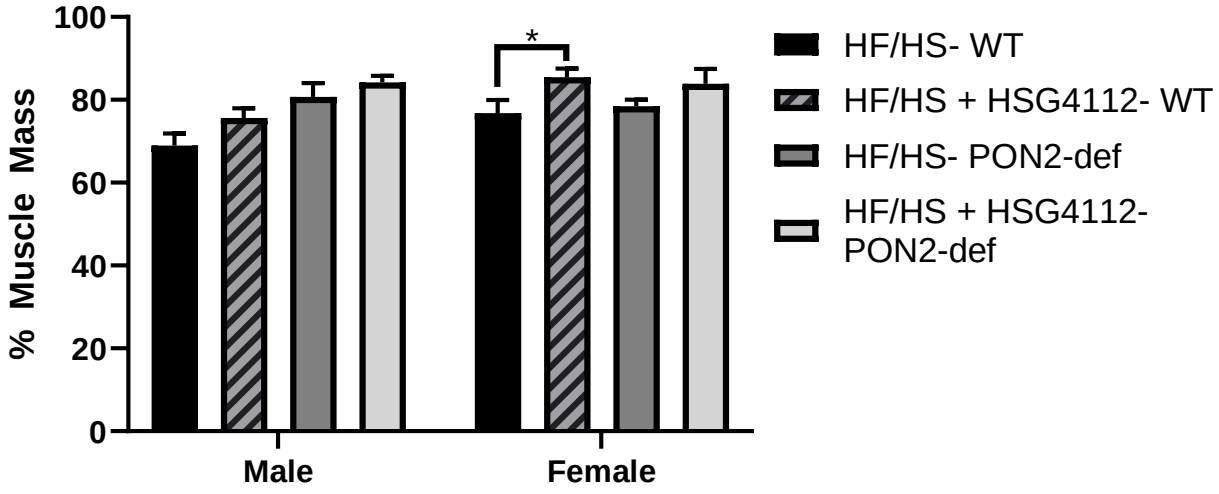

Figure 25E

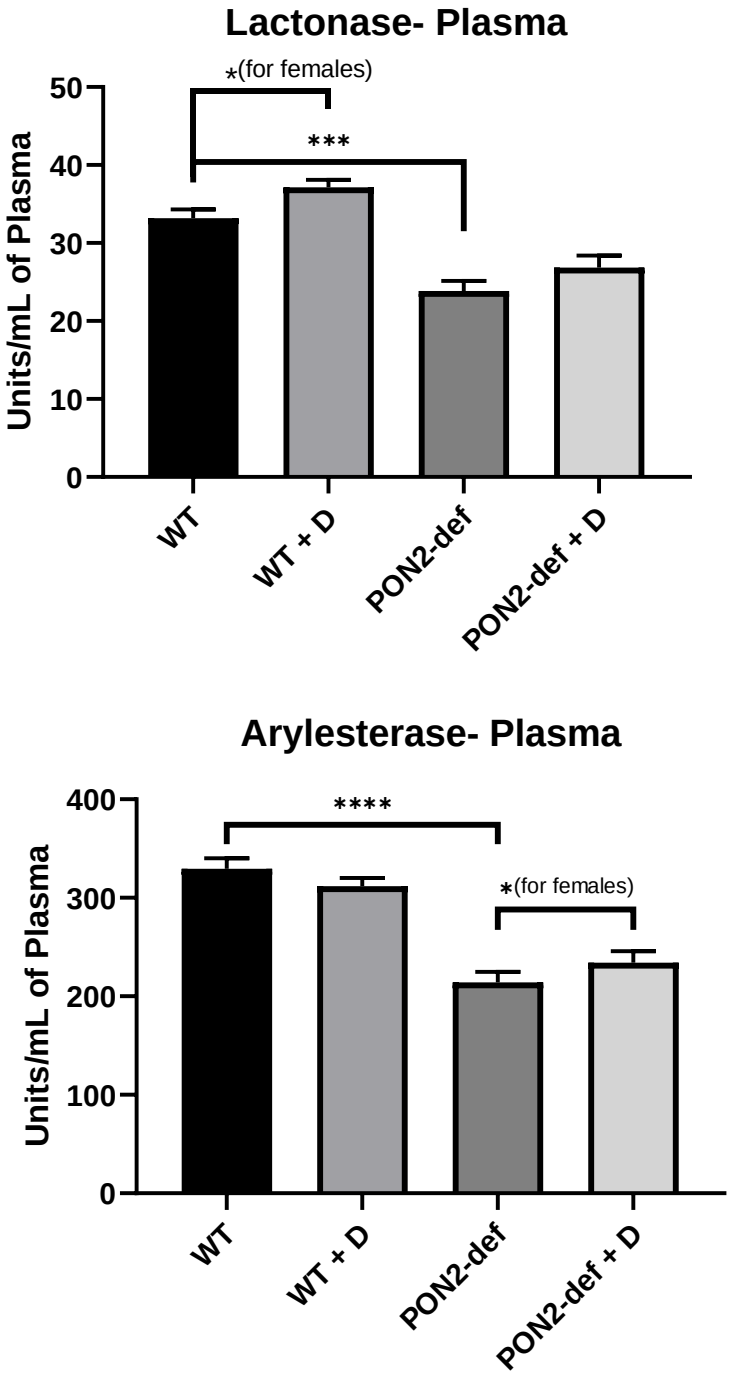
Lactonase- Plasma
*(for females)
***
Units/mL of Plasma
50
40
30
20
10
0
WT
WT + D
PON2-def
PON2-def + D
Arylesterase- Plasma
****
*(for females)
Units/mL of Plasma
400
300
200
100
0
WT
WT + D
PON2-def
PON2-def + D

Figure 25F

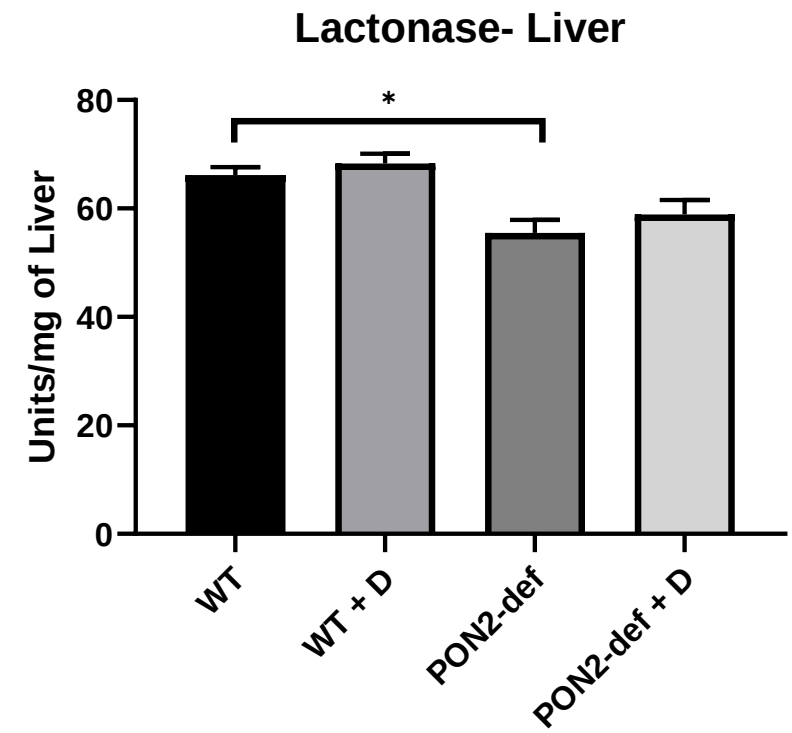
Lactonase- Liver
Units/mg of Liver
80
60
40
20
0
*
WT
WT + D
PON2-def
PON2-def + D

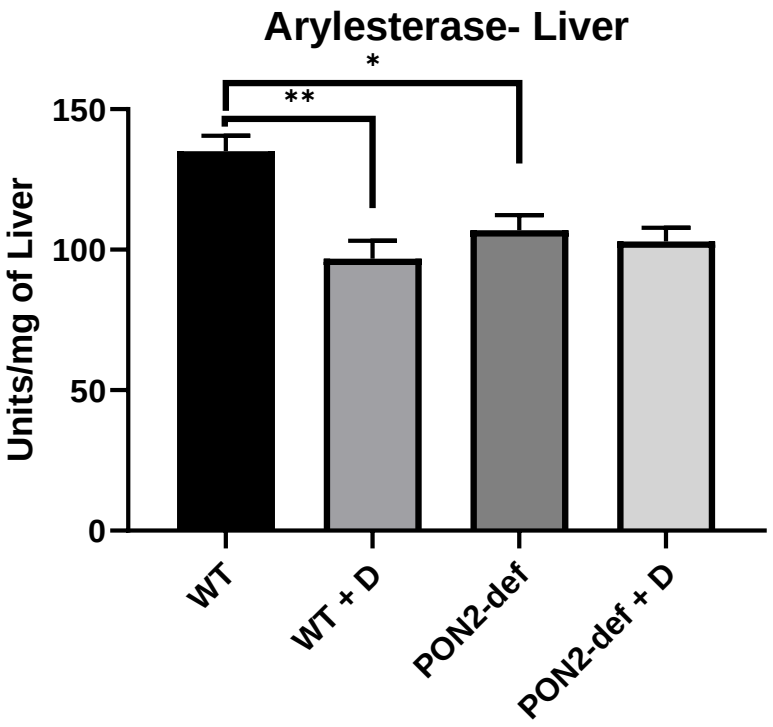
Arylesterase- Liver
Units/mg of Liver
150
100
50
0
*
**
WT
WT + D
PON2-def
PON2-def + D

Figure 25: Role of PON2 in modulating the protective effects of HSG4112. (A) WT (C57BL/6J) and PON2-def mice were utilized to investigate the role of PON2 in modulating the protective effects of HSG4112 against diet-induced obesity. Mice were fed High Fat/High Sucrose (HF/HS) with and without HSG4112 for 3 weeks. Dosing of HSG4112 was at 100mg/kg. Both male and female mice, between 9-20 weeks of age, with 5 mice per group were used for this study. The mice were weighed prior to the start of the experiment. At the end of third week of feeding, the experiment was terminated. (B) Changes in weight (grams) were determined between the weight of the mice before the start of the experiment and weights collected at the end of 2 weeks of diet. (C) Fat mass changes were assessed and quantified as percentage of final fat mass (grams) over total body weight (grams) x 100. (D) Muscle (lean) mass were assessed and quantified as percentage of final muscle mass (grams) over total body weight (grams) x 100. Arylesterase and lactonase activities were assessed in the terminal collections of plasma (E) and livers (F). 1 unit=μmole of dihydrocumarin (for lactonase) or phenyl acetate (for arylesterase) hydrolyzed per minute. The data is represented as Mean ± SEM and statistically significant data is noted as *p<0.05,**p<0.01, ***p<0.001, ****p<0.0001.

Figure 26A

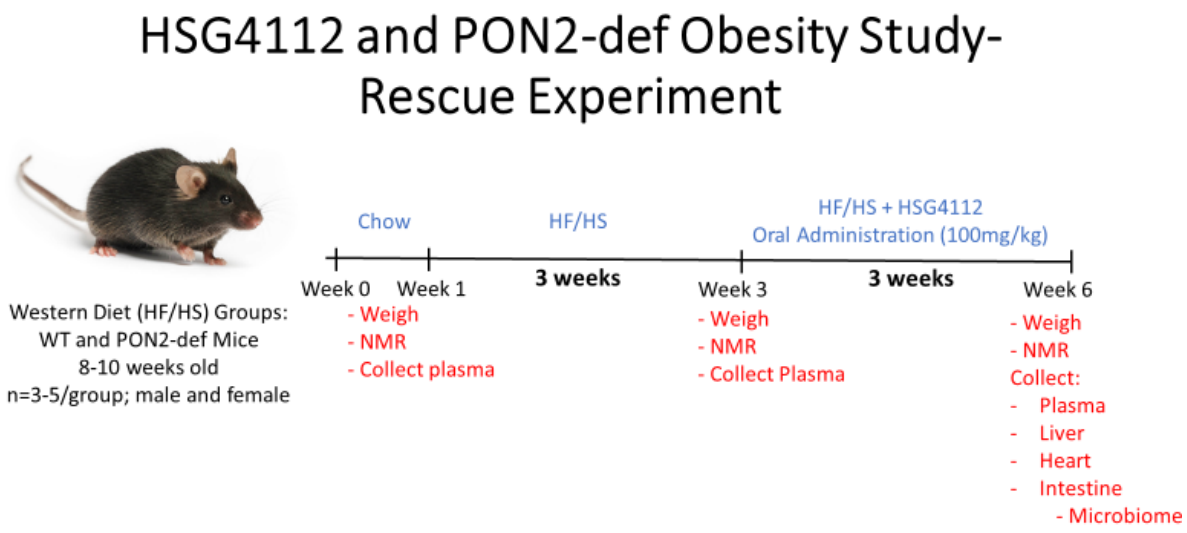
HSG4112 and PON2-def Obesity Study-
Rescue Experiment
Western Diet (HF/HS) Groups:
WT and PON2-def Mice
8-10 weeks old
n=3-5/group; male and female
Chow
HF/HS
HF/HS + HSG4112
Oral Administration (100mg/kg)
Week 0
Week 1
3 weeks
Week 3
3 weeks
Week 6
- Weigh
- NMR
- Collect plasma
- Weigh
- NMR
- Collect Plasma
- Weigh
- NMR
Collect:
- Plasma
- Liver
- Heart
- Intestine
- Microbiome

Figure 26B

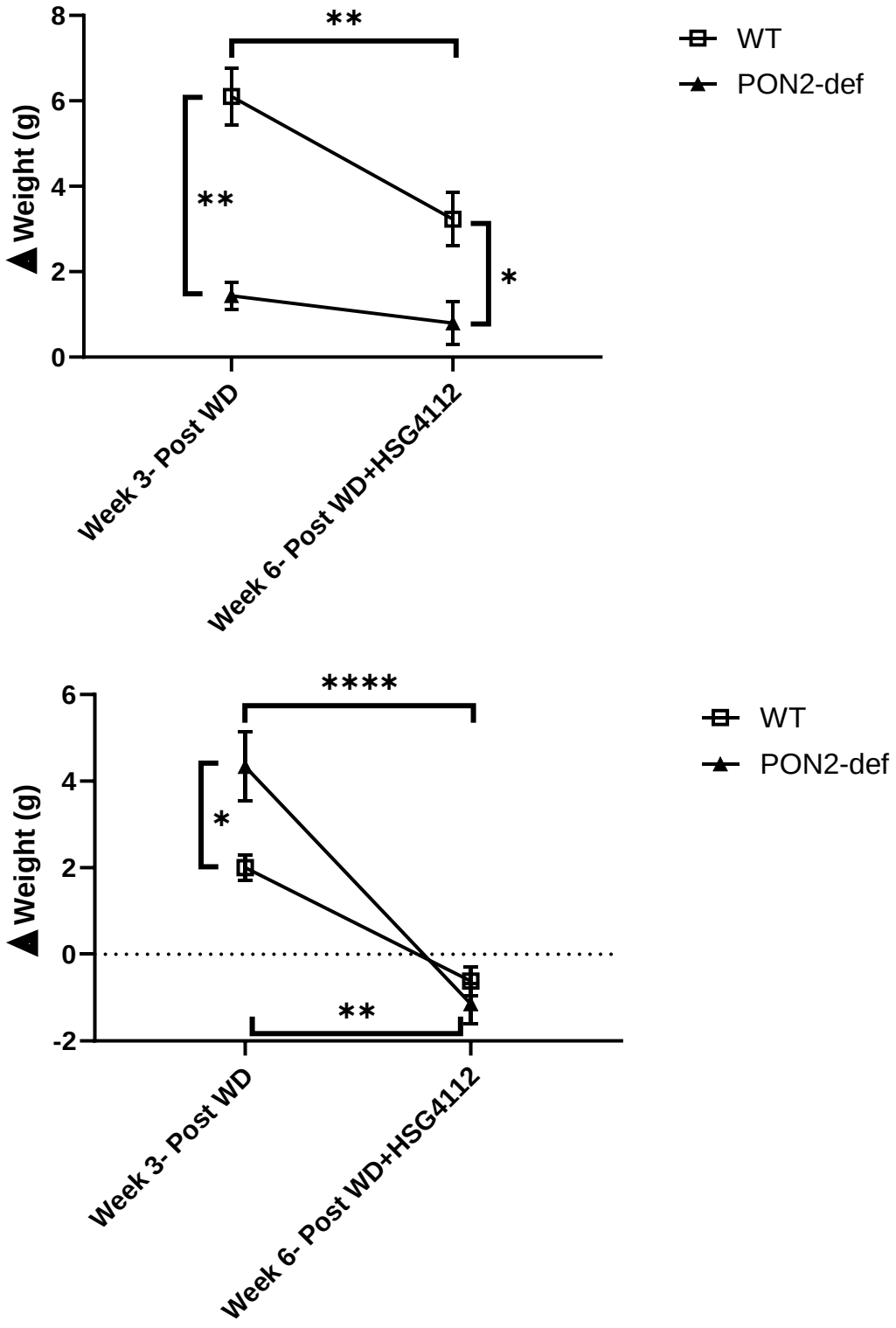
8
6
4
2
0
Weight (g)
**
**
*
WT
PON2-def
Week 3- Post WD
Week 6- Post WD+HSG4112
6
4
2
0
-2
Weight (g)
****
*
**
WT
PON2-def
Week 3- Post WD
Week 6- Post WD+HSG4112

Figure 26C

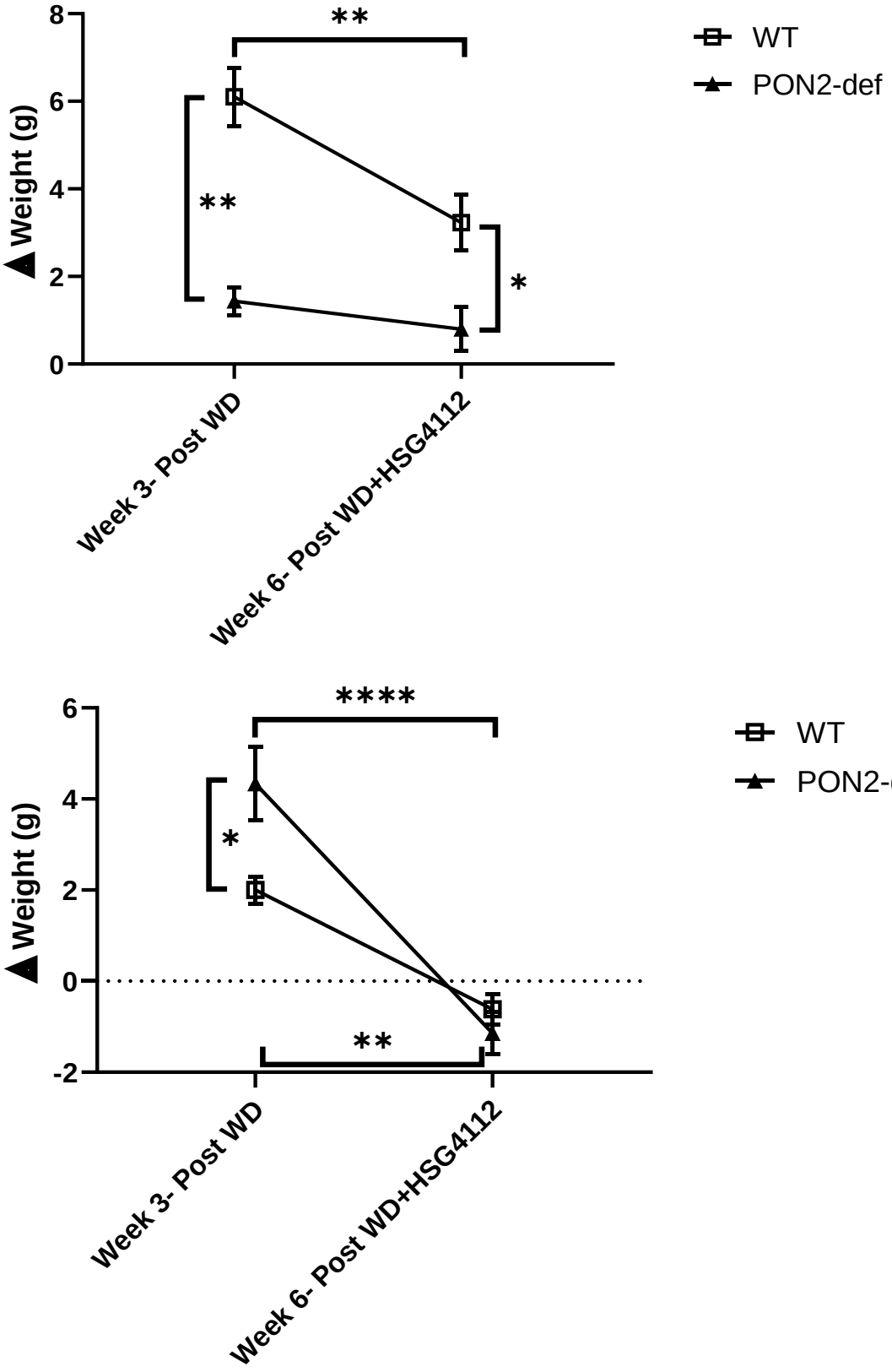
8
6
4
2
0
Weight (g)
**
**
*
WT
PON2-def
Week 3- Post WD
Week 6- Post WD+HSG4112
6
4
2
0
-2
Weight (g)
****
*
**
WT
PON2-def
Week 3- Post WD
Week 6- Post WD+HSG4112

Figure 26D

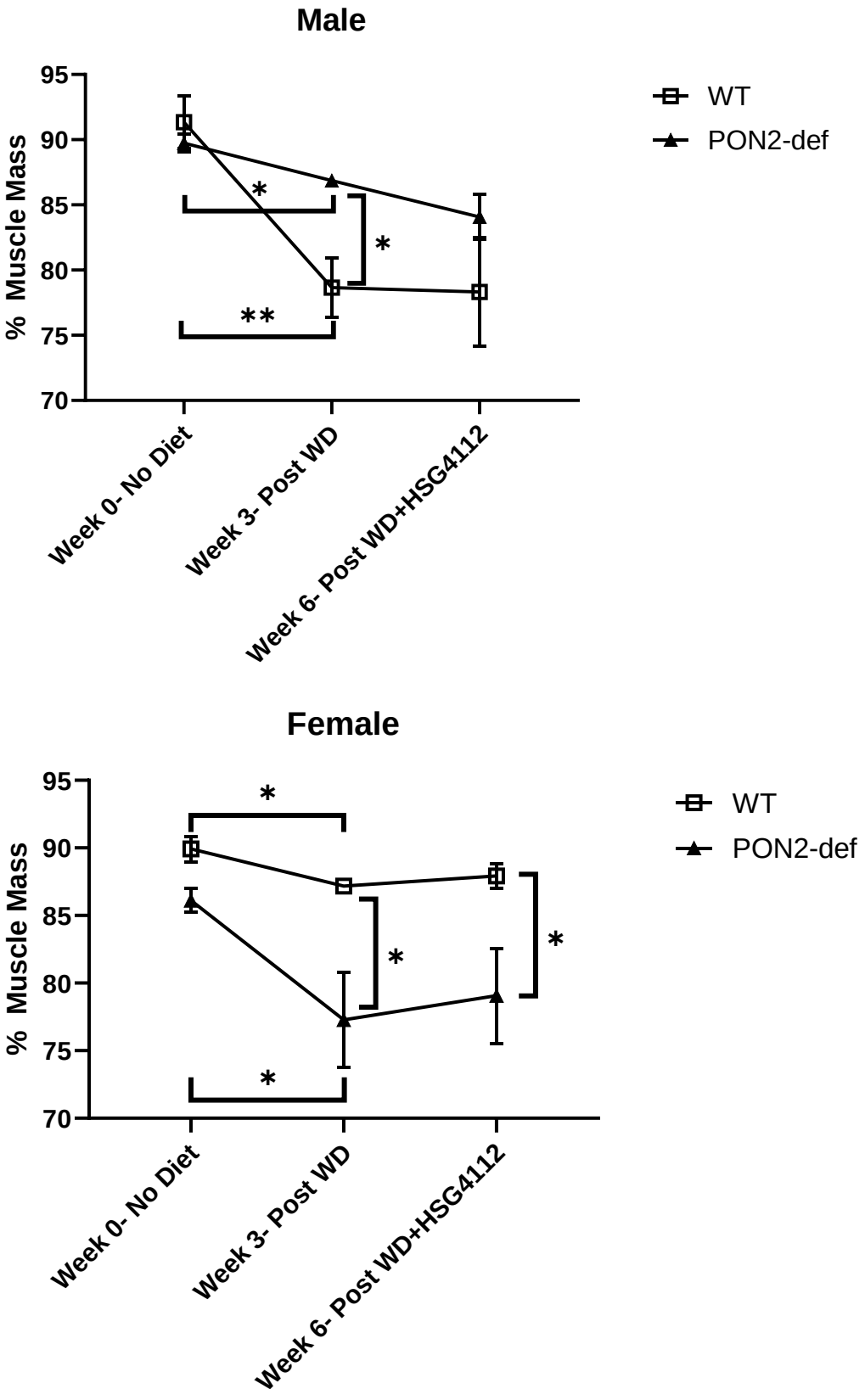
Male
% Muscle Mass
95
90
85
80
75
70
*
*
**
WT
PON2-def
Week 0- No Diet
Week 3- Post WD
Week 6- Post WD+HSG4112
Female
% Muscle Mass
95
90
85
80
75
70
*
*
*
*
WT
PON2-def
Week 0- No Diet
Week 3- Post WD
Week 6- Post WD+HSG4112

Figure 26E

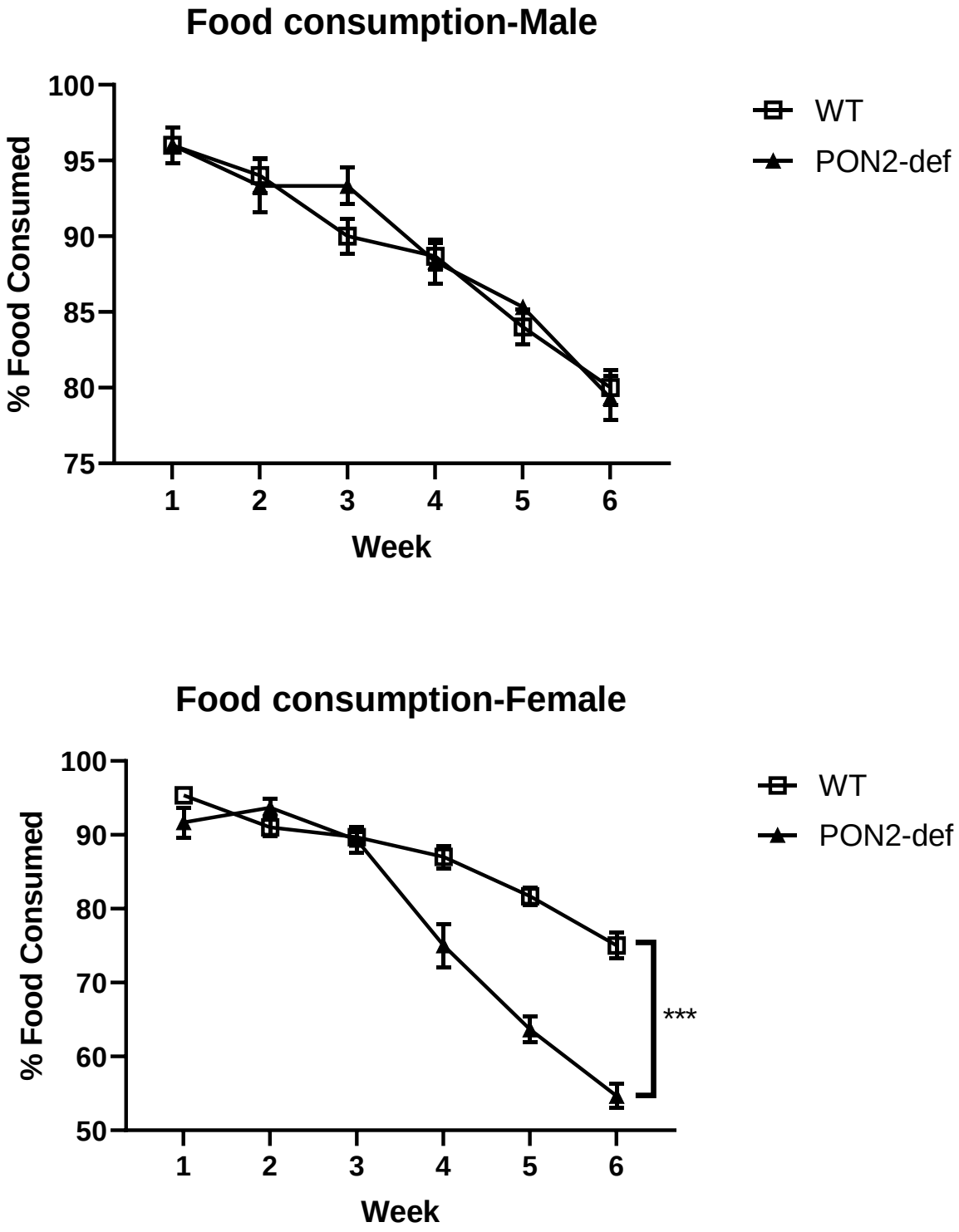
Food consumption-Male
% Food Consumed
100
95
90
85
80
75
1
2
3
4
5
6
Week
WT
PON2-def
Food consumption-Female
% Food Consumed
100
90
80
70
60
50
1
2
3
4
5
6
Week
***
WT
PON2-def

Figure 26: Limited capacity of HSG4112 to rescue obesity phenotype in PON2-def mice. (A) WT (C57BL/6J) and PON2-def mice were utilized to investigate the rescue potential of HSG4112 against diet-induced obesity, while concurrently determining the role PON2 in modulating the protective effects of HSG4112. Both male and female mice, between 8 - 10 weeks of age, with 5 mice per group were used for the study. One week prior to the start of the experiment, mice were weighed, bled for plasma, and NMR was performed to measure fat and lean mass. After one week of recovery, mice were fed HF/HS for 3 weeks. Three days prior to the third week of feeding, the mice were weighed, bled for plasma, and NMR was performed to measure fat and lean mass. Subsequently, the mice were given 3 days to recover (still on HF/HS diet) and were then placed on a HF/HS + HSG4112 (100mg/kg) at the start of fourth week for another 3 weeks of feeding. The end of sixth week of feeding, the experiment was terminated. (B) Changes in weight (grams) were determined between the weight of the mice at week 1 and week 3, and at week 3 and 6. Changes in fat mass (C) and muscle mass (D) in the mouse groups fed HF/HS for three weeks, followed by HF/HS + HSG4112 diet for another 3 weeks were assessed. Data was quantified as percentage of final fat/muscle mass (grams) over total body weight (grams) x 100, at the start of the experiment (week 0), as well as the

end of week 3 and 6. (E) Food consumption was measured per mouse cage with every food change over the course of the six week diet study for male and female, WT and PON2-def mice. The percent of food consumed was determined as the amount of food consumed over the total amount of food originally provided per food container x 100. The data is represented as Mean ± SEM and statistically significant data is noted as *$p<0.05$, **$p<0.01$, and ****$p<0.0001$.

Figure 27A

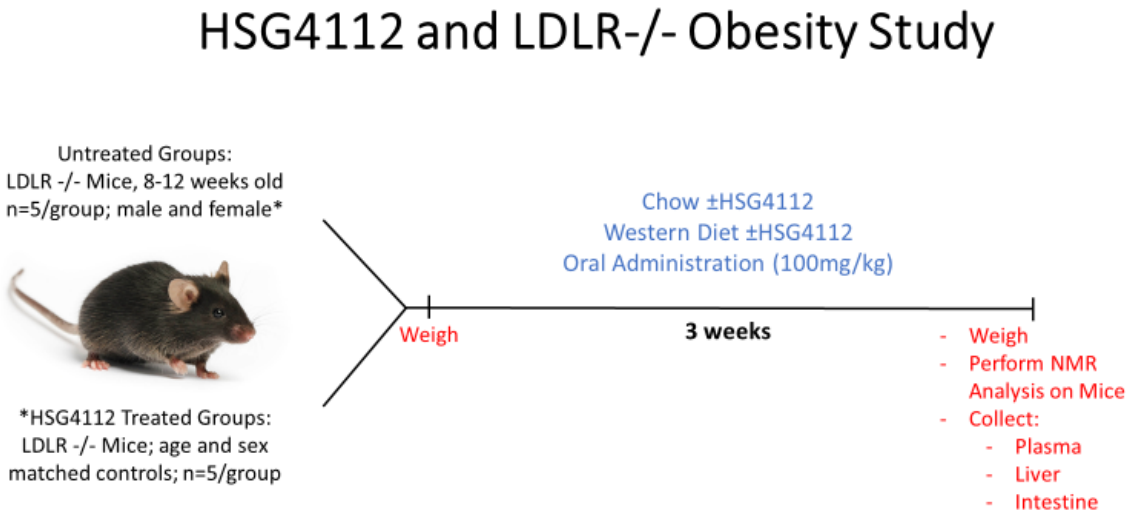

Figure 27B

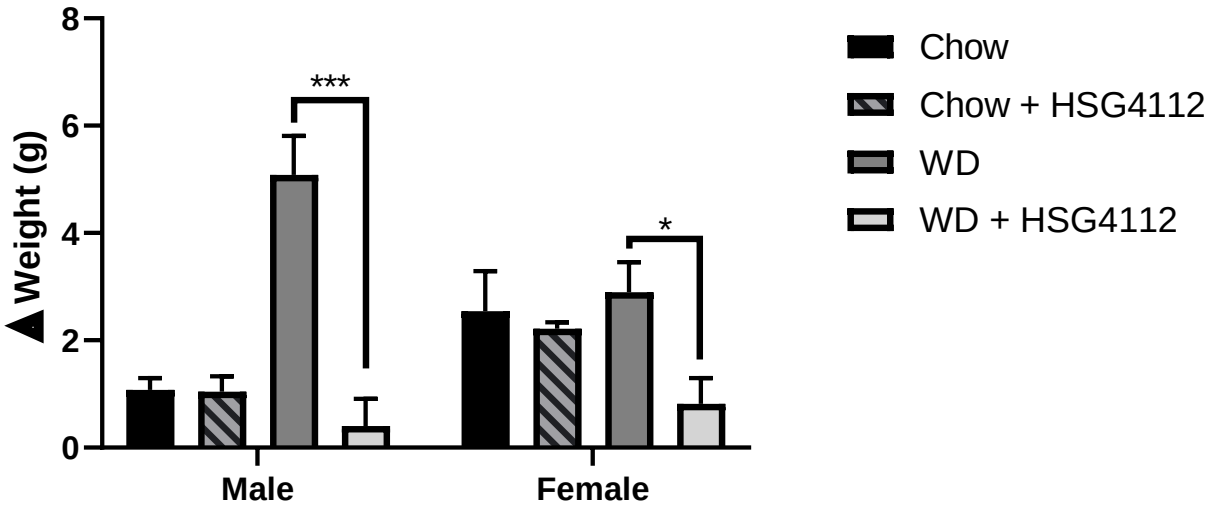

Figure 27C

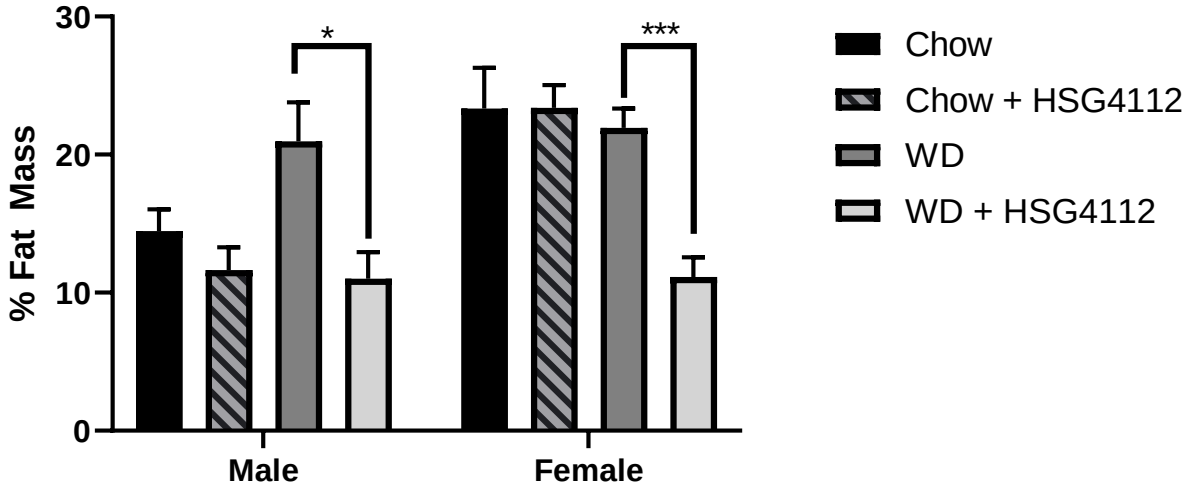

Figure 27D

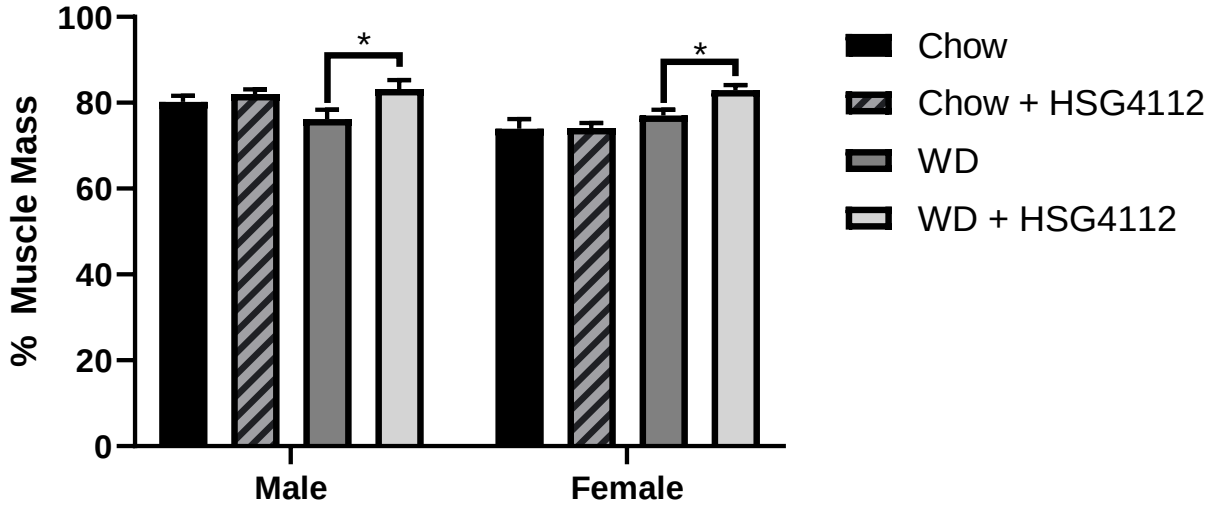

Figure 27E

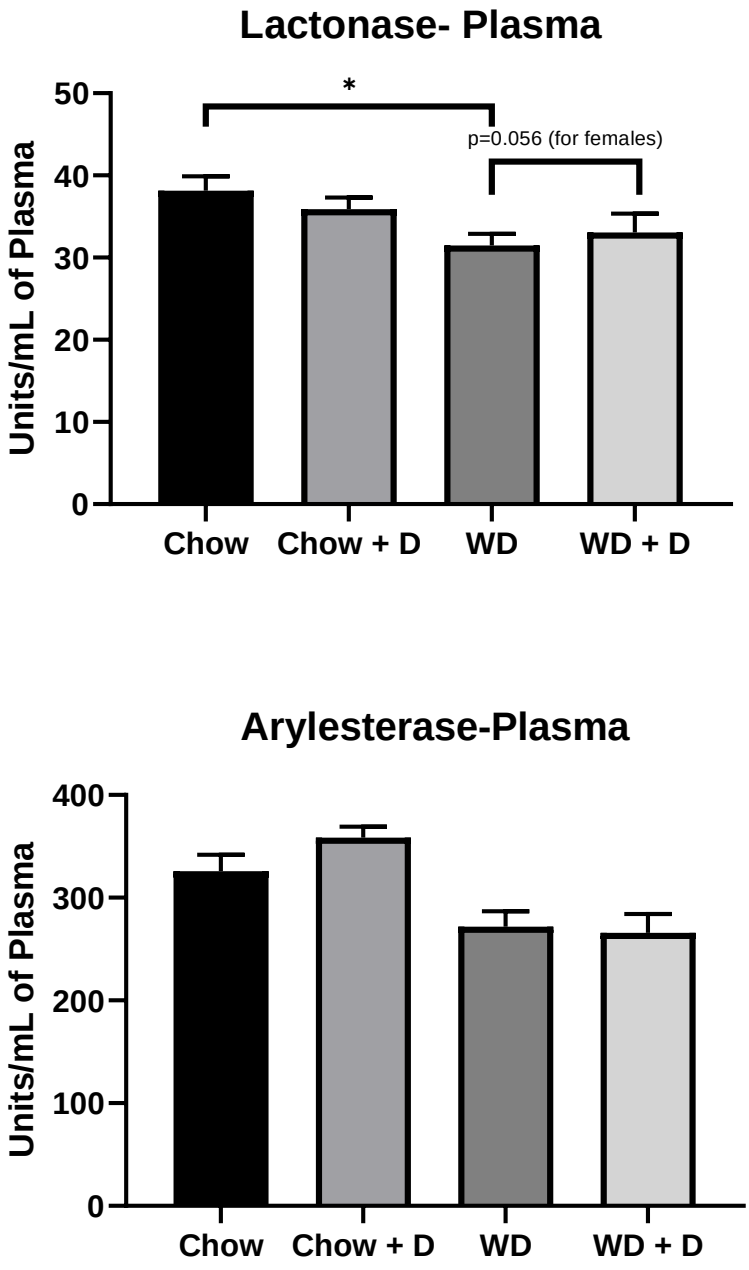
Lactonase- Plasma
*
p=0.056 (for females)
Units/mL of Plasma
50
40
30
20
10
0
Chow
Chow + D
WD
WD + D
Arylesterase-Plasma
Units/mL of Plasma
400
300
200
100
0
Chow
Chow + D
WD
WD + D

Figure 27F

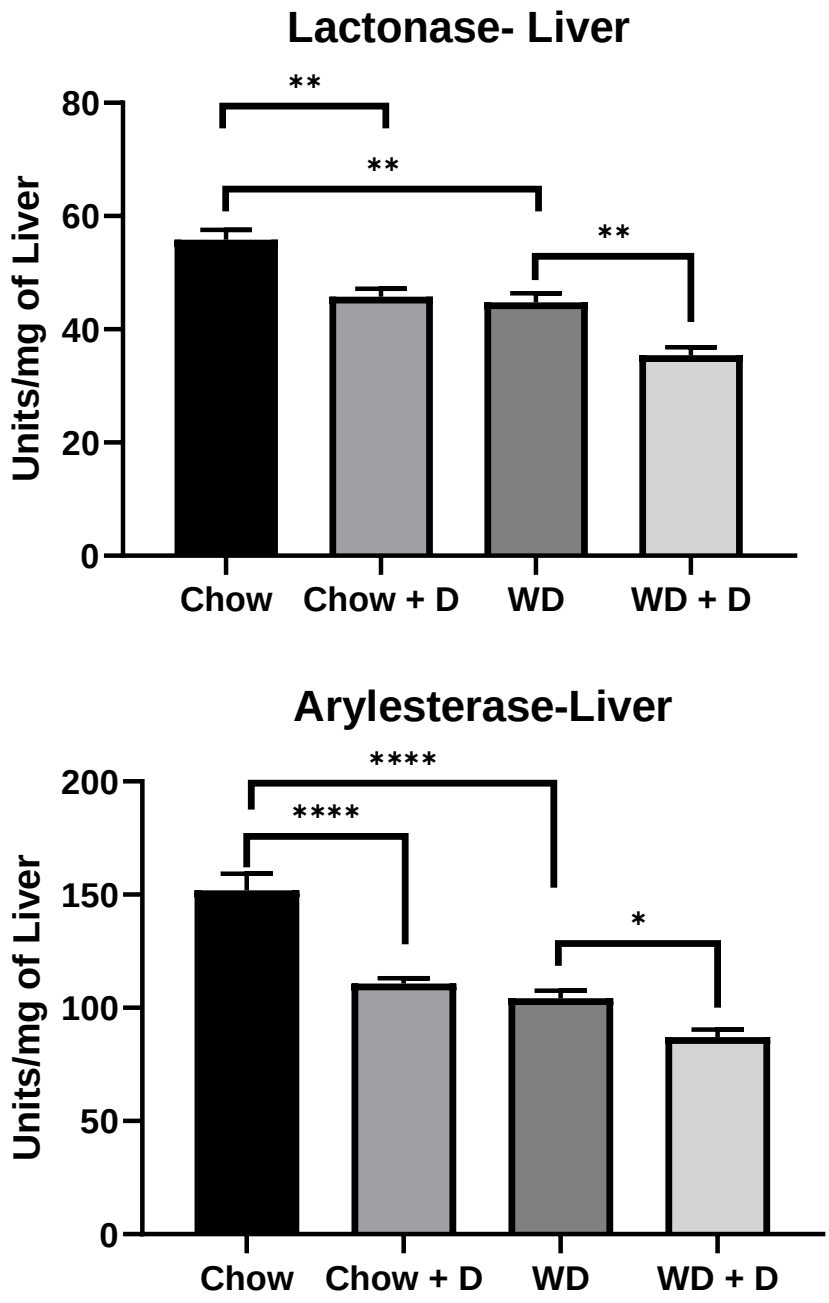
Lactonase- Liver
Units/mg of Liver
80
60
40
20
0
**
**
**
Chow
Chow + D
WD
WD + D
Arylesterase-Liver
Units/mg of Liver
200
150
100
50
0
****
****
*
Chow
Chow + D
WD
WD + D

Figure 27: HSG4112 Protection Against Diet-Induced Obesity in Hyperlipidemic Mice. (A) LDLR-KO mice were utilized to investigate the role of HSG4112 against diet-induced obesity. Mice were fed 4 different diets for 3 weeks: Chow ± HSG4112 or Western Diet (WD) ± HSG4112. Dosing of HSG4112 was at 100mg/kg. Both male and female mice, between 8-12 weeks of age, with 5 mice per group. The mice were weighed prior to the start of the experiment. At the end of third week of feeding, the experiment was terminated. (B) Changes in weight (grams) were determined between the weight of the mice before the start of the experiment and final weights prior to termination. (C) Fat mass changes were assessed and quantified as percentage of final fat mass (grams) over total body weight (grams) x 100. (D) Muscle (lean) mass changes were assessed and quantified as percentage of final muscle mass (g) over total body weight (grams) x 100. Arylesterase and lactonase activities were determined in plasma (terminal plasma collection) (E) and livers (F). 1 unit=μmole of dihydrocumarin (for lactonase) or phenyl acetate (for arylesterase) hydrolyzed per minute. The data is represented as Mean ± SEM and statistically significant data is noted as *p<0.05,**p<0.01, ***p<0.001, ****p<0.0001.

Supplementary Figure 6A

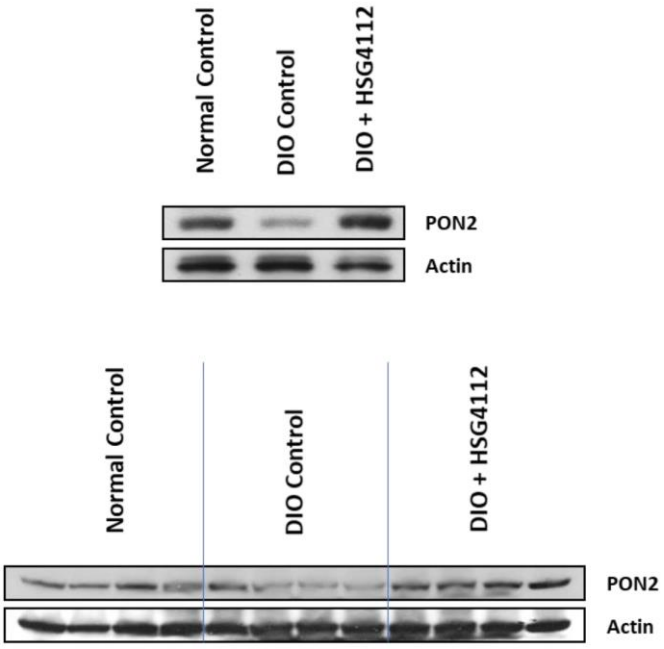

Supplementary Figure 6B

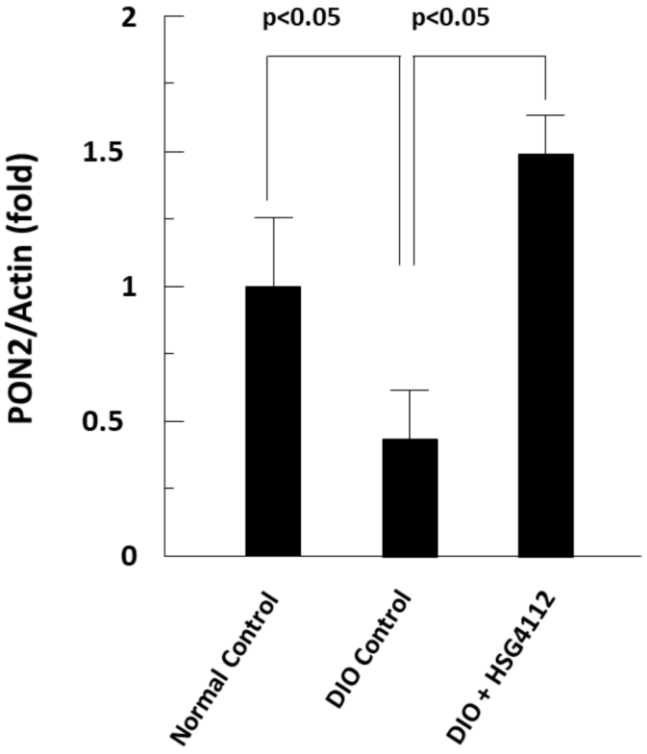

Supplementary Figure 6C

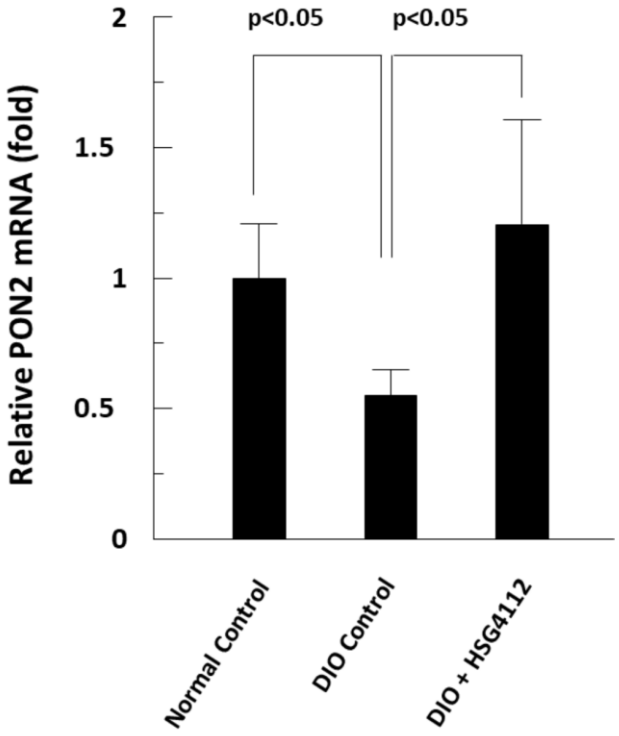

Supplementary Figure 6: PON2 induction by HSG4112 in a Diet-Induced Obesity Model. WT, C57BL/6J mice were fed normal, chow diet or an obesifying diet with and without HSG4112 (100mg/kg) for 6 weeks. In the livers, protein expression was assessed via western blot (A) and quantified as fold change (B). Also, PON2 gene expression was determined (C). [Data from Glaceum, Inc.; data unpublished]

Table 4: Plasma lipid panel and glucose levels of WT/PON2-def mice fed a HF/HS ± HSG4112 Diet for 3 weeks.

WT/PON2-def: Male

Group	*n*	TG	TC	HDL	UC	Glucose
WT- WD	4	40.25 ± 1.5	149.5 ± 29.6	119 ± 18.2	22.5 ± 5.4	189.7 ± 3.5
WT- WD + HSG4112	4	103.75 ± 32.9	147.75 ± 42.8	108 ± 28.7	28 ± 4.8	136 ± 20.7
p value		0.008	0.95	0.54	0.18	0.03
PON2-def- WD	6	59 ± 13.4	118.8 ± 12.9	98.2 ± 12.7	17.3 ± 2.8	126.7 ± 11.6
PON2-def- WD + HSG4112	6	70.3 ± 22.3	125.3 ± 7.3	102.2 ± 4.7	19.8 ± 2.2	106.5 ± 18.1
p value		0.31	0.31	0.49	0.12	0.04

WT/PON2-def: Female

Group	*n*	TG	TC	HDL	UC	Glucose
WT- WD	5	32 ± 12.1	101.2 ± 8.6	81.4 ± 5.1	11.4 ± 1.1	131.8 ± 24.1
WT- WD + HSG4112	5	35.8 ± 12.6	98 ± 13.6	71.6 ± 7.8	15.6 ± 5.4	112.2 ± 15.7
p value		0.64	0.67	0.04	0.13	0.17
PON2-def- WD	5	39.4 ± 7.8	106.2 ± 5.8	87.2 ± 3.8	13 ± 1.6	115.6 ± 17.8
PON2-def- WD + HSG4112	5	26.4 ± 5.6	109.8 ± 17.1	85.4 ± 17.0	15.8 ± 3.3	114.2 ± 25.9
p value		0.02	0.67	0.82	0.12	0.92

Values are represented as mean ± standard deviation. Units are in mg/dl.
Abbreviations: TG: triglycerides, TC: total cholesterol, HDL: high density lipoprotein, and UC: unesterified cholesterol.

Table 5: Plasma lipid panel and glucose levels of LDLR-KO mice fed a Chow ± HSG4112 or WD ± HSG4112 for 3 weeks.

LDLR-KO: Male

Group	*n*	TG	TC	HDL	UC	Glucose
Chow	4	40.7 ± 2.1	274.5 ± 24.2	112 ± 9.7	64.5 ± 13.7	210.5 ± 98.7
Chow + HSG4112	5	112.4 ± 14.5	278 ± 22.4	102.4 ± 14.9	71.6 ± 5.2	113.4 ± 45.5
p value		0.0002	0.83	0.30	0.32	0.09
WD	5	105 ± 50.2	1118 ± 127.5	90.2 ± 17.5	314.4 ± 42.6	196.4 ± 55.1
WD + HSG4112	5	122.8 ± 24.5	914.8 ± 124.2	87.8 ± 22.1	272.4 ± 32.8	147.8 ± 49.5
p value		0.5	0.03	0.85	0.12	0.18

LDLR-KO: Female

Group	*n*	TG	TC	HDL	UC	Glucose
Chow	5	50 ± 12.3	261.6 ± 13.2	87 ± 15.7	62.8 ± 4.6	196 ± 28.5
Chow + HSG4112	5	116 ± 10.4	311.2 ± 53.3	78.6 ± 17.3	88.4 ± 25.3	98.6 ± 19.1
p value		6.01E-05	0.08	0.45	0.06	0.0002
WD	5	74.4 ± 41.2	1030.4 ± 133.3	95.4 ± 11.0	290.8 ± 37.8	188.25 ± 34.4
WD + HSG4112	5	117.2 ± 30.3	932 ± 106.2	77.6 ± 11.3	272.8 ± 36.9	142.4 ± 29.2
p value		0.09	0.23	0.04	0.47	0.06

Values are represented as mean ± standard deviation. Units are in mg/dl.
Abbreviations: TG: triglycerides, TC: total cholesterol, HDL: high density lipoprotein, and UC: unesterified cholesterol.

Chapter 6: Conclusion and Future Direction

Abbreviations:

CVD	Cardiovascular Disease
CHD	Coronary Heart Disease
CAD	Coronary Artery Disease
PON	Paraoxonase
3OC12-HSL	N-(3-oxododecanoyl)-1-homoserine lactone
WT	Wild-type
PON2-def	PON2-deficient
LDLR-KO	Low density lipoprotein receptor knock-out
WD	Western diet
HF/HS	High fat/high sucrose
ROS	Reactive oxygen species
RISK	Reperfusion injury salvage kinase
HETE	5-Hydroxyeicosatetraenoic acid
POVPC	1-palmitoyl-2-(5'-oxo-valeroyl)-sn-glycero-3-phosphocholine
PGPC	1-palmitoyl-2-glutaryl-sn-glycero-3-phosphocholine
AA	Arachidonic acid
LA	Linoleic acid
$cPLA_2$	Cytoplasmic phospholipase A_2
5-HETEL	(±) 5-hydroxy-6 E,8 Z,11 Z, 14 Z-eicosatetranenoic acid 1,5-lactone.

PON2 has a plethora of anti-oxidant and anti-inflammatory properties that affect a variety of disease models, including cancer, cardiovascular disease (atherosclerosis), and obesity.[4, 6] The protective capacity of PON2 against CVD was thoroughly explored in this thesis, specifically expanding our novel understanding of PON2's protection against myocardial IRI and its potentially casual role in mediating the protective effects of a novel therapeutic, HSG4112, against one of the leading CVD risk factors, diet-

induced obesity. Many of the antioxidant properties of PON2 converge on the mitochondria, a fundamental organelle affected by myocardial IRI, leading me to hypothesize that PON2 has a protective capacity against myocardial IRI by modulating mitochondrial dysfunction, oxidative stress, and lipid peroxidation.

My recent publication (Chapter 2) demonstrated the cardioprotective role that PON2 possesses against myocardial IRI in cardiomyocytes, specifically by mitigating mitochondrial dysfunction (preserving mitochondrial membrane potential and calcium retention capacity) and oxidative stress (reduction of ROS production), and reducing cell apoptosis/necrosis.[50] Additionally, the RISK signaling pathway (PI3K, Akt, GSK-3β) was determined to be a potential mechanism by which PON2 modulates myocardial IRI. Given the pivotal role that PON2 plays within the mitochondria during myocardial IRI, particularly in mitigating ROS production, I explored PON2's capacity to modulate mitochondrial lipotoxicity, both in membrane phospholipids and as esterified and unesterified eicosanoids and prostanoids, the oxidation products of LA and AA (Chapter 3). I found that PON2 deficiency leads to an increase in both mitochondrial phospholipid oxidation (POVPC and PGPC) and eicosanoid production and a decrease in prostanoid production post-myocardial IRI; all of which is rescued, at least in part, by PON2 overexpression. Additionally, the ability of PON2 to modulate mitochondrial lipid peroxidation of AA and downstream eicosanoid and prostanoid production, points to potentially novel substrates/mechanism of action for PON2. The increased unesterified eicosanoid production, although partly explained by the increased expression of cPLA2, is still far from being resolved. It still remains to be determined whether PON2 modulates lipoxygenase enzymatic function to produce the increase of eicosanoids or

whether PON2 is interacting directly with the unesterified AA, potentially revealing novel substrates for PON2. In fact, the potential interaction of PON2 with AA products is not new. It has been shown *in vitro* that PON2 metabolizes 5-HETEL, which is a product of both enzymatic and nonenzymatic oxidation of AA.[100] Therefore, evaluating PON2 binding affinity to various eicosanoids, particularly 12-HETE and 15-HETE, is of great importance. Also, the decrease in mitochondrial prostanoid production in PON2-def mice further suggests the potential interaction of PON2 with cyclooxygenase (COX1 and 2), another avenue crucial to investigate.

An interesting observation made during these studies was the susceptibility of PON2-def mice to small, yet significant, injuries under baseline, untreated conditions. For example, the mitochondria of PON2-def mice had reduced calcium retention capacity (Chapter 2) and increased lipid peroxidation in the form of HETE and POVPC production (Chapter 3). Although these injuries do not culminate in any overt pathogenic phenotype, their presence indicates that PON2 deficiency primes the tissue for increased injury when a stressor is introduced, such as myocardial IR in these studies.

The PON2-deficient mouse model utilized in the various experiments throughout this thesis is a global “knock-out” of PON2, creating a limitation in understanding the role of PON2 exclusively in the heart and more specifically within cardiomyocytes, the key cellular subtype affected by myocardial IRI.[44] Therefore, generating cardiac-specific PON2 knock-out (KO) mouse models allows for the investigation of the role that PON2 plays specifically in the cardiomyocytes, while minimizing any off-target or compensatory responses that can arise from the global PON2 “knock-out” model. Consequently, I generated two novel cardiomyocyte-specific, PON2 KO mouse models

using a CRISPR/Cas9 and FLP-Cre Recombinase system (Chapter 3). Although I have not been able to use these mice due to time constraints, there are two fundamental experiments that I would like to perform using them. The first would be characterizing the mice under baseline, untreated conditions. This would include isolating different tissue types (liver, spleen, lungs, etc.) as well isolating the cardiomyocytes from both the control and cardiomyocyte-specific PON2-KO mice and determining the expression of PON2, enzymatic capacity (lactonase and arylesterase activity), oxidative stress (ROS production), and mitochondrial bioenergetics (oxygen consumption rate). Nevertheless, these novel transgenic mice strains are fundamental in enabling a robust and effective model for the investigation of PON2 in myocardial IR injury, as well as other cardiovascular disease paradigms. The extensive data that I have generated (Chapters 2 and 3) during the course of my studies greatly supports the hypothesis that PON2 is protective against myocardial IRI, particularly in the cardiomyocytes, by modulating mitochondrial dysfunction, oxidative stress, and lipid peroxidation. Accordingly, my second experiment would be subjecting the cardiomyocyte-specific PON2-KO mice to myocardial IRI. I hypothesize that PON2 deficiency only in cardiomyocytes will be sufficient to lead to an exasperated myocardial IRI phenotype. This would include the induction of a larger infarct size, greater mitochondrial dysfunction (reduced mitochondrial membrane potential and calcium retention capacity) and oxidative stress (increase ROS production), and increased mitochondrial lipid peroxidation (increased eicosanoid formation and phospholipid oxidation).

I was very fortunate to have the opportunity to investigate the role of a novel compound, HSG4112, against diet-induced obesity and the potential role that PON2

plays in modulating its protective effects (Chapter 5). Diet-induced obesity is one the lead risk factors leading to CVD, particularly CHD. Therefore, finding therapeutic targets that can mitigate this destructive risk factor is of critical importance. HSG4112 increased PON1 and PON3 expression and enhanced lactonase and arylesterase activity in the plasma and livers of WT, PON1-KO, and PON2-def mice under baseline, chow fed conditions, suggesting that the drug's protective effects are, at least in part, through the Paraoxonase gene family. As noted earlier, Glaceum found that PON2 was induced with HSG4112 in diet-induced obesity studies. Therefore, I performed two diet-induced obesity studies using our PON2-def mouse line to evaluate the potentially casual role that PON2 plays in HSG4112 protection. Although there was a significant decrease in body weight in both male and female, WT and PON2-def mice, the female, PON2-def mice had a reduced change in body weight, no fat mass loss, no gain of muscle mass, no decrease in plasma glucose levels, or enhanced (plasma) lactonase activity when compared to the WT controls. Therefore, based on these studies, PON2 deficiency, in females, significantly reduces, although not completely, the protective capacity of HSG4112. This suggests, that some of HSG4112's protective effects are independent of PON2. Consequently, I wanted to evaluate the protective capacity of HSG4112 against another model of diet-induced obesity, one that involves hyperlipidemia. HSG4112 significantly reduced body weight and fat mass, while increasing muscle mass in hyperlipidemic, LDLR-KO mice (male and female) fed a western diet with HSG4112. It is worth noting that these protective effects were not observed in the LDLR-KO, chow fed group with the drug, suggesting that an external

stressor, in this case obesifying diet, is required in spite of being predisposed to hyperlipidemia.

Lastly, another important avenue to explore is the potential of HSG4112 to modulate mitochondrial lipid peroxidation. According to data from Glaceum, a key mechanism of action of HSG4112's protection in diet-induced obesity is the reduction of mitochondrial dysfunction, through the reduction of ROS generation and increase in ATP production (data unpublished). This data, coupled with the capacity of HSG4112 to induce PON2 expression, further supports the hypothesis that PON2 modulates the protective properties of HSG4112. Therefore, given my observations on the protective role that PON2 plays in reducing mitochondrial dysfunction and oxidative as well reducing mitochondrial lipid peroxidation, I hypothesize that part of HSG4112's protective properties include it's ability to reduce mitochondrial lipid peroxidation. As a result, HSG4112 has the potential to be utilized as a therapeutic agent against myocardial IRI. Two experiments can be performed to test my hypothesis. The first would be a quick cell culture experiment where I would subject H9c2 cells to my established *in vitro* HRI protocol with and without HSG4112 treatment. I would then isolate mitochondria from these cells and determine the mitochondrial lipid peroxidation using our existing mass spectrometry method. The second experiment would involve feeding my newly generated cardiomyocyte-specific KO mice (and controls) with HSG4112 for 3 weeks, after which I would subject the mice to myocardial IRI. Mitochondria will then be isolated from these mice and mitochondrial lipid peroxidation will be determined via mass spectrometry. I hypothesize that HSG4112 treatment will

protect against myocardial IRI by reducing cell death (decreased infarct size) and protecting against mitochondrial dysfunction and lipid peroxidation.

My dissertation work has explored the protective capacity of PON2 against CVD, specifically expanding our understanding of its cardioprotective role against acute myocardial IRI. This protective capacity is largely rooted in PON2's modulation of mitochondrial dysfunction and oxidative stress, particularly lipid lipotoxicity. In addition, I investigated the protective role of HSG4112, a novel drug that protects against diet-induced obesity, and the potentially causal role that PON2 plays as its mode of action. In conclusion, these studies help determine possible physiological substrates and molecular mechanisms of PON2, which remain largely unknown, as well as targets for therapeutic intervention against myocardial IRI and diet-induced obesity.

Bibliography

1. Benjamin EJ, Muntner P, Alonso A, Bittencourt MS, Callaway CW, Carson AP, Chamberlain AM, Chang AR, Cheng S, Das SR, Delling FN, Djousse L, Elkind MSV, Ferguson JF, Fornage M, Jordan LC, Khan SS, Kissela BM, Knutson KL, Kwan TW, Lackland DT, Lewis TT, Lichtman JH, Longenecker CT, Loop MS, Lutsey PL, Martin SS, Matsushita K, Moran AE, Mussolino ME, O'Flaherty M, Pandey A, Perak AM, Rosamond WD, Roth GA, Sampson UKA, Satou GM, Schroeder EB, Shah SH, Spartano NL, Stokes A, Tirschwell DL, Tsao CW, Turakhia MP, VanWagner LB, Wilkins JT, Wong SS, Virani SS, American Heart Association Council on E, Prevention Statistics C and Stroke Statistics S. Heart Disease and Stroke Statistics-2019 Update: A Report From the American Heart Association. *Circulation*. 2019;139:e56-e528.
2. Fryar CD, Chen TC and Li X. Prevalence of uncontrolled risk factors for cardiovascular disease: United States, 1999-2010. *NCHS Data Brief*. 2012:1-8.
3. Heron M. Deaths: Leading Causes for 2016. *Natl Vital Stat Rep*. 2018;67:1-77.
4. Devarajan A, Shih D and Reddy ST. Inflammation, infection, cancer and all that...the role of paraoxonases. *Adv Exp Med Biol*. 2014;824:33-41.
5. Devarajan A, Bourquard N, Hama S, Navab M, Grijalva VR, Morvardi S, Clarke CF, Vergnes L, Reue K, Teiber JF and Reddy ST. Paraoxonase 2 deficiency alters mitochondrial function and exacerbates the development of atherosclerosis. *Antioxid Redox Signal*. 2011;14:341-51.
6. Shih DM, Meng Y, Sallam T, Vergnes L, Shu ML, Reue K, Tontonoz P, Fogelman AM, Lusis AJ and Reddy ST. PON2 Deficiency Leads to Increased Susceptibility to Diet-Induced Obesity. *Antioxidants (Basel)*. 2019;8.
7. Li W, Kennedy D, Shao Z, Wang X, Kamdar AK, Weber M, Mislick K, Kiefer K, Morales R, Agatisa-Boyle B, Shih DM, Reddy ST, Moravec CS and Tang WHW. Paraoxonase 2 prevents the development of heart failure. *Free Radical Biology and Medicine*. 2018;121:117-126.
8. Camps J, Marsillach J and Joven J. The paraoxonases: role in human diseases and methodological difficulties in measurement. *Crit Rev Clin Lab Sci*. 2009;46:83-106.
9. Chen ML, Zhao H, Liao N and Xie ZF. Association Between Paraoxonase 2 Ser311Cys Polymorphism and Coronary Heart Disease Risk: A Meta-Analysis. *Med Sci Monit*. 2016;22:3196-201.
10. Chen Q, Reis SE, Kammerer CM, McNamara DM, Holubkov R, Sharaf BL, Sopko G, Pauly DF, Merz CN, Kamboh MI and Group WS. Association between the severity of angiographic coronary artery disease and paraoxonase gene polymorphisms in the National Heart, Lung, and Blood Institute-sponsored Women's Ischemia Syndrome Evaluation (WISE) study. *Am J Hum Genet*. 2003;72:13-22.
11. Martinelli N, Girelli D, Olivieri O, Stranieri C, Trabetti E, Pizzolo F, Friso S, Tenuti I, Cheng S, Grow MA, Pignatti PF and Corrocher R. Interaction between smoking and PON2 Ser311Cys polymorphism as a determinant of the risk of myocardial infarction. *Eur J Clin Invest*. 2004;34:14-20.
12. Leus FR, Zwart M, Kastelein JJ and Voorbij HA. PON2 gene variants are associated with clinical manifestations of cardiovascular disease in familial hypercholesterolemia patients. *Atherosclerosis*. 2001;154:641-9.
13. Pan JP, Lai ST, Chiang SC, Chou SC and Chiang AN. The risk of coronary artery disease in population of Taiwan is associated with Cys-Ser 311 polymorphism of human paraoxonase (PON)-2 gene. *Zhonghua Yi Xue Za Zhi (Taipei)*. 2002;65:415-21.
14. Hausenloy DJ and Yellon DM. Myocardial ischemia-reperfusion injury: a neglected therapeutic target. *J Clin Invest*. 2013;123:92-100.
15. Kalogeris T, Baines CP, Krenz M and Korthuis RJ. Cell biology of ischemia/reperfusion injury. *Int Rev Cell Mol Biol*. 2012;298:229-317.

16. Sanada S, Komuro I and Kitakaze M. Pathophysiology of myocardial reperfusion injury: preconditioning, postconditioning, and translational aspects of protective measures. *Am J Physiol Heart Circ Physiol*. 2011;301:H1723-41.
17. Verma S, Fedak PWM, Weisel RD, Butany J, Rao V, Maitland A, Li R-K, Dhillon B and Yau TM. Fundamentals of Reperfusion Injury for the Clinical Cardiologist. *Circulation*. 2002;105:2332-2336.
18. Turer AT and Hill JA. Pathogenesis of myocardial ischemia-reperfusion injury and rationale for therapy. *Am J Cardiol*. 2010;106:360-8.
19. Ott M, Gogvadze V, Orrenius S and Zhivotovsky B. Mitochondria, oxidative stress and cell death. *Apoptosis*. 2007;12:913-22.
20. Piot C, Croisille P, Staat P, Thibault H, Rioufol G, Mewton N, Elbelghiti R, Cung TT, Bonnefoy E, Angoulvant D, Macia C, Raczka F, Sportouch C, Gahide G, Finet G, Andre-Fouet X, Revel D, Kirkorian G, Monassier JP, Derumeaux G and Ovize M. Effect of cyclosporine on reperfusion injury in acute myocardial infarction. *N Engl J Med*. 2008;359:473-81.
21. Ibanez B, Heusch G, Ovize M and Van de Werf F. Evolving therapies for myocardial ischemia/reperfusion injury. *J Am Coll Cardiol*. 2015;65:1454-71.
22. Gomez L, Thiebaut PA, Paillard M, Ducreux S, Abrial M, Crola Da Silva C, Durand A, Alam MR, Van Coppenolle F, Sheu SS and Ovize M. The SR/ER-mitochondria calcium crosstalk is regulated by GSK3beta during reperfusion injury. *Cell Death Differ*. 2016;23:313-22.
23. Gomez L, Paillard M, Thibault H, Derumeaux G and Ovize M. Inhibition of GSK3beta by postconditioning is required to prevent opening of the mitochondrial permeability transition pore during reperfusion. *Circulation*. 2008;117:2761-8.
24. Li J, Iorga A, Sharma S, Youn JY, Partow-Navid R, Umar S, Cai H, Rahman S and Eghbali M. Intralipid, a clinically safe compound, protects the heart against ischemia-reperfusion injury more efficiently than cyclosporine-A. *Anesthesiology*. 2012;117:836-46.
25. Rahman S, Li J, Bopassa JC, Umar S, Iorga A, Partownavid P and Eghbali M. Phosphorylation of GSK-3β mediates Intralipid-induced cardioprotection against Ischemia/Reperfusion injury. *Anesthesiology*. 2011;115:242-253.
26. Osman C, Voelker DR and Langer T. Making heads or tails of phospholipids in mitochondria. *J Cell Biol*. 2011;192:7-16.
27. Chen J, Henderson GI and Freeman GL. Role of 4-hydroxynonenal in modification of cytochrome c oxidase in ischemia/reperfused rat heart. *J Mol Cell Cardiol*. 2001;33:1919-27.
28. Fukai M, Hayashi T, Yokota R, Shimamura T, Suzuki T, Taniguchi M, Matsushita M, Furukawa H and Todo S. Lipid peroxidation during ischemia depends on ischemia time in warm ischemia and reperfusion of rat liver. *Free Radic Biol Med*. 2005;38:1372-81.
29. Xiao CY, Yuhki K, Hara A, Fujino T, Kuriyama S, Yamada T, Takayama K, Takahata O, Karibe H, Taniguchi T, Narumiya S and Ushikubi F. Prostaglandin E2 protects the heart from ischemia-reperfusion injury via its receptor subtype EP4. *Circulation*. 2004;109:2462-8.
30. Goto S, Kim YI, Kawano K, Kai T and Kobayashi M. Efficacy of PGI2 analog in preventing ischemia reperfusion damage of liver grafts from living donors. *Transpl Int*. 1992;5 Suppl 1:S366-9.
31. Simpson PJ, Mitsos SE, Ventura A, Gallagher KP, Fantone JC, Abrams GD, Schork MA and Lucchesi BR. Prostacyclin protects ischemic reperfused myocardium in the dog by inhibition of neutrophil activation. *Am Heart J*. 1987;113:129-37.
32. Hohlfeld T, Strobach H and Schror K. Stimulation of endogenous prostacyclin protects the reperfused pig myocardium from ischemic injury. *J Pharmacol Exp Ther*. 1993;264:397-405.
33. Van der Vusse GJ, Reneman RS and van Bilsen M. Accumulation of arachidonic acid in ischemic/reperfused cardiac tissue: possible causes and consequences. *Prostaglandins Leukot Essent Fatty Acids*. 1997;57:85-93.

34. Katsumata Y, Shinmura K, Sugiura Y, Tohyama S, Matsuhashi T, Ito H, Yan X, Ito K, Yuasa S, Ieda M, Urade Y, Suematsu M, Fukuda K and Sano M. Endogenous prostaglandin D2 and its metabolites protect the heart against ischemia-reperfusion injury by activating Nrf2. *Hypertension*. 2014;63:80-7.
35. Brown DA, Sabbah HN and Shaikh SR. Mitochondrial inner membrane lipids and proteins as targets for decreasing cardiac ischemia/reperfusion injury. *Pharmacology & therapeutics*. 2013;140:258-66.
36. Paradies G, Petrosillo G, Pistolese M, Di Venosa N, Federici A and Ruggiero FM. Decrease in mitochondrial complex I activity in ischemic/reperfused rat heart: involvement of reactive oxygen species and cardiolipin. *Circulation research*. 2004;94:53-9.
37. Petrosillo G, Ruggiero FM, Pistolese M and Paradies G. Ca2+-induced reactive oxygen species production promotes cytochrome c release from rat liver mitochondria via mitochondrial permeability transition (MPT)-dependent and MPT-independent mechanisms: role of cardiolipin. *J Biol Chem*. 2004;279:53103-8.
38. Orrenius S and Zhivotovsky B. Cardiolipin oxidation sets cytochrome c free. *Nat Chem Biol*. 2005;1:188-9.
39. Primo-Parmo SL, Sorenson RC, Teiber J and La Du BN. The human serum paraoxonase/arylesterase gene (PON1) is one member of a multigene family. *Genomics*. 1996;33:498-507.
40. Martinelli N, Consoli L, Girelli D, Grison E, Corrocher R and Olivieri O. Paraoxonases: ancient substrate hunters and their evolving role in ischemic heart disease. *Adv Clin Chem*. 2013;59:65-100.
41. Chistiakov DA, Melnichenko AA, Orekhov AN and Bobryshev YV. Paraoxonase and atherosclerosis-related cardiovascular diseases. *Biochimie*. 2017;132:19-27.
42. Horke S, Xiao J, Schutz EM, Kramer GL, Wilgenbus P, Witte I, Selbach M and Teiber JF. Novel Paraoxonase 2-Dependent Mechanism Mediating the Biological Effects of the Pseudomonas aeruginosa Quorum-Sensing Molecule N-(3-Oxo-Dodecanoyl)-L-Homoserine Lactone. *Infect Immun*. 2015;83:3369-80.
43. Li XC, Wang C, Mulchandani A and Ge X. Engineering Soluble Human Paraoxonase 2 for Quorum Quenching. *ACS Chem Biol*. 2016;11:3122-3131.
44. Ng CJ, Bourquard N, Grijalva V, Hama S, Shih DM, Navab M, Fogelman AM, Lusis AJ, Young S and Reddy ST. Paraoxonase-2 deficiency aggravates atherosclerosis in mice despite lower apolipoprotein-B-containing lipoproteins: anti-atherogenic role for paraoxonase-2. *J Biol Chem*. 2006;281:29491-500.
45. Altenhofer S, Witte I, Teiber JF, Wilgenbus P, Pautz A, Li H, Daiber A, Witan H, Clement AM, Forstermann U and Horke S. One enzyme, two functions: PON2 prevents mitochondrial superoxide formation and apoptosis independent from its lactonase activity. *J Biol Chem*. 2010;285:24398-403.
46. Horke S, Witte I, Wilgenbus P, Altenhofer S, Kruger M, Li H and Forstermann U. Protective effect of paraoxonase-2 against endoplasmic reticulum stress-induced apoptosis is lost upon disturbance of calcium homoeostasis. *Biochem J*. 2008;416:395-405.
47. Devarajan A, Grijalva VR, Bourquard N, Meriwether D, 3rd, Imaizumi S, Shin BC, Devaskar SU and Reddy ST. Macrophage paraoxonase 2 regulates calcium homeostasis and cell survival under endoplasmic reticulum stress conditions and is sufficient to prevent the development of aggravated atherosclerosis in paraoxonase 2 deficiency/apoE-/- mice on a Western diet. *Mol Genet Metab*. 2012;107:416-27.
48. Horke S, Witte I, Wilgenbus P, Kruger M, Strand D and Forstermann U. Paraoxonase-2 reduces oxidative stress in vascular cells and decreases endoplasmic reticulum stress-induced caspase activation. *Circulation*. 2007;115:2055-64.

49. Witte I, Altenhofer S, Wilgenbus P, Amort J, Clement AM, Pautz A, Li H, Forstermann U and Horke S. Beyond reduction of atherosclerosis: PON2 provides apoptosis resistance and stabilizes tumor cells. *Cell death & disease*. 2011;2:e112.
50. Sulaiman D, Li J, Devarajan A, Cunningham CM, Li M, Fishbein GA, Fogelman AM, Eghbali M and Reddy ST. Paraoxonase 2 protects against acute myocardial ischemia-reperfusion injury by modulating mitochondrial function and oxidative stress via the PI3K/Akt/GSK-3beta RISK pathway. *J Mol Cell Cardiol*. 2019;129:154-164.
51. Meriwether D, Sulaiman D, Volpe C, Dorfman A, Grijalva V, Dorreh N, Solorzano-Vargas RS, Wang J, O'Connor E, Papesh J, Larauche M, Trost H, Palgunachari MN, Anantharamaiah GM, Herschman HR, Martin MG, Fogelman AM and Reddy ST. Apolipoprotein A-I mimetics mitigate intestinal inflammation in COX2-dependent inflammatory bowel disease model. *J Clin Invest*. 2019;130:3670-3685.
52. Mozaffarian D, Benjamin EJ, Go AS, Arnett DK, Blaha MJ, Cushman M, de Ferranti S, Despres JP, Fullerton HJ, Howard VJ, Huffman MD, Judd SE, Kissela BM, Lackland DT, Lichtman JH, Lisabeth LD, Liu S, Mackey RH, Matchar DB, McGuire DK, Mohler ER, 3rd, Moy CS, Muntner P, Mussolino ME, Nasir K, Neumar RW, Nichol G, Palaniappan L, Pandey DK, Reeves MJ, Rodriguez CJ, Sorlie PD, Stein J, Towfighi A, Turan TN, Virani SS, Willey JZ, Woo D, Yeh RW, Turner MB, American Heart Association Statistics C and Stroke Statistics S. Heart disease and stroke statistics--2015 update: a report from the American Heart Association. *Circulation*. 2015;131:e29-322.
53. Robertson KS, Hawe E, Miller GJ, Talmud PJ, Humphries SE and Northwick Park Heart S, II. Human paraoxonase gene cluster polymorphisms as predictors of coronary heart disease risk in the prospective Northwick Park Heart Study II. *Biochim Biophys Acta*. 2003;1639:203-12.
54. Rodriguez-Esparragon F, Lopez-Fernandez JC, Buset-Rios N, Garcia-Bello MA, Hernandez-Velazquez E, Cappiello L and Rodriguez-Perez JC. Paraoxonase 1 and 2 gene variants and the ischemic stroke risk in Gran Canaria population: an association study and meta-analysis. *Int J Neurosci*. 2017;127:191-198.
55. Sanghera DK, Aston CE, Saha N and Kamboh MI. DNA polymorphisms in two paraoxonase genes (PON1 and PON2) are associated with the risk of coronary heart disease. *Am J Hum Genet*. 1998;62:36-44.
56. Gonzalez-Castro TB, Tovilla-Zarate CA, Juarez-Rojop IE, Hernandez-Diaz Y, Lopez-Narvaez ML, Rodriguez-Perez C, Gonzalez-Hernandez YK and Ramos-Mendez MA. PON2 and PPARG polymorphisms as biomarkers of risk for coronary heart disease. *Biomark Med*. 2018;12:287-297.
57. Li J, Chen X, McClusky R, Ruiz-Sundstrom M, Itoh Y, Umar S, Arnold AP and Eghbali M. The number of X chromosomes influences protection from cardiac ischaemia/reperfusion injury in mice: one X is better than two. *Cardiovascular research*. 2014;102:375-84.
58. Li J, Umar S, Iorga A, Youn JY, Wang Y, Regitz-Zagrosek V, Cai H and Eghbali M. Cardiac vulnerability to ischemia/reperfusion injury drastically increases in late pregnancy. *Basic research in cardiology*. 2012;107:271.
59. Li D, Wu J, Bai Y, Zhao X and Liu L. Isolation and culture of adult mouse cardiomyocytes for cell signaling and in vitro cardiac hypertrophy. *Journal of visualized experiments : JoVE*. 2014.
60. Louch WE, Sheehan KA and Wolska BM. Methods in cardiomyocyte isolation, culture, and gene transfer. *J Mol Cell Cardiol*. 2011;51:288-98.
61. Sverdlov AL, Elezaby A, Qin F, Behring JB, Luptak I, Calamaras TD, Siwik DA, Miller EJ, Liesa M, Shirihai OS, Pimentel DR, Cohen RA, Bachschmid MM and Colucci WS. Mitochondrial Reactive Oxygen Species Mediate Cardiac Structural, Functional, and Mitochondrial Consequences of Diet-Induced Metabolic Heart Disease. *J Am Heart Assoc*. 2016;5.

62. Ebert J, Wilgenbus P, Teiber JF, Jurk K, Schwierczek K, Dohrmann M, Xia N, Li H, Spiecker L, Ruf W and Horke S. Paraoxonase-2 regulates coagulation activation through endothelial tissue factor. *Blood*. 2018.
63. Pei JF, Yan YF, Tang X, Zhang Y, Cui SS, Zhang ZQ, Chen HZ and Liu DP. Human paraoxonase gene cluster overexpression alleviates angiotensin II-induced cardiac hypertrophy in mice. *Sci China Life Sci*. 2016;59:1115-1122.
64. Devarajan A, Bourquard N, Grijalva VR, Gao F, Ganapathy E, Verma J and Reddy ST. Role of PON2 in innate immune response in an acute infection model. *Mol Genet Metab*. 2013;110:362-70.
65. Jean S and Kiger AA. Classes of phosphoinositide 3-kinases at a glance. *J Cell Sci*. 2014;127:923-8.
66. Tsuruta F, Masuyama N and Gotoh Y. The phosphatidylinositol 3-kinase (PI3K)-Akt pathway suppresses Bax translocation to mitochondria. *J Biol Chem*. 2002;277:14040-7.
67. Marín-García J. *Heart failure : bench to bedside*. New York: Humana Press; 2010.
68. Marín-García J, Akhmedov A, Rybin V and Moe GW. *Mitochondria and their role in cardiovascular disease*. New York: Springer; 2013.
69. Harel M, Aharoni A, Gaidukov L, Brumshtein B, Khersonsky O, Meged R, Dvir H, Ravelli RB, McCarthy A, Toker L, Silman I, Sussman JL and Tawfik DS. Structure and evolution of the serum paraoxonase family of detoxifying and anti-atherosclerotic enzymes. *Nat Struct Mol Biol*. 2004;11:412-9.
70. Devarajan A, Epand RF, Epand RM and Reddy ST. Potential Role for Paraoxonase 2 in Cardiolipin Transport. *Free Radical Biology and Medicine*. 2011;51:S144-S144.
71. Michael A, Haq S, Chen X, Hsich E, Cui L, Walters B, Shao Z, Bhattacharya K, Kilter H, Huggins G, Andreucci M, Periasamy M, Solomon RN, Liao R, Patten R, Molkentin JD and Force T. Glycogen synthase kinase-3beta regulates growth, calcium homeostasis, and diastolic function in the heart. *J Biol Chem*. 2004;279:21383-93.
72. Rizzuto R, Marchi S, Bonora M, Aguiari P, Bononi A, De Stefani D, Giorgi C, Leo S, Rimessi A, Siviero R, Zecchini E and Pinton P. Ca(2+) transfer from the ER to mitochondria: when, how and why. *Biochim Biophys Acta*. 2009;1787:1342-51.
73. Devarajan A, Epand RF, Epand RM and Reddy ST. Potential Role for Paraoxonase 2 in Cardiolipin Transport. *Free Radical Biology and Medicine*. 2011;51, Supplement:S144.
74. Huang CC, Chang MT, Leu HB, Yin WH, Tseng WK, Wu YW, Lin TH, Yeh HI, Chang KC, Wang JH, Wu CC, Shyur LF and Chen JW. Association of Arachidonic Acid-derived Lipid Mediators with Subsequent Onset of Acute Myocardial Infarction in Patients with Coronary Artery Disease. *Sci Rep*. 2020;10:8105.
75. Prasad MR, Popescu LM, Moraru, II, Liu XK, Maity S, Engelman RM and Das DK. Role of phospholipases A2 and C in myocardial ischemic reperfusion injury. *Am J Physiol*. 1991;260:H877-83.
76. Suzuki J, Ogawa M, Watanabe R, Takayama K, Hirata Y, Nagai R and Isobe M. Roles of prostaglandin E2 in cardiovascular diseases. *Int Heart J*. 2011;52:266-9.
77. Vu HS, Shiva S, Roth MR, Tamura P, Zheng L, Li M, Sarowar S, Honey S, McEllhiney D, Hinkes P, Seib L, Williams TD, Gadbury G, Wang X, Shah J and Welti R. Lipid changes after leaf wounding in Arabidopsis thaliana: expanded lipidomic data form the basis for lipid co-occurrence analysis. *Plant J*. 2014;80:728-43.
78. Watson AD. Thematic review series: systems biology approaches to metabolic and cardiovascular disorders. Lipidomics: a global approach to lipid analysis in biological systems. *Journal of lipid research*. 2006;47:2101-11.
79. Cummings BS, McHowat J and Schnellmann RG. Phospholipase A(2)s in cell injury and death. *J Pharmacol Exp Ther*. 2000;294:793-9.
80. Sun GY, Chuang DY, Zong Y, Jiang J, Lee JC, Gu Z and Simonyi A. Role of cytosolic phospholipase A2 in oxidative and inflammatory signaling pathways in different cell types in the central nervous system. *Mol Neurobiol*. 2014;50:6-14.

81. Jezek J, Jaburek M, Zelenka J and Jezek P. Mitochondrial phospholipase A2 activated by reactive oxygen species in heart mitochondria induces mild uncoupling. *Physiol Res*. 2010;59:737-47.
82. De Windt LJ, Reneman RS, Van der Vusse GJ and Van Bilsen M. Phospholipase A2-mediated hydrolysis of cardiac phospholipids: the use of molecular and transgenic techniques. *Mol Cell Biochem*. 1998;180:65-73.
83. Otani H, Prasad MR, Jones RM and Das DK. Mechanism of membrane phospholipid degradation in ischemic-reperfused rat hearts. *Am J Physiol*. 1989;257:H252-8.
84. Adams JA, Uryash A and Lopez JR. Cyclooxygenase inhibition prior to ventricular fibrillation induced ischemia reperfusion injury impairs survival and outcomes. *Med Hypotheses*. 2020;135:109485.
85. Guo Y, Nong Y, Tukaye DN, Rokosh G, Du J, Zhu X, Book M, Tomlin A, Li Q and Bolli R. Inducible cardiac-specific overexpression of cyclooxygenase-2 (COX-2) confers resistance to ischemia/reperfusion injury. *Basic research in cardiology*. 2019;114:32.
86. Berliner JA and Watson AD. A role for oxidized phospholipids in atherosclerosis. *N Engl J Med*. 2005;353:9-11.
87. Watson AD, Subbanagounder G, Welsbie DS, Faull KF, Navab M, Jung ME, Fogelman AM and Berliner JA. Structural identification of a novel pro-inflammatory epoxyisoprostane phospholipid in mildly oxidized low density lipoprotein. *J Biol Chem*. 1999;274:24787-98.
88. Yeang C, Hasanally D, Que X, Hung MY, Stamenkovic A, Chan D, Chaudhary R, Margulets V, Edel AL, Hoshijima M, Gu Y, Bradford W, Dalton N, Miu P, Cheung DY, Jassal DS, Pierce GN, Peterson KL, Kirshenbaum LA, Witztum JL, Tsimikas S and Ravandi A. Reduction of myocardial ischaemia-reperfusion injury by inactivating oxidized phospholipids. *Cardiovascular research*. 2019;115:179-189.
89. Skarnes WC, Rosen B, West AP, Koutsourakis M, Bushell W, Iyer V, Mujica AO, Thomas M, Harrow J, Cox T, Jackson D, Severin J, Biggs P, Fu J, Nefedov M, de Jong PJ, Stewart AF and Bradley A. A conditional knockout resource for the genome-wide study of mouse gene function. *Nature*. 2011;474:337-42.
90. Coleman JL, Brennan K, Ngo T, Balaji P, Graham RM and Smith NJ. Rapid Knockout and Reporter Mouse Line Generation and Breeding Colony Establishment Using EUCOMM Conditional-Ready Embryonic Stem Cells: A Case Study. *Front Endocrinol (Lausanne)*. 2015;6:105.
91. Agah R, Frenkel PA, French BA, Michael LH, Overbeek PA and Schneider MD. Gene recombination in postmitotic cells. Targeted expression of Cre recombinase provokes cardiac-restricted, site-specific rearrangement in adult ventricular muscle in vivo. *J Clin Invest*. 1997;100:169-79.
92. Sander JD and Joung JK. CRISPR-Cas systems for editing, regulating and targeting genomes. *Nat Biotechnol*. 2014;32:347-55.
93. Carroll KJ, Makarewich CA, McAnally J, Anderson DM, Zentilin L, Liu N, Giacca M, Bassel-Duby R and Olson EN. A mouse model for adult cardiac-specific gene deletion with CRISPR/Cas9. *Proc Natl Acad Sci U S A*. 2016;113:338-43.
94. Benjamin EJ, Blaha MJ, Chiuve SE, Cushman M, Das SR, Deo R, de Ferranti SD, Floyd J, Fornage M, Gillespie C, Isasi CR, Jiménez MC, Jordan LC, Judd SE, Lackland D, Lichtman JH, Lisabeth L, Liu S, Longenecker CT, Mackey RH, Matsushita K, Mozaffarian D, Mussolino ME, Nasir K, Neumar RW, Palaniappan L, Pandey DK, Thiagarajan RR, Reeves MJ, Ritchey M, Rodriguez CJ, Roth GA, Rosamond WD, Sasson C, Towfighi A, Tsao CW, Turner MB, Virani SS, Voeks JH, Willey JZ, Wilkins JT, Wu JH, Alger HM, Wong SS and Muntner P. Heart Disease and Stroke Statistics—2017 Update: A Report From the American Heart Association. *Circulation*. 2017.
95. Bournat JC and Brown CW. Mitochondrial dysfunction in obesity. *Curr Opin Endocrinol Diabetes Obes*. 2010;17:446-52.
96. Marseglia L, Manti S, D'Angelo G, Nicotera A, Parisi E, Di Rosa G, Gitto E and Arrigo T. Oxidative stress in obesity: a critical component in human diseases. *Int J Mol Sci*. 2014;16:378-400.

97. Monteiro R and Azevedo I. Chronic inflammation in obesity and the metabolic syndrome. *Mediators Inflamm*. 2010;2010.
98. Shih DM, Xia YR, Wang XP, Wang SS, Bourquard N, Fogelman AM, Lusis AJ and Reddy ST. Decreased obesity and atherosclerosis in human paraoxonase 3 transgenic mice. *Circulation research*. 2007;100:1200-7.
99. Draganov DI. Lactonases with organophosphatase activity: structural and evolutionary perspectives. *Chem Biol Interact*. 2010;187:370-2.
100. Draganov DI, Teiber JF, Speelman A, Osawa Y, Sunahara R and La Du BN. Human paraoxonases (PON1, PON2, and PON3) are lactonases with overlapping and distinct substrate specificities. *Journal of lipid research*. 2005;46:1239-47.
101. Chun CK, Ozer EA, Welsh MJ, Zabner J and Greenberg EP. Inactivation of a Pseudomonas aeruginosa quorum-sensing signal by human airway epithelia. *Proc Natl Acad Sci U S A*. 2004;101:3587-90.
102. Stoltz DA, Ozer EA, Ng CJ, Yu JM, Reddy ST, Lusis AJ, Bourquard N, Parsek MR, Zabner J and Shih DM. Paraoxonase-2 deficiency enhances Pseudomonas aeruginosa quorum sensing in murine tracheal epithelia. *Am J Physiol Lung Cell Mol Physiol*. 2007;292:L852-60.
103. Shih DM, Yu JM, Vergnes L, Dali-Youcef N, Champion MD, Devarajan A, Zhang P, Castellani LW, Brindley DN, Jamey C, Auwerx J, Reddy ST, Ford DA, Reue K and Lusis AJ. PON3 knockout mice are susceptible to obesity, gallstone formation, and atherosclerosis. *FASEB journal : official publication of the Federation of American Societies for Experimental Biology*. 2015;29:1185-97.
104. Ng CJ, Wadleigh DJ, Gangopadhyay A, Hama S, Grijalva VR, Navab M, Fogelman AM and Reddy ST. Paraoxonase-2 is a ubiquitously expressed protein with antioxidant properties and is capable of preventing cell-mediated oxidative modification of low density lipoprotein. *J Biol Chem*. 2001;276:44444-9.
105. Kim JB, Xia YR, Romanoski CE, Lee S, Meng Y, Shi YS, Bourquard N, Gong KW, Port Z, Grijalva V, Reddy ST, Berliner JA, Lusis AJ and Shih DM. Paraoxonase-2 modulates stress response of endothelial cells to oxidized phospholipids and a bacterial quorum-sensing molecule. *Arterioscler Thromb Vasc Biol*. 2011;31:2624-33.
106. Schweikert EM, Amort J, Wilgenbus P, Forstermann U, Teiber JF and Horke S. Paraoxonases-2 and -3 Are Important Defense Enzymes against Pseudomonas aeruginosa Virulence Factors due to Their Anti-Oxidative and Anti-Inflammatory Properties. *J Lipids*. 2012;2012:352857.
107. Ruiz-Larrea MB, Mohan AR, Paganga G, Miller NJ, Bolwell GP and Rice-Evans CA. Antioxidant activity of phytoestrogenic isoflavones. *Free Radic Res*. 1997;26:63-70.
108. Lampe JW. Isoflavonoid and lignan phytoestrogens as dietary biomarkers. *J Nutr*. 2003;133 Suppl 3:956S-964S.
109. Simmler C, Pauli GF and Chen SN. Phytochemistry and biological properties of glabridin. *Fitoterapia*. 2013;90:160-84.
110. Yehuda I, Madar Z, Leikin-Frenkel A, Szuchman-Sapir A, Magzal F, Markman G and Tamir S. Glabridin, an isoflavan from licorice root, upregulates paraoxonase 2 expression under hyperglycemia and protects it from oxidation. *Mol Nutr Food Res*. 2016;60:287-99.
111. Aviram M and Rosenblat M. Paraoxonases (PON1, PON2, PON3) analyses in vitro and in vivo in relation to cardiovascular diseases. *Methods Mol Biol*. 2008;477:259-76.
112. Humbert R, Adler DA, Disteche CM, Hassett C, Omiecinski CJ and Furlong CE. The molecular basis of the human serum paraoxonase activity polymorphism. *Nat Genet*. 1993;3:73-6.
113. Giordano G, Cole TB, Furlong CE and Costa LG. Paraoxonase 2 (PON2) in the mouse central nervous system: a neuroprotective role? *Toxicol Appl Pharmacol*. 2011;256:369-78.

114. Giordano G, Tait L, Furlong CE, Cole TB, Kavanagh TJ and Costa LG. Gender differences in brain susceptibility to oxidative stress are mediated by levels of paraoxonase-2 expression. *Free Radic Biol Med*. 2013;58:98-108.
115. Tamir S, Eizenberg M, Somjen D, Stern N, Shelach R, Kaye A and Vaya J. Estrogenic and antiproliferative properties of glabridin from licorice in human breast cancer cells. *Cancer Res*. 2000;60:5704-9.